Sustainable Strategies for the Scalable Production of Widely Used Small Precursors

YINGFENG ZHANG

Durham University

Sustainable Strategies for the Scalable Production of Widely Used Small Precursors

A thesis submitted for the degree of
Doctor of Philosophy

By
Yingfeng Zhang

Under the Supervision of
Prof. Ian R. Baxendale

10-2024

Acknowledgement

I am deeply grateful to my supervisor, Prof. Ian Baxendale, and co-supervisor, Prof. David Hodgson, for their invaluable support, and to Dr. Mark Fox for his expertise in electronic structure calculations. My thanks also extend to the Baxendale research group members—Alexander J. Nicholls, Camila R. de Souza Bertallo, Guido Gambacora, Eilish S. Bonner, Haijing Wang, Diego Alvares Bustos, and Haoyang Wang, as well as the dedicated staff at Durham University's analytical services (NMR, Mass Spectrometry, Elemental Analysis, Chromatography, and X-Ray Crystallography) and workshops (mechanical, electrical and glass-blowing workshops). Special thanks go to my lecturers, teaching lab demonstrators who have illuminated the beauty of chemistry during my academic journey. I'd like to express my heartfelt gratitude to the event organizers for their excellent training courses, lectures, symposiums, and leisure events. I am sincerely grateful to my family and friends, whose support has been unwavering. I also want to thank large language models for answering many many questions.

Lastly, I am very grateful to myself—not for any particular talent but for the enduring joy I find in science. This journey was not a childhood dream, but rather a series of unexpected, rewarding surprises. Reflecting on this journey, I appreciate the personal growth and unexpected discoveries that research has brought. Beyond the foundational knowledge presented in this thesis, one takeaway as a student is seeing how everything ultimately comes together. As noted by educators in *Experiential Learning: Experience as the Source of Learning and Development*, the order and nature of learning experiences vary across individual. While research often focuses on specific targets and societal applications, some of the most remarkable discoveries, like penicillin or drug repurposing, arise outside of intended design.

To myself, I simply say: keep at it and enjoy science.

Declaration

The work in this thesis is based on research carried out within the Baxendale laboratory, in the Department of Chemistry at Durham University, UK. No part of this thesis has been submitted elsewhere for any other degree or qualification and it is the author's own work unless indicated otherwise in the text; for example, where the referential work of previous project is taken as a reference.

Statement of Copyright

Preface by the Author

Chemistry serves as a bridge between the macrocosm and the microcosm, offering a unique lens through which to perceive the world. It reveals that substances, despite their apparent differences to the naked eye, often share similar elemental compositions at a microscopic level. Foundational knowledge of quantum mechanics and molecular orbitals enhances our understanding of wave-particle duality, molecular structures, and interactions. Reaction mechanism is one of the most fascinating tools in chemistry, capable of explaining and predicting a wide range of experimental outcomes. This was flourished around 1940s, 1950s and continues to evolve today.[1] However, this is also an area that poses challenges for many undergraduate students. Numerous exceptional lecturers offer valuable insights into learning established reactions and mechanisms, each with their own approach—some emphasizing p*Ka*, while others effortlessly recalling named reactions, etc.[2] The key takeaway for students might be developing the strategy of embracing teaching styles, others' experiences, and ultimately to cultivate a personalized learning pathway.

Beyond chemistry, fields such as Experiential Learning, neuroscience and psychology also play significant roles in shaping learning experiences. As someone who self-identifies with congenital aphantasia—a condition only recently explored in literature reviews from 2018 and 2019,[3, 4] I wish to share my personal experiences and supplementary tools for learning reaction mechanisms. While my approach may not be universally applicable, I hope it serves as an inspiration for those passionate about chemistry and encourages them to pursue their career aspirations despite external doubts.

Congenital aphantasia (or simply aphantasia) is an emerging topic in neuroscience, with theories still developing.[4, 5] A brief explanation, provided by Zeman *et al*. 2015, describes aphantasia as "reduced or absent voluntary imagery."[6] Individuals with aphantasia are unable to visualize images in their mind's eye, making it difficult to imagine pictures such as faces or a sunset. This condition has gained attention on social media, as it impacts various daily tasks,[5] such as visual memory exercises relying on mental imagery.[7-9] In contrast, many people can voluntarily form vivid mental images, and in some cases, strong imagery has been linked to anxiety disorders.[4]

In practical scenarios, memorizing reaction mechanisms through models (grouped information) is less effective than relying on logical deductions for me. Supplementary learning in quantum chemistry—including quantum mechanics[10] and electronic structure calculation methods[11]—as well as the history of molecular structure development,[1] was invaluable alongside foundational knowledge of organic chemistry. While quantum chemistry builds upon quantum mechanics, it also provides predictive tools for analysing electronic interactions, often facilitated by computational software such as Gaussian. The connection between mathematical functions and graphical representations enhances the understanding of reaction mechanisms. Additionally, although historical insights may not directly explain logical reasoning, they offer valuable perspectives on the progression of research. The current stage of molecular understanding is not one in which a fully established logical theory exists; rather, named reactions represent breakthroughs achieved by pioneers who expanded the boundaries of knowledge at a time when theoretical frameworks were still developing.[1] While theoretical knowledge certainly informs research, the discoveries made by early chemists marked monumental shifts from the unknown to the known, laying the groundwork for modern organic chemistry—an ever-evolving field.

To maximize the value of these pioneering developments, effective learning techniques for memory tasks, taught by different practitioners are summarized as 8 tips:

1. **Clarify unfamiliar terminology** – Look up unknown words or phrases using a dictionary, large-language models, or other reference tools depending on context. For complex or awkward sentences, read them multiple times and engage in deep thinking exercises.
2. **Copy key sentences** – Record important sentences based on their contextual significance and learning purposes.
3. **Identify conceptual similarities** – Recognize sentences that convey similar meanings to reinforce understanding.
4. **Summarize and reframe** – Rewrite the chapter outline to grasp its structure.
5. **Recognize cross-chapter connections** – Learn to summarize the broader structure of a book by linking related concepts across different sections. A helpful tip: once you understand how the book is written, you can analyze it using the same method. (*The Pyramid Principle: Logic in Writing and Thinking*[12] serves as a useful example.)

6. **Understand genre and writing style** – Identify the book's genre and typical stylistic approach to deepen comprehension.
7. **Expand beyond a single book** – Determine which parts resonate with or complement other books. Some may convey the same ideas, while others expand on a topic with different emphases. Identifying these patterns can accelerate reading speed—a strategy also beneficial for crafting lesson plans and educational handouts.
8. **Critically evaluate content** – Reflect on whether the ideas within these books reveal deeper connections or expose unresolved questions. By continuously applying previous steps, you will begin to see not just the "cement" but the "reinforcing steel" beneath the texts.

Organic synthesis, often regarded as an artistic pursuit, showcases human creativity and innovation, with applications in energy, pharmaceuticals, food preservation, energy, housing and personal care products.[13] As society continues to explore and harness nature's resources, the imperative to give back has become increasingly pressing.[13-15] Sustainable development is gaining attention, signalling a shift toward environmentally friendly chemical synthesis, strategic methodologies, theoretical advancements, and cutting-edge technologies—topics that will be further explored in the remainder of this chapter.

Table of Contents

List of Figures

List of Schemes

List of Tables

List of Equations

List of Abbreviations

δ	Chemical shift (NMR spectroscopy)
ν	Wavenumber (IR spectroscopy)
API	Active pharmaceutical ingredients
BOD	Biochemical oxygen demand
br.	Broad (NMR spectroscopy)
BRP	Back pressure regulator
CBS	Combinatorial library synthesis
cm^{-1}	Inverse centimetre
COD	Chemical oxygen demand
CW	Cheese whey
d	Doublet (NMR spectroscopy)
DFT	Density functional theory
DMSO	Dimethyl sulfoxide
DOS	Diversity oriented synthesis
d.r.	Diastereomeric ratio
equiv.	Equivalents
et al.	Et alia
FGA	Functional group adjustment
FT-IR	Fourier-transform infrared
g	Grams
GMP	Good manufacturing practices
h	Hour
HF	Hartree-Fock
HOMO	Highest occupied molecular orbital
HRMS	High resolution mass spectrometry
Hz	Hertz
J	Coupling constant (NMR spectroscopy)

LC-MS	Liquid chromatography mass spectrometry
LUMO	Lowest occupied molecular orbital
m	Medium intensity (IR spectroscopy)
m	Multiplet (NMR spectroscopy)
M	Moles per litre
min	Minutes
mL	Millilitres
mol	Moles
NB	Nota Bene
nm	Nanometres
NMR	Nuclear magnetic resonance
PI	Process intensification
ppm	Parts per million
PTC	Phase transfer catalyst
q	Quartet (NMR spectroscopy)
QPSA/QP-SA	Amberlyst^{TM} 15(H), ion exchange resin
R_t	Retention time
r.t.	Room temperature
RXN Time	Reaction Time
s	Strong intensity (IR spectroscopy)
t	Triplet (NMR spectroscopy)
Temp	Temperature
THF	Tetrahydrofuran
TLC	Thin layer chromatography
TOS	Target oriented synthesis
w	Weak intensity (IR spectroscopy)

Abstract

The aim of this thesis is to design and apply enabling technologies such as flow chemistry, microwave reactors, immobilised reagents and scavengers to expedite complex chemical syntheses of widely used small precursors.

Chapter 1 introduces the significance of sustainable synthesis, contextualising current methodologies and technologies within broader societal and industrial demands. The increasing need for affordable, efficient, and scalable chemical products continues to drive innovation in safer, environmentally conscious, and sustainable synthesis strategies. The research comprises three interconnected projects, grouped into two thematic parts:

- Part I: Sustainable valorisation of recycled materials containing carbohydrate sources
- Part II: Methodology development for small, broadly applicable building blocks: 2-hydroxy-6-methoxyacetophenone and 2-hydroxy-6-methoxybenzaldehyde.

Part I explores laboratory synthesis optimisation for industrial-scale applications, addressing real-world environmental challenges. A key focus is the valorisation of lactose derived from cheese whey waste. This project applies the García González reaction in flow reactors to convert carbohydrates into high-value C-glycosalfuran derivatives (Figure 1). Using *D*-(+)-glucose and *D*-(+)-galactose as model monosaccharides, reaction yields ranged from 78% to 85%. The García González reaction achieved 98% lactose consumption, yielding products with exceptional stability in aqueous media—making them promising candidates for synthesising materials requiring robust water-phase resilience.

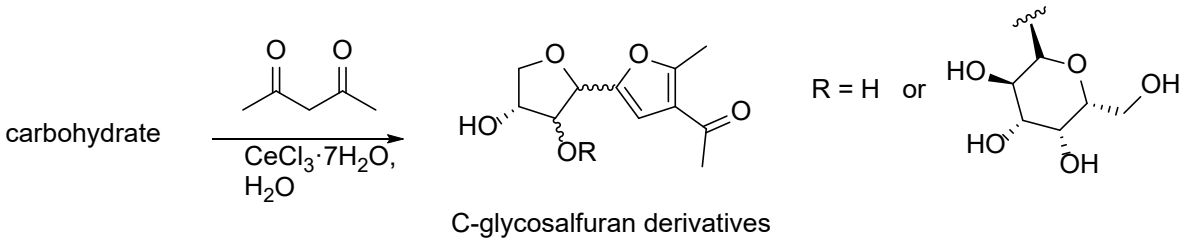

Scheme 1. Garcia Gonzale reaction to convert carbohydrate into C-glycosalfuran derivatives

Part II comprises two projects addressing regioselectivity challenges frequently encountered in electrophilic aromatic substitution reactions. Specifically, the focus lies in synthesising two target compounds: *2-hydroxy-6-methoxybenzaldehyde* and *2-hydroxy-6-methoxyacetophenone*. The benzaldehyde derivative was synthesised via a three-step sequence employing the Casnati–Skattebøl reaction, which enabled ortho-selective formylation using an Et_3N–$MgCl_2$ system (Scheme 2). To access the acetophenone analogue, a novel synthetic approach was developed. This involved the preparation of the coumarin precursor *5-methoxy-4-methylcoumarin*, followed by ozonolysis to achieve complete functional conversion of the alkene moiety, ultimately yielding *2-hydroxy-6-methoxyacetophenone* (Scheme 3).

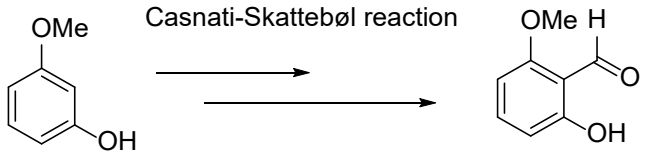

Scheme 2. Preparation of 2-hydroxy-6-methxoybenzaldehyse via Casnati-Skattebøl reaction.

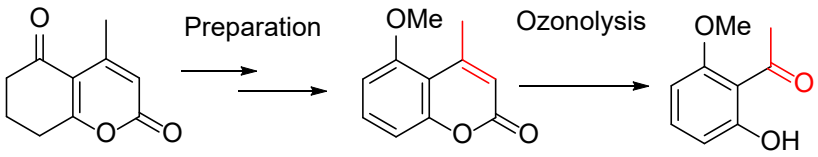

Scheme 3. Noval synthetic strategy of synthesizing 2-hydroxy-6-methoxyacetophenoe.

Chapter 1

Introduction

1.1 Sustainable development of chemicals: A historical context

The usage of chemicals has grown significantly throughout the 20th century, spanning many sectors such as health, textiles, food, household products, and transportation. By 2020, over 350,000 chemicals and mixture of chemicals have been registered for production and use, more are claimed as confidential (over 50,000) or ambiguously described (up to 70,000),[13] and are still growing by many hundreds each year.[15, 16] Whilst these chemical products provide significant benefits, their large scale production also contributes to environmental issues like global warming, toxic waste generation which creates safety concerns during production. As a result, there has been a substantial rise in discussions on how to maintain the advantages of chemistry-based products in a more environmentally responsible and sustainable way. To protect the long-term ecosystem, we have recognized the importance of staying within the Earth's natural capacity to manage waste and pollution. In 1987, the United Nations Commission on Environment and Development (Brundtland Commission) defined sustainable development as: "… meeting the needs of the present without compromising the ability of future generations to meet their own needs."[17] Later, the term "Green Chemistry" was introduced to describe the approach of conducting chemistry and engineering in a sustainable manner. The 12 Principles of Green Chemistry outlined best practices across the entire product life cycle (Table 1).[18] The 12 Principles of Green Engineering serve as a guiding framework for scientists and engineers in the design of new materials, products, processes, and systems that prioritize human health and environmental sustainability (Table 2).[19] Since their introduction, innovative synthetic methods and technologies have flourished significantly.

Table 1. Twelve principles of Green Chemistry.

1. Prevent waste
2. Maximize atom economy
3. Design less hazardous chemical syntheses
4. Design safer chemicals and products
5. Use safer solvents and reaction conditions
6. Increase energy efficiency
7. Use renewable feedstocks
8. Avoid chemical derivatives
9. Use catalysts, not stoichiometric reagents
10. Design chemicals and products to degrade after use
11. Analyze in real time to prevent pollution
12. Minimize the potential for accidents

Table 2. Twelve Principles of Green Engineering

1. Designers need to strive to ensure that all material and energy inputs and outputs are as inherently non-hazardous as possible.
2. It is better to prevent waste than to treat or clean up waste after it is formed.
3. Separation and purification operations should be designed to minimize energy consumption and materials use.
4. Products, processes, and systems should be designed to maximize mass, energy, space, and time efficiency.
5. Products, processes, and systems should be "output pulled" rather than "input pushed" through the use of energy and materials.
6. Embedded entropy and complexity must be viewed as an investment when making design choices on recycle, reuse, or beneficial disposition.
7. Targeted durability, not immortality, should be a design goal.
8. Design for unnecessary capacity or capability (e.g., "one size fits all") solutions should be considered a design flaw.
9. Material diversity in multicomponent products should be minimized to promote disassembly and value retention.
10. Design of products, processes, and systems must include integration and interconnectivity with available energy and materials flows.
11. Products, processes, and systems should be designed for performance in a commercial "afterlife".
12. Material and energy inputs should be renewable rather than depleting.

1.2 Sustainable chemical synthesis

Chemical synthesis

Chemical synthesis serves as a means to manipulate the molecular architecture of the microscopic world, enabling the construction of both natural and artificial compounds through the manipulation of atoms, ions, and molecules. Today, a major branch of chemical synthesis is organic synthesis which specifically deals with carbon-based compounds (in contrast to inorganic synthesis) and is the core of this thesis. One thing worth mentioning is that the concept of (chemical) synthesis has evolved overtime (Table 3), hence, throughout this work, the terms "chemical synthesis" and "organic synthesis" will be used as defined in the referenced literature.

Table 3. Selected definitions of (chemical) synthesis.[20]

Year	Word/phrase	Description
1860	Chemical synthesis	"Having completed his analytical work, the chemist proposes to re-compose what he has destroyed; he takes as his point of departure the ultimate of analysis, that is, simple bodies, and he compels them to unite with each other and by their combination to re-form the same natural principles which constitute all material beings. Such is the object of chemical synthesis."
1987	Synthesis	a) formation of a natural organic product from any other simpler natural prduct. b) formation of a natural organic product from an artificial product. c) formation of a natural organic product from the elements directly. d) formation of an artificial organic product from any other artificial product. e) formation of an artificial organic product from the elements directly. f) formation of an artificial organic product from a natural one of simpler structure.

One of the major strengths of chemical synthesis is its flexibility in designing a wide range of molecular structures with specific functions. Many new methodologies have been implemented for improving aspects of chemical synthesis. The creation of compound libraries, which increases the likelihood of identifying successful drug candidates is a notable example. Various synthetic strategies can be employed to build these libraries, which will be introduced in section 1.3.[21]

Synthetic chemistry can also play a pivotal role in shaping the physical properties of various compounds. This is evident in the development of radiolabeled compounds used in drug metabolism and pharmacokinetic studies,[22] as well as materials used in dye-sensitized solar cells[23] and fluorescent probes[24]. Another field that has seen remarkable progress over the past 25 years is synthetic biology, where assembling biological components, such as DNA-binding proteins and the sequences they target, to create new systems with useful functions has become common parctice.[25, 26] For instance, the microbial production of artemisinic acid has enabled large-scale, sustainable synthesis of complex natural molecules like qinghaosu (artemisinin) derivatives (Figure 1).[27] As such there is much debate regarding the direction of chemical synthesis and biosynthesis, but when asked, large language models (e.g., GPT-4) suggest a likely convergence between the two fields. Synthetic biology may excel in producing complex natural molecules, leveraging evolution, while chemical synthesis will continue to dominate the production of materials, fine chemicals, and small-molecule drugs. Increasing collaboration between these disciplines, coupled with advancements in manufacturing technologies and artificial intelligence, promises a more sustainable future for both fields.

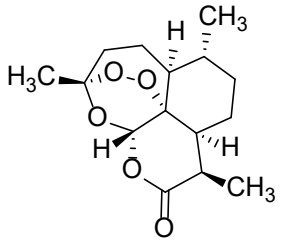

Figure 1. Structure of qinghaosu (artemisinin).

Interdisciplinary approaches have been crucial for development of organic chemistry since the late 18th century, indeed the advancement of organic synthesis has been closely intertwined with the establishment of fundamental theories and advances in instrumentation. As students today learn, Avogadro's constant represents the number of units in one mole of any substance. Historically, the balanced equation by Avogadro's hypothesis, which involves the small whole numbers (i.e., the number of moles of each element), helped reconcile Dalton's law of multiple proportions with Gay-Lussac's law of combining volumes (e.g., Equation 1). Avogadro's hypothesis was later confirmed and advanced by his student Stanislao Cannizzaro (1826–1910, a chemist), leading to universal agreement on atomic weights and chemical formulas at the Karlsruhe Conference.[1] One

of the attendees of this conference was Dmitri I. Mendeléev (1834–1907, a chemist) who later developed the first version of the periodic table. His work was subsequently revised and supplemented with newly discovered elements, eventually forming the periodic table.

$$H_2 + \frac{1}{2}O_2 = H_2O$$

Equation 1. Balanced equation of one unit water made by one unit hydrogen gas and a half unit of oxygen gas.

The pictorial representation of invisible entities, such as molecules marked a significant advancement in organic synthesis by allowing the spatial arrangements of molecules to be considered.[1, 28] In 1865, Kekulé (1829 – 1896, a chemist) published the ring structure of benzene and later predicted the bonding of atoms to tetravalent carbon, which became known as the *Structural Theory of Organic Compounds*. The three-dimensional arrangement of substituents attached to tetravalent carbon, positioned at the four corners of a tetrahedron, was introduced by Jacobus van't Hoff (1852–1911, a physical chemist) and Joseph Le Bel (1847–1930, a chemist). Additionally, Jean-Baptiste Biot (1774–1862, a physicist, astronomer, and mathematician) discovered optical activity in several organic compounds. Among the many contributors to the application of quantum mechanics in chemistry, Linus C. Pauling (1901–1994, a chemist, biochemist, chemical engineer, peace activism, author, and educator) had the most profound influence. His book, *The Nature of the Chemical Bond*, first published in 1939, introduced theories such as hybrid atomic orbitals, making these concepts accessible to chemists in practical terms rather than as purely mathematical wavefunctions.[29] The development of quantum theory not only advanced the ability to synthesize more complex structures and explain fundamental chemical phenomena but it also impacted other fields, including biochemistry and structural biology.[1] This also coincided with a revolution in analytical instrumentation which began in the 1950s, dramatically increasing the efficiency of structural identification.[30] Prior to the advent of techniques like infrared (IR), ultraviolet (UV), nuclear magnetic resonance (NMR) spectroscopy, mass spectrometry, and X-ray crystallography, it took scientists over 60 years to fully determine the structure of compounds such as strychnine, despite its empirical formula being established in 1838 (Figure 2).[31] The development of these methods led to a step change in reaction mechanism studies, providing more rational and reliable explanations for chemical reactions and enhancing their design.

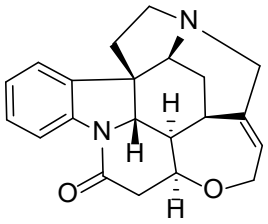

Figure 2. Structure of strychnine.

The Evolving Role of Organic Synthesis: Market Demands and Green Chemistry

Moving into the 21st century, organic synthesis continues to play a pivotal role in many applications, importantly a balance is being aimed for addressing market demands while adhering to green chemistry principles. Also due to the sophistication in our ability to make new chemical entities and our improved understanding of molecular interactions, current synthetic efforts are increasing focused on the functional properties of the targets.[32] To highlight this, a brief example from the field of drug discovery is offered here. A comprehensive statistical review by Newman and Cragg (2020) analyzed approved therapeutic agents for all diseases (from 01/01/1980 to 30/09/2019) and all antitumor drugs (earliest records from ~1946 to 30/09/2019).[33] The sources of these compounds were classified as shown in Table 4. Out of 1,881 newly approved drugs (from 01/01/1981 to 30/09/2019), 1,394 (74%) were small molecules, while the remaining 487(26%) were biological macromolecules and vaccines. ("*Small-molecule drugs are chemical compounds with a molecular weight in the range of 0.1–1 kDa. They are smaller than biologics or bio-therapeutic modalities, which are generally more than 1 kDa in molecular size*."[34]) Among the small molecules, 33% were purely synthetic, 36% included synthetic and natural components (S or S* included), a further 31% involved no synthetic components (no S or S*). Figure 3 illustrates these findings. Notably, between 01/01/2011 and 30/09/2019, there was a significant rise in approved small molecules in the S*/NM category, followed by S, S/NM, and ND categories since all categories are defined in the literature (Figure 4).[33, 35] While natural sources have inspired many drug molecules, synthetic compounds continue to dominate the field of small-molecule drugs. The convergence of synthetic and natural approaches has also become increasingly important. An exemplary case is the development of eribulin, a derivative of halichondrin B, which was approved in 2010 by the US FDA as HALAVEN® for the treatment of breast cancer and liposarcoma (Figure 5).[36-41] This compound, with a molecular weight of 730 Da, showcases the developmental journey from a

potent marine-derived antitumor compound to its large-scale production via total synthesis, adhering to good manufacturing practices (GMP).[42] Lifecycle assessments also reported that synthetic chemistry plays a crucial role in reducing the environmental impact of active pharmaceutical ingredients (API) synthesis.[43] Pharmaceutical companies focused on traditional medicinal chemistry goals like potency and dosage can decrease the amount of API that is required to be synthesized. In parallel, breakthroughs in bond formation methods can streamline synthesis pathways, and novel manufacturing techniques can cut down on production-related waste.

Table 4. Code and definition of categories for approved new drugs 01/01/1981 – 30/09/2019.[33]

Code	Brief definition [introduced reference]	Explanation[33]
B	Biological macromolecule[44]	Usually a large (>50 residues) peptide or protein either isolated from an organism/cell line or produced by biotechnological means in a surrogate host
V	Vaccine[45]	Vaccine
S	Synthetic drug[44]	Totally synthetic drug, often found by random screening/modification of an existing agent
S*	Synthetic drug (NP pharmacophore)[44]	Made by total synthesis, but the pharmacophore is/was from a natural product
N	Unaltered natural product[44]	Natural product
NB	Botanical drug (defined mixture)[35]	Natural product "Botanical" (in general these have been recently approved)
ND	Natural product derivative[44]	Derived from a natural product and is usually a semisynthetic modification.
/NM	Mimic of natural product[45]	A sub-division used with S or S*, meaning mimic of natural product. (Please refer detailed definition to the reference.)

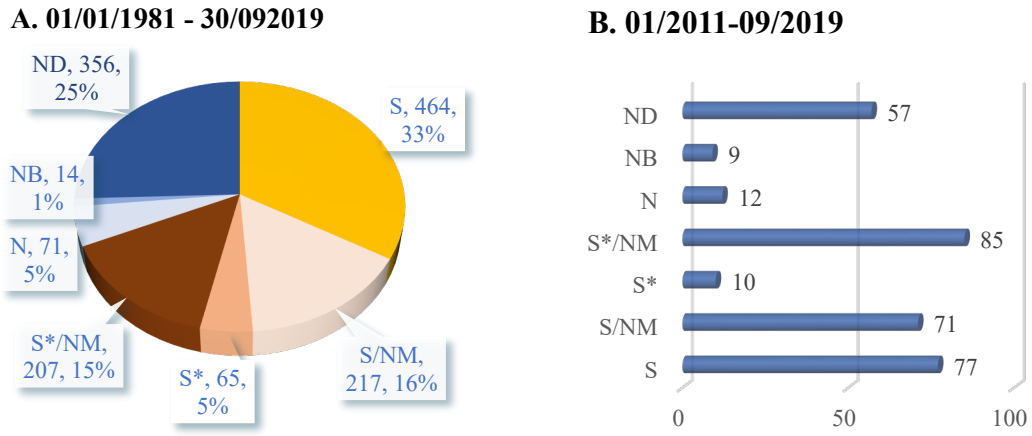

Figure 3. A. The percentage distribution approved new drugs of small molecules.[33] B. Increased small molecules of approved new drugs from June 2006 to September 2019.[33, 35, 46, 47]

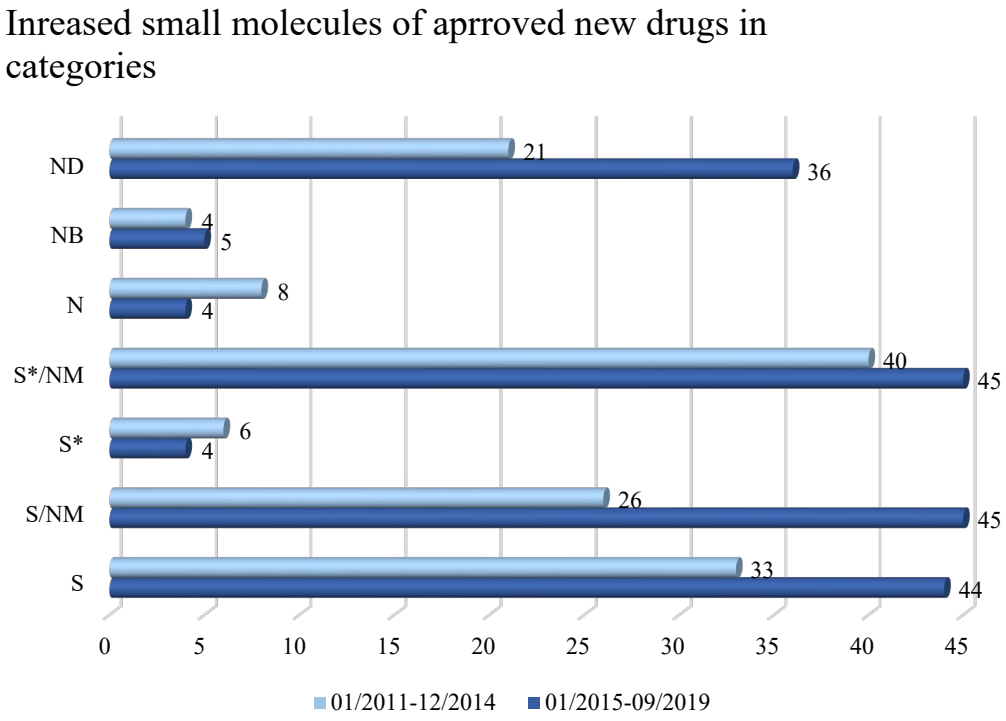

Figure 4. Summarized increase in approved new drugs of small molecules from referenced literatures since all categories were identified in literatures.[33, 35]

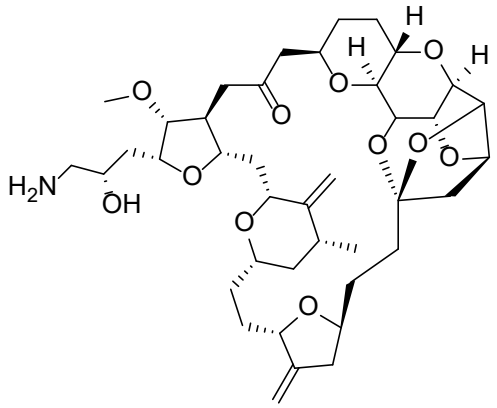

Figure 5. Structure of Eribulin (Halaven®).[48]

Although organic synthesis has undergone significant development, there is still much to discover. Many areas in organic chemistry continue to evolve or to be reinvestigated as technology improves; for example, *retrosynthesis*, *frontier orbitals*, *electronic structure calculations*, *flow chemistry*, *microwave synthesis*, and *photochemical reactions*. These cutting-edge techniques are integral to modern, sustainable molecular synthesis, and were incorporated into three case studies of small molecules: the synthesis of C-glycosalfuran derivatives, 2-hydroxy-6-methoxybenzaldehyde (**20**), and 2-hydroxy-6-methoxyacetophenone (**21**). The C-glycosal furan derivatives are rich in functional groups with great potential as building blocks. Compounds **20** and **21** introduced in Chapter 3 and Chapter 4 are not widely commercially available but are frequently involved in synthesizing a range of different compounds such as secondary metabolites including coumarin derivatives and chalcone derivatives. Throughout the thesis, both successful and failed attempts are documented, as Sierra and co-workers have noted that deviations from the original synthetic plans often align with the evolutionary process leading to the final synthesis.[49] Including these details will provide valuable insights for future reference. Other emerging tools, such as artificial intelligence, while not covered here, offer exciting potential for future sustainable synthesis and are recommended for further exploration in this field. To set the stage for the synthesis discussions, concise explanations of key concepts are provided. For those interested in further reading, relevant literature and book recommendations will be listed, as a detailed discussion of each topic is beyond the scope of this thesis.

1.3 Synthetic methodologies and strategies

The rapid progress in theoretical and analytical chemistry makes it feasible to synthesize highly intricate structures.[1] Nonetheless, the drive to meet green chemistry principles necessitate updates to traditional synthetic protocols, aiming to replace hazardous reagents and adopt energy-efficient, high-yielding approaches and to design functionally enriched chemical compounds.[17, 50, 51] As such, carefully designed and executed organic synthesis strategies are more essential than ever, and this section will review some of the most effective techniques utilized in synthesis.

Retrosynthesis

Given a target compound, retrosynthetic analysis can be applied to design the synthesis using commercially available starting materials. This methodology is used for 'Target-oriented syntheses' (as detailed in Figure 7A, from the Compound Library section). The target molecule is systematically "disconnected" into simpler fragments, called *synthons*, modified through functional group interconversions (FGI), (such as oxidation or reduction), or functional group addition (FGA, required where reactions like Friedel-Crafts acylation avoids problems found for Friedel-Crafts alkylation) to develop an efficient synthetic pathway.[52] In Figure 6, two example retrosynthetic analysis and corresponding forward synthetic schemes are presented. In example A, the antihypertensive drug ofornine is disconnected at the amide bond, converting the resultant acyl chloride to a carboxylic acid, and finally disconnecting the secondary amine.[53] In example B, the need for functional group adjustment (FGA) is demonstrated to achieve the target compound in the forward synthesis. However, it's noted that the alkylation method in this scheme will produce *tert*-butyl substituents rather than the desired *iso*-butyl substituents.[52] Nevertheless, in a real-world scenario, this disconnection approach is far more complicated with order of multiple site disconnection, reagent choice, etc. Practical laboratory experience is essential to apply these retrosynthetic guidelines thoughtfully, allowing researchers to select less-toxic reagents or adapt established methods that may not initially have been the most suitable or sustainable choice. The essence of retrosynthesis is however undoubtedly useful to plan organic synthesis.

A. A Disconnection Example

ofornine retrosynthesis analysis

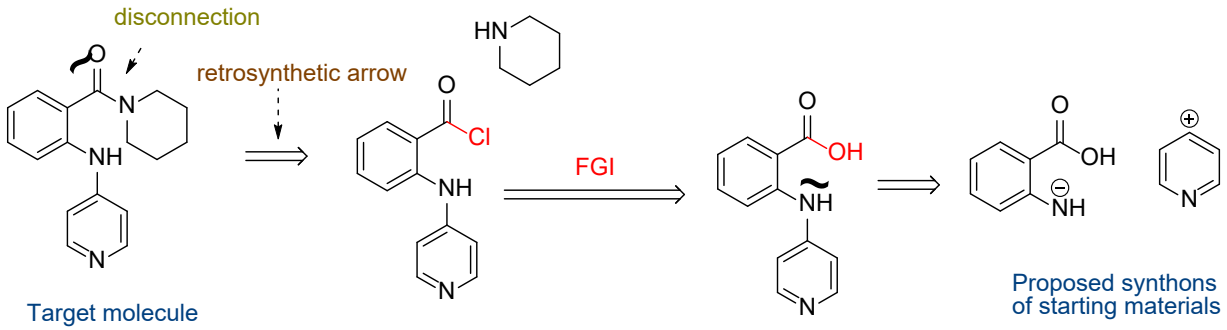

ofonine synthesis:

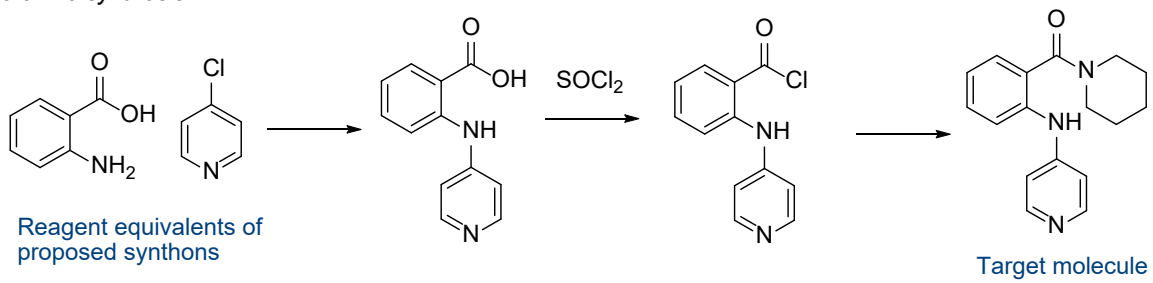

B. A functional group addition (FGA) example

Retrosynthesis:

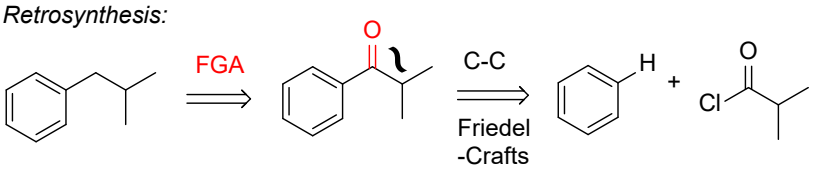

Synthetic scheme via Friedel-Crafts acylation

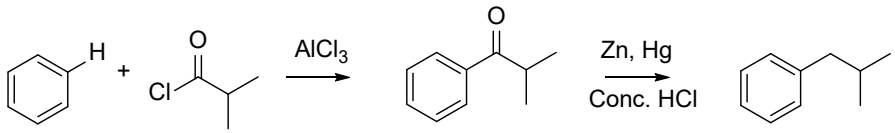

Wrong products derived via Friedel-Crafts alkylation

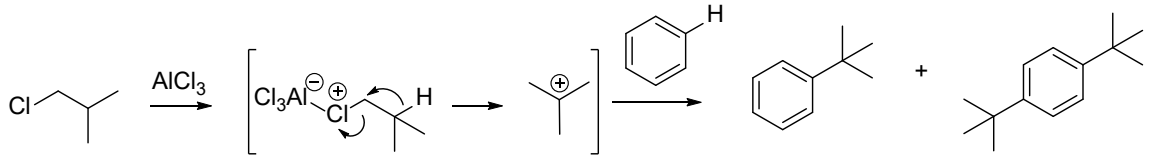

Figure 6. A. A disconnection approach of ofornine, an antihypertensive drug. B. A disconnection approach via functional group addition.

Compound Libraries

Collections of synthetic compounds (compound libraries) are created for structure-activity studies such as in drug discovery and chemical biology.[54, 55] The varied molecular frameworks allow them to interact effectively with structurally diverse macromolecules and the collection improves the chances of identifying target molecules capable of modulating biological macromolecules by exploring a greater area of chemical space. Traditionally, target orientated synthesis (TOS) (Figure 7A) uses retrosynthesis of one specific structure to deduce an appropriate starting material. To expand structure diversity, two other strategies — combinatorial library synthesis (CBS) and diversity-oriented synthesis (DOS) were popularised (Figure 7B, 7C).[55] CBS utilizes retrosynthetic strategy, to produce a collection of analogues of a target structure having known or predicted properties, using a one-synthesis/one-skeleton method.[56] This method biases available structures toward specific biological targets,[56, 57] covering a functionally dense chemical space, aiming to understand both known and novel biological activities from closely related compounds.[57] Diversity-oriented synthesis (DOS) has emerged as a forward synthesis strategy, focusing on producing a variety of molecular structures aimed at expanding novel hits in patent free chemical space. Syntheses of diverse structures generally depend on high-yield, broadly applicable synthetic methods that accommodate a wide range of substrates and functional groups, i.e. supported by prior literature.

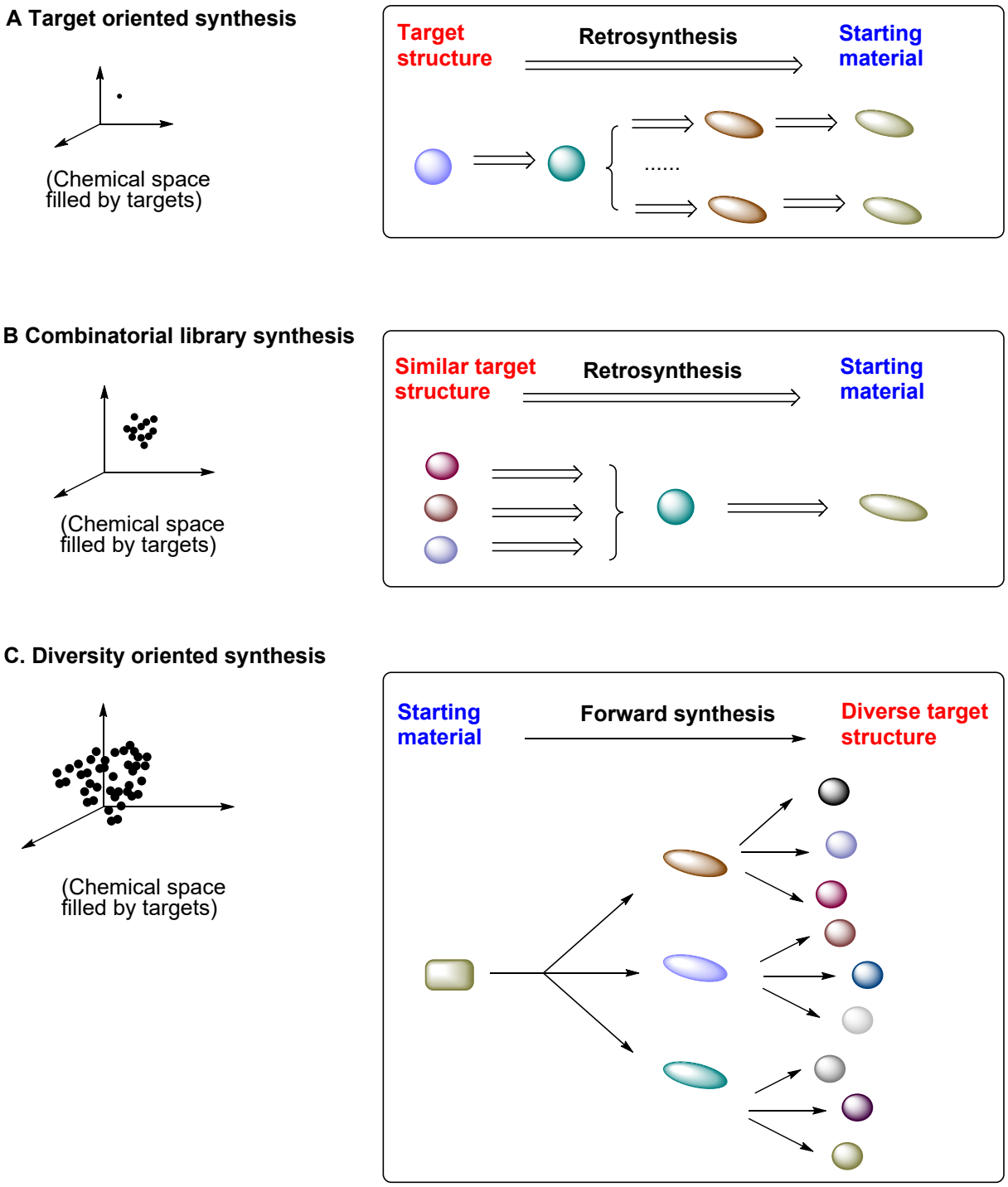

Figure 7. Summary of synthetic strategies of A. Target oriented synthesis, B. Combinatorial Library Synthesis, and C. Diversity oriented synthesis.

1.4 Quantum chemistry in organic synthesis

The modeling of reaction components, such as reactants and reaction progress, has been made possible by advancements in quantum chemistry and modern computing technologies.[58] Unlike classical mechanics, which governs the macroscopic world, quantum mechanics describes the behaviour of particles like electrons at the microscopic level, providing essential tools for studying chemical reactions. This shift in understanding has empowered chemists to analyze or predict molecular properties, investigate reaction mechanisms, and interpret complex NMR spectra with greater precision.

Reactions do not occur randomly, rather, they follow principles governed by the second law of thermodynamics, which states: "In a spontaneous process, the entropy of the Universe increases." Thus the change in entropy of the Universe is the sum of the entropy changes in the system and its surroundings (Equation 2).

$$\Delta S_{univ} = \Delta S_{surr} + \Delta S_{sys}$$

Equation 2. Entropy change of the universe is the sum of the entropy change of the surroundings and the entropy change of the system. ΔS_{univ} is the entropy change of the universe. ΔS_{surr}, the entropy change of the surroundings. ΔS_{sys}, the entropy change of the system.

To relate chemical reactions more directly, Gibbs free energy of the system (ΔG_{sys}) is more often calculated instead of entropy change of the universe (ΔS_{univ}) and the interconversion between these two is shown by Equation 3A. For chemical reactions, ΔG_{sys} is favourable when $G_{products} < G_{reactants}$, meaning ΔG_{sys} is negative (Equation 3B). Moreover, the energy absorbed and released in chemical reactions corresponds to bonds breaking and forming, understanding molecular bonding is essential for accurately modeling these reactions.

$$A.\ \Delta S_{univ} = -\frac{\Delta G_{sys}}{T_{sys}},$$

$$B.\ \Delta G_{sys} = G_{products} - G_{reactants}$$

Equation 3. The equation representing relationship of A. Entropy change of the universe (ΔS_{univ}) and B. Gibbs free energy of the system (ΔG_{sys})., T_{sys}, Absolute temperature in kelvin (assume, system and surrounding are at the same temperature, $T_{sys} = T_{surr}$).$G_{reactant}$, Gibbs energy of reactant. $G_{product}$, Gibbs energy of product.

Bonding results from electrostatic interactions between electrons and charged nuclei, holding multiple atoms together as a molecule. The most stable geometry of an molecule is achieved when bonding optimally balance the attraction of opposite charges and repulsion of like charges. In molecular orbital theory, the Schrödinger equation is used to describe electron dynamics (Equation 4A) and by solving the Schrödinger equation for required conditions, acceptable energies can be derived(e.g. Equation 4B). Unlike classical mechanics, which permits a continuous range of energy values (by $E = mc^2$), quantum mechanics allows only specific energy levels (Equation 4B). These discoveries about energy levels are crucial for explaining reaction mechanisms, as will be illustrated below and later in Section 1.5 in regard to photochemical reactions.

$$A.\quad \frac{d^2\psi}{dx^2} + \frac{8\pi^2 m}{h^2}(E - V)\psi = 0$$

$$B.\quad E_n = \frac{n^2 h^2}{8\pi^2 m r^2} \quad n = 0,1,2, \ldots$$

Equation 4. A. The Schrödinger equation for a one-dimensional, single-electron system applied to a conservative system, where no interactions with the surroundings occur. **B**. The quantized energy of the electron when it is constrained to move in a circle of radius r; x is the distance parameter along the edge of the circle (x = rθ); V = 0 at the circumference of the circle and V = ∞ elsewhere.[10, 59] E, Total energy. V: Potential energy. φ: Wavefunction. x, The distance parameter. m, mass of the particle (in this case, the electron). h, Plank's constant.

Molecular orbitals (MOs) are formed as linear combinations of atomic orbitals that spreads over multiple atoms with each MO having specific allowed energy levels. The highest occupied molecular orbital (HOMO) and the lowest unoccupied molecular orbital (LUMO), play critical

roles in reaction mechanisms. As molecules approach one another, their orbitals interact, forming bonding and antibonding orbitals through constructive and destructive interference respectively (Figure 8). The orbital interactions that significantly lower energy are the filled ones (HOMO) with unfilled ones (LUMO) (Figure 9).

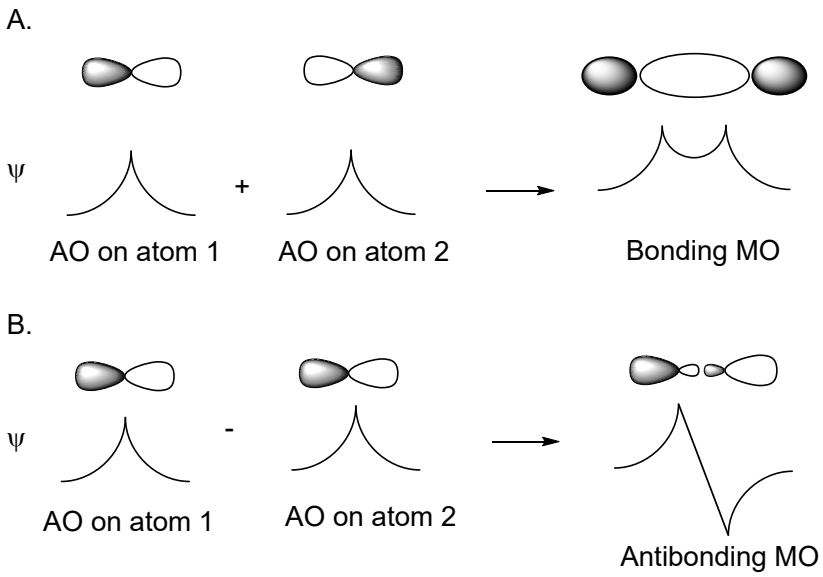

Figure 8. An example to present the linear combination of two atomic orbitals (AO) to form two molecular orbitals (MO) through bonding and antibonding interactions. A. Bonding interaction of two $2p_x$ atomic orbitals. B. Antibonding interaction. illustration of two $2p_x$ atomic orbitals. ψ: wavefunctions.

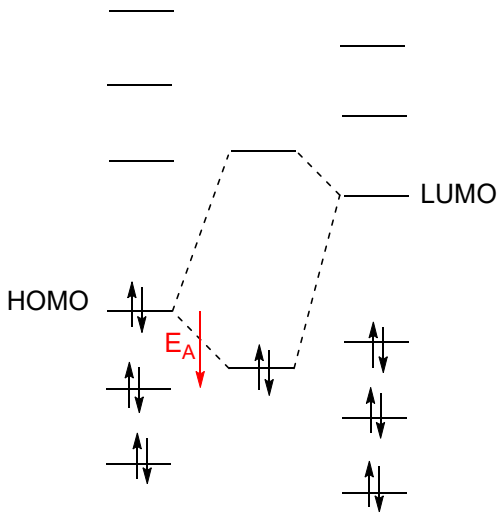

Figure 9. Interaction of the HOMO of one molecule with the LUMO of another molecule.

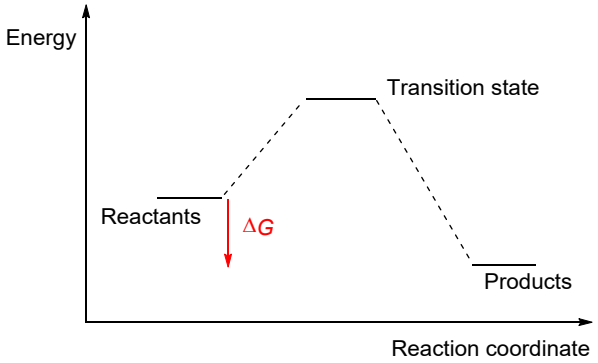

Figure 10. Plot of energy against reaction coordinate of reactants, transition state, and products.

When experimental data on transition states is limited (Figure 10), as these intermediate structures are challenging to isolate, modeling the reactants' frontier orbitals can provide some insight for predicting product formation. This approach is supported to some extent by the Hammond postulate, which suggests that the transition state for an exothermic reaction resembles the reactant most closely. A good example is the nitration of aromatic compounds, where electron densities in frontier orbitals have been compared with experimental nitration sites. In most cases, high absolute values of orbital coefficients correctly predict nitration positions, though slight anomalies, such as with pyrrocoline, are observed (Figure 11).

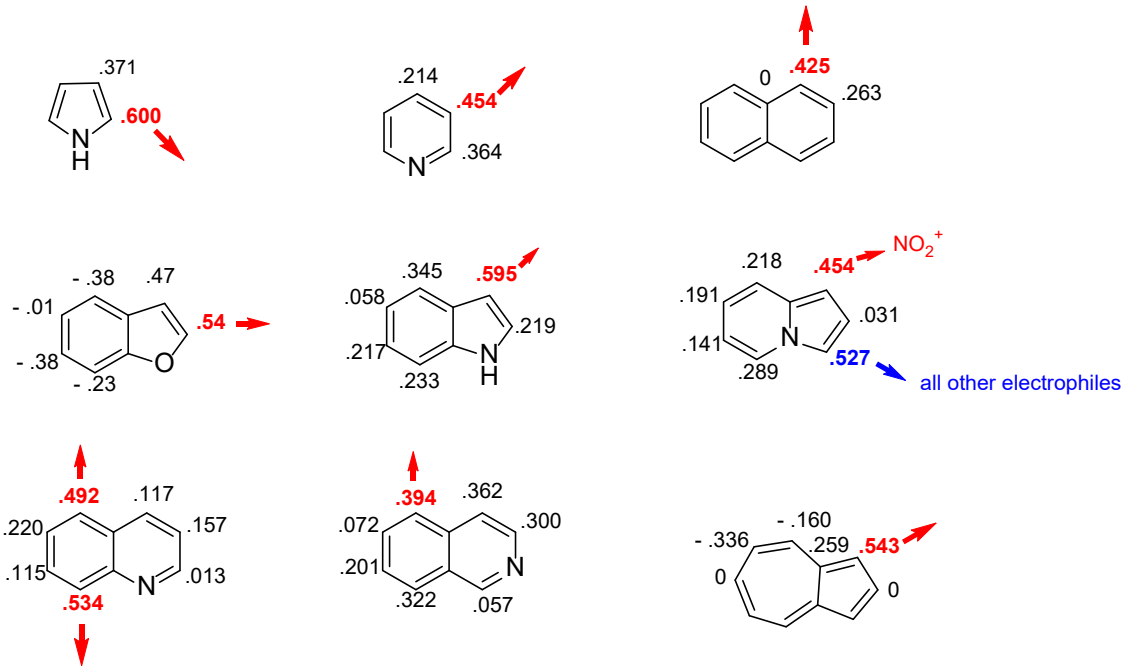

Figure 11. Electron densities in frontier orbitals compared with experimental nitration sites.[60]

The qualitative aspects of these calculations have been further explained by equation 5 using perturbation theory which rationalizes the contribution of overall charge (second term) and frontier orbitals (in third term) to energy changes to explain more complexed situations. These calculations are not to be treated as accurate as experimental result but instead provide probably outcomes for use in planning reactions (see Chapter 3 and Chapter 4). For example, electrophilic aromatic substitution is in general *ortho* and *para* directing for electron donating substituents or *meta* directing for electron withdrawing substituents. However, this site selectivity can be more accurately analyzed by electronic structure methods, where the energy gained and lost when orbitals of one reactant overlap with those of another is expressed with the equation below by Klopman and Salem (Equation 5).[60] Overall charge distribution is important for the orange term of the equation and the frontier orbitals contributed most for the green term. The first term is less important when we explain the features of differential reactivities.

$$\Delta E = -\sum_{ab}(q_a + q_b)\beta_{ab}S_{ab} + \sum_{k<1}\frac{Q_k Q_l}{\varepsilon R_{kl}} + \sum_{r}^{occ.}\sum_{s}^{unocc.} - \sum_{s}^{occ.}\sum_{r}^{unocc.}\frac{2(\sum_{ab} c_{ra}c_{sb}\beta_{ab})^2}{E_r - E_s}$$

Equation 5. First term in blue colour, second term in orange colour, third term in green colour. q_a and q_b are electron populations (often loosely called electron densitities) in the atomic orbitals *a*

and *b*. β and S are the resonance and overlap integrals. Q_k and Q_l are the total charges on atoms *k* and *l*. ε is the local dielectric constant. R_{kl} is the distance between the atoms *k* and *l*. C_{ra} is the coefficient of atomic orbital *a* in molecular orbital *r*, where *r* refers to the molecular orbitals on one molecule and *s* refers to those on the other. E_r is the energy of molecular orbital *r*.

Although the Schrödinger Equation of a one-dimensional single electron is ideal, current computing resources are challenged to calculate this for reactions. In practice, chemists use approximation methods to model chemistry based upon the Schrödinger wave equation, often via desktop software like Gaussian 16ts. This allows research chemists to select appropriate parameters to model their reactions using appropriately selected basis sets.

A basis set defines the quantum mechanical wavefunctions and consists of a set of mathematical functions with varying levels of electron movement. Larger basis sets with fewer constraints on electrons typically yield more accurate results but come with a heavier processing requirement. Approximation methods like Hartree-Fock (HF) and Density Functional Theory (DFT) approach electron behaviour differently: HF simplifies calculations by neglecting certain electron interactions, while DFT uses electron density distributions to account for the associated properties and energy. Although HF is computationally efficient, DFT typically provides more accurate results. As molecule size increases, however, the computational demands grow, so hybrid methods (e.g., B3LYP) are often preferred to balance accuracy with computational resource. In addition various modifications can be applied such as specifying a solvent model. There are also options for closed-shell versus open-shell molecules, where open-shell systems can be analyzed with spin-restricted or spin-unrestricted methods, depending on selected parameters.

Beyond energy calculations, the software can produce molecular orbital images, electron density maps, and predictions for spectroscopic data (Figures 12 and 13).

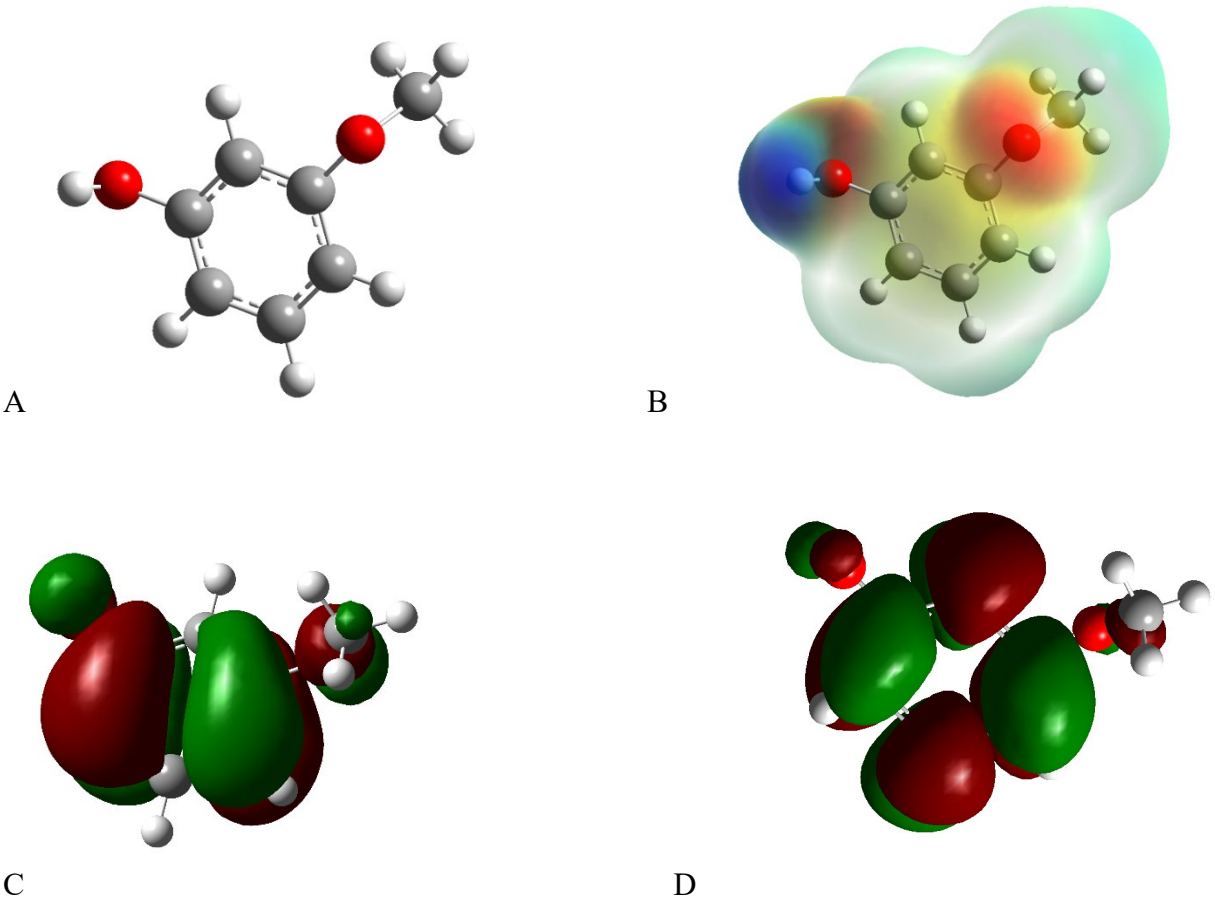

Figure 12. Pictorial illustration of a calculation result for 3-methoxyphenol. A. Minimum energy geometry. B. Electron density from Total SCF density. C. HOMO. D. LUMO.

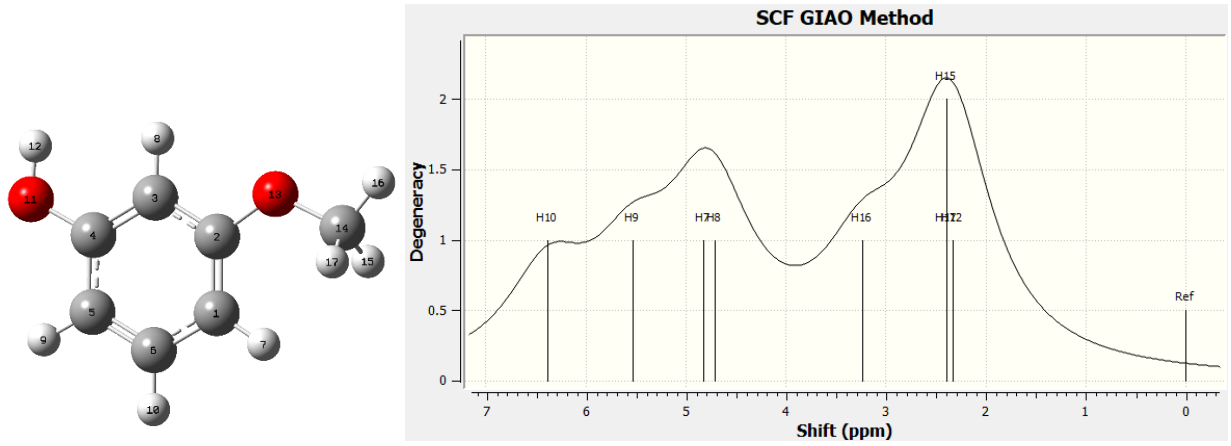

Figure 13. Predicted ^{1}H-NMR of 3-methoxyphenol by Gaussian 16.

1.5 Cutting-edge technologies

The efficiency of reactions and overall process economics depends significantly on the methods of chemical transformation, choice of reagent and/or catalyst, and reactor type.[61] Besides conventional chemical synthesis, process intensification (PI) is widely recognized in chemical engineering as a means to reduce the environmental impact of processes throughout their life cycle.[62-56] Four general principles of PI have been outlined with four approaches which are accepted worldwide Figure 14.[61, 63, 64]

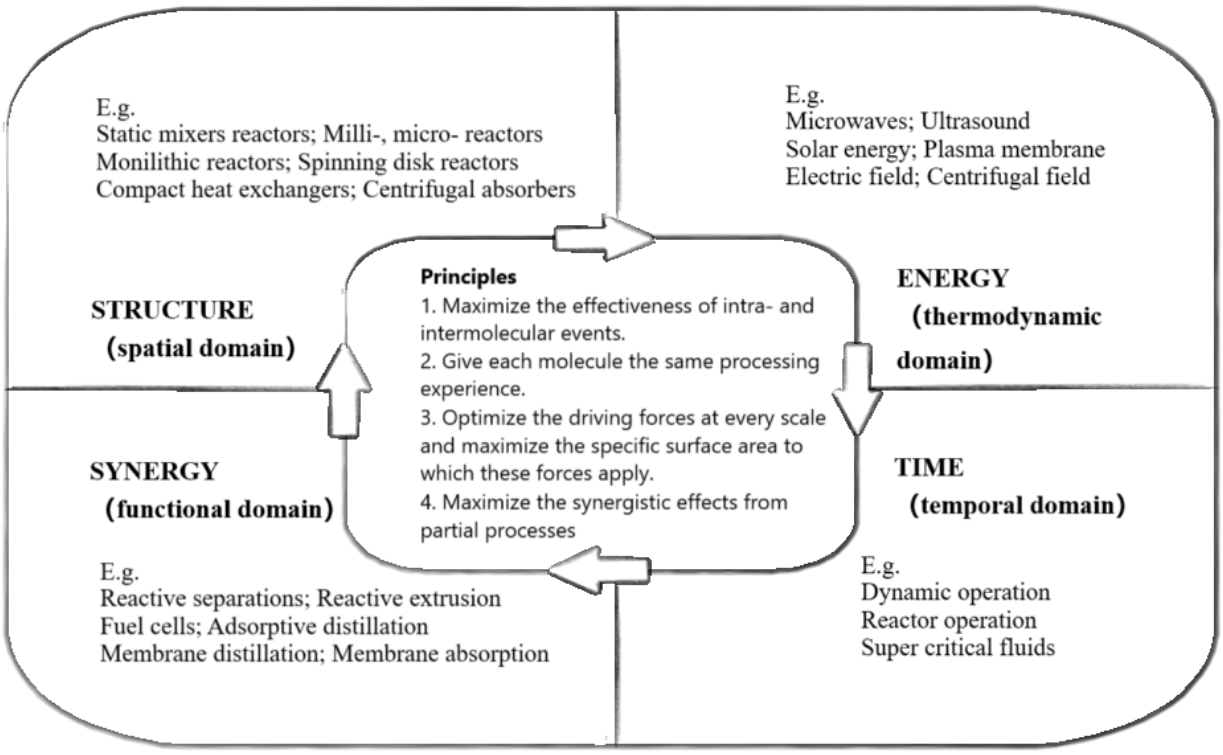

Figure 14. Four principles and approaches of principles (structure, energy, time, synergy) of process intensification with examples.[61, 63, 64]

These technologies enable process developments that are more compact, cleaner, safer, and energy efficient. Later disclosed work will indicate a focus on experimenting with alternative reactor types and employing innovative energy sources, such as flow reactors, photochemical reactors, and microwave reactors. In this section, these concepts are briefly introduced and their applications will be explored in subsequent chapters.

Flow reactions

Continuous flow synthesis is often the preferred approach for bulk chemical production in industry.[65] At laboratory scales, flow reactions are processed under rigorously controlled conditions in a confined space through multi-purpose micro or meso flow units (Figure 15) in contrast to conventional round bottom flasks.[66]

Figure 15. A modular assembly flow reactor from Vapourtec.

The use of smaller reactor volumes and increased containment provided by the sealed reactor system negates many problematic issues associated with synthesis such as potential toxic reagent contact, explosion risks and dangers relating to extreme exothermic behaviour. This includes the generation and handling of reactive and dangerous intermediates or waste streams. In addition, the more effective quenching, extraction, and work-up procedures often achieved in microreactors or in combination with other designed apparatus can help improve the downstream elements of the synthesis. Reaction efficiency may well also be improved with incorporated technologies such as microwave irradiation, polymer supported reagents, and photochemistry, allowing integrated processes and multi-step operations to be conducted as a seamless synthesis solution.[66] For example, the drawbacks of using diethylamino sulfur trifluoride (DAST) reagent in halogenation

chemistry includes its volatility, sensitivity to water, readily dismutation to SF_4 and $(Et_2N)_2SF_2$ when heating beyond 90 °C, and safety concerns based upon the liberation of corrosive hydrofluoric acid.[67] While the contact-free process in flow reactors avoids most of these drawbacks, the incorporation of direct in-line work-up facilitates the consumption of inorganic fluoride, excess reagents and side products in a scavenging process further simplifying and improving the process.[66]

The advantages in handling hazardous compounds and automation of several integrated processes have been demonstrated numerous times in fine chemicals or Active Pharmaceutical Ingredients (APIs) preparation in recent years.[65] While there is a growing demand for safer, greener, and more efficient synthesis, flow technology will continue to be one of the most promising universal tools for the development of new routes to these future chemicals.[65] An integrated upgrading approach that encompasses renewable feedstock, traditional synthesis, and scaling with state-of-the-art technology offers significant potential for large-scale applications. In the following chapters, two alternative energy sources used in organic reactions will be explored, focusing on how these energies influence the reaction medium compared to conventional heating.

Microwave-assisted organic synthesis

Microwave wavelengths range from 1 cm to 1 m, with frequencies between 300 GHz and 300 MHz, positioned within the electromagnetic spectrum between infrared and radar regions (Figure 16). To avoid interference with telecommunication and cellular phone frequencies, most household and laboratory microwaves are set to work at 2.45 GHz.[68]

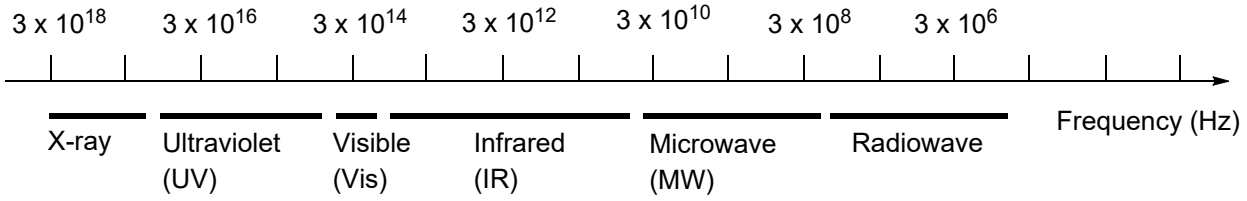

Figure 16. Position of microwave in the electromagnetic spectrum.

In microwave-assisted organic synthesis, microwaves—high-frequency electromagnetic waves—serve as an alternative energy source to conventional heating methods for chemical reactions.[51] This heat is produced via *dielectric loss* in the reaction medium when microwaves are applied. In electrical engineering, dielectric loss describes a material's capacity to dissipate electromagnetic

energy as heat.[69] While dielectric loss is generally undesirable in conventional electrical applications (e.g., capacitors) due to energy loss, in reactions, this generated heat is beneficial as activation energy. The reaction mixture is the dielectric that exhibit varying abilities to absorb and dissipate microwave energy, optimizing reaction efficiency.[68] When an external electric field ($\overrightarrow{E_0}$) is applied to a dielectric material, molecules align with the field: polar molecules align according to the charge, while non-polar molecules align with the induced dipole moment (Figure 17A and B).[70] Inside the dielectric, opposing charges/ dipoles neutralize each other, except at the boundaries, where equal and opposite charges/ dipoles accumulate (Figure 17 B). These induced surface charges/ dipoles create an additional electric field ($\overrightarrow{E_i}$) that opposes the external field (Figure 17 C).[70] This dipolar polarization, along with dc conduction, is a primary source of heat generation.[71]

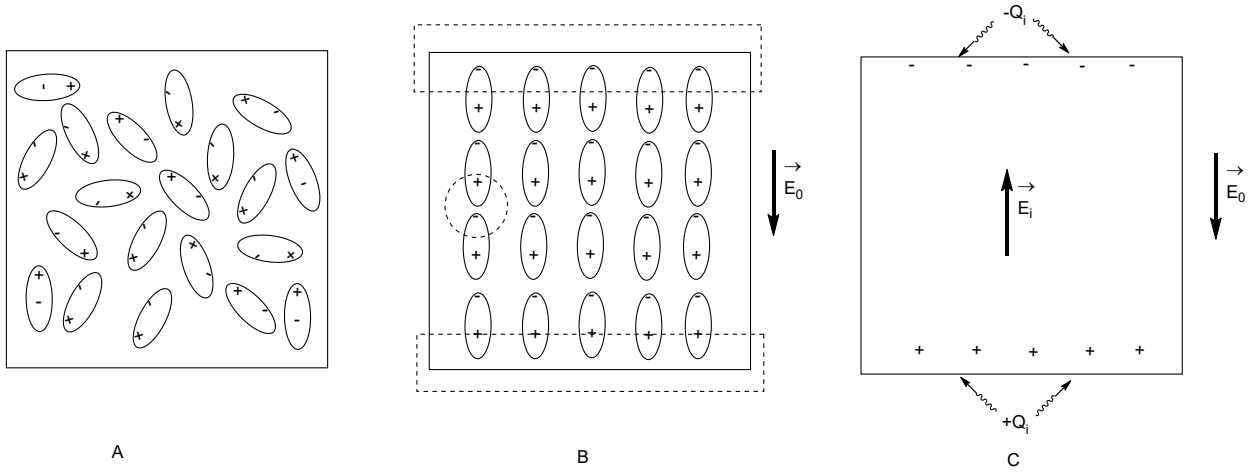

Figure 17. The dielectric representation of polar molecules. A. In the absence of the external field, polar molecules are randomly distributed. B. when an external field is applied, the charges are aligned and neutral as circled by dashed line and charges accumulates at the surface. C. The induced surface charge Q_i produced the internal field $\overrightarrow{E_i}$.

When an alternating electric field is applied, it induces the displacement and re-orientation of charges. If this re-orientation stays in phase with the external field or is too slow, no heat loss occurs. However, when the dipole rotation lags behind the field by an angle δ, resistive heating is generated in the medium and this is quantified by dielectric properties of the reaction medium, specifically described by dielectric constant (ε_r'), dielectric loss (ε_r''), and dielectric loss tangent ($tan\delta$) (See Table 5).[72] This phenomenon is analogous to mechanical systems, as explained by Ohring (1995)[69]: if a material under elastic tension is cyclically loaded and unloaded, no energy is lost because strain and stress remain in phase. Similarly, at very low frequencies, dipole

polarization is "elastic" and energy loss is minimal. While in between these two extremes, polarization causes a shift in energy level population, and the friction from polar molecule reorientation relative to neighbours together with other mechanisms results in energy being ultimately dissipated as heat. Efficient microwave absorption and rapid heating occur when the overall reaction medium, including solvents, reagents and any polar additives, exhibits a high $tan\delta$ value. For practical guidance, solvents are categorized based on their $tan\delta$ values into three absorption levels: low ($tan\delta$<0.1), medium (0.1< $tan\delta$<0.5), and high ($tan\delta$>0.5), examples are given in Table 6. These categories assist in selecting optimal reaction conditions for laboratory microwave system.

Table 5. The meaning of dielectric constant, dielectric loss and dielectric loss tangent.[72]

Name	Meaning
Dielectric constant (ε_r')	A measure of the ability of the molecules to be polarized by an external electric field.
Dielectric loss (ε_r'')	A measure of the efficiency with which electromagnetic energy can be converted into heat.
Dielectric loss tangent ($tan\delta$)	The $tan\delta$ is the ratio of ε_r'' to ε_r'. This defines the ability of a material to convert electromagnetic energy into heat energy at a given frequency and temperature.

Table 6. tanδ value of some solvents in groups of high, medium, and low absorption levels.[68]

Solvent	tanδ (high)	Solvent	$tan\delta$ (medium)	Solvent	$tan\delta$ (low)
Ethylene glycol	1.35	2-Butanol	0.447	Chloroform	0.091
Ethanol	0.941	1,2-Dichlorobenzene	0.28	Acetonitrile	0.062
DMSO	0.825	N-Methyl-2-pyrrolidone	0.275	Ethyl acetate	0.059
2-Propanol	0.799	Acetic acid	0.174	Acetone	0.054
Formic acid	0.722	DMF	0.161	Tetrahydrofuran	0.047
Methanol	0.659	1,2-Dichloroethane	0.127	Dichloromethane	0.042
Nitrobenzene	0.589	Water	0.123	Toluene	0.04
1-Butanol	0.571	Chlorobenzene	0.101	Hexane	0.02

The advantages of microwave reactions are the instantaneous increase in temperature (square heating profile as the reaction can be actively cooled upon completion), reduced reaction times as the enclosed reaction can be heated in excess of the solvent boiling point, and improved or changed

selectivity of products, coupled with increased reproducibility. The increase in rate of the reaction is simply explained by Arrhenius law where the rate of the reaction (k) is dramatically enhanced with increased temperature (T) (Equation 6). Since the 1980s, microwave-assisted synthesis has gained popularity, prompting the publication of numerous reviews and books on the topic (theories,[69, 71, 73] synthesis,[68, 74, 75] and both[76]). This method is regarded as an energy-efficient approach that can integrate well with flow reactors to enhance reaction efficiency. While the reaction scale is sometimes limited by microwave reactor dimensions, microwave-assisted synthesis remains a powerful tool for efficiently screening of reaction conditions, as discussed in Section 4.3.2.

$$k = Ae^{-\frac{E_a}{RT}}$$

Equation 6. Arrhenius Equation. k: Rate constant, A: Pre-exponential factor, E_a: Activation energy, R: Gas constant, T: Temperature.

Photochemical transformation

Photochemical transformations are widespread in nature, utilizing solar energy to drive processes such as photosynthesis in plants.[77] In organic synthesis, materials absorb light to undergo photochemical transformations, where light (electromagnetic radiation) serves as a form of energy exhibiting both wave-like and particle-like characteristics. The wave-like nature of light accounts for many intrinsic properties, such as propagation, reflection, interference, and polarization. Light propagates at approximately 3×10^{-8} ms^{-1} in a vacuum and the wavelength (or frequency) of its transverse oscillations determines its characteristic colour. Meanwhile, the energy of electromagnetic radiation with frequency ν is quantized as hν, 2hν, …, representing 0, 1, 2, particle(s) called photons, with each photon carrying an energy of hν and can be measured experimentally (Equation 7).[10]

$$E = h\upsilon = \frac{hc}{\lambda}$$

Equation 7. Energy of photons calculated by frequency (ν) or wavelength (λ), where h is Plank's constant, and c is the speed of light (approximately 3×10^{-8} m s^{-1}).

The energy carried by photons is absorbed when they interact with atoms or molecules. According to the Stark-Einstein Law, for each photon of light absorbed by a chemical system, only one

molecule is typically activated for subsequent reaction, although exceptions exist.[78] This implies that the energy available to each individual species is consistently fixed at hν. The intensity of radiation which relates to the number of photons per unit time, affects only the number of excited species not the energy available to each individual molecule. Photon-induced excitation of molecules leads to a change in their electronic state (Figure 18).

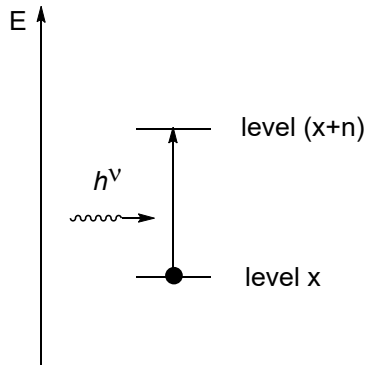

Figure 18. Excitation by absorption of radiation.

Due to the new electronic arrangement in the excited state, species possess greater energy and altered reactivity compared to their ground state, allowing further reactions. Thus, photoactivated compounds can:

- undergo unimolecular transformations,
- participate in bimolecular reactions with ground-state molecules,
- engage in bimolecular reactions with other electronically excited molecules,
- activate another substrate molecule through energy transfer or electron transfer, acting as a photosensitizer,
- serve as a photoinitiator, such as in photochemically induced radical chain reactions.

In later sections, an intramolecular process that induces *E*/*Z* isomerization (Section 4.3.1)will be explored and photoredox catalysis (Section 4.3.2). These reactions are conducted using photochemical reactors designed to facilitate flow reactions and optimize energy transfer[10, 77-80].

1.6 Conclusion

Overall, this chapter has outlined the need for sustainable chemical development and the vital role of organic synthesis. Progress in the development of more sustainable synthesis practices arise not only from production methods and experimental research but also from foundational theories and analytical tools, which have dramatically accelerated organic synthesis since the late 18th century. The design of organic compounds has become more efficient through systematic approaches like retrosynthesis, and for projects requiring multiple targets with specific functional activities, combinatorial library synthesis (CLS) allows for the exploration of a larger chemical space. For libraries that prioritize functional diversity among small molecules, diversity-oriented synthesis (DOS) covers an even broader chemical space than CLS. In cases where reaction mechanisms require in-depth analysis, quantum chemistry can model and explain reactions at a microscopic scale. Software like Gaussian 16 offers convenient electronic structure calculations, allowing experimental chemists to apply theoretical insights practically. When considering using such software or artificial intelligence aided tools, it is important to note that computational tools analyze data based on existing datasets. This reliance may limit exploration in underrepresented areas. Consequently, researchers must critically assess computational results rather than treating them as definitive conclusions, and, as with experimental work, verifying reproducibility is essential. Advanced technologies, such as flow synthesis, microwave-assisted synthesis, and photochemical activation, play pivotal roles in process intensification within chemical engineering. While academic laboratories often conduct organic synthesis on a relatively small scale compared to industry, testing these technologies in laboratory settings helps to facilitate a seamless transition from research outcomes to industrial applications. It is worth noting that while these technologies are valuable contributors to green chemistry principles, green chemistry does not rely solely on them; in some cases, conventional synthesis may perform better depending on the reaction condition.

In this project aim is to achieve the sustainable synthesis of several small organic molecules with high functional density on a large scale. As briefly mentioned in Section 1.2, small molecules play a crucial role in drug development. Among the compounds selected are secondary metabolites, which have significant applications in human health and disease management, including roles as dietary antioxidants and as ingredients in cosmetics and dermatological products.[81-84] However,

selective synthesis of the chosen compounds remains a challenge in the literature, with many examples overlooked, a gap also reflected in recent group research project.

Part I

Sustainable valorisation of recycled carbohydrate sources

Chapter 2

Introduction

Green Chemistry considerations are an idealised concept which can be applied to resolve environmental hazards, health issues and increase safety.[85,50] A number of established APIs synthesis has been redesigned to meet Green Chemistry principles, considering cost effectiveness, percentage of yield and amount of waste produced.[86-107,108, 109] One key consideration when considering the Green credentials of a synthesis is the origin of the starting materials.

Biomass is one of the most easily accessible and renewable material sources , derived mainly from plants but also from animals.[110] The annual production of plant based biomass is estimated as 170 billion metric tons per year delivered primarily through photosynthesis.[110] Some derived biomasses are recognized as potential stock building blocks for existing chemicals or potential new industrial demand feedstock chemicals.[111] Interestingly, around three fourths of the total biomass production can be assigned to carbohydrates where these are recognized as promising green chemistry feedstocks for future chemical generation.

In this vain, valorization of biomass into more value-added chemicals is an attractive starting point for synthetic design based on the general principle of Green Chemistry to produce pharmaceuticals.[50] This is termed as "biorefinery" – "a sustainable approach to biotransform raw materials (Figure 19) e.g. biomass into energy and a wider spectrum of everyday commodities in an economical and eco-friendly manner".[112]

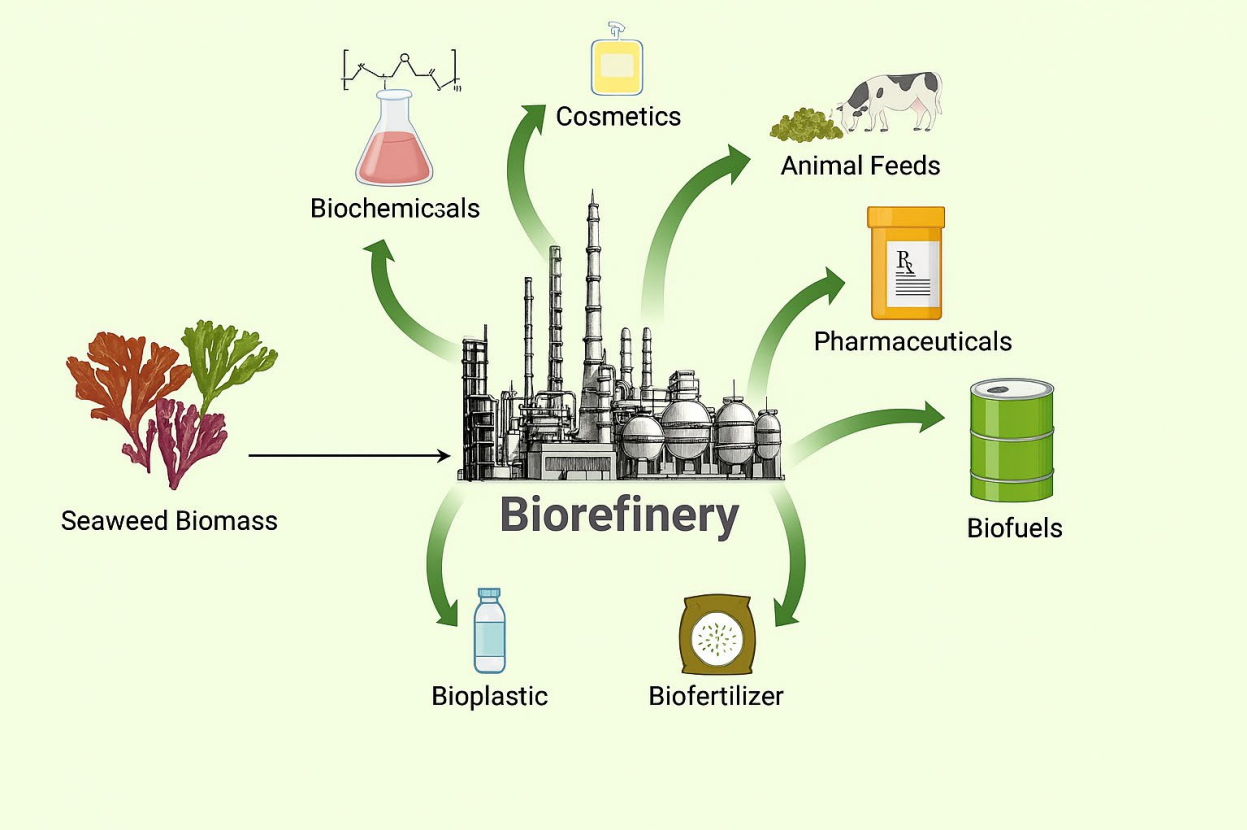

Figure 19. The holistic biorefinery concept. (The template is provide by BioRender.[113])

Most of the current research in this area documents the derivatization of monomers already obtained from primary processing of raw biomass materials , however this is a fast developing area and more integrated processes are the obvious way forward.[114, 115] To obtain pure target sugar monomers, components are often extracted and processed from raw materials requiring high energy input. Some examples are starch from corn grain,[112] simple sugar from sugar cane and beets [116], cellulose, and hemicellulose from lignocellulose biomass[117]. Although sugar monomers can be afforded from starch (a polysaccharide with 1,4'-α-glycosidic linkage) by acids or enzyme attack, there is a large demand for such substances by the food market.[27] Alternative supply chains can be considered through lignocellulose which is accessed from wood, bamboo, and agricultural residues.[114] Access to cellulose which contains sugar monomers in lignocellulose is often restricted by complex higher-order structures in plants. Strong intermolecular interactions in cellulose result in a natural resistance to enzymatic deconstruction. More energy sustainable pretreatment to

overcome these barriers are still being developed.[114, 115, 117] Lactose (**1**), however, is another type of biomass that can be obtained from dairy products, it accounts for 70% of the solid components of industrial wastewater cheese whey (CW) (Figure 20).[118]

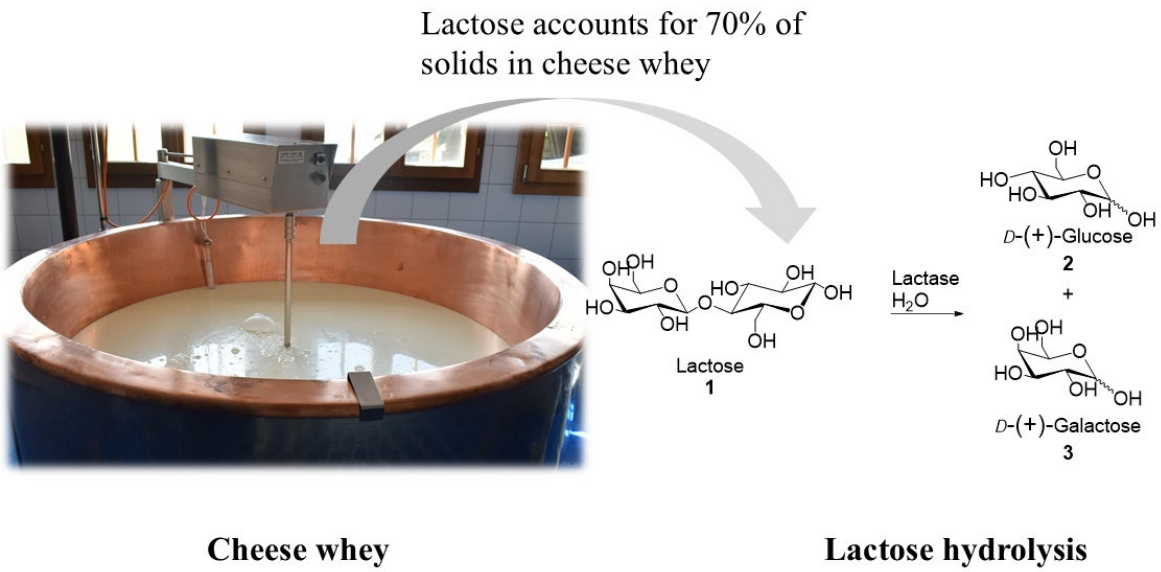

Figure 20. Cheese whey, lactose, and lactose hydrolysis.

Annually, around 201 million metric tons of cheese whey was produced in 2023 (estimated by a 9 fold multiplication of the annual cheese production), equivalent to roughly 19,900 Eiffel Towers.[119,120] Although lactose has found a few applications in food, cosmetics, and pharmaceuticals, the vast majority of generated lactose is a waste product and contributes to high Biochemical Oxygen Demand (BOD) and Chemical Oxygen Demand (COD) of cheese whey waste streams in the enviroment.[118, 120] The sequential effects of reduced oxygen concentration poses sever risks to the environment, aquatic life, and human health.[118] Potentially, more cheese whey could be recycled however this is a logistical issue as many small to medium sized dairies lack the infrastructure and investment to enable this efficently.[118]

Researchers have explored various strategies to upgrade lactose into value-added compounds (Table 7). A common approach involves enzymatic or acidic hydrolysis of lactose into galactose and glucose, which serve as sweeteners or precursors for further synthesis (Entry 1). Additionally, lactose can undergo fermentation or oxidation, yielding biofuels and biomaterials for diverse

applications (Entries 2 and 3). Reduction of lactose produces lactitol, a widely used low-calorie sweetener (Entry 4).[121] Esterification of lactose and its monosaccharides, catalyzed by Amberlyst™ 15, leads to biodegradable surfactants with potential industrial applications (Entry 5). While these transformations generate readily usable products, they often result in a loss of inherent molecular functionality. Advancing green synthesis methods could enable the production of more complex structures with higher-added value. Herein, our research in this area aims to develop monosaccharide and disaccharide transformations towards efficient conversion of cheese whey waste into heterocyclic fragments. These fragments can be subsequently used to synthesize compounds such as anti-cancer agents,[122] and are useful building blocks for the total synthesize of natural products.

Table 7. Reactions of making value added compounds from Lactose.

Entry	Reaction Type	Enzyme/Catalyst	Products	Example of Uses
1	Hydrolysis[123]	Lactase (*β*-galactosidase), Acid (HCl, H_2SO_4)	*D*-(+)-Glucose (**2**), *D*-(+)-Galactose (**3**)	Sweetener (Glucose syrup, Glucose-galactose syrup)[124]
2	Fermentation[125]	Engineered Saccharomyces cer -evisiae yeast	Lactic Acid, Ethanol	Lactic acid for biodegradable plastics[126]; Ethanol in biofuels[127]
3	Oxidation[128]	Cellobiose dehydrogenase	Lactobionic Acid	Galactonic acid in biomaterials[129]
4	Reduction[121]	Silica supported Cu	Lactitol	Used as a low-calorie sweetener[121]
5	Esterification[130]	Amberlyst™ 15	Lactose-Based Esters	Used in biodegradable surfactants[130]

2.1 Review of sugar based Knoevenagel reaction

2.1.0 Introduction

The origin of the target synthesis dates from the 1950s, where chemists developed a synthetic scheme for converting glucose to polyhydroxyalkyl and C-glycosyl furan derivatives (Scheme 4). The furan class of heterocycles are interesting as they are bioactive and display prominent pharmacological activities, such as antifungal, anti-trypanosomal, gastrointestinal motility activity and farnesyl and can be bioisosteres for other aromatic compounds (classically furan is a medicinal chemistry replacement for benzene) (Figure 21).[131] As such furan and furan derivatives are valuable chemical entities and therefore routes that can rapidly assemble novel functionalised furan structure are of general interest to pharmaceutical manufactures and more widely the chemical industry. An excellent example of this is the general chemistries that have arisen around the biomass derived synthesis of 5-hydroxymethylfurfural (HMF) (Figure 22).[132] It is therefore of interest to consider other chemical approaches to furan derivatives that may themselves find value as commodity or specialist chemicals. The compounds in Scheme 4 have potential uses as novel therapeutics including anti-cancer and as components of fluorescent probes.[133,134]

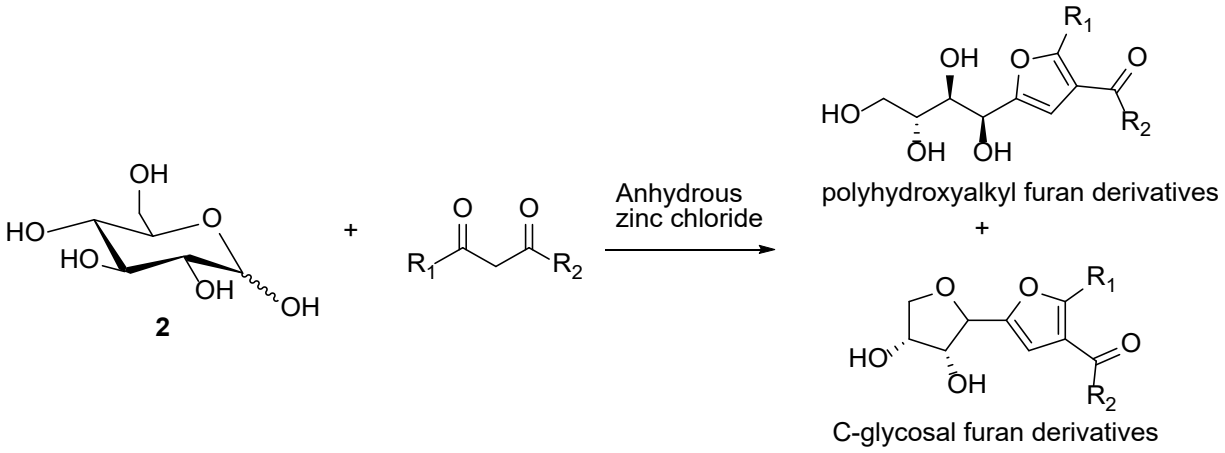

Scheme 4. Synthesis of polyhydroxyalkyl- and C-glycosal-furan derivatives from glucose.[134]

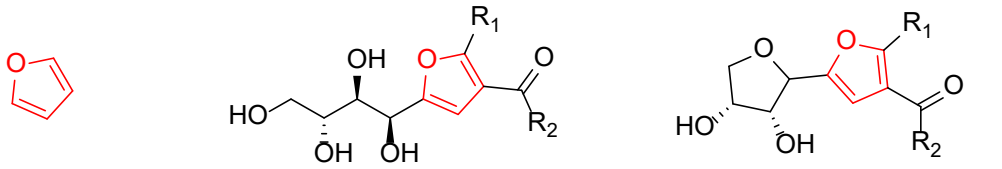

Figure 21. Structures of furan, polyhydrocyalkyl furan derivatives and C-glycosal furan derivatives.

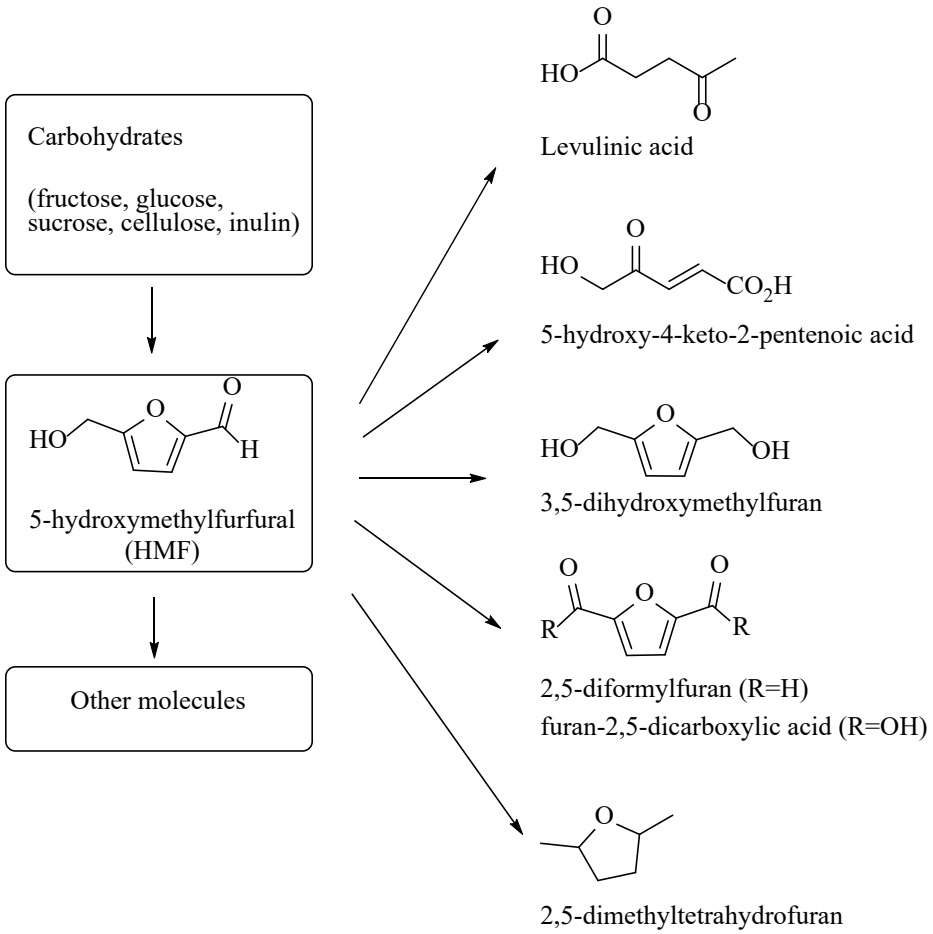

Figure 22. The general compounds formed from 5-hydroxymethylfurfural (HMF) as suggested by Rosatella *et al*. 2011.[132]

Although having been first developed in the 1950's this transformation then became essentially forgotten for over 30 years.[133] The reaction was next explored in the 1980s and described as progressing through a Knoevenagel condensation.[135] In general, the reaction is a modified Aldol condensation with C-C bond formation occurring with the ring opened aldehyde form of the sugar (Scheme 4). Besides the sustainable starting materials (hexoses) and green solvent (water) used, the other reagent 2,4-pentanedione (**5**) has also been synthesized by researchers to allow for potentially fully renewable production. Although commercially, 2,4-pentanedione (**5**) is available at a low cost £101/2.5 L derived from fossil sources.[136] In 2004, Zha *et al*. reported the biosynthesis of triacetic acid lactone (**4**) can be obtained from *D*-(+)-glucose (**2**) by *Brevibacterium ammoniagenes* fatty acid synthase B (FAS-B).[137] The triacetic acid lactone (**4**) undergoes ring-opening and decarboxylation in water to afford 2,4-pentanedione (**5**) (Scheme 5).[138]

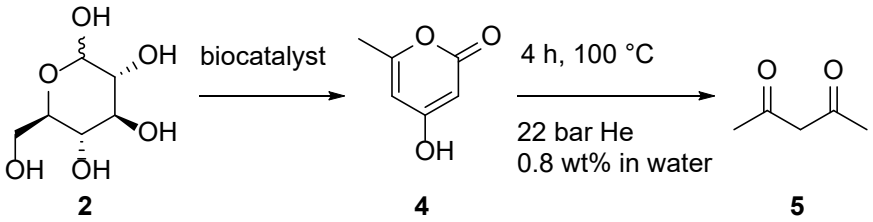

Scheme 5. The scheme of 2,4-pentanedione (**5**) synthesis from *D*-(+)-glucose (**2**).[138]

The reaction mechanism of linear sugar and *β*-dicarbonyl under basic condition is shown (Scheme 6) and the need for the linear sugar (open chain form, step 1) has been shown to be key to the successful use of other carbohydrate starting materials in the same general transformation.

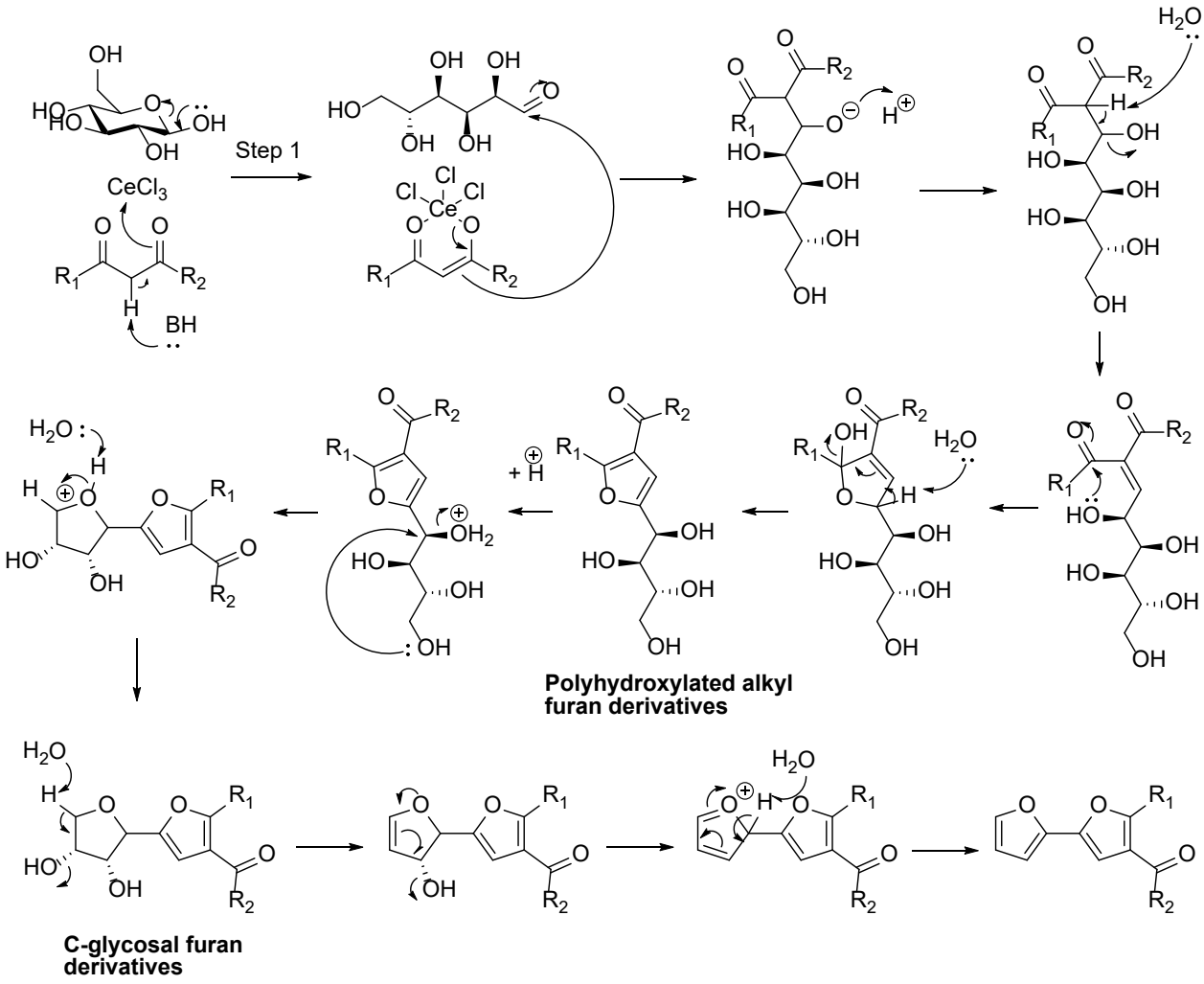

Scheme 6. Reaction mechanism of Lewis acid catalysed Knoevenagel condensation from a sugar and *α*,*β*-dicarbonyl.

This corresponding Lewis acid catalysed reaction became known as the Garcia Gonzales reaction and has over the years been revisited by several other chemists, exploring many parameters such as solvent, choice of Lewis catalyst, reaction time, temperature, and obtaining various yield improvements as well as obtaining polyhydroxy alkyl furan derivatives and C-glycosal furan derivatives respectively. The scope of the synthesis has also been developed incorporating other monosaccharides, disaccharides, oligosaccharides (starch), and substituted hexoses.[134, 139-148] Table 8 showed a summary of reaction conditions used to synthesise these C-glycosal furan derivatives.

Table 8. Summary of key literature synthesis of Garcia Gonzales reaction and the yields of C-glycosal furan derivatives.

Entry	Equivalents of Catalyst	Catalyst	Solvents	Temp.	Time	Yield/%	Ref.
1	0.6	anhydrous $ZnCl_2$	MeOH	Boiling water bath	30 min	31	[134, 140]
	0.1	aqueous acetic acid					
2	0.1	$Yb(OTf)_3$	H_2O	60 °C	20 h	39	[139]
3	0.25	$CeCl_3 \cdot 7H_2O$	H_2O	90 °C	6 - 10 h	75 - 93	[144]
4	0.10	$InCl_3$	H_2O	80 °C	3 - 7 h	76 - 93	[146]
5	0.02 – 0.078	$(FeOTf)_3$	H_2O	Reflux	1– 3 days	47 - 85	[145]
6	0.1	$ZrCl_4$	H_2O/D_2O	50 °C	4 - 16 h	38 - 88	[141]
7	0.1	$FeCl_3$	$EtOH/H_2O$	90 °C	3 - 7 h	76 - 93	[147]

A previous 4th year MChem research student within the Baxendale group[149] had conducted a literature review and identified the optimized batch process as outlined in Scheme 7 through screening of catalyst and reaction conditions, adapted from Entry 3 Table 8.

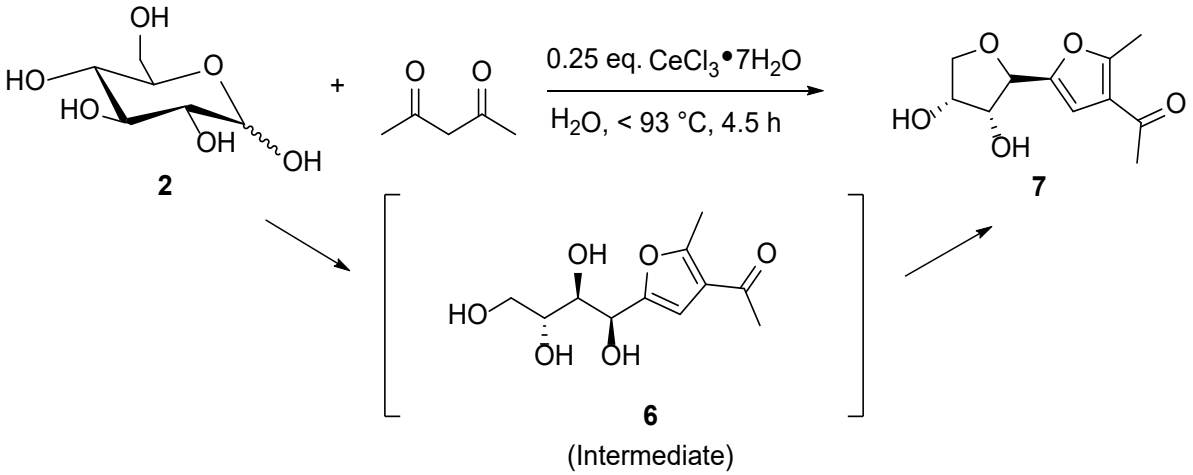

Scheme 7. The reaction scheme to produce 1-(5-(3,4-dihydroxytetrahydrofuran-2-yl)-2-methylfuran-3-yl)ethenone (**7**) previously optimized in the Baxendale group.[149]

To establish a foundation for the flow synthesis, the batch reaction conditions, and solvent extraction efficiency were first optimized (Sections 2.1.1 and 2.1.2, respectively). These optimized parameters were then adapted for flow, as discussed in Section 2.2.

2.1.1 Reproduction and testing of the previously identified batch conditions

The previously identified reaction conditions applying $CeCl_3 \cdot 7H_2O$ catalyst (Scheme 4, Table 9 Entry 7) were further investigated (Table 9) with various equivalents of reagents and concentration of the solution. Lower equivalents of diketone and reaction concentration resulted in decreased yields (Entries 1–6, Table 9). In contrast, increasing the relative concentration of *D*-(+)-glucose significantly improved the mass yield from 50% to 95% (Entries 3, 7, and 8, Table 9). Thus Entry 8 was selected for later flow-based processing tests.

Table 9. Parameter analysis of batch process in Scheme 7.

Entry	Scale/ mmol	Diketone equivalent	Catalyst equivalent	Temp/ °C	Time/ h	Water/ mL	NMR yield/ %
1	50	1	0.25	90	4.5	100	24
2	50	1	1	90	4.5	100	42
3	50	1.5	0.25	90	4.5	100	50
4	50	1	0.25	90	4.5	50	63
5	50	1	0.25	90	4.5	25	72
6	50	1	0.25	90	4.5	12.5	82
7	50	1.5	0.25	90	4.5	50	84
8	50	1.5	0.25	90	4.5	25	95
9	75	2/3[a]	0.17	90	4.5	100	23

[a]50 mmol

The key challenge remained demonstrating the reaction's scalability and establishing an effective catalyst recycling mechanism to ensure better commercial viability. The Knoevenagel reaction provides a strong foundation for a one-pot, coherent process that can be optimized using flow techniques to enhance throughput and catalyst recycling. In this project, a consolidated approach that utilizes sustainable and readily available materials to synthesize C-glycosyl furan derivatives via scalable flow technologies for intended industrial applications is presented.

2.1.2 Extraction Solvent test

Although the solvent, water, for the system is inherently green, the product needs to be extracted from the aqueous media in order to facilitate its purification and isolation. In the process, all starting materials and the catalyst are highly water soluble. Therefore, it was anticipated that if the product could be efficiently extracted, the aqueous phase could be readily recycled in subsequent

runs. To maximise the recovery of target compound in the extracted organic phase, the extraction solvent was reviewed. The selected solvents were ethyl acetate, trifluorotoluene, hexane, 4-methyltetrahydropyran, chloroform, diethyl ether, and toluene. These were selected to cover a range of polarities and also with an industrial consideration on availability and their green characteristics. The reaction was performed for 4.5 h using the conditions in Scheme 7. For every 50 mmol scale of products, 4 × 100 mL of extraction solvent was used. The presented calculated yields of target compound **7** was determined by calculation of target compounds in crude reaction mixture by NMR integrals as shown in Table 10 with the selected proton signals used for NMR integration. The solvents EtOAc and $CHCl_3$ gave the highest quantities of extracted products (Table 10, Entry 1 and 4).

Table 10. NMR integrals and the percentage of target compound **2** of the derived mass in Table 5. Protons of **6**, **7**, **5**, and **5a** were identified with corresponding NMR of the isolated material. The compound **7a** is a proposed side product in NMR of compound **7**.

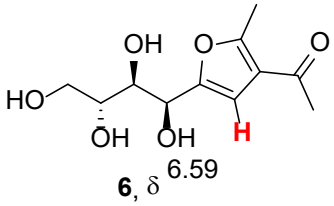

6, δ 6.59

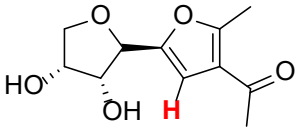

7, δ 6.79

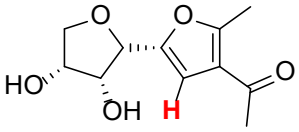

7a, δ 6.69

(predicted structure)

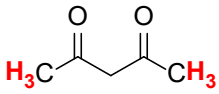

5, δ 2.14

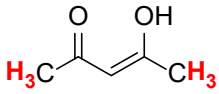

5a, δ 2.03

Entry	Solvents	δ 6.79 (**7**)	δ 6.69 (**7a**)	δ 6.59 (**6**)	δ 2.14 (**5,** proton*6)	δ 2.03 (**5a,** proton*6)	Mass of crude mixture/ g	Estimated mass of **7**/ g
1	EtOAc	1.00	0.16	0.31	2.14	3.02	14.6	6.27*
2	MTHP	1.00	0.16	0.16	0.33	0.44	6.4	4.42
3	Et_2O	1.00	0.16	0.04	5.04	7.51	4.8	1.46
4	$CHCl_3$	1.00	0.17	0.0	4.08	5.97	23	8.08
5	Toluene	1.00	0.11	0.0	0.49	0.53	0.8	0.63
6	Hexane	1.00	1.39	0.0	947.85	1372.02	0.5	0.00
7	$PhCF_3$	1.00	0.13	0.0	7.29	3.20	0.4	0.14

Exemplary calculation: 14.6(1/1+0.16+0.31+2.14/6+2.03/6) = 6.27 g

Although $CHCl_3$ was a more effective extraction solvent for **7** this solvent falls into the non—ideal solvent category suggested by ranking of major organic solvents in the form of hazardous impact, and was classified as highly hazardous.[50, 150] The selection of organic solvents has become

increasingly important as large quantities are often required but does not contribute to building the molecular structure directly. Researchers nowadays require more analysis of topics such as environmental impact, regulation (waste, toxicity), worker health and safety, sustainability and life cycle while selecting the reaction solvent.[2] In particular, the purity of pharmarceutical products leads to more waste per kilogram of product than other industrial products. Four classes of solvents were defined by the Centre for Drug Evaluation and Research (CDER) of the USA Food and Drug Administration (FDA) and Centre for Biologics Evaluation and Research (CBER)[151]:

Recommended

Problematic

Hazardous

Highly Hazardous.

While $CHCl_3$ is highly hazardous, EtOAc is recommended. Hence, for this reaction, EtOAc was used as the ideal extraction solvent for green synthesis.

2.2 Results and Discussion

2.2.1 Introduction of project Aims

The aim of this project was to explore the valorization of readily accessible carbohydrates, including lactose (**1**), *D*-(+)-glucose (**2**) and *D*-(+)-galactose (**3**) in a continuous-flow system. In principle, these carbohydrates are widely available from industrial whey waste from cheese manufacturing and require proper valorization to reduce potential pollution. This chapter introduced the assessment of **1**, **2** and **3** from the lactose hydrolysis reaction through literature review and experimental studies (Scheme 8) [152] and how these carbohydrates were transformed into C-glycosyl furan derivatives in flow (Scheme 9).

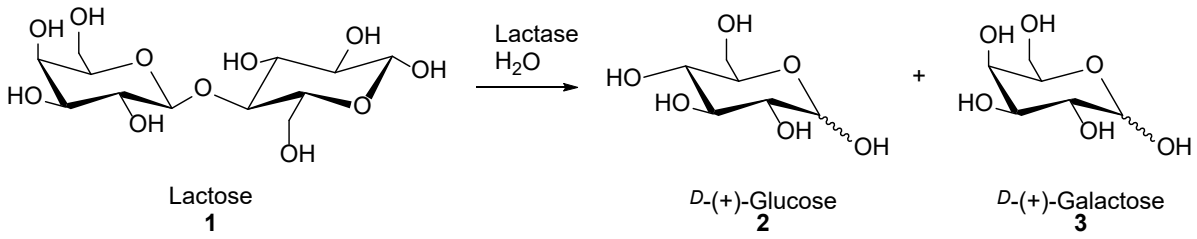

Scheme 8. Lactose enzymatic hydrolysis reaction.

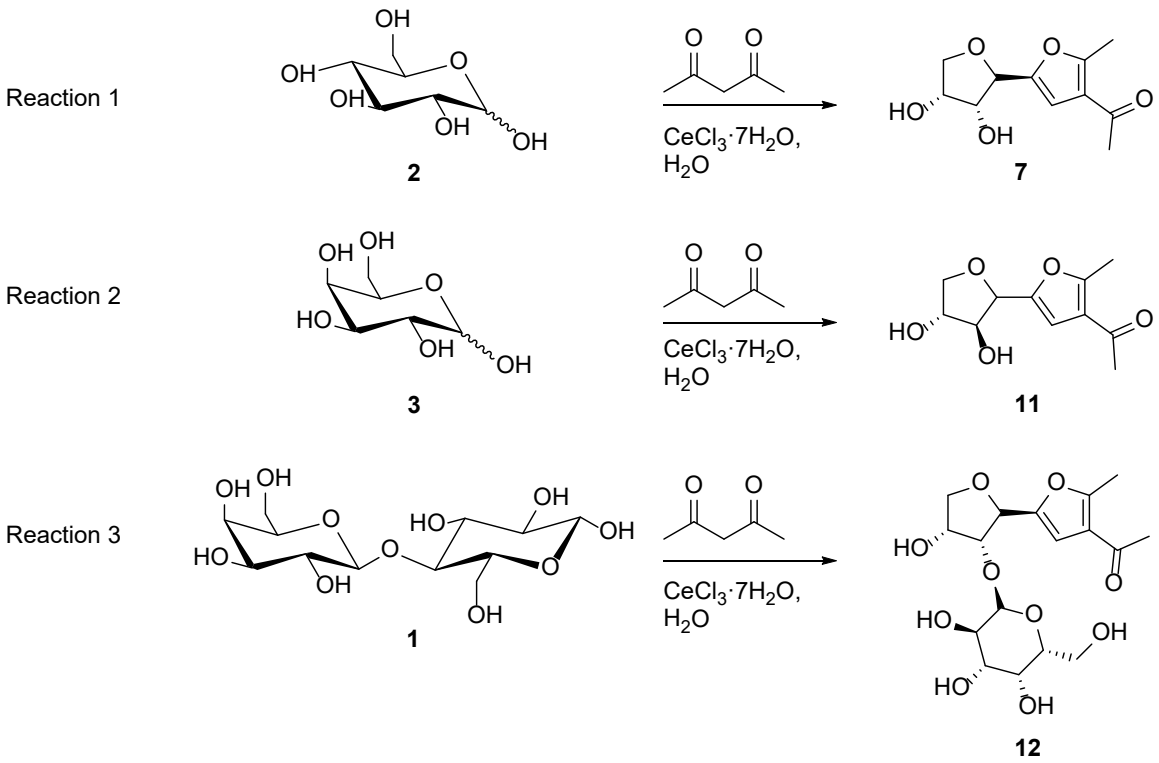

Scheme 9. The conversion of Sugar compounds **2**, **3** and **1** to furans **7**, **11**, **12** via Lewis acid Knoevenagel reaction.

In summary, the subsequent sections of this chapter are structured according to the following objectives:

Project aims:

(1) Assess the feasibility of lactose hydrolysis through experimental studies and literature review.

(2) Investigate the Lewis acid-catalyzed Knoevenagel reaction using *D*-glucose as a model system by:

- Re-evaluating reaction parameters and optimizing flow conditions.
- Testing yields in both small- and large-scale reactions to assess industrial applicability.
- Evaluating the sustainability and reusability of the catalyst.

(3) Extend the optimized flow conditions from Aim 2 to *D*-galactose and lactose

2.2.2 Lactose derivation and lactose hydrolysis (Aim 1)

As introduced above, scientists have been searching for protocols to produce higher added value products from carbohydrates due to their ready abundance of natural sources. In this respect lactose is one of the most easily accessible by-products from the major solid components of cheese whey (CW). In the literature, researchers have shown that the suspended solids and solutes of molecular weight higher than 8000 Da in CW are removed by ultrafiltration allowing isolation of lactose.[120, 153] Two monosaccharides, *D*-glucose and *D*-galactose are known to be synthesized via lactose hydrolysis. For this transformation, the selection of the catalysts is the key to the success of this reaction. Both acids and lactase enzyme can be used to catalyze this reaction, although the enzyme methodology is normally preferred due to its mild reaction conditions.[154]

According to *Project Aim 1* lactose hydrolysis reactions were tested to achieve the desired monosaccharides **2** and **3** through the preparation of heterogeneous beads made from lactase enzyme, sodium alginate, and $CaCl_2$ solution.[155, 156] The easily accessible lactase enzyme (for dietary supplements) is provided as pills or drops, but contain additional components such as glycerol, sodium acetate, etc.[157, 158] The enzymes prepared at research grade are very expensive, for instance, Native Kluyveromyces lactis β-Galactosidase: ≥2600 units/g, were sold as $328/50ml, $785/250ml.[159] To improve the sustainability of this catalyst for large scale synthesis, several heterogeneous lactase enzyme systems have been developed with many different immobilising phases, for example, porous silica carrier,[160] polymer nanofibers,[161] and sodium alginate beads[155, 162, 163] for use in packed bed reactors.[161, 163, 164] Sodium alginate beads can be easily generated under mild conditions, making this method a suitable choice for later experimentation. Alginate is a naturally occurring anionic polymer typically isolated from brown seaweed.[165, 155] Sodium alginate is the sodium salt of alginic acid, an acid copolymer of two uronic acid: *β*-*D*-mannuronic acids (**1a**) and *α*-*L*-glucuronic (**1b**) (Figure 23), linearly linked to each other by 1–4 glycosidic bonds. [166-171] The structure of sodium alginates with corresponding sources, combining different ratios of **1a** and **1b** and the lengths of the chain varies.[172, 173] The alginate beads (Figure 24) were prepared by dropwise addition of a solution of lactase enzyme and sodium alginate into a solution of calcium chloride. A preliminary assessment of the immobilized lactase showed that lactose was successfully cleaved to yield increasing quantities of glucose as demonstrated by glucose test strips

(Figure 25). However, the product mixture could not be separated by our Interchim Puriflash systems to obtain proper data analysis.

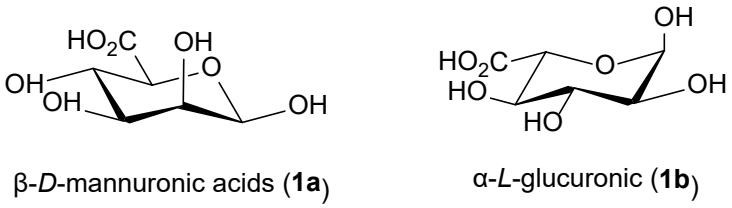

Figure 23. Structure of sodium alginate.[155]

Figure 24. Filtered sodium alginate beads in Buchner funnel.

Figure 25. Glucose test strips at various times. Top to bottom: a to f, A. Lactose; B. just dissolved, C. >10 min D. >20 min, E. > 50 min, F. >90 min.

Returning to the literature, Majore and Ciprovica had analysed enzymatic lactose hydrolysis of both sweet whey and acid whey (Sweet whey is produced when rennet is used to coagulate cheese. Acid whey, also known as sour whey, is produced when acid (like lactic acid bacteria) is used to curdle cheese.). They achieved 78-97% lactose hydrolysis and the percentage of glucose, galactose, and lactose is shown in Table 11 with different tested enzymes.[174] Three types of *β*-galactosidases were selected: **Ha-Lactase 5200** produced by *Kluyveromyces lactis*, the activity is expressed in Neutral Lactase Units (NLU): 5200 NLU·g^{-1}; **NOLA Fit5500** produced by *Bacillus LicheniformisI,* the activity is expressed in Bifido Lactase Units (BLU): 5500 BLU·g^{-1} (Chr.HANSEN, Denmark); **GODO-YNL2** produced by Kluyveromyces lactis, activity 5000 NLU·g^{-1}.[174,175] The reaction conditions were based upon 20% of the initial whey solids concentration, 0.05% of the chosen *β*-galactosidases, which were incubated at 42.5 °C for 4 h. The carbohydrates (glucose, galactose, fructose, and lactose) were analyzed by high-performance liquid chromatographic analysis (Shimadzu LC-20).

Table 11. Percentage of Glucose, galactose, lactose after lactose hydrolysis.[174]

Sweet whey permeate (pH 6.2 ± 0.1)			
Enzyme	Glucose/%	Galactose/%	Lactose/%
NOLA fit5500	43.9 ± 1.4	16.4 ± 0.9	22.1 ± 0.5
Ha-Lactase 5200	51.0 ± 3.4	20.9 ± 1.1	2.1 ± 0.6
GODO-YNL2	36 ± 0.3	15.2 ± 0.1	13.9 ± 0.6
Acid whey permeate (pH 4.5 ± 0.1)			
Enzyme	Glucose/%	Galactose/%	Lactose/%
N5500	43.5 ± 1.6	25.3 ± 1.7	19.8 ± 0.5
H5200	50.6 ± 2.1	22.4 ± 1.4	5.9 ± 0.3
GODO-YNL2	32.5 ± 1.7	17.2 ± 1.6	20.2 ± 1.0

The successful conversion of lactose into glucose, as demonstrated by the test strip analysis, confirms the carbohydrate source. A comprehensive analysis of all components in cheese whey would require an additional PhD-level investigation, as indicated by the literature, and thus falls beyond the scope of this project. Therefore, established publications were relied upon for relevant data. Based on the results of lactose hydrolysis and literature evidence identifying glucose, galactose, and residual lactose as hydrolysis products, *Project Aim 1* was met. Further insights into the lactose hydrolysis method can be found in existing literature, such as studies on the inhibitory effects of galactose and fructose on whey lactose hydrolysis[176] and a general predictive mathematical model for a packed-bed enzyme reactor in lactose hydrolysis.[177] For more comprehensive investigation, additional literature reviews are provided for reference.[123, 178]

2.2.3 *D*-(+)-glucose conversion in flow (Aim 2)

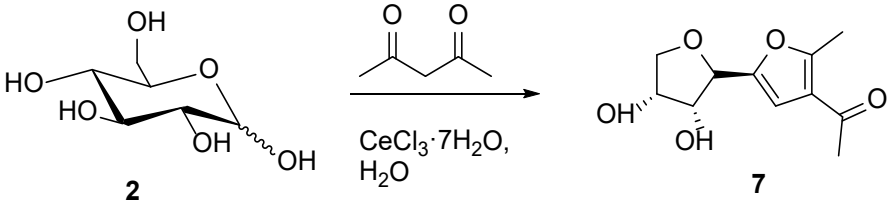

Scheme 10. Conversion of *D*-(+)-glucose **2** into furan **7**.

As mentioned in section 1.5, flow synthesis is often the preferred approach for bulk chemical production in industry.[65] At laboratory scales, flow reactions are processed under rigorously controlled conditions in a confined space through multi-purpose micro or meso flow systems in

contrast to conventional round bottom flasks.[66] As such, homogeneous solutions are pumped through reactors tubular or catalyst packed columns, and activated through applied temperature, sonication or photo activation. To increase productivity, the test reactions (Scheme 7) were explored at raised temperatures.

It should be noted that some parameters when using flow systems differ from those in batch reactions and require reassessment during translation. Hence, before delving into the synthesis, these concepts will be outlined first in the context of our reaction.

2.2.3.1 Concepts of flow parameters

Two parameters often used in flow are flow rates of the reagents streams (Q), and space-time-yield (STY). The flow rate is expressed by Equation 8, where Q_T is the total flow rate in mL min^{-1}, v is volume of the reactor system in mL and t is the residence time in minutes (or seconds). These are often indicated in the flow diagram as shown coloured red.

$$Q = \frac{V}{t}$$

Equation 8. Flow rate (Q_T) is equal to volume (V) divided by residence time (t).[179]

The space-time-yield refers to the amount of product achieved for given volume and residence time. This is expressed by Equation 9, where m_p is the mass of product, V is the volume of the flow reactor and t is the residence time. This is often expressed in kilogram per liter per hour (due to its origin in heterogenous catalysis engineering), but for laboratory operation this is more typically given as g/mL/min due to the differences in processing scales.

$$STY = \frac{m_p}{V \times t}$$

Equation 9. Space time yield (STY) is given by mass of product(s) divided by the product of volume (V) and residence time (t).

2.2.3.2 Optimisation of residence time and space-time-yield

It is often quoted that economics is everything, hence why process intensification is an important aspect of optimization in chemical manufacturing. Thus, the aim was to improve the space-time yield (STY) compared to the batch reaction (Scheme 11) and test the scalability of this reaction for potential industrial application in section 2.2.4. Assuming constant reactor volume and product mass, STY increases with reduced reaction time (Equation 9). The precise and efficient temperature control of flow reactors can facilitate this improvement through elevated reaction temperatures impacting reaction kinetics. For the target reaction, the batch solution is warmed up over 20 minutes using conventional conductive methods. In flow the reaction solution is rapidly heated to the required temperature within seconds of entering the reactors in a confined space. This can equate to increased yield or a reduction in the necessary residence time (compared to the reaction time in batch).

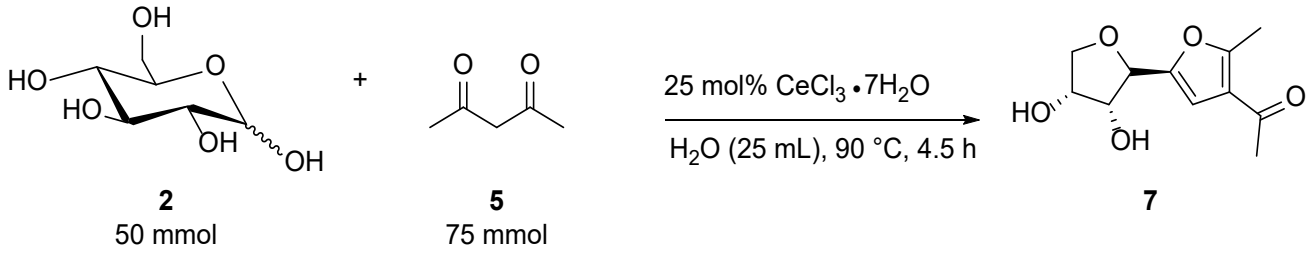

Scheme 11. Optimised conditions developed using batch methods in sections 2.1.1 (Table 9 Entry 8). NB: for this batch reaction, 250 mL round bottom flask is required since 50 mmol of D-(+)-glucose require space.

To determine the ideal residence time, the consumption of *D*-(+)-glucose (**2**) was monitored through its batch reactions. Given one mole of product is obtained by one mole of starting material (Scheme 12), **7** is synthesized via intermediate **6** from **2**, the consumption of starting material can be monitored by measuring the sum amount of product and intermediate.

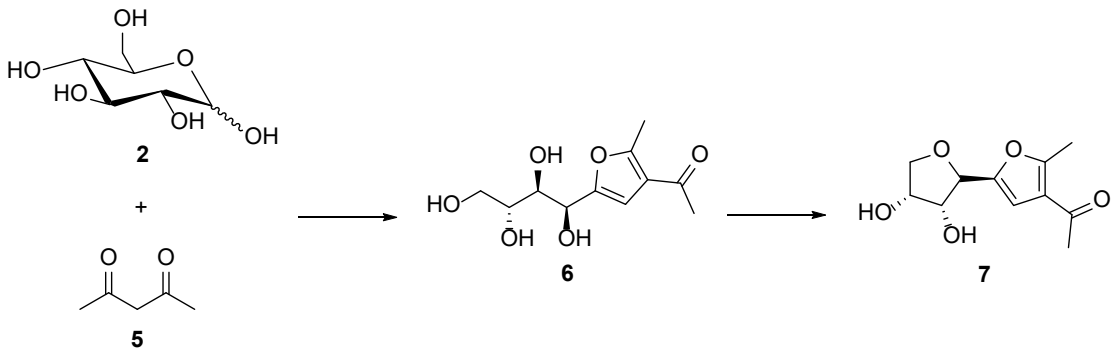

Scheme 12. The process of making **7** from **2** and **5**.

The integral of the proton peak in NMR can be used to estimate the amount of the corresponding compound with an internal standard when the mass of internal standard is known (Equation 10).

$$n_p = \frac{\frac{I_p}{N_p}}{\frac{I_{is}}{N_{is}}} \times n_{is}$$

p (product)

is (internal standard)

n (number of moles)

I (integral)

N (Number of protons)

Equation 10. The equation used to estimate the amount of product produced based on integral analysis of a product proton peak versus an internal standard proton peak. -

If the proton shift of the product or intermediate represents a single proton, the proton shift of the internal standard represents two protons and the integral of the internal standard is set at 2, i.e.

$$N_p = 1$$

$$\frac{I_{is}}{N_{is}} = \frac{2}{2} = 1$$

then substitute these two values into Equation 10 to get Equation 11:

$$n_p = \frac{\frac{I_p}{1}}{1} \times n_{is} = I_p \times n_{is}$$

Equation 11. Simplified equation with given values of $N_p = 1$, $I_{is} = 2$, $N_{is} = 2$.

If n_{is} is a constant value, then the change of n_p is proportional to the change of I_p, in this scenario I_p is the sum integral of proton peaks chosen from **6** and **7**. Hence, as long as I_p is a positive constant, the trend (of increasing or decreasing) of the plot will not be affected whether this is 1 or 1.3333, or another positive constant. As a result, the plot of estimated consumption of starting material can be produced as the sum of integrals against reaction time. The cyclised compound **7** was represented by the proton peak at 6.74 ppm (furan C-H), the acyclic compound **6** was represented by a peak at 6.60 ppm corresponding to the furan C-H signal (Figure 26). Besides, another peak at 6.67 ppm was identified in previous research and the structure (Figure 26, **7a**) was predicted as the stereoisomer of **2**. Hence the sum integral of **6**, **7a**, **7** (Figure 26) were used to monitor the consumption of starting materials, i.e. the progression of the reaction. A water-soluble internal standard, 3-(trimethylsilyl)-1-propanesulfonic acid sodium salt (**8**) was used to avoid overlapping proton shifts of other compounds. The structure of the compound and the NMR peaks were shown in Figure 27.

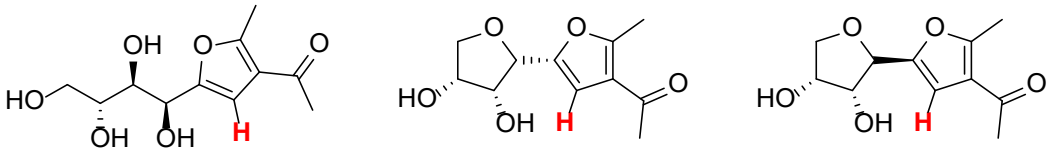

6 **7a** **7**

(predicted structure)

Figure 26. NMR reference peaks of **6**, **7a**, **7** synthesis from *D*-(+)-glucose (**2**).

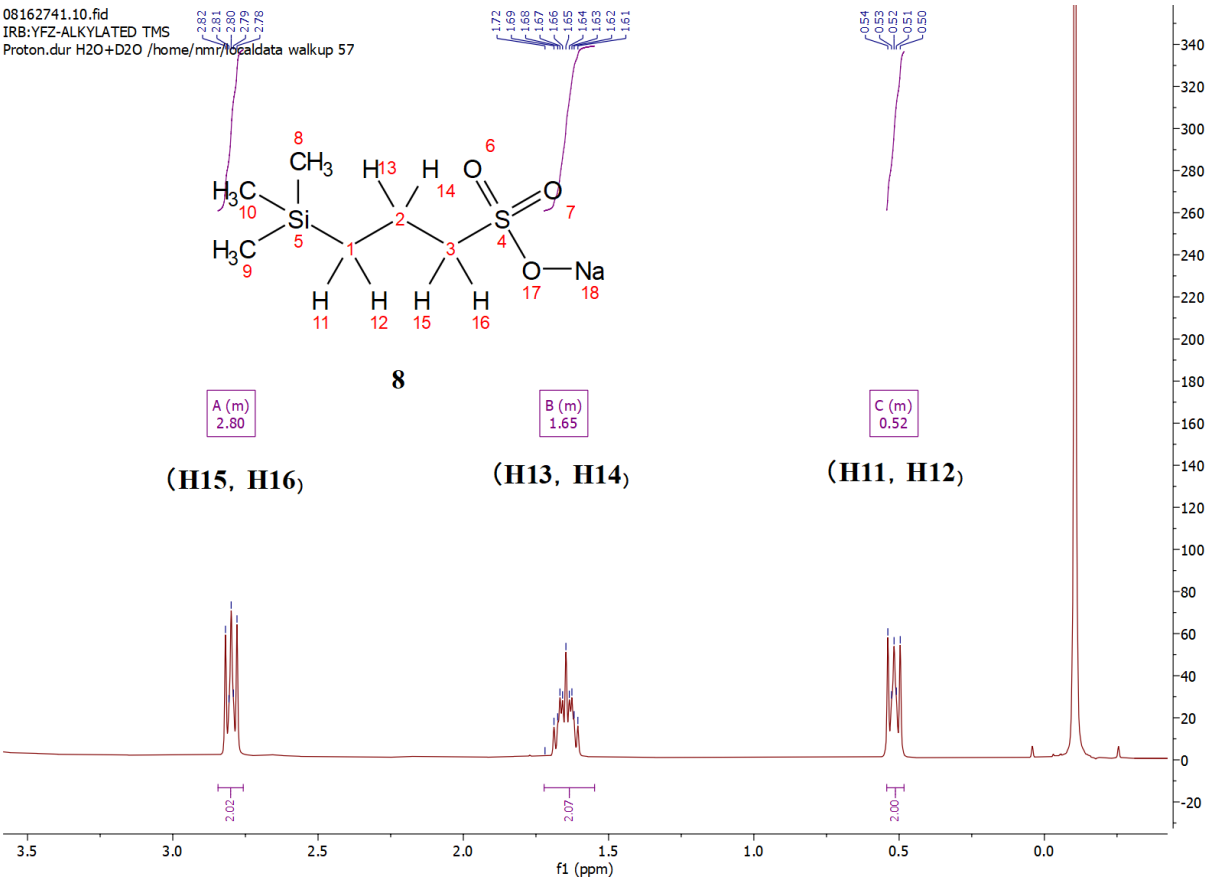

Figure 27. The structure of the water-soluble internal standard, 3-(trimethylsilyl)-1-propanesulfonic acid sodium salt (**8**) and its corresponding ^{1}H NMR spectrum.

Figure 28 presents an example of the NMR spectrum used for quantification. One of the three internal standard protons was selected as the reference and assigned an integral value of 2 (hence, I_{is} = 2). The integrals of the target protons corresponding to compounds **6**, **7a**, and **7** were then assigned manually as I_p (= 0.11, 0.05, 0.55 respectively). Other peaks are ignored since it is difficult to discriminate against all the other proton peaks. Since the number of moles of internal standard ($n_{is} = \frac{mass\ (internal\ standard)}{molecular\ weight\ (internal\ standard)}$) can be derived with recorded mass. The number of moles of **6**, **7a** and **7** in the mixture are then derived by substituting I_p and n_{is} values in Equation 11. Although this estimation method involves inaccuracies, such as measurement uncertainty in balance-determined weight that may propagate through subsequent calculations (Section 2.5 Appendix, Internal standard calculations), it remains a valid and efficient approach for monitoring the reaction and approximating an optimized reaction time. The CH_2 peak of 3-(trimethylsilyl)-1-propanesulfonic acid sodium salt (**8**) appears at ~0.49 ppm and was assigned

with a constant integral value (=2) while the aromatic peaks of the target compounds were monitored (Figure 28). To allow a time course for the reaction a sample of the reaction was taken every 30 minutes from 0.5 h to 4.5 h with a consistent volume. The cyclisation of intermediate **6** was tracked by integral change of the proton peak at 6.60 ppm (Figure 29). The estimated consumption of starting material was calculated by sum of integrals at 6.60 pm, 6.67 ppm, and 6.74 ppm in Figure 30.

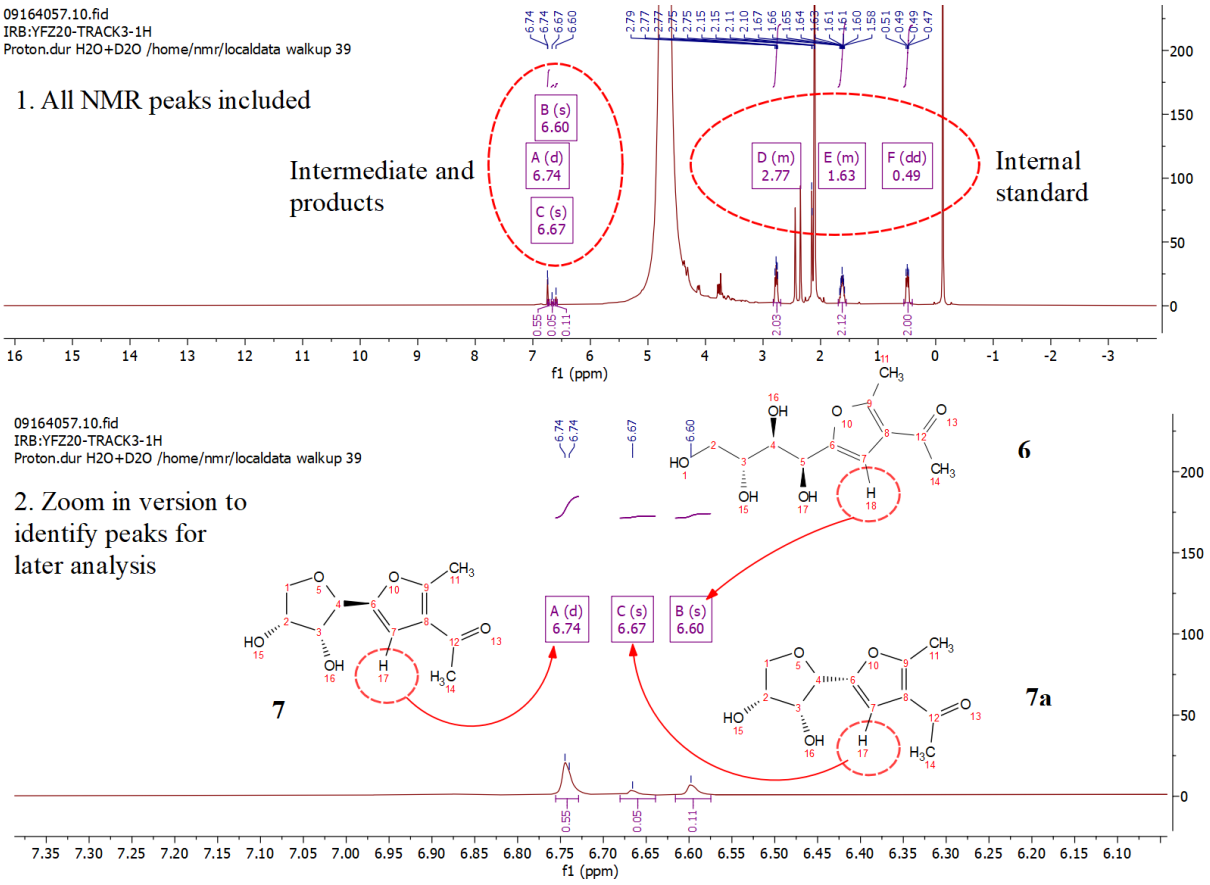

Figure 28. An illustration of the proton peaks identified for later monitoring of reaction. The proton peak at 6.60 ppm represents **6**, 6.67 ppm represent **7a**, 6.74 ppm represents **7**. The ^{1}H NMR references were derived from the analytical data of the isolated material. This assignment is further supported by the subsequent cyclisation analysis (Scheme 13), in which the referential proton integrals of compounds **6** and **7a** exhibited characteristic changes upon conversion from **6** to **7a**—specifically, a decrease in the integral corresponding to **6** and a concomitant increase in that of **7a** within the reaction mixture.

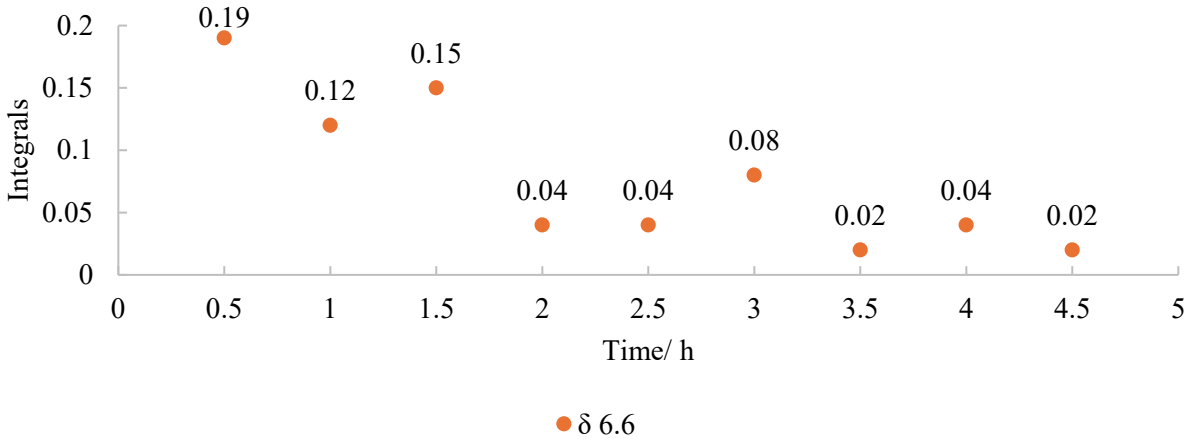

Figure 29. The scatter plot compared integrals of ^{1}H NMR peaks of acyclic intermediate **6** (6.60 ppm) over 4.5 h reaction time. A decreased trend was observed possibly due to the cyclisation of intermediate **6** as shown in Scheme 12.

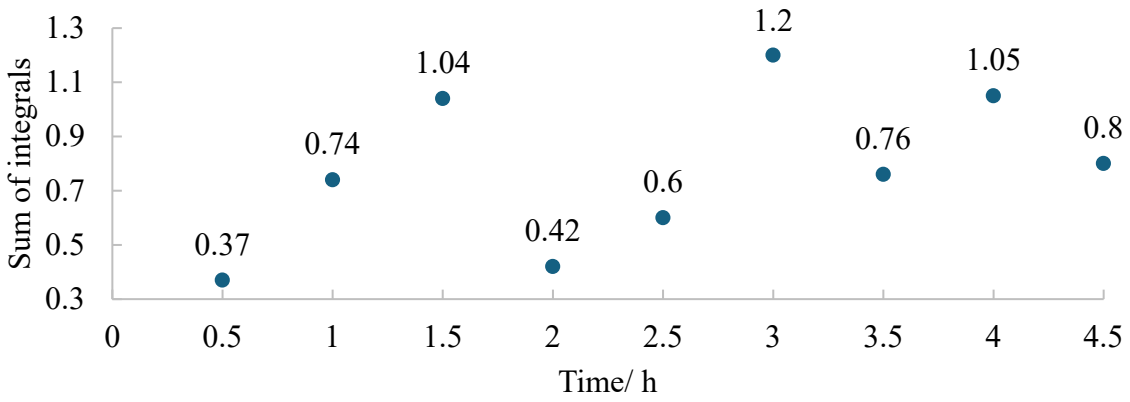

Figure 30. The scatter plot shows the sum of ^{1}H NMR integrals at 6.60 ppm, 6.68 ppm and 6.75 ppm representing **6**, **7a** and **7** over 4.5 h, giving estimated consumpation of starting material of Scheme 12.

At 2 h, the conversion reached 1.04 (Figure 30), with 96% of the integral attributed to the C-glycosyl furan derivatives (Figure 29 *vs*. Figure 30 at 1.5 h). The sample was mixed with a pre-prepared internal standard solution. Due to the small volume required for analysis—approximately 50 µL—handling during mixing and transfer to the NMR tube may introduce inaccuracies, potentially affecting the reliability of the measurement and resultingfluctuations after 2 h. To confirm this finding, batch reactions were repeated at three different reaction times (Table 12, Entries 1–3). The presented yields of target compound **7** were determined by calculation of target compounds in the crude reaction mixture by NMR integrals as shown in Table 13 with the selected

proton signals used for NMR integration. The reaction times included variable warm-up periods (Table 13), and fluctuations which made it challenging to maintain a consistent reaction temperature of 90 °C and resulted in inconsistent yields. A subsequent experiment conducted under reflux conditions (30-minute warm-up followed by 2 h at reflux – entry 4, Table 11) afforded a calculated yield of 81%. Given that shorter reaction times are advantageous for improving space-time yield (STY) within a fixed reactor volume, the equivalent reflux conditions (98 °C) were emplotedfor flow reactor trials.

Table 12. Isolated yield from batch reactions. 50 mmol of *D*-(+)-glucose, 1.5 equivalent of 2,4-pentanedione (**8**), 0.25 equivalent of catalyst and 25 mL of water. The calculated yield was derived from NMR estimation, excluding the peaks of minor distereoisomer **7a**, acyclic compound **1**, 2,4-pentanedione **5**, and ethyl acetate. One of the examples is illustrated below in Table 13.

Entry	Time/ h	Mass/g	Isolated mass/ g	Calculated yield/ %	Temp. 90 °C Time taken to reach temp.
1	1.5	11.3	9.3	82	~40 min; controlled temperature was around 92 ℃
2	2.5	12.3	7.0	62	~30 min; temperature 92 – 88 ℃ (longer time at 88 ℃))
3	3.5	12.2	6.9	61	~30 min; temperature 95-85 ℃ (longer time at 85 and 88 ℃)
4	2.5	12.5	9.2	81	Heated at reflux 98 °C;~30

Table 13. ^{1}H NMR integrals and the percentage of target compound **7** of the derived mass in Table 6

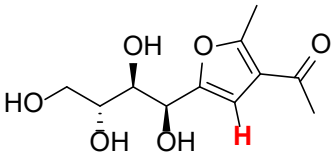

6 δ 6.59

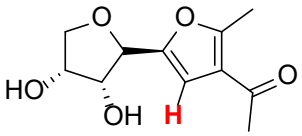

7 δ 6.79

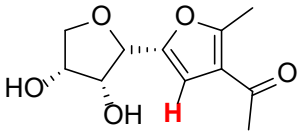

7a δ 6.69

(predicted structure)

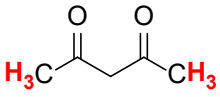

5 δ 2.14

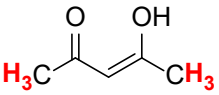

5a δ 2.03

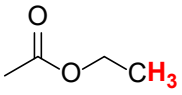

Ethyl acetate δ 1.99

Entry	δ 6.79 (**7**)	δ 6.69 (**7a**)	δ 6.59 (**6**)	δ 2.14 (**5** proton*6)	δ 2.03 (**5a** proton*6)	δ 1.99 (EtOAc proton*3)	Percentage of compound **7** %
1	1.00	0.13	0.08	0.05	0.03	0.00	82*
2	1.00	0.12	0.10	0.69	1.01	0.71	57
3	1.00	0.12	0.06	0.66	0.95	0.94	57

4	1.00	0.12	0.03	0.41	0.50	0.17	74

*Exemplary calculation: 1/(1 + 0.13 + 0.08 + 0.05/6 + 0.03/6 + 0/3) = 82%.

Additionally, if the remaining intermediate **6** can be converted to **7**, the overall yield can be maximised further. The use of a heterogenous catalyst (Quadrapure^{TM}-sulfonic acid (QP-SA) was tested to promote the cyclisation of compound **6** (Scheme 13). The crude mixture containing **6**, **7**, and **7a** was dissolved in ethyl acetate with an additional amount of QP-SA and the disappearance of the proton peak of **6** was tracked by NMR (Figure 31, 32). The integral at 6.58 ppm (representing **6**) was completely reduced after 1 h reaction time, the integral at 6.78/6.79 ppm (representing **7**) increased from 0.84 to 0.95, the integral at 6.68 (representing **7a**) hence indicating that compound **6** was successfully cyclised to 7. This indicates a conversion time of between 0.5 and 1 h.

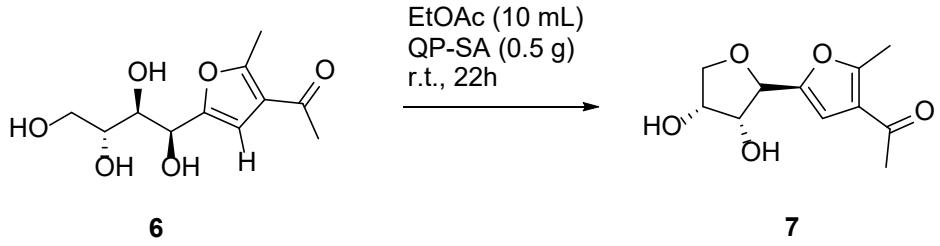

6 **7**

Scheme 13. The reaction of converting **6** to **7** by QP-SA at room temperature. The starting material was The crude mixture (0.365 g) containing 6, 7, 7a obtained from Scheme 12 was used as the starting material for this reaction.

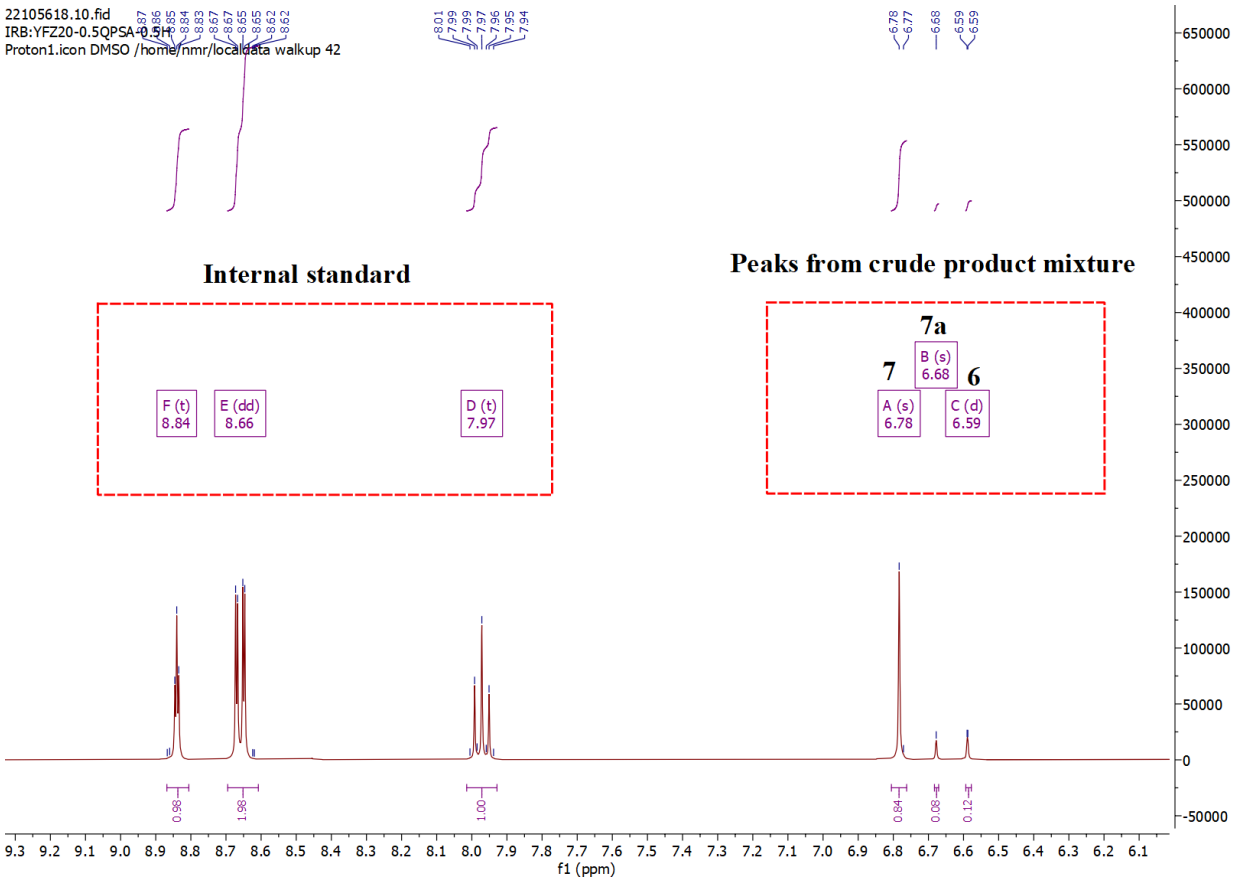

Figure 31. The exemplary NMR data of converting compounds **6** to **7** with QP-SA. The internal standard is 1,3-dinitrobenzene.

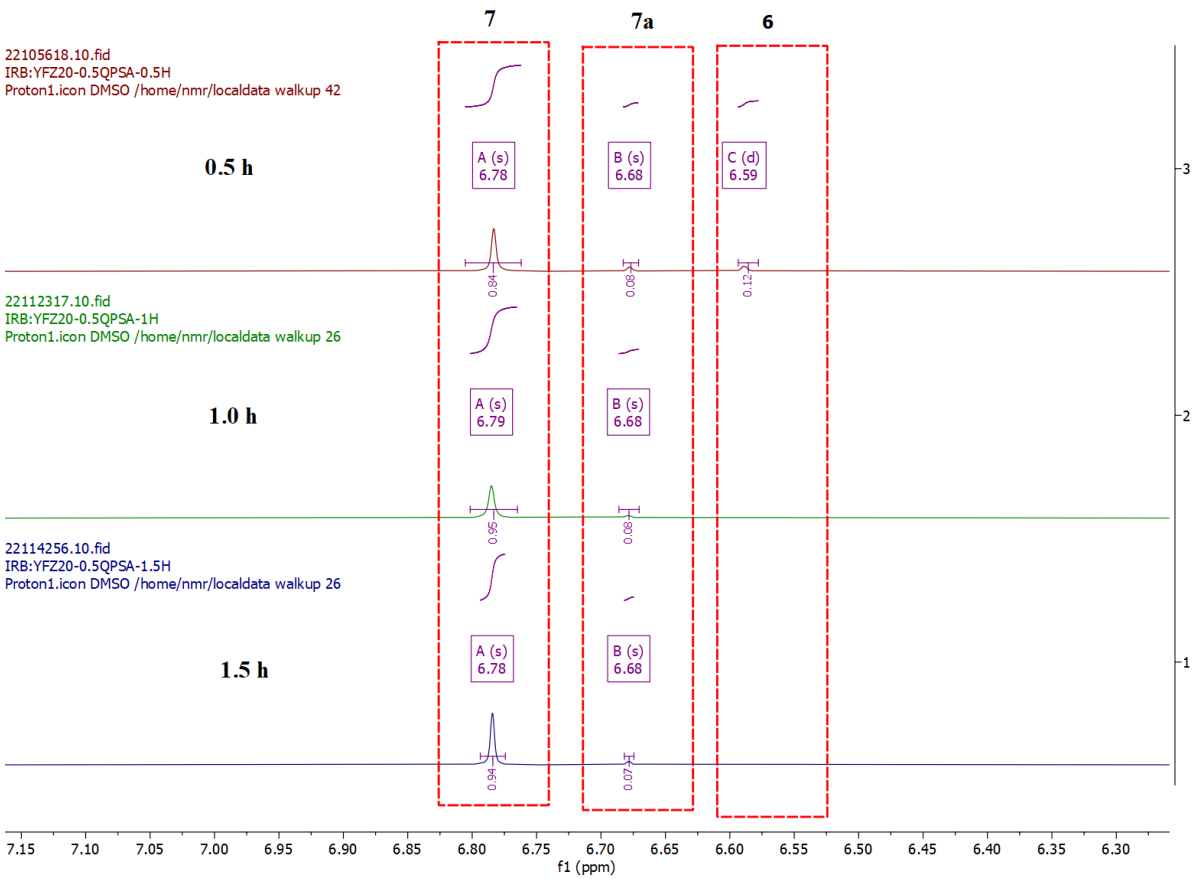

Figure 32. The NMR data of converting **6** to **7** with QP-SA with reaction times of 0.5 h, 1.0 h, and 1.5 h. The peak at 6.58 ppm is absent at 1 h and 1.5 h.

2.2.3.3 Establishing a flow set up

Following work in batch it was decided to translate the optimized reaction protocol to flow. The flow reactor set up comprised of two peristaltic pumps named A and B (max flow rate 10 mL per pump) (Figure 33). Pump A provided an aqueous stream of carbohydrate (monosaccharide or disaccharide) and catalyst; Pump B delivered a stream of 2,4-pentanedione (**6**) since this is not fully dissolved with other reagents at the required concentration. The solubility of 2,4-pentanedione (**6**) is 16 g/ 100 mL in water (20 °C),[180] consequently around 46.9 mL of water was required for a 50 mmol scale. The reactor volume of the flow system is 60 mL and can produce a residence time of 180 minutes (2.5 h). As a general set up pump A was set at 0.321 mL min^{-1} and B was set at 0.079 mL min^{-1} using Equation 8. These solutions were combined using a T-piece connector and processed through the 60 mL heated reactor coil (made from 6 × 10 mL PTFE

tubular coils). A comprehensive calculation of flow rate and residence time can be found in Section 2.5 Appendix.

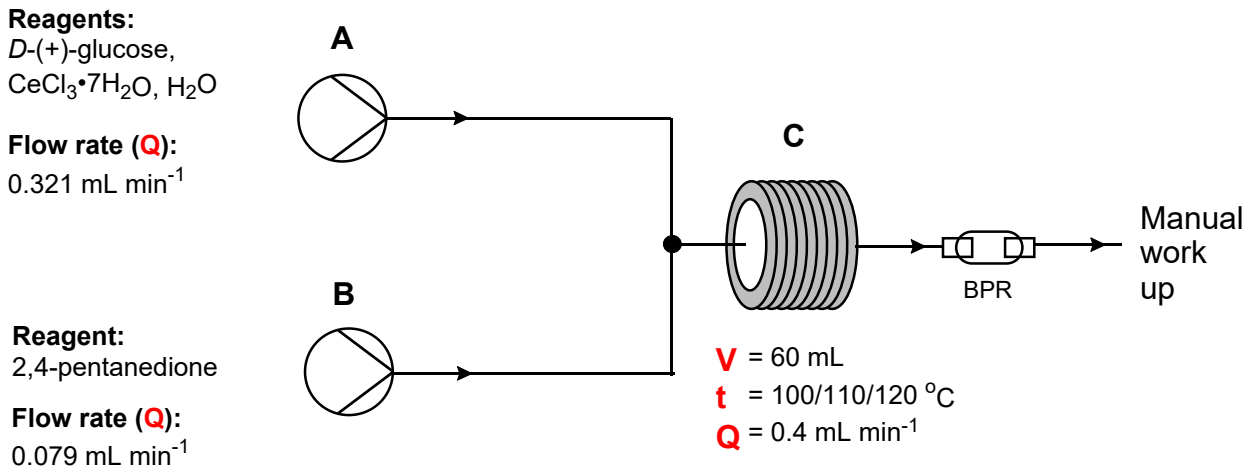

Figure 33. The flow set-up for preparation of 1-(5-((2*S*,3*R*,4*R*)-3,4-dihydroxytetrahydrofuran-2-yl)-2-methylfuran-3-yl)ethan-1-one (**7**). Pump A was controlled by the easy-MedChem E-Series, B was a vapourtec SF10, C is standard coiled tubular reactor (PTFE).

A screening of conditions was performed using 50 mmol processing amounts (Table 14). Reaction temperature was further investigated at 100 ℃, 110 ℃, and 120 ℃ as flow reactors allow operation beyond the reflux temperature. The yield increased with increased temperature, at 100 ℃, 110 ℃, 120 ℃, the yields were 37%, 60%, and 70% respectively (Table 14, Entry 1-3). However, the yields obtained were lower than found in the batch process (95%). The first proposed reason for this was due to insufficient reagent supply to reach continuous steady state of the flow reactor. There are many explanations of steady state with various contexts as summarised in Table 15. [181-186] In flow chemistry, steady state refers to the condition where the system's key parameters — such as concentration, temperature, pressure, and flow rate — become constant over time at any given point in the reactor. This doesn't mean the reaction stops; rather, it means the system reaches a dynamic equilibrium where inputs and outputs are balanced. For this project, the concept will be used in Section 2.2.4 where cases were examined in which the solution volume exceeded twice the reactor volume—a condition recognized as a minimum threshold for reaching steady-state flow, which correlates with production yield in flow.

Table 14. Conditions used in flow reaction.

Entry	Vol/ mL	Res Time/ h	Temp/ °C	Mass recovery/ g	Calc mass (yield)/ g	Calc Yield/%	Water pH
1	60	2.5	100	12.7	4.19	37	> 7
2	60	2.5	110	8.6	6.78	60	> 7
3	60	2.5	120	11.8	7.90	70	> 7
4	60	2.5	100	7.9	6.54	58	= 7
5	60	2.5	110	9.6	7.85	69	= 7
6	60	2.5	110	9.6	7.77	69	= 1*

* 1 mL of 1 M HCl was added.

Table 15. A selection of "steady state" description references.

Entry	Source	Description	Reference
1	IUPAC Gold Book – Steady State (S05962)	Defines steady state in the context of stirred flow reactors, emphasizing time-independent concentrations.	[183]
2	Flow Chemistry Overview – Organic Chemistry Portal	Offers a comprehensive introduction to flow chemistry, including steady state, residence time, and reactor types.	[184]
3	Unlocking Flow Chemistry – fReactor	Explains how steady state is achieved and maintained in various flow reactor designs, including CSTRs and PFRs.	[185]
4	Theoretical Foundations of Chemical Engineering (Springer)	Analyzes the stability of steady state in flow reactors, including oscillatory regimes and kinetic modeling.	[186]

In addition, the water pH used in the reactions was analyzed because it was noted that the departmental supply of deionized water had pH > 7 (Table 14, Entry 4-6). This was important as the base catalysed Knoevenagel reaction can lead to other products as shown in Figure 34.[187] The characteristic proton peaks for CH_2 and CH_3 of **9** and **10** were however not observed in the ^1H NMR analysis of Entries 1-3, Table 14. Hence, the reduced yield was possibly due to the increased pH of the water. In addition, it was found that adding hydrochloric acid (pH = 1) had no impact on the yield (Table 14, Entry 6).

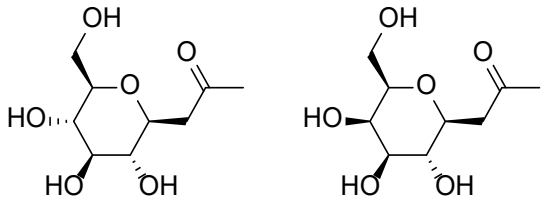

9 **10**

Figure 34. The products **9** and **10** from the base catalysed Knoevenagel reaction of *D*-(+)-Glucose (**2**) and *D*-(+)-Galactose (**3**) respectively.[187]

In summary, the reaction was influenced by water pH values above 7, whereas a neutral pH (pH = 7) consistently yielded reproducible results. Therefore, pH 7 was selected for further investigation. Although elevated temperatures of 110 °C and 120 °C improved yields, they also yielded solid by-products within the reaction mixture. These solids blocked the tubing during a test trail of scale-up. To mitigate this issue, the conditions specified in Table 14, Entry 4 were adopted in subsequent experiments.

2.2.4 Scalability test (Aim 2)

The 24-hour scalability test for *D*-(+)-glucose (**2**) conversion requires overnight monitoring to ensure consistent reaction conditions. To facilitate remote supervision, a webcam and Wi-Fi–enabled smart plug were employed (Figure 35). The webcam enabled researchers to verify the positioning of the stock solution tube in real time. If the tube was displaced beyond the solution surface or blockages were observed, the reaction could be stopped using the smart plug, avoiding any potential safety risks or loss of data. The set up is given by Figure 36.

Figure 35. The webcam monitoring (left) and wifi smart plug (right).

Figure 36. The flow set up with web cam monitoring and wifi smart plug to monitor overnight reaction.

A large-scale reaction was performed scaling from 50 to 735 mmol, using a reactor temperature of 100 °C, and a combined flow rate of 0.4 mL min^{-1} (Table 16, Entry 3), achieving 81.8% calculated yield. The scale has increased to run over24 h with continuous feed of stock solution forscalability test, (the aqueous phase of the reaction from Entry 3 was kept for later catalyst sustainability testing as reported in section 2.2.5). To test consistency a repeat run (Entry 5) was performed. In addition, this 24 h run includes the steady state analysis of this flow reaction. The steady state is defined as 'a situation in which all variables are constant, for example, the process temperature and reagent feed flow rates are constant' in 'chemical flow' by AM Technology Engineering Chemistry. In this scenario, a constant yield should be obtained after 2.5-fold of the reactor volume as proven below. The reduced yield from 81% (Entry 1) to 58% (Entry 2) at 50 mmol scale was potentially due to this systematic problem. This was tested by Entry 4 with exit flow directed through a fractional collector (Figure 37), allowing analysis of the output and determination of consistency and regions of the steady state operation. The amount of product obtained during each hour segment of the 24 h run was recorded and is presented in Figure 38. A sum of 26 samples were collected to ensure the diffused solution mixture at the start and end of the solution mixture were also included. The amount of product obtained became consistent within experimental errors from the 4th hour of collection - indicating steady state. The yield stayed within 5% after continuous steady state and the space-time yield of flow reactions are 2.4 times higher than the batch process (Entry 1).

Table 16. Calculated yields and space-time-yields of **7** by *D*-(+)-glucose (**2**) conversion. [a]Batch reaction with 250 mL round bottom flask (Scheme 11). [b]Flow reaction, water pH 7, volume of coils = 60 mL, Flow rate = (0.321 + 0.079) mL min^{-1} = 0.4 mL min^{-1}. [c]The catalyst recycling test in section 2.2.5.

Entry	Reaction type	Scale/ mmol	Calculated Yield of **7**/%	S.T.Y $*10^{-4}$/ g min^{-1} mL^{-1}
1[a]	batch	50	81	6.1
2[b]	flow	50	58	7.3
3[b]	flow	735	82	15.7
3-catalyst[c]	flow	735	77	14.7
4[b]	flow	735	80	15.4
5[b]	flow	735	83	15.9

Figure 37. The fractional collector (time segmented) connected after the BPR in set-up as shown in Figure14.

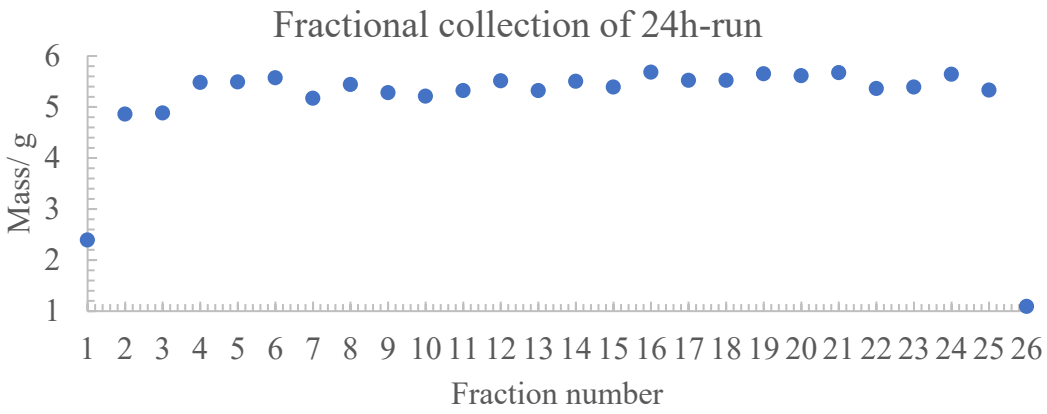

Figure 38. 24 h segmented flow run analysis of reaction in Table 16 Entry3-catalyst. The fraction was collected for an hour.

2.2.5 Catalysts sustainability (Aim 2)

Another sustainable feature of this Knoevenagel reaction is the desire to recycle the catalyst. In theory, $CeCl_3 \bullet 7H_2O$ can be collected in the aqueous phase after the liquid-liquid extraction process and re-used. To test the feasibility of recycling the catalyst, the extracted aqueous solution (Table

17, Entry 3 catalyst) was reacted with additional *D*-(+)-glucose (**2**) and 2,4-pentanedione (**5**). The initial reaction was performed at 100 mmol scale using the same reaction conditions as previously used in section 2.2.4. The yields recorded for various trials are reported in Table 16, since large-scale reaction processing has shown that the, steady state would not be reached at 100 mmol scale, a run at 735 mmol scale was also performed (Entry 5). In general, the single use recycling showed consistent results at ~70%.

Table 17. Scale and calculated yield of **7** of flow reactions.

Entry	Scale/mmol	Calculated Yield/%*
1	100	75
2	100	71
3	100	68
4	100	73
5	735	77

*Calculation method is given in Table 13, Section 2.2.3.2.

Next, we investigated repeated recycles at 100 mmol scale, and the catalyst was recycled five times with the recycled aqueous phase solution after each extraction. The sequential yields are recorded in Table 18. The recovery of material was boosted for 1st, 2nd, 4th, and 5th recycled runs, maintaining yield of **7** greater than Entry 1 while the catalyst was recycled for the 5th time. This would be consistent with increased material extraction based upon residual starting material and/ or intermediates in collected aqueous phase being converted to product and isolated in progressive runs.

Table 18. Mass yield and calculated yield of **7** based upon 100 mmol recycle tests.

	Mass yield/ %	Calculated yield/%
Initial reaction	86	73
Recycle-1	99	77
Recycle-2	97	81
Recycle-3	89	75
Recycle-4	100	87
Recycle-5	96	80

*Calculation method is given in Table 13, Section 2.2.3.2.

2.2.7 Investigation of Galactose as a substrate

After the success of performing the Lewis acid catalysed Knoevenagel reaction in flow, the same procedure was investigated for the reaction of *D*-(+)-galactose (**3**) (Scheme 14). Two different scales were tested, a 50 mmol scale and 175 mmol scale (137.2 mL solution) and the results are summarized below in Table 18.

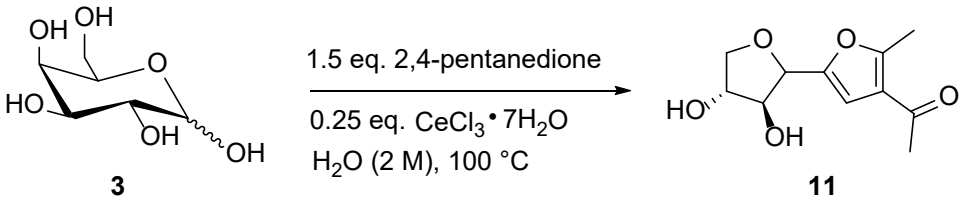

Scheme 14. The synthetic scheme of 1-(5-((3*S*,4*R*)-3,4-dihydroxytetrahydrofuran-2-yl)-2-methylfuran-3-yl)ethan-1-one (**11**).

The reaction of *D*-(+)-galactose (**3**) gave a mixture of two diastereoisomers. The ratios of the diastereoisomers and yields were estimated by ^{1}H NMR integration analysis and are reported in Table 19. Entry 1 and 4 showed similar yields between the batch and flow reactions at 50 mmol scale. When continuous steady state was achieved at 175 mmol, the yield was slightly higher than 50 mmol scale. The catalyst could be recycled as shown by Entry 3.

Table 19. Reaction conditions of synthesis from *D*-(+)-galactose.

Entry	scale/ mmol	mass/ g	Ratio of diastereoisomers	Calculated yield of both diastereoisomers/ %
1 flow	50	10.2	1.9:1	78
2 flow	175	44.4	1.9:1	85
3 flow-recycle	175	46.0	1.9:1	80
4 batch	50	12.6	1.8:1	73

2.2.8 Exploring the reaction of Lactose

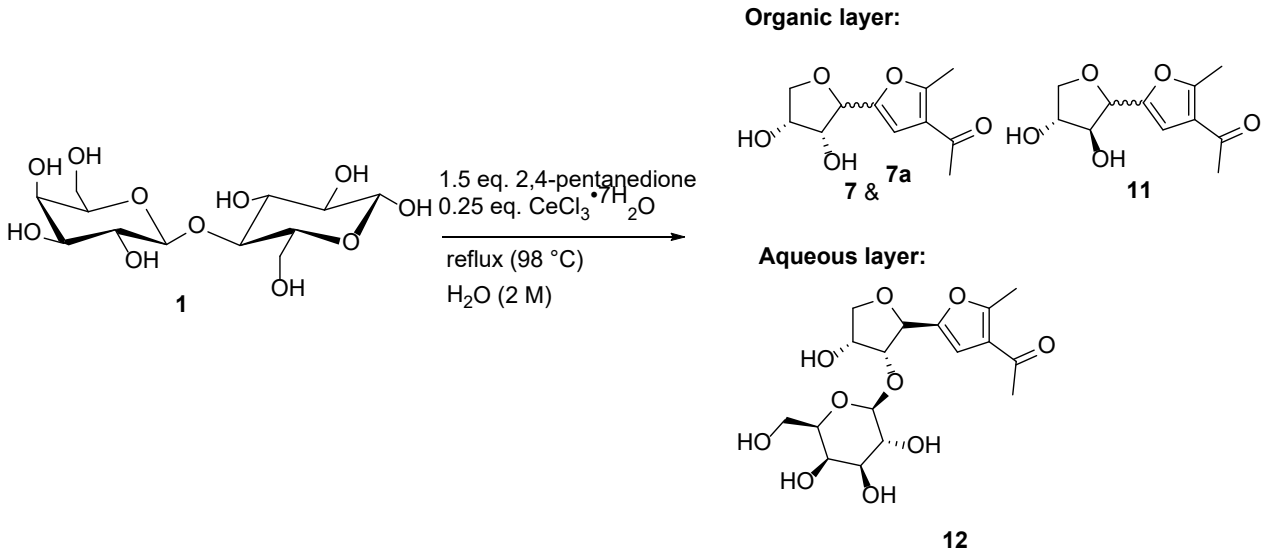

Scheme 15. Batch conditions for synthesis of **9** from **1** via Knoevenagel reaction.

Having shown the feasibility of reacting *D*-(+)-glucose (**2**) and *D*-(+)-galactose (**3**) independently the processing of the more complex sugar, lactose (Scheme 15) was investigated. Initially, the standard batch synthesis conditions was applied to test the lactose conversion. Following solvent extraction with ethyl acetate, we obtained a mixture of products in the organic layer was obtained. These products were the proposed as the C-glycosal furan derivatives **7**, **11** previously synthesised using by *D*-(+)-glucose and *D*-(+)-galactose. The overall conversion for the reaction was based upon NMR analysis as shown in Figure 39. The dimer target compound was detected in the aqueous phase, the structure of the compound was then confirmed with evidence from LC-MS, NMR, and crystallography analysis (Figure 40, 41, and 42). The progression of the reaction was tracked with an internal standard (**8**). The formation of **7** and **12** were tracked by NMR integral ratios for comparison analysis (Figure 43, 44). There was a reduction in amount of **7** represented by the peak at δ 6.79. The blue spots (Figure 44) representing **12** (δ 6.84) showed a consistent integral area at 1 h, 1.75 h, and 2.5 h giving 92% conversion.

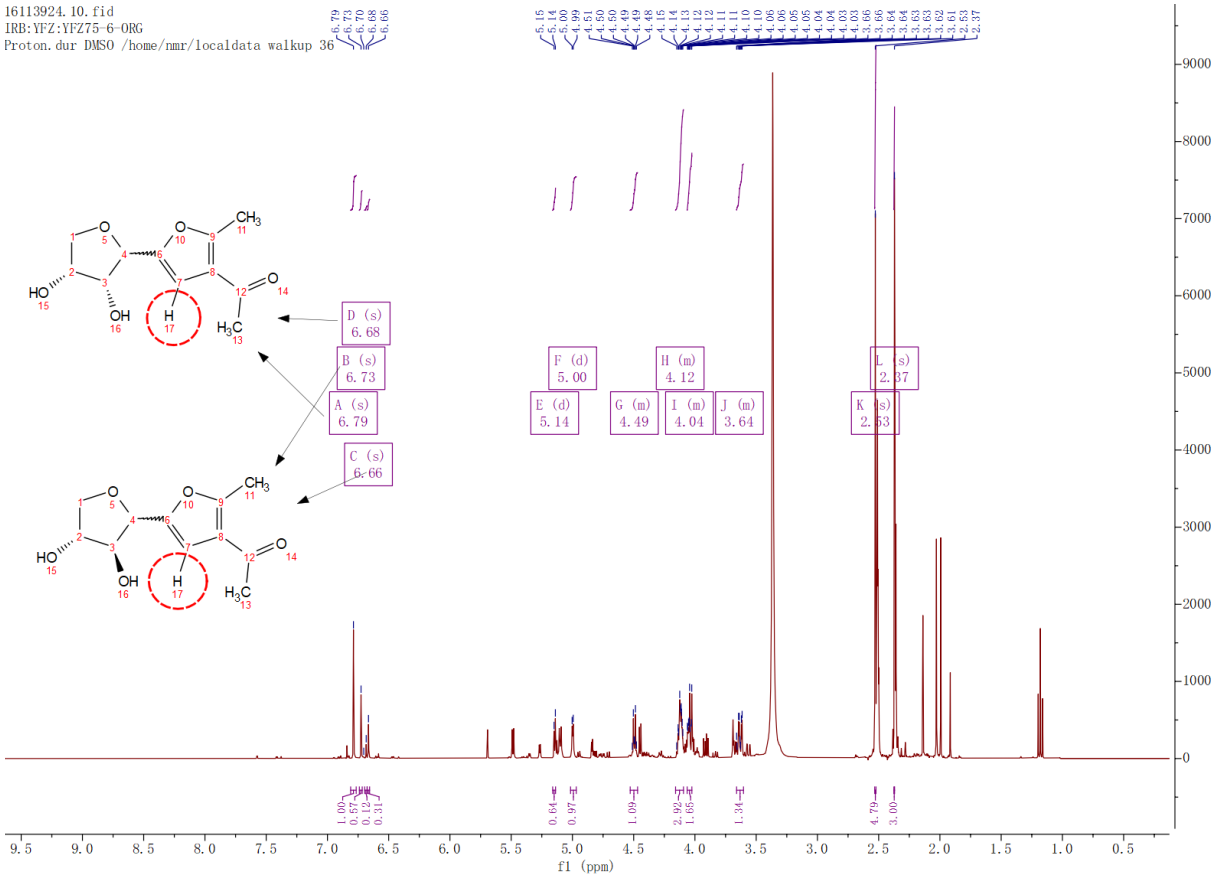

Figure 39. ^{1}H NMR spectroscopy for Organic layer. Proton 17 was assigned using data from the isolated material and used as an internal reference to analyze the mixture. The remaining baseline signals, corresponding to hydrogens on carbons 1-4, could not be unambiguously assigned in the crude mixture and were therefore not characterized.

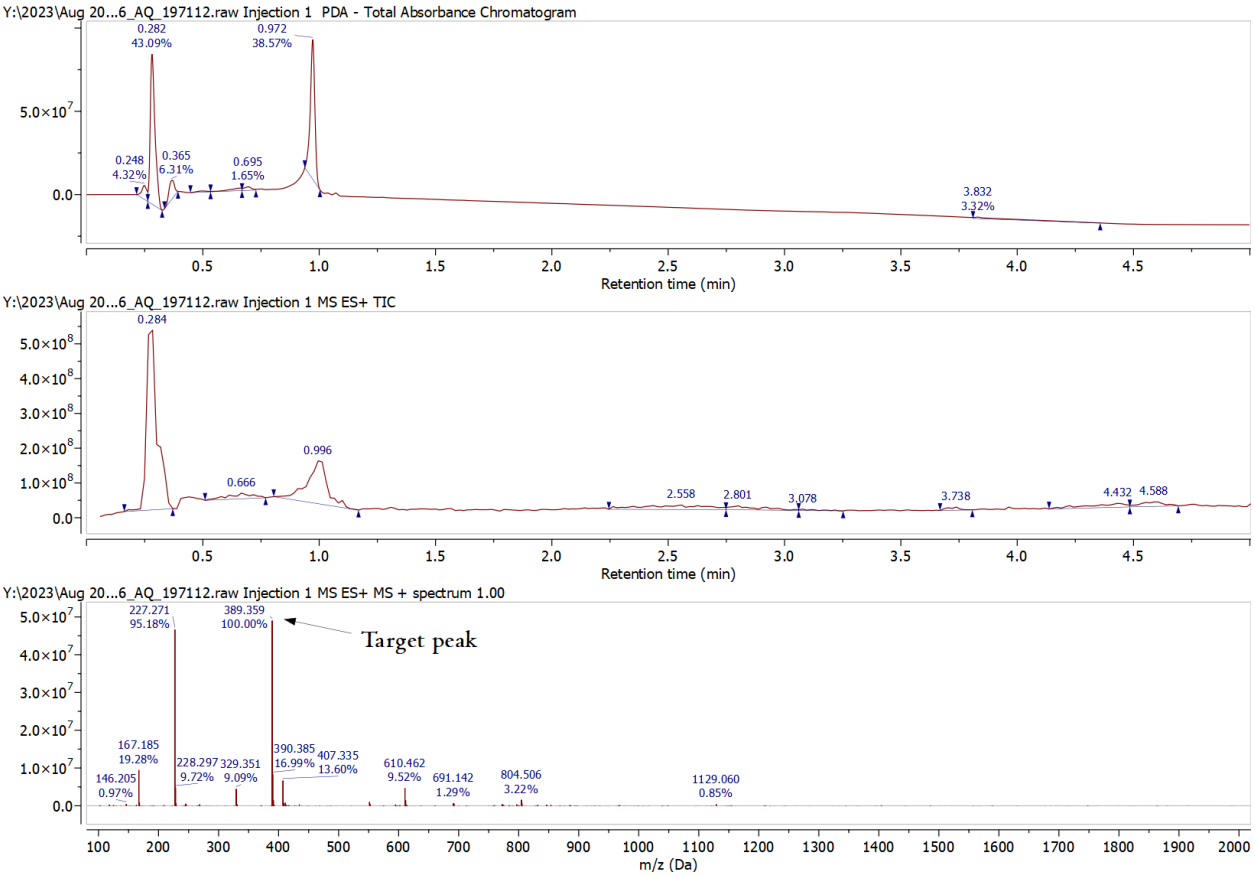

Figure 40. LC-MS for Aqueous layer with target peak of compound **12** after 2.5 h reaction**.**

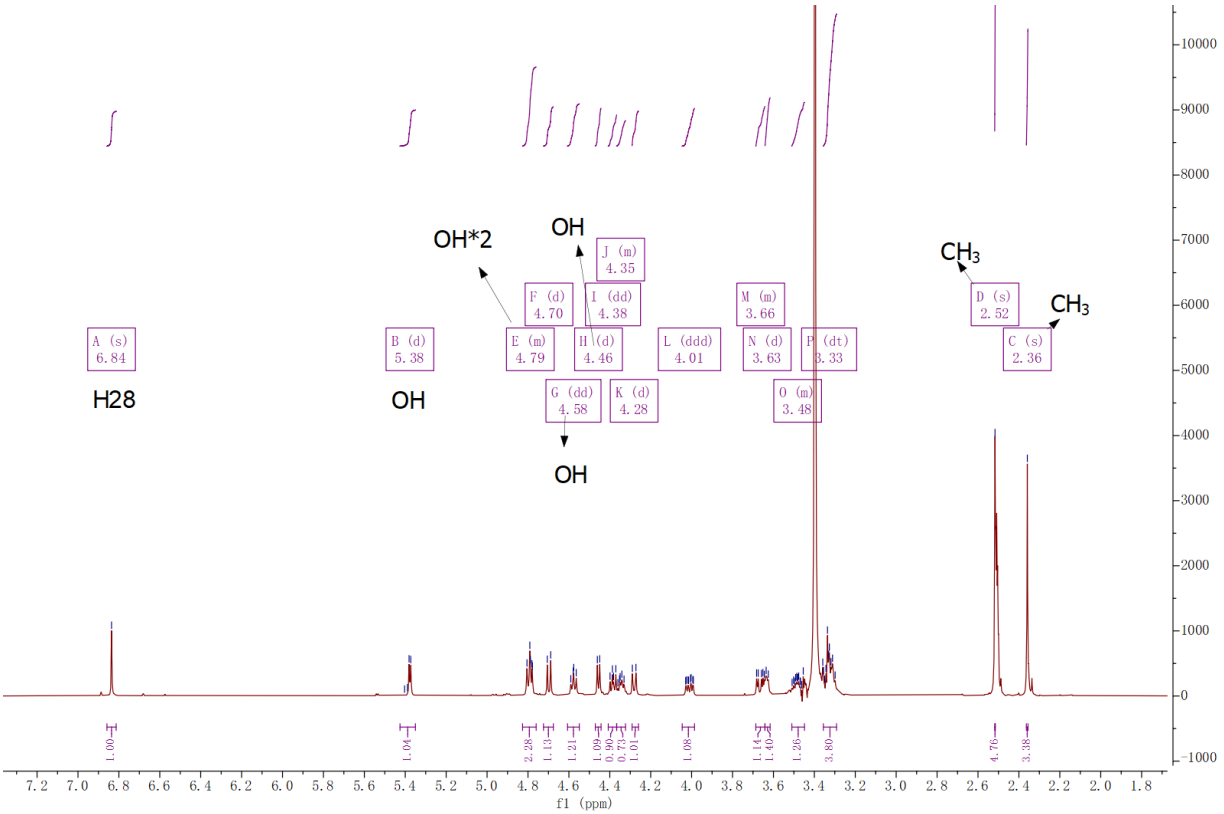

Figure 41. ^{1}H NMR spectroscopy of aqueous layer, illustrating structure of target compound **12**. (Assigned protons were derived from 2D NMR spectroscopy as illustrated in Section 2.4).

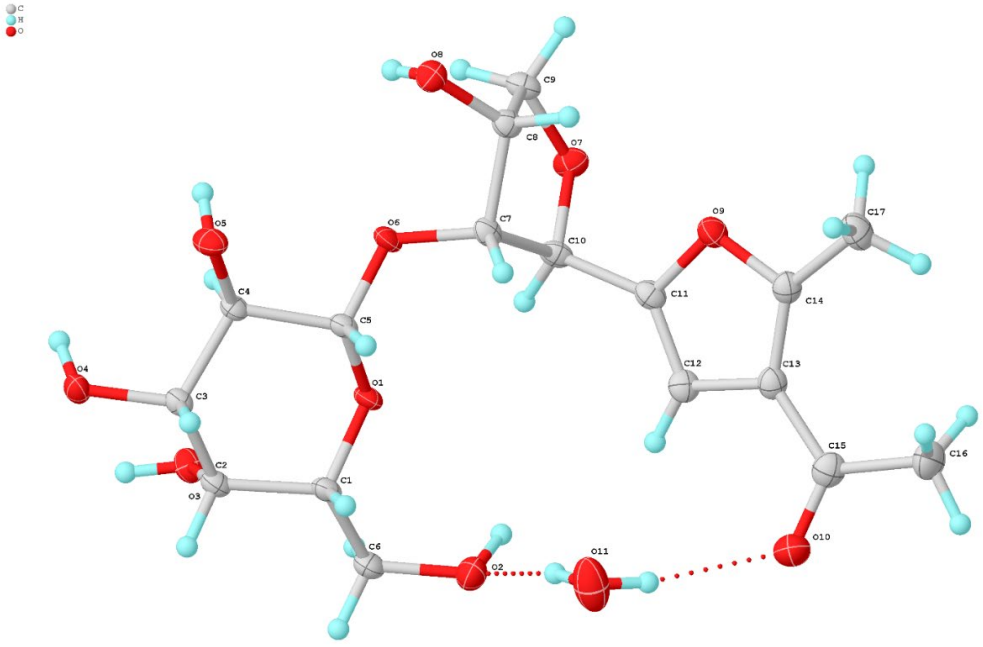

Figure 42. Crystal structure of **12** crystalised from Aqueous phase.

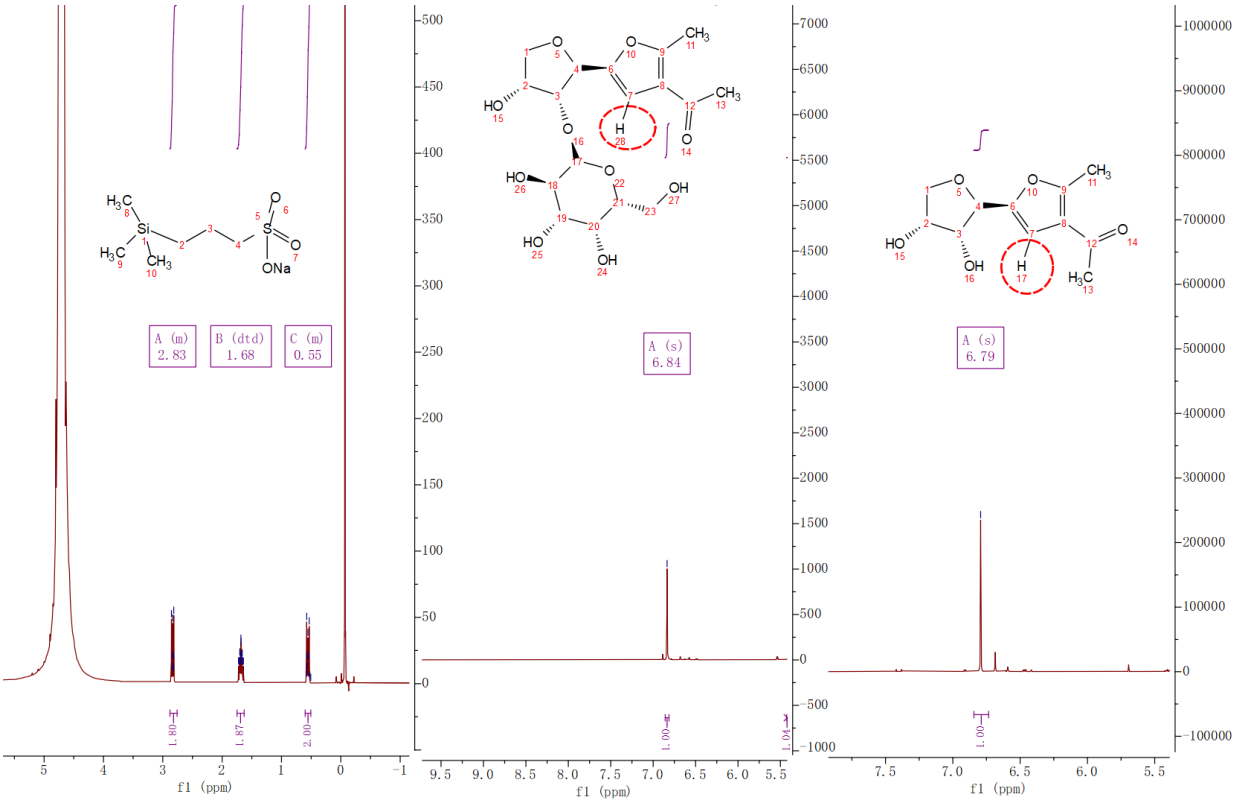

Figure 43. The internal standard reference, and the protons picked to track the reaction.

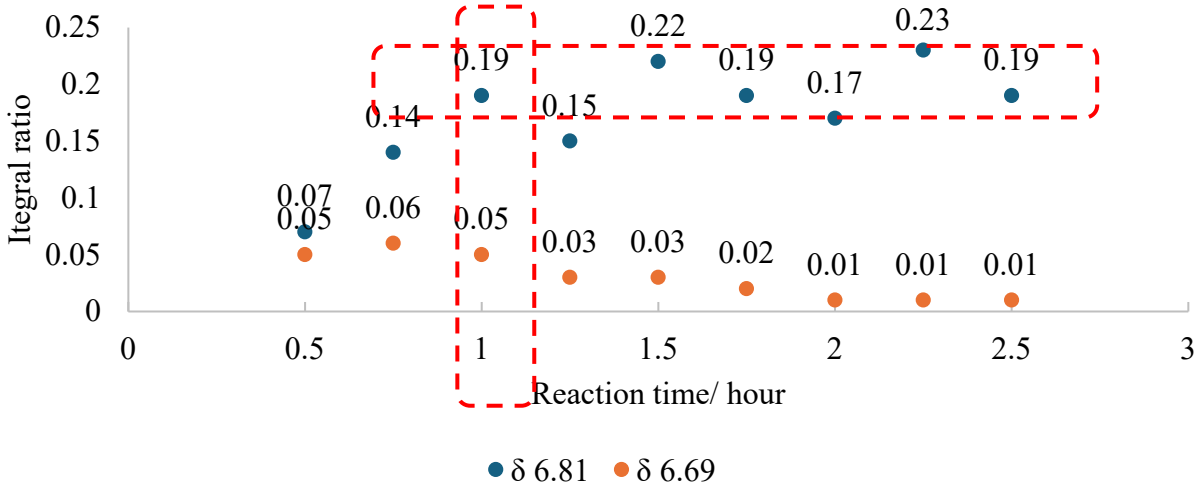

Figure 44. The plot of integral over reaction time to track reaction process by internal standard references in ^{1}H NMR spectroscopy.

Considering the high efficiency of the reaction in batch, a 1 h and 2 h residence time in flow reactor were evaluated. The stock solution prepared by lactose, water and cerium chloride heptahydrate required warming to obtain a homogeneous solution (Figure 45) as lactose is less soluble in water than either *D*-(+)-galactose (**3**) or *D*-(+)-glucose (**2**). Comparing the ^{1}H NMR spectra of the progressing reaction solutions, a 2 h residence time resulted in high conversion to the target compound **12** (Figure 46). A 98% conversion was achieved for this process in flow as estimated by ^{1}H NMR spectroscopy with an internal standard at 25 mmol scale.

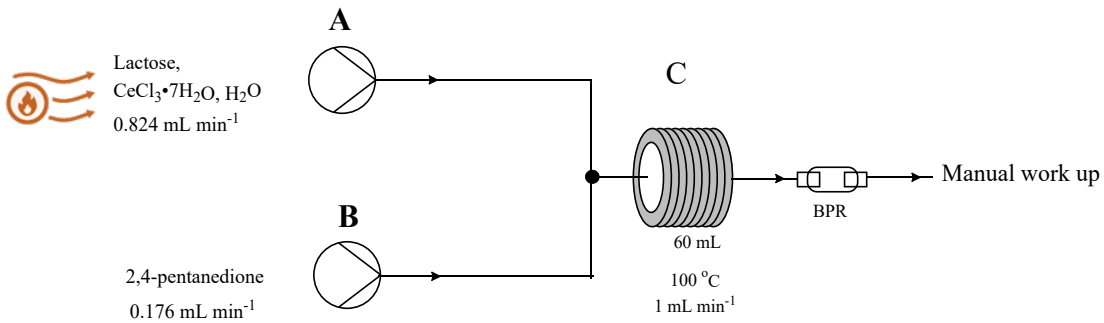

Figure 45. The Knoevenagel reaction of Lactose in flow reactors. The solution of lactose, $CeCl_3 \cdot 7H_2O$ and water was heated to around 60 °C to obtain a homogenous solution. Reactor volume = 60 mL, residence time = 1 h, flow rate = (0.824+0.176) mL min^{-1} = 1.0 mL min^{-1}.

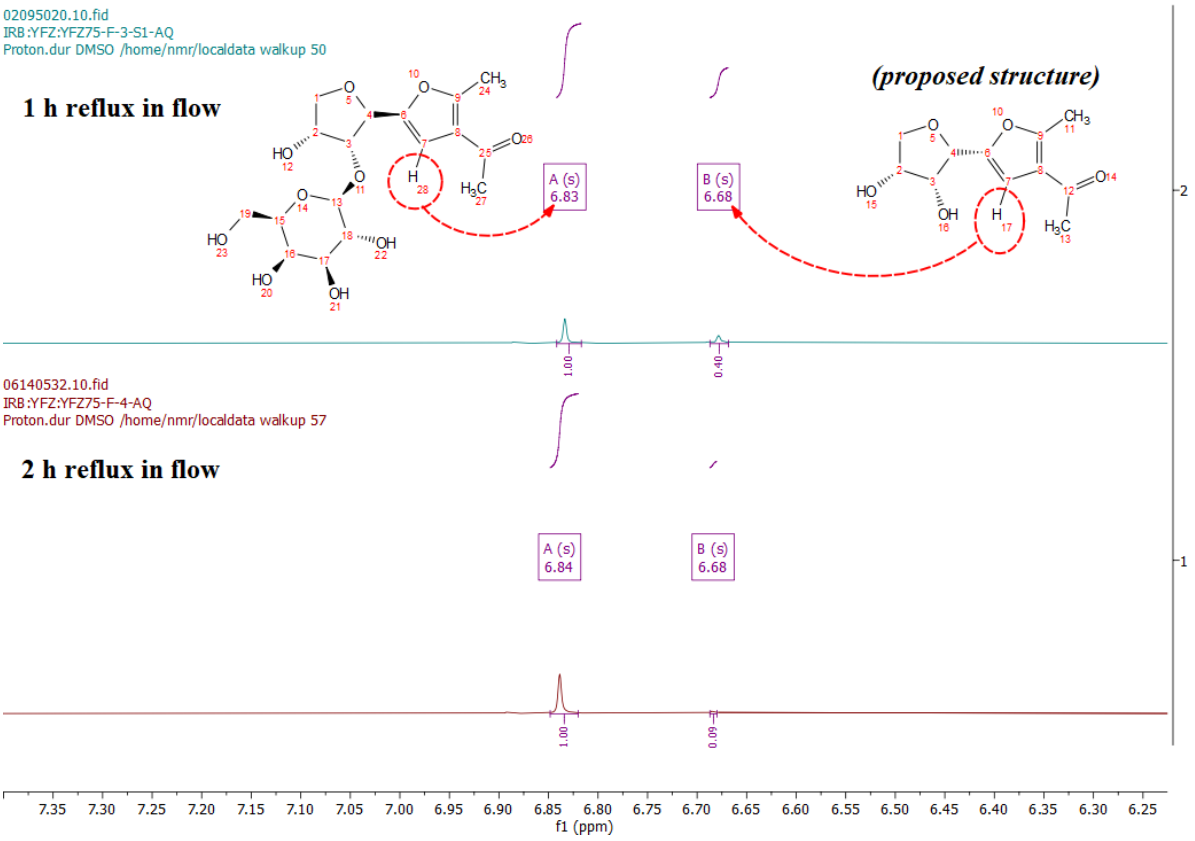

Figure 46. The residence time test in flow with 1 or 2 h reaction. The integral at 6.68 ppm has reduced from 0.40 to 0.09 while the integral at 6.84 ppm were set at 1.00, meaning less side product was formed and more target compound obtained.

Extraction methodology

In literatures, compound **12** was isolated by conventional methods of acetylation (condition: A portion of the crude mass was acetylated conventionally using Ac_2O and pyridine at room temperature, which after column chromatography over SiO_2 afforded the acetylated furan derivative in quantitative yield) and column purification (condition: a Teledyne ISCO Combiflash Rf in conjunction with Redi Sep Rf Gold C8 150 g column, using a combination of water and acetonitrile as the eluent mixture) as,[141, 144] alternative green strategies of isolating these compounds were considered. The current extraction involved using 4 × 100 mL of ethyl acetate based upon a 50 mmol of starting material reaction scale. This solvent was selected after testing as explained in Section 2.1.2, but in this case the target molecule **12** remained in the aqueous phase. This increased solubility in the aqueous phase is evidently due to the extensive hydrogen bonding

created with the multiple hydroxyl groups of this compound and the water environment. To increase the intermolecular forces of this compound in an organic solvent, to facilitate extraction, a series of derivatives were selected for synthesis as listed in Figure 47 and as shown in Scheme 16. The sulfonylation reaction was employed, which could be performed in an aqueous system—a limitation of many other chemistries considered. This approach also took advantage of the inherent selectivity of the sugar unit, which preferentially reacts with the less hindered primary alcohol group, with all other hydroxyl groups being secondary.

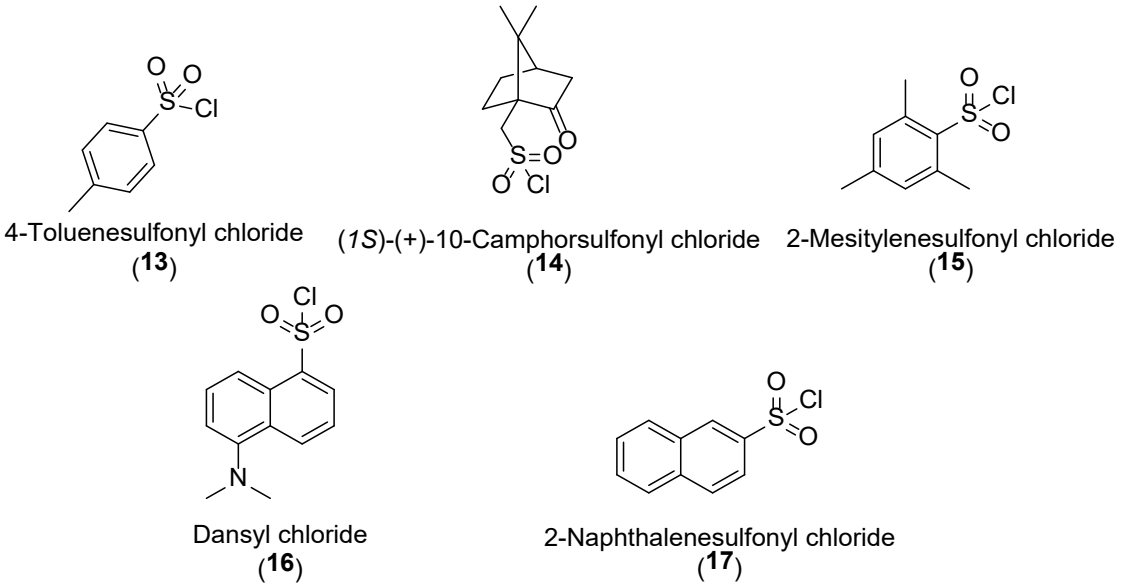

Figure 47. Selected sulfonyl chloride compounds investigated.

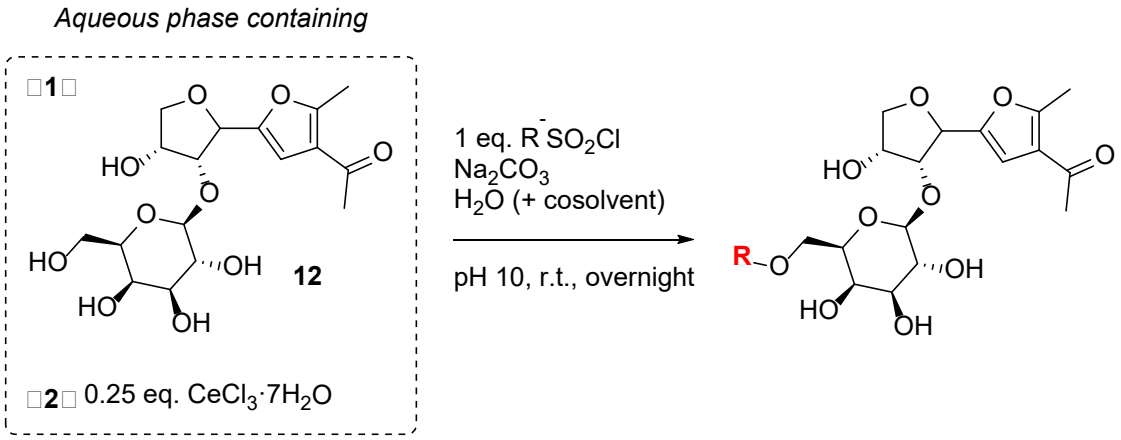

Scheme 16. Sulfonylation of alcohol groups in compound **12**.

The sulfonylated products (Scheme 16) were analyzed with NMR spectroscopy and LC-MS. Each reaction progressed to completion and was subsequently extracted with ethyl acetate to determine the partitioning of the newly formed derivative. The material synthesized from **13**-**17** (Figure 51) all remained in the aqueous phase. The starting materials **16** and **17** were less soluble in water, and consequently cosolvent was used to aid solvation (Table 20; Entry 1 and 2). The LC-MS analysis of the reactions showed the desired molecular ion peaks for both target compounds while **17** had less side product peaks. The reaction was repeated with **17** this time using acetonitrile as the cosolvent to fully dissolve the starting materials. After extraction with ethyl acetate (4 × 100 m withL) the desired product synthesized by 17 was found in the organic phase with no molecular ion peak for the product being detected in aqueous phase indicating a full extraction.

Table 20. Reaction conditions with dansyl chloride (DC, **16**) and 2-naphthalene sulfonyl chloride (NC, **16**) as RSO_2-Cl compound. Co-solvent was added to help dissolve the catalyst. The reactions were conducted at pH 10 through the addition of Na_2CO_3 prior to addition of RSO_2-Cl.

Entry	Scale/ mmol	RSO_2-Cl	Eq. of RSO_2-Cl	Vol. (H_2O)	Co-solvent	Time	Temp.
1	4	DC	1	25 mL	Acetone, 10 mL	Overnight	r.t.
2	4	NC	1	50 mL	MeCN, 15 mL	Overnight	r.t.
3	10	DC	1	25 mL	MeCN, 50 mL	Overnight	r.t.

As the aim was to enact functionalization to enable extraction of the product into the organic phase with optimum conversion, we continued exploring the reaction conditions using **17**. More crude mixture was isolated from the organic phase by increasing the equivalents of **17** from 1 to 2.5 (Table 21, Entry 1 and 2). However, only <1.00 g of target compound was isolated with reaction conditions in Entry 2. Extending the reaction time and increasing the temperature also failed to improve the reaction (Entry 3 and 4) as no target m/z were identified in LC-MS analysis.

Table 21. Reaction conditions with 2-naphthylsulfonyl chloride (**17**) at 10 mmol scale. The target m/z 579 were found at 2.8 – 2.9 min in LC-MS analysis.

Entry	Equiv. of NC	H_2O/ mL	MeCN/ mL	Time/ h	Temp/ °C	Mass of crude mixture/ g	Total area% of target m/z in LC-MS
1	1	25	50	16	18 – 23	1.67	46.27
2	2.5	25	100	16	18 - 23	6.95	38.06
3	1	50	75	72	50 – 80	1.41	0.00
4	1.5	50	75	16	50	2.95	0.00
5	1.8	50	85	21	50	5.60	0.00

In summary, the desired sulfonyl derivative compounds were derived with **13**-**17** but the generated products remained in the aqueous phase after attempted extraction. The product derived from dansyl chloride (**16**) and 2-naphthalene sulfonyl chloride (**17**) could be extracted into the organic phase but were accompanied by many other side products leading to a poor yield.

2.2.9 Development of continuous flow system

In this scenario, the implementation of a fully continuous flow system enables reaction processes, automated extraction of the organic phase, recycling of the aqueous phase, and precise reagent addition. This configuration substantially minimizes manual handling, requiring only remote supervision for monitoring and intervention. Such automation contributes to streamlined operation and aligns with the principles of sustainable process design. To generate this system, a specifically designed separation was performed by a gravity extraction device (65 mL, Figure 48). The aqueous phase was connected to circulate back to the aqueous feed bottle (Figure 49, 50, 51) and a powder doser was installed to continuously add *D*-(+)-glucose (**2**) at a constant rate (Figure 51H).

The flow reactor was set up with three peristaltic pumps named A, B, C (max flow rate 10 mL per pump) which were all set with the same flow rate (Figure 49). Pump A provided a stream of ethyl acetate used to extract out the organic phases in the separating glassware (65 mL); Pump B delivered an aqueous solution of reagents which was processed through a 60 mL of heated reactor coil (made from 2/6 × 10 mL PTFE tubular coils). The processed solution was combined with the ethyl acetate stream using a T-piece connector. The commercially available construction units and designed glassware of flow system are introduced below in Figure 50 and Figure 51. For the convenience of testing, concentration of solution was set at the level to fully dissolve 2,4-pentanedione (**5**).

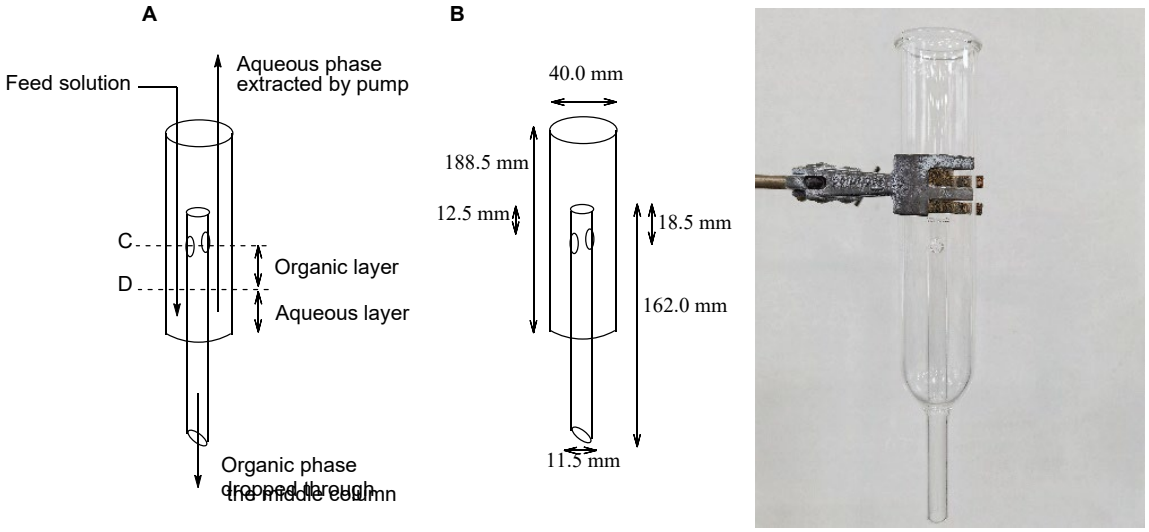

Figure 48. The phase separation glassware was made by the custom glass blowers resident in the Department of Chemistry at Durham University. As depicted in illustration A, the operational principle involves filling the outer column with the reaction mixture to level C, enabling gravitational separation of the organic and aqueous phases. The lower-density organic phase enters the inner column and is drawn off for collection. A pump extracts the accumulated aqueous phase from the top of the outer column at a flow rate calibrated to match the input feed, ensuring stable operation. The design dimensions are specified in B, alongside a photograph of the fabricated unit.

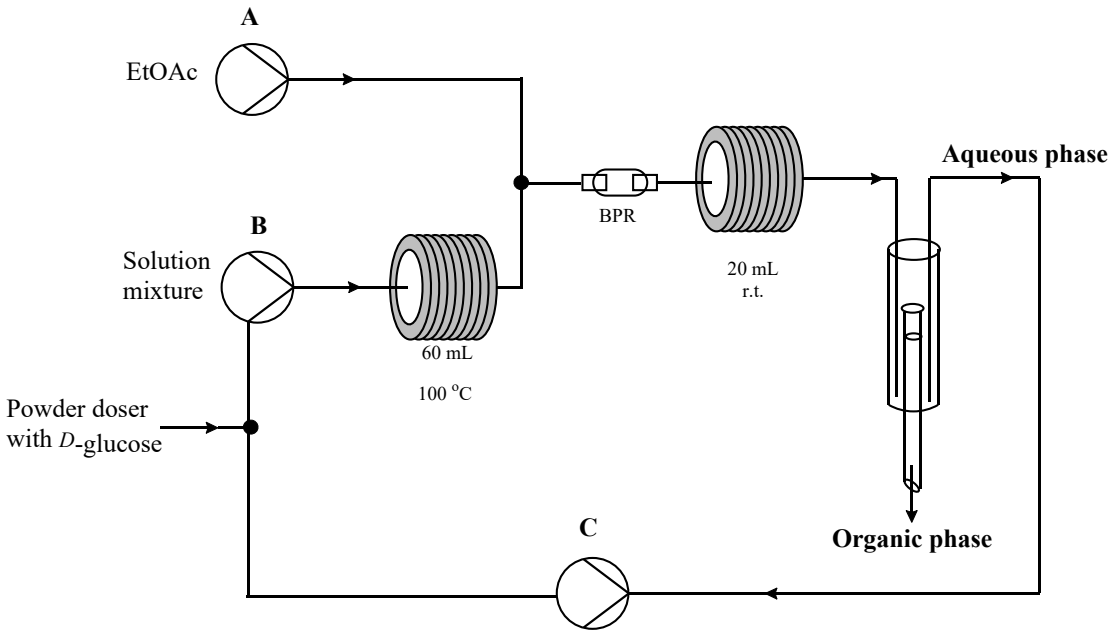

Figure 49. The design of flow set-up to cyclise the aqueous phase of the reaction.

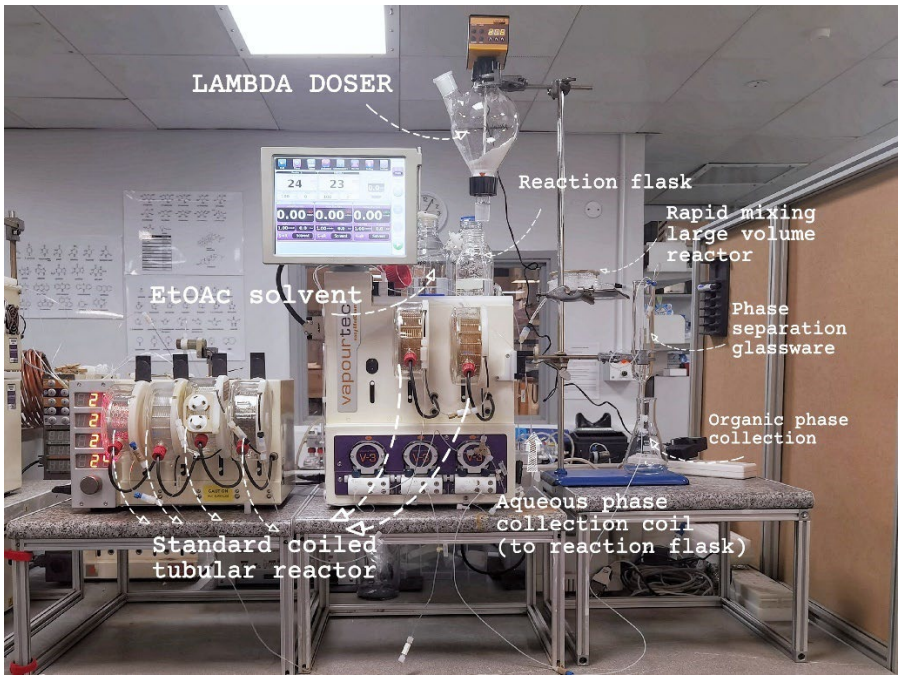

Figure 50. The flow set-up for preparation of 1-(5-(3,4-dihydroxytetrahydrofuran-2-yl)-2-methylfuran-3-yl)ethenone (**2**). A, B, C are pumps on easy-MedChem E-Series, D is standard coiled tubular reactor (PTFE), E is Rapid mixing large volume reactor.

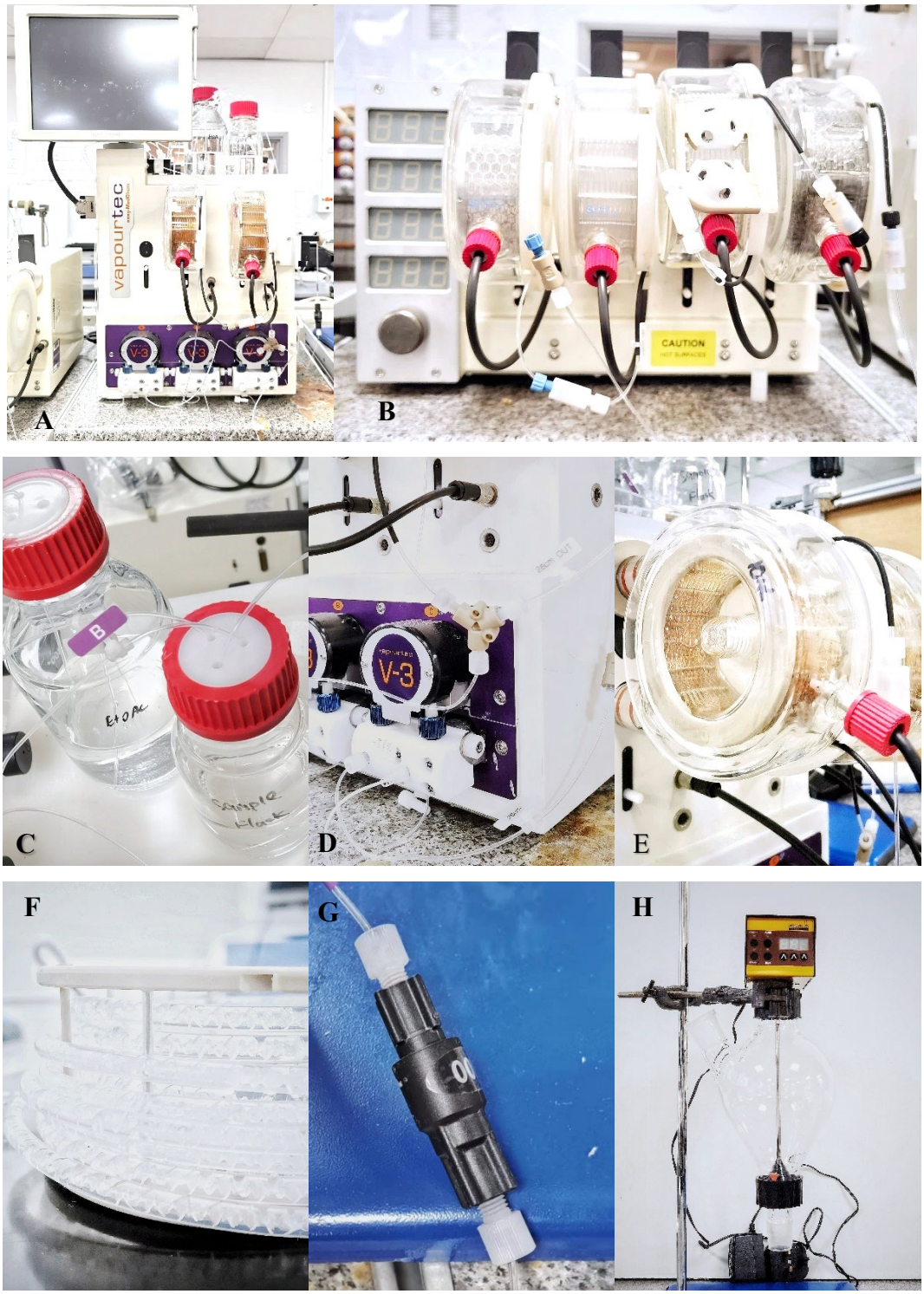

Figure 51. A The easy-MedChem E-Series with two standard coiled tubular reactor (10 mL); **B** R4 Reactor heater/ cooler module with four standard coiled tubular reactor (10 mL); **C** Reaction flask; **D** The Y-piece connector; **E** Standard coiled tubular reactor (10 mL); **F** Rapid mixing large volume reactor (20 mL); **G** The in-line back pressure regulator (BRP). **H** LAMBDA Doser.

The minimum calibrated feed rate given on the company website for the solid doser is 50 mg min^{-1} based on the dispensing of NaCl.[188] To test its delivery and ensure calibration of the *D*-(+)-glucose (**2**) a dosing profile was established as shown in Figure 52. Unfortunately, this shows that a constant dosing regime at the minimal values required could not be achieved and based upon the time allowed no other commercially available powder doser was found to enable this task. Designs for bespoke, custom-made units have been prepared but these still require building and testing.

Although not optimal, the system was run as a proof of concept showcasing potential for continuous extraction and recirculation of the aqueous phase containing any unreacted sugar and the Lewis acid catalyst (which could be reused as previously demonstrated). This solution could be supplemented with fresh sugar starting material enabling replenishment of the input solution. This by necessity required manual operation of the doser to limit the quantities of sugar added per unit time. Work is ongoing to improve on this and validate the potential for truly continuous operation.

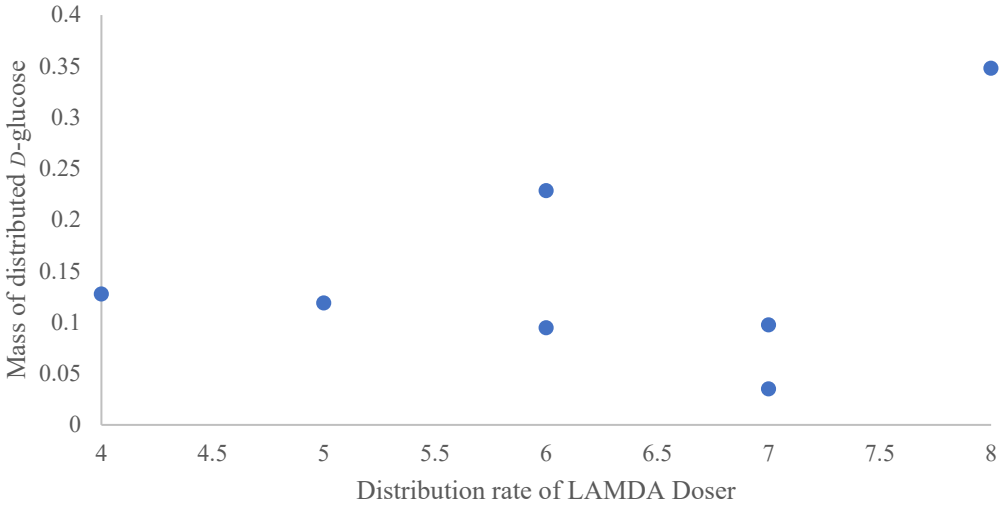

Figure 52. Calibration plot of LAMDA Doser.

2.3 Conclusion

The starting materials of *D*-(+)-glucose (**2**) and *D*-(+)-galactose (**3**) can be sourced from easily accessible biomass or derived from sources such as lactose through enzymatic hydrolysis. In this work the model reaction using *D*-(+)-glucose (**2**) was re-evaluated to estimate the parameter set-up for flow processing. The tracked reaction monitored through the use of an internal standard showed a conversion of 91% representing the combined acyclic **6** and cyclised **7** compounds after 2 h reaction time at 90 ℃. At a higher reaction temperature of 98 ℃, an 83% isolated yield of compound **7** was obtained.

The starting point for the design of experiments in flow were selected based on these batch processes - using Q = 0.4 mL min^{-1} and T = 100, 110, 120 °C. It was found that water sources in our laboratory which were found to be basic could have contributed to the reduced yield of compound **7**. At an elevated temperature of 110-120 °C and 0.4 mL min^{-1}, significant decomposition was observed. An extended 24 h process run showed steady state operation from 4 h and gave a consistent recovery of product. Trials to demonstrate the catalyst sustainability through recycling over five sequential reuses proved viable. The crystal structure of **7** was obtained, while the other diastereoisomer **7a** was not isolated by HPLC chromatographyand the structure can only be proposed as shown in the Experimental procedure section. The work pioneered using *D*-glucose was repeated with *D*-(+)-galactose (**3**) at two scales yielding 78% (50 mmol) and 85% (175 mmol) respectively. This transformation produced a mixture of diastereoisomers in a 1.9 to 1 ratio and when using the recycled stock this did not show a significant change in diastereoisomer ratio.

Overall, the translation of the Lewis-catalysed Knoevenagel reaction with *D*-(+)-glucose (**2**) and *D*-galactose (**3**) were established, affording C-glycosal furan derivatives in flow in 83% (**7**) and 85% (**12**) at steady state (calculated yield by ^{1}H NMR spectroscopy analysis) respectively, and indicating potential industrial viability. A 98% consumption of lactose (**1**) was also achieved as estimated by NMR spectroscopic data but this requires further extraction methodology to allow isolation of the product. Initial attempts to derivatize the product through sulfonylation have produced mixed results. The green chemistry metrics for Scheme 9 (2.2.1 Project aim), including atom economy and reaction mass efficiency are summarized in Table 21.

Table 22. Summary of Green metrics of Scheme 9. AE = atom economy, RME = reaction mass efficiency. *Consumption of Lactose.

Reaction	Reactor	Scale/ mmol	Yield/%	AE/%	RME/%
1	batch	50	83	35	29
	flow	735	82	35	29
2	batch	50	78	35	27
	flow	175	85	35	30
3	batch	50	98*	48	47

2.4 Experimental procedure

General Information

Unless specified, reagents were obtained from commercial sources and used without further purification. Organic solutions were concentrated under reduced pressure using a Buchi rotary evaporator and high vacuum was achieved using an Edwards RV5 pump and Schlenk line.

Solvents and liquids

Table 23. Lists of solvents and liquids.

Name	Grade	Catalogue No.	Volume/ L	Brand
Acetone	AR	A/0600/17	2.5	Fisher Scientific UK LTD
Acetonitrile	HPLC	A/0627/15	2.5	Fisher Scientific UK LTD
Acetonitrile	99.9%, Extra Dry over Molecular Sieve, AcroSeal™	10363413	0.5	Fisher Scientific UK LTD
Chloroform	99+%	10236110	2.5	Fisher Scientific UK LTD
Dichloromethane	AR	10784941	2.5	Fisher Scientific UK LTD
Diethyl ether	SLR	D/2400/17	2.5	Fisher Scientific UK LTD
N,N-Dimethylformamide	HPLC	D/3846/17	2.5	Fisher Scientific UK LTD
Ethanol	Absolute Reagent Grade (99.8%)	E/0650DF/17	2.5	Fisher Scientific UK LTD
Ethyl acetate	AR	E/0900/17	2.5	Fisher Scientific UK LTD
Hexane				
Hydrochloric acid	37% aq.	10000180	2.5	Fisher Scientific UK LTD
2-Propanol	SLR	P/7490/17	2.5	Fisher Scientific UK LTD

Liquid Nitrogen	/	557	25	British Oxygen Company
Methanol	AR	M/4000/17	2.5	Fisher Scientific UK LTD
4-Methyltetrahydrofuran				
Tetrahydrofuran	SLR	T/0700/PB17	2.5	Fisher Scientific UK LTD
Tetrahydrofuran	99.85%, Extra Dry, Unstabilized, AcroSeal™	15245508	1	Fisher Scientific UK LTD
Toluene	AQ	T/2300/17	2.5	Fisher Scientific UK LTD
Trifluorotoluene	≥99%	547948-2L	2	Merck Life Science UK Ltd

GAS

Oxygen Cylinder size W, 1-W, British Oxygen Company.

Guidelines for Using Purified vs. Crude Material in synthetic sequence

Crude reaction mixtures were employed in subsequent synthetic steps when spectroscopic analysis confirmed that side products did not interfere with the desired transformation. Compounds were consistently found to be more tractable to purify in the later stages of the synthetic sequence. For any reactions proceeding with crude material, yields are reported as estimates. Unless otherwise specified, a small portion of the material was purified for all analytical characterization.

Flash Chromatography

Unless specified, flash chromatography was performed using Merck Silica gel high-purity grade (9385), pore size 60 Å, 230-400 mesh particle size.

TLC

Thin-Layer Chromatography was performed using Merck TLC silica gel 60 with glass support and visualised by UV-irradiation or a $KMnO_4$ stain. The retention factor (R_f) is given by

$$\textbf{Equation 12}.\ R_f = \frac{\text{Distance traveled by the compound}}{\text{Distance traveled by the solvent front}}$$

and reported in 2 decimal places under specified solvent ratio.

Calculated yield

This is estimated by ^{1}H NMR spectroscopic integration analysis, excluding peaks from ethyl acetate, 2,4-pentanedione, diastereoisomer and 1-(2-methyl-5-(1,2,3,4-tetrahydroxybutyl)furan-3-yl)ethenone.

For calculations of estimated yield by NMR

Equations 13 and **14** below describe the method for calculating the estimated yield using NMR with an internal standard.

Equation 13. $$n_p = \frac{\frac{I_p}{N_p}}{\frac{I_{is}}{N_{is}}} \times n_{is}$$

Equation 14. $$Yield = \frac{n_p \times Mr_p \times \frac{m_p}{m_{p-nmr}}}{n_{sm} \times Mr_p} \times 100$$

The variables used are defined as follows:

p (product)

is (internal standard)

n (number of moles)

I (integral)

N (number of protons),

Mr (molecular mass),

m (mass),

p-nmr (product in NMR sample),

sm (starting material).

NMR Spectroscopy

Nuclear Magnetic Resonance (NMR) spectra were recorded on:

Table 24. A summary of spectrometer used to obtain NMR spectra.

Spectrometer	Operating frequencies for ^{1}H/ Hz	Operating frequencies for ^{13}C/ Hz
Bruker 700 MHz spectrometer (name: E7)	699.73	175.95
Varian 600 MHz P6 spectrometer (name: P6)	599.42	150.72
Bruker 400 MHz spectrometer (name: N4)	400.20	100.63
Bruker 400 MHz spectrometer (name: B4)	400.07	100.60
Bruker 400 MHz spectrometer (name: A4)	399.95	100.57

Data for ^{1}H NMR are reported as follows:

^{1}H NMR (Operating frequency, solvent) δ/ ppm chemical shift (multiplicity, coupling constant (Hz), integration, ^{1}H assignment).

- ^{1}H NMR are reported relative to residual solvent: $CDCl_3$ (δ 7.26 ppm), DMSO-d_6 (δ 2.50 ppm), MeOD-d_4 (δ 3.31 ppm), MeCN-d_3 (δ 1.94 ppm).
- Multiplicities are reported as follows: s = singlet, d = doublet, t = triplet, q = quartet, sept. = septet, m = multiplet.
- Coupling constants (*J*) were measured to the nearest 0.1 Hz.
- ^{1}H assignment numbers were highlighted in red, consistent with those shown in the skeletal structure in ChemDraw.

Data for ^{13}C NMR are reported as follows:

^{13}C NMR (Operating frequency, solvent) δ/ ppm chemical shift (carbon assignment)

- ^{13}C NMR spectra are reported relative to CDCl3 (δ 77.16 ppm) and DMSO-d_6 (δ 39.52 ppm), MeOD-d_4 (δ 49.00 ppm), MeCN-d_3 (δ 1.32 ppm).
- ^{13}C assignment numbers were highlighted in red, consistent with those shown in the skeletal structure in ChemDraw.

DEPT-135, COSY, HSQC, HMBC, PSYCHE and NOESY experiments were used in structural assignments for key molecules. For example, carbon assignments were made only when supported by HSQC and HMBC evidence; otherwise, these were left unassigned.

IR

Infrared spectra were recorded neat on a Perkin-Elmer Spectrum Two FT-IR spectrometer. The absorbency of the peaks was defined as: weak (w, < 40% of most the intense peak), medium (m, 40 - 75% of the most intense peak), strong (s, > 75% of the most intense peak) and broad (br).

Mass spectroscopy

Both low- and high-resolution mass spectrometry were performed using the indicated techniques.

1. Low-resolution gas chromatography–mass spectrometry, EI GC non polar SLOW GRADIENT (Ultra) analyses, was conducted using a Shimadzu QP2010-Ultra system equipped with an Rxi-5Sil MS column (0.15 μm × 10 m × 0.15 mm). Electron ionization (EI) mode was employed with helium as the carrier gas (flow rate: 0.41 mL min^{-1}). The oven temperature was programmed from 30 °C to 300 °C at a rate of 15 °C min^{-1}. A 0.5 μL sample was injected using a 5:1 split/splitless ratio.
2. Low-resolution liquid chromatography–mass spectrometry (LC-MS) analyses were conducted using an SQD mass spectrometer coupled with an Acquity UPLC system (Waters Ltd., UK) through flow injection analysis (FIA). The solvent flow from the UPLC system was introduced into the electrospray ionisation (ESI) source, generating alternating positive and negative ions. The system operated over a mass range of 100–2000 u. UV absorbance data were collected using an Acquity photodiode array detector across the 210–400 nm wavelength range. Either ESI-LC C18 MeOH or ESI-LC C18 MeCN methods was employed as given below:

Table 25. The summarised information of ESI-LC C18 MeOH or ESI-LC C18 MeCN methods.

RA4 Experiment	**Column (Dimensions)**	**Mobile phase**	**Gradient**			
			Time (min)	**Flow Rate (mL min^{-1})**	**%A**	**%B**
ESI-LC C18 MeOH (SQD)	Acquity UPLC BEH C_{18} 1.7 μm (2.1 mm × 50 mm)	Water containing formic acid (0.1% $\frac{v}{v}$):Methanol	0	0.6	95	5
			0.2	0.6	95	5
			4	0.6	5	95
			4.5	0.6	5	95
			5	0.6	95	5
			0	0.6	95	5

ESI-LC C18	Acquity	Water containing	0.2	0.6	95	5
MeCN	UPLC BEH	formic acid	4	0.6	5	95
(SQD)	C_{18} 1.7 µm	(0.1% $\frac{v}{v}$):Acetonitrile	4.5	0.6	5	95
	(2.1 mm ×		5	0.6	95	5
	50 mm)					

3. High-resolution mass spectrometry (accurate mass) analyses were performed using a QToF Premier mass spectrometer coupled with an Acquity UPLC system (Waters Ltd., UK). Flow injection analysis (FIA), loop injection, and ultra-performance liquid chromatography (UPLC) methods were employed, depending on the analysis requirements. The solvent stream from the UPLC system was introduced into the electrospray ionisation (ESI) source, which generated either positive or negative ions, as specified. The standard operating mass range was 100–2000 u. UV absorbance data were collected using an Acquity photodiode array detector across the 210–400 nm wavelength range.

   - *FIA:* The sample solution was infused (~10 µL min^{-1}) into a continuous solvent stream (0.2 mL min^{-1}) of acetonitrile or methanol.
   - *Loop injection:* The sample was directly injected into a solvent flow (0.2 mL min^{-1}) of acetonitrile or methanol.
   - *UPLC:* Reverse-phase chromatography was available to support tailored separations, although not applied in this thesis.

   Accurate mass measurements were reported in parts per million (ppm) and millidaltons (mDa), with a deviation tolerance of 3 mDa, in accordance with the Journal of Organic Chemistry Author Guidelines[189] and 5 ppm (EI and CI) or 10 ppm (FAB or LSIMS) with Experimental details and characterisation required for journal articles by Royal Society of Chemistry.[190]

Melting point

Melting points were recorded on an Optimelt automated melting point system and are uncorrected. The heating ramp gradient was set at 5 – 10 °C min^{-1}.

X-ray crystal analysis

X-Ray crystal structure determination was performed by crystallographers at the Department of Chemistry, University of Durham on a Bruker D8 Venture diffractometer with PHOTON 100 CMOS area detector, using Mo-Kα radiation from Incoatec IμS microsources with focusing mirrors. The crystals were cooled using a Cryostream 700 (Oxford Cryosystems, (Oxford, Oxfordshire, UK) open-flow N_2 gas cryostat. The structures were solved by dual-space intrinsic phasing (SHELXT program)[191] and refined by full-matrix least squares using SHELXL[192] software on Olex2 platform.[193]

The probability level of the thermal ellipsoids is 50% for all the samples.

1-(5-(3*R*,4*R*-dihydroxytetrahydrofuran-2-yl)-2-methylfuran-3-yl)ethenone (7) [144]

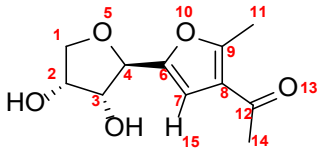

Chemical Formula: $C_{11}H_{14}O_5$
Exact Mass: 226.08

Batch process:

The monosaccharide *D*-(+)-glucose (**2**) (9.0 g, 50.0 mmol), 2,4-pentanedione (**5**) (7.5 g, 75.0 mmol), and $CeCl_3.7H_2O$ (4.7 g, 12.5 mmol) were dissolved in distilled water (25 mL, pH 7) at room temperature. The reaction mixture was heated at reflux (98 °C) for 2 h 30 min. The organic layer was extracted with ethyl acetate (4 x 100 mL), concentrated in vacuo to give a yellow-brown solid (Calculated yield: 9.2 g, 85%). The solid was recrystallised from acetone to afford the white crystal for crystal analysis below.

Flow synthesis:

The monosaccharide *D*-(+)-glucose (**2**) (132.4 g, 735.0 mmol) and $CeCl_3 \cdot 7H_2O$ (68.5 g, 183.8 mmol) were dissolved in distilled water (367.5 mL, pH 7) at room temperature. The solution (Flow rate: 0.321 mL min^{-1}) and 2,4-pentanedione (**5**) (110.4 g, 1102.5 mmol, Flow rate: 0.079 mL min^{-1}), were joined with a T-connector and were progressed (combined flow rate: 0.4 mL/min) into a 60 mL PTFE reactor which was set at 100 °C (Run time of the stock = 24 h). The organic layer was extracted with ethyl acetate (1470 mL × 4) into a reaction flask, dried over Na_2SO_4, and concentrated *in vacuo* to afford the titled compound. (Calculated yield: 136.0 g, 82%).

^{1}H NMR (400 MHz, DMSO) δ/ppm 6.80 (s, 1H, H7), 5.13 (d, *J* = 6.2 Hz, 1H, H15), 5.03 (d, *J* = 3.6 Hz, 1H, H16), 4.49 (d, *J* = 6.8 Hz, 1H, H4), 4.12 (m, 2H, H2+H3), 4.02 (m, 2H, H1), 3.65 – 3.59 (m, 1H, H1), 2.57 – 2.47 (m, 3H, H14), 2.37 (d, 3H, H11);

^{13}C NMR (101 MHz, DMSO) δ/ppm 194.20 (C12), 157.86 (C9), 151.58 (C6), 122.19 (C3), 109.59 (C7), 76.47 (C2), 74.98 (C4), 73.22 (C3), 70.89 (C1), 29.65 (C11), 14.55 (C14);

LC-MS R_t = 1.41 min m/z = 227.5 $[M]^+$.

The structure and connectivity were confirmed by single crystal X-ray crystallography, performed by Dr Dmitry S. Yufit of the Durham University X-Ray Crystallography Service and has the unique identifier of '22srv258'.

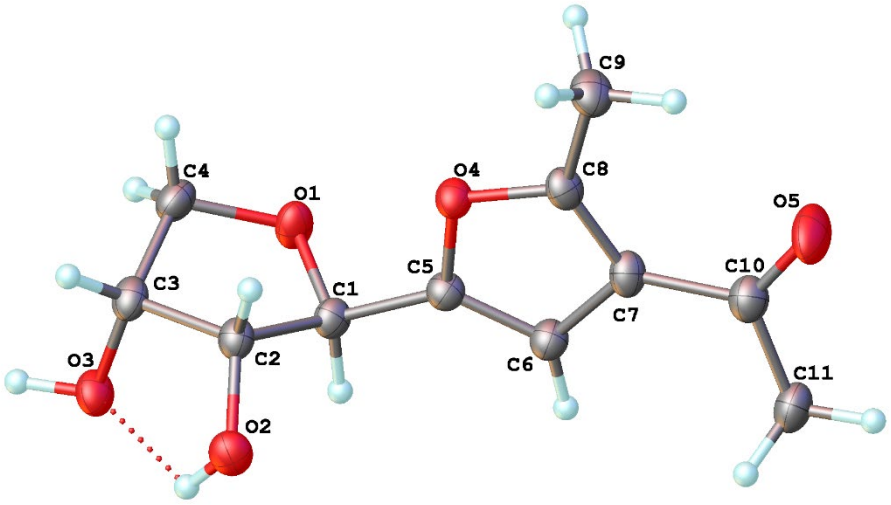

Space group	$P2_1$
a/Å	9.7418(4)
b/Å	6.0691(2)
c/Å	9.9186(4)
α/°	90
β/°	112.534(2)
γ/°	90

1-(2-methyl-5-(1,2,3,4-tetrahydroxybutyl)furan-3-yl)ethenone (6) [134]

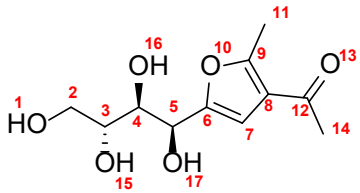

Chemical Formula: $C_{11}H_{16}O_6$
Exact Mass: 244.0947

A byproduct of synthesizing **7**.

Isolated yield: ~20 mg.

^{1}H NMR (400 MHz, DMSO) δ/ppm 6.59 (d, *J* = 0.9 Hz, 1H, H7), 5.13 (d, *J* = 7.3 Hz, 1H, H5), 4.75 (appt. ddd, *J* = 7.4, 2.3, 1.0 Hz, 1H, H4), 4.65 (d, *J* = 5.5 Hz, 1H, H2), 4.57 (d, *J* = 7.2 Hz, 1H, H2), 4.38 (t, *J* = 5.6 Hz, 1H, H3), 3.52 (m, H1+H15+H16+H17), 2.51 (q, *J* = 2.0 Hz, 3H, H11), 2.36 (s, 3H, H14).

^{13}C NMR (101 MHz, DMSO) δ/ppm 194.24 (C12), 156.38 (C9), 155.55 (C6), 122.19 (C8), 107.26 (C7), 72.96 (C5), 71.39 (C4), 66.32 (C3), 63.77 (C2), 29.63 (C14), 14.54 (C11).

IR (neat) ν = 3288 (br, OH) 1677 (C=O) 1640 (C=O).

LC-MS: R_t = 0.27 min, m/z 245.29 $[M+H]^+$.

Melting point: 145-147.5 °C, literature 152 ℃.[134]

1-(5-((3*S*,4*R*)-3,4-dihydroxytetrahydrofuran-2-yl)-2-methylfuran-3-yl)ethan-1-one (11)

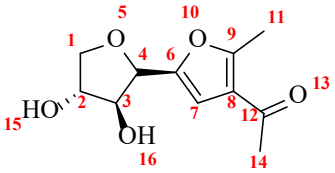

Chemical Formula: $C_{11}H_{14}O_5$
Exact Mass: 226.08

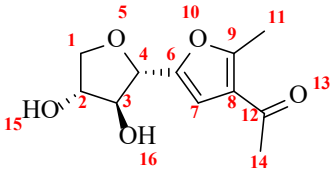

Chemical Formula: $C_{11}H_{14}O_5$
Exact Mass: 226.08

NB: The predicted structures of this reaction are provided. The reaction provided a mixture of two compounds and were separated by HPLC column. Both compounds are brown-orange oil and no crystal structure was confirmed. The remaining experimental procedure and data analysis are presented below.

Batch process:

Follow the procedure to synthesize **6** and use *D*-(+)-galactose (**3**) (50 mmol) instead of *D*-(+)-glucose (**2**). The product was a brown-orange oil. The diastereoisomers mixture was prepared as 20 mg/ mL in deionized water and were separated by Interchim Puriflash with acetonitrile and water (5:95).

Flow synthesis:

Follow the procedure to synthesize **6** and use *D*-(+)-galactose (**3**) (175 mmol).

Minor diastereoisomer

Yield: Batch 2.9 g (26%); flow 11.5 g (29%).

^{1}H NMR (599 MHz, d_6-DMSO) δ/ppm 6.63 (s, 1H,H7), 5.23 (s, 1H,H15 or H16), 5.10 (s, 1H,H15 or H16), 4.80 (d, J = 3.6 Hz, 1H,H4), 4.08 (dt, J = 3.9, 1.7 Hz, 1H,H3), 4.03 (dd, J = 9.0, 4.1 Hz, 1H,H1), 3.95 (dd, J = 3.7, 1.7 Hz, 1H,H2), 3.53 (dd, J = 9.0, 1.5 Hz, 1H,H1), 2.47 (d, J = 2.3 Hz, 3H,H14), 2.32 (s, 3H,H11).

^{13}C NMR (151 MHz, d_6-DMSO) δ/ppm 194.17 (C9), 156.94 (C12), 150.34 (C6), 122.20 (C8), 109.21 (C7), 77.46 (C2), 76.97 (C3), 76.53 (C4), 73.45 (C1), 29.55 (C14), 14.49 (C11).

LC-MS: R_t = 0.87 min, m/z 227.16 $[M+H]^+$; HR-MS calculated for $C_{11}H_{15}O_5$ 227.0919, found 227.0928 (Δ = 0.9 mDa; 4.0 ppm).

Optical rotation: + 2.15˚.

Major diastereoisomer

Yield: Batch 5.3 g (46%); Flow 22 g (56%).

^{1}H NMR (599 MHz, d_6-DMSO) δ/ppm 6.69 (s, 1H, H7), 5.48 (s, 1H, H15 or H16), 5.13 (s, 1H, H15 or H16), 4.41 (d, J = 5.2 Hz, 1H, H4), 4.07 (dd, J = 5.2, 3.3 Hz, 1H, H3), 4.02 (dt, J = 5.4, 3.5 Hz, 1H, H2), 3.87 (dd, J = 9.2, 5.4 Hz, 1H, H1), 3.63 (dd, J = 9.2, 3.7 Hz, 1H, H1), 2.49 (s, 3H, H14), 2.33 (s, 3H, H11).

^{13}C NMR (151 MHz, d_6-DMSO) δ/ppm 194.10 (C9), 157.51 (C12), 151.67 (C6), 122.23 (C8), 109.02 (C7), 80.96 (C3), 79.82 (C4), 77.41 (C2), 73.40 (C1), 29.58 (C11), 14.49 (C14). LC-MS R_t = 1.20 min m/z = 227.1 $[M]^+$.

LC-MS: R_t = 1.22 min, m/z 227.19 $[M+H]^+$; HR-MS calculated for $C_{11}H_{15}O_5$ 227.0919, found 227.0932 (Δ = 1.3 mDa; 5.7 ppm).

Optical rotation: + 12.50˚

1-(5-((2*S*,3*R*,4*R*)-4-hydroxy-3-(((2*R*,3*R*,4*S*,5*R*,6*R*)-3,4,5-trihydroxy-6-(hydroxymethyl)tetrahydro-2*H*-pyran-2-yl)oxy)tetrahydrofuran-2-yl)-2-methylfuran-3-yl)ethan-1-one (12)

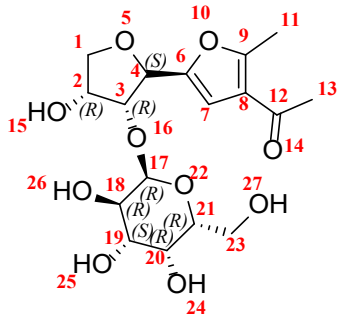

Chemical Formula: $C_{17}H_{24}O_{10}$
Exact Mass: 388.1369

Batch process:

A sample of lactose (**1**) (17.1 g, 50.0 mmol), 2,4-pentanedione (**5**) (7.5 g, 75.0 mmol), and $CeCl_3.7H_2O$ (4.7 g, 12.5 mmol) were dissolved in distilled water (25 mL, pH 7) at room temperature and heated to reflux (~ 25 min). The reaction mixture was heated at reflux (98 °C) for 2 h. The organic layer was extracted with ethyl acetate (3 × 50 mL) to remove side products. The target compound remained in the aqueous phase and crystals was discovered following slow evaporaton..

Flow synthesis:

A sample of lactose (**1**) (8.56 g, 25 mmol) and $CeCl_3 \cdot 7H_2O$ (2.33 g, 6.25 mmol) were dissolved in distilled water (12.5 mL, pH 7) and warmed to 80 °C until a homogenous solution was obtained. This solution mixture (Flow rate: 0.824 mL min^{-1}) and 2,4-pentanedione (**5**) (3.75 g, 37.5 mmol, flow rate: 0.176 mL min^{-1}), were joined with a T-connector and were progressed (combined flow rate: 1 mL/min) into a 60 mL PTFE reactor which was set at 100 °C (Residence time = 1 h). The organic layer was extracted with ethyl acetate (3 × 25 mL) to remove side products. The target compound remained in the aqueous phase and can be crystallized by slow evaporation.

White crystal

^{1}H NMR (599 MHz, DMSO) δ/ppm 6.81 (s, 1H, H7), 5.35 (d, *J* = 3.5 Hz, 1H, OH), 4.80 – 4.74 (m, 2H, OH), 4.67 (d, *J* = 6.8 Hz, 1H), 4.58 – 4.51 (m, 1H, OH), 4.43 (d, *J* = 4.6 Hz, 1H, OH), 4.36 (dd, *J* = 6.9, 4.6 Hz, 1H), 4.31 (p, *J* = 3.6 Hz, 1H), 4.25 (d, *J* = 7.3 Hz, 1H), 4.01 – 3.96 (m, 1H), 3.64 (dd, *J* = 9.4, 3.0 Hz, 1H), 3.61 (t, *J* = 3.9 Hz, 1H), 3.50 – 3.42 (m, 1H), 3.35 – 3.23 (m, 4H), 2.49 (s, 3H), 2.33 (s, 3H).

^{13}C NMR (151 MHz, DMSO) δ/ppm 194.18, 157.92, 150.85, 122.17, 109.92 (C7), 103.67, 81.69, 75.67, 74.81, 73.54, 72.59, 71.26, 69.74, 68.21, 60.39, 29.54, 14.51.

IR (neat) ν = 3392 (br, OH) 2914 (m) 1641 (s, C=O) 1567 (m, aromatic C-C).

LC-MS R_t = 1.39 min, m/z 389.40 $[M-H]^+$; HR-MS calculated for $C_{17}H_{25}O_{10}$ at 389.1448, found 389.1443 (Δ = -0.5 mDa; - 1.3 ppm).

The structure and connectivity were confirmed by single crystal X-ray crystallography, performed by Dr Toby Blundell of the Durham University X-Ray Crystallography Service and has the unique identifier of '23srv280'.

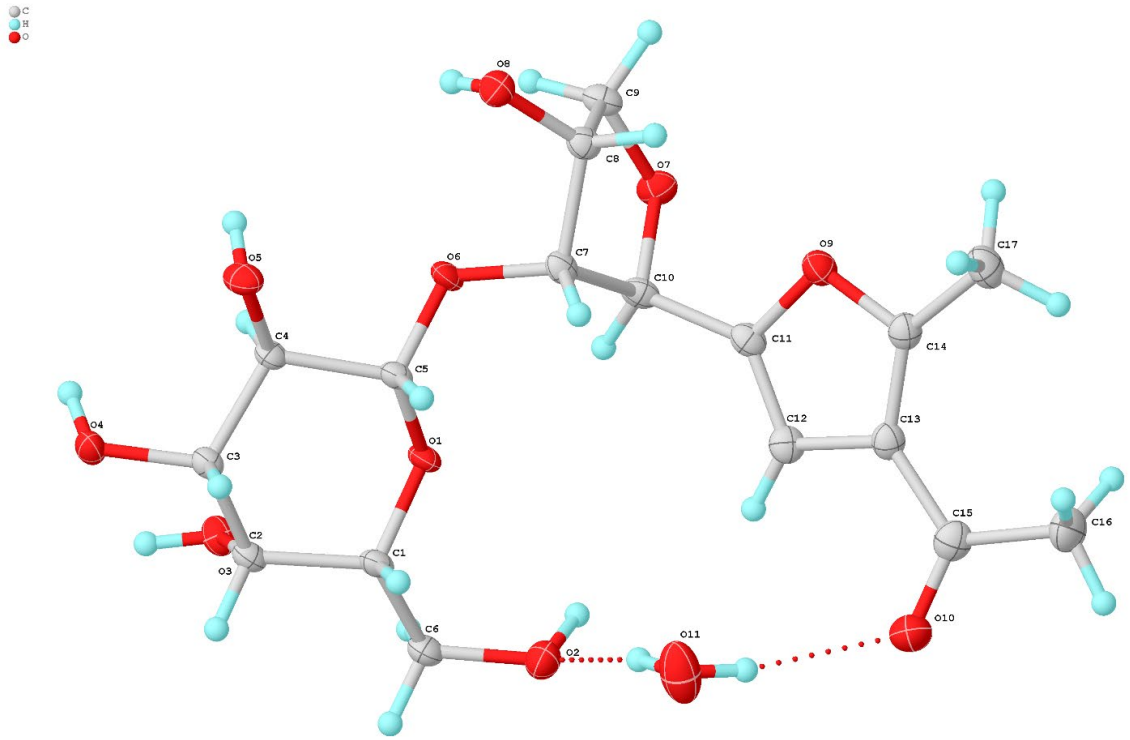

Space group	$P2_12_12_1$
a/Å	4.7326(2)
b/Å	9.9969(5)
c/Å	38.1294(18)
α/°	90
β/°	90
γ/°	90

Reference[144]

2.5 Appendix

Internal standard calculations

A stock solution of the internal standard was prepared. The standard was added after the sample was taken from the reaction mixture and the time was recorded once the internal temperature reached 90 ℃. (To get a better resolution of the ^{1}H NMR spectra, the sample was prepared with 10 mg, 3-(trimethylsilyl)-1-propanesulfonic acid sodium salt in 50 μL of D_2O and 387.5 μL of H_2O and 50 μL of solution mixture.)

Note that, as 50 μl could result in the error of integral analysis (as shown in the charts below), a better way is to add the internal standard in the reaction mixture at the beginning.

Calculation of flow parameters in chapter 2

Known information:

The reagents used in this reactions were A, B, C, and D listed below.

A. *D*-(+)-glucose 9.0 g, 50 mmol
B. $CeCl_3 \cdot 7H_2O$ 7.51 g, 75 mmol
C. H_2O, 25 mL
D. 2,4-pentanedione, 4.66 g, 12.5 mmol

The solution pumped at the rate Q_{pump_A} has a volume of V1:

V1 = Volume (A + B + C) = 31.5 mL (by measurement)

The 2,4-pentane-dione pumped at the rateQ_{pump_B} has a volume of V2:

V2 = Volume (D) = mass (D)/ density (D) = $\frac{n(D) \times Mr\ (D)}{\rho\ (D)} \approx 7.7\ mL$

Flow rate calculation:

Q_{pump_A} and Q_{pump_B} can be calculated by

Sum of the flow rate equals the flow rate of pump A plus the flow rate of pump B:

$$Q_{total} = \frac{\text{Volume}}{\text{Residence time}} = \frac{60\ \text{mL}}{150\ \text{min}} = 0.4\ \text{mL min}^{-1}$$

$Q_{total} = 0.4\ \text{mL min}^{-1} = Q_{pump\_A} + Q_{pump\_B}$

The time required to pump the solution from pump A and pump B are the same:

$$t_{pump\_A} = t_{pump\_B} \Rightarrow \frac{V1}{Q_{pump\_A}} = \frac{V2}{Q_{pump\_B}} \Rightarrow \frac{31.5\ mL}{Q_{pump\_A}} = \frac{7.7\ mL}{Q_{pump\_B}}$$

Hence,

$Q_{pump\_A} = 0.321\ \text{mL min}^{-1}$

$Q_{pump\_B} = 0.079\ \text{mL min}^{-1}$

Time estimations:

For a single unit, the volume of reaction mixture is smaller than reactor coils:

Residence time = Volume of reactor coils/ flow rate = 60 mL/ 0.4 mL min^{-1} = 150 min

There are three time points that require attention in this flow reaction:

E. time to change the receiver flask.
F. time to change solution supply to water (pure solvent).
G. Time to complete the collection of the reacted solution.

Figure 53 below shows the time E, F, G for a single unit run:

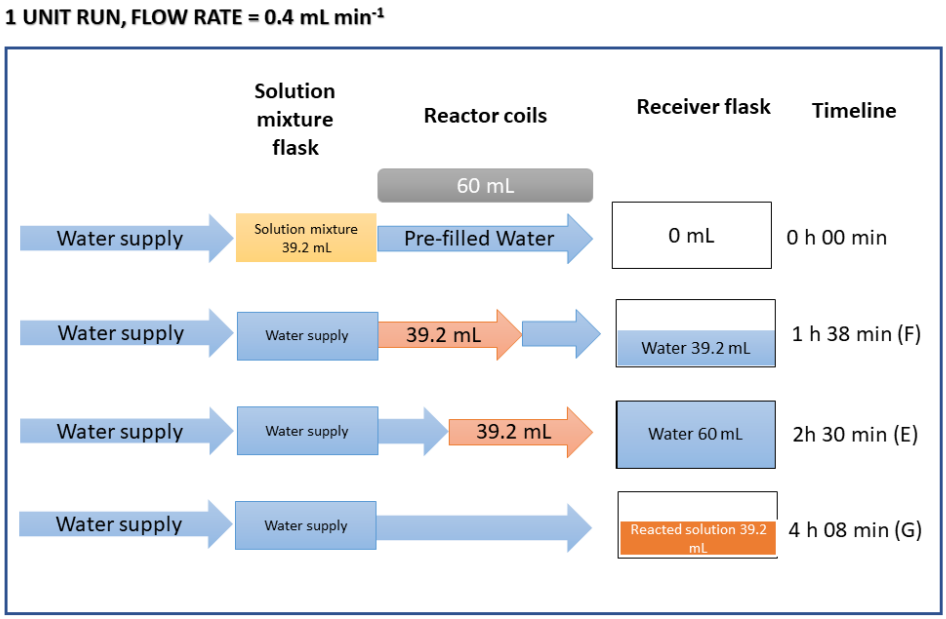

Figure 53. Calculation methodologies for 1 unit run of flow reaction.

For 2 units run, the volume of reaction mixture is greater than the volume of reactor coils, the order of time E and F is changed (Figure 54). For N (N>1) units run, the time requried for E, F, and G for this flow reaction can be calculated by the formula given in Figure 55. While the volume of solution mixture is greater than the volume of reactor coils,

Residence time = (Volume of single unit * multiples)/ flow rate (= 0.4 mL min^{-1})

Hence, Multiples (24 h run) = (residence time * flow rate)/ volume of single unit ≈ 14.7

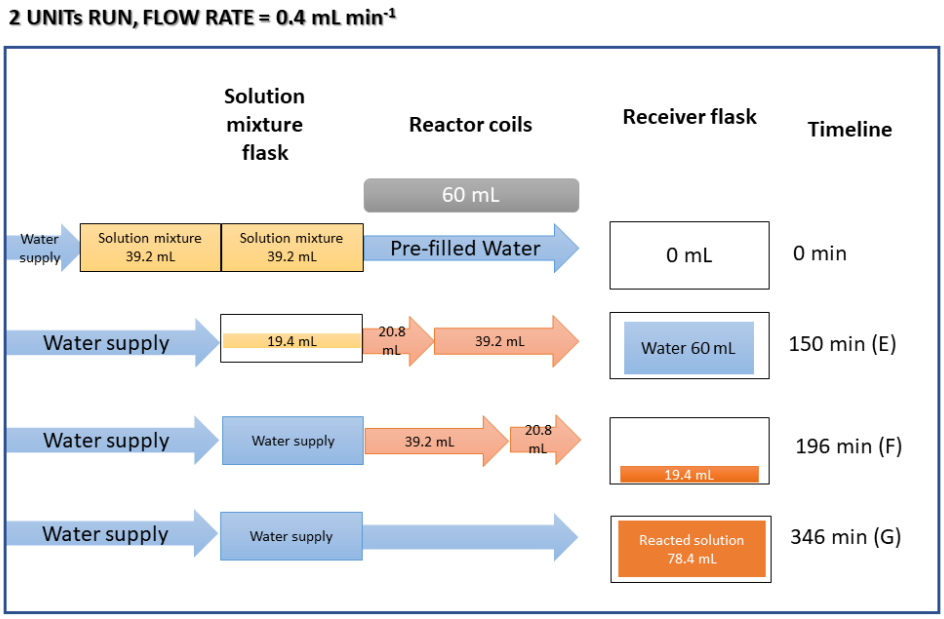

Figure 54. Calculation methodologies for 1 unit run of flow reaction.

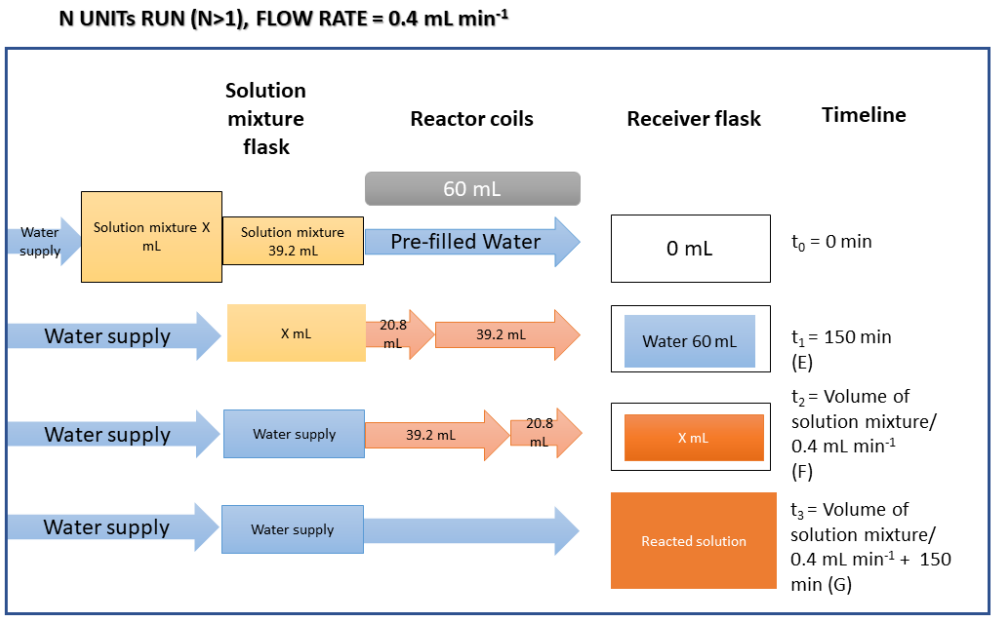

Figure 55. Calculation methodologies for N (N>1) unit run of flow reaction.

Part II

Methodology development

for small, broadly applicable

building blocks:

- 2-hydroxy-6-methoxybenzaldehyde
- 2-hydroxy-6-methoxyacetophenone

Introduction

Plant secondary metabolites are produced as adaptive responses to various biotic and abiotic stresses, including drought, salinity, UV radiation, pathogens, and herbicide exposure. Many of these metabolites have been isolated and evaluated for their bioactive properties, with numerous compounds demonstrating potential for treating human diseases, such as cancer. Benzaldehyde derivatives (Figure 56, **18**) represent a class of aromatic secondary metabolites naturally found in plants, fruits, fungi, and microorganisms Figure 56, **19**.[194-197] Researchers have isolated these compounds and identified a broad spectrum of bioactivities, including anti-inflammatory,[198, 199] cytotoxic,[200] anti-fungal,[196] antitrypanosomal,[201] and Alzheimer's disease inhibitory properties.[202] Beyond their pharmacological applications, benzaldehyde derivatives also serve as precursors in the synthesis of other secondary metabolites such as chalcones,[203] function as organic catalysts in photoinduced polymerization[204] and are integrated as part of biocidal polymers with antimicrobial properties.[205]

Alongside benzaldehydes, acetophenones represent another class of secondary metabolites. In these compounds, an acetyl group replaces the aldehyde group on the phenyl ring (Figure 56, **19** vs **18**). Acetophenone derivatives have been found in more than 24 plant families and fungi strains with diverse biological activities and multiple applications across industries (plant examples are shown in Figure 57).[206-208] Their antifungal properties are utilized in eco-friendly synthetic pesticides.[206] Compounds such as paeonol (2-hydroxy-4-methoxyacetophenone)[209] and apocynin (4-hydroxy-3-methoxyacetophenone),[210] noted in various traditional herbal medicine used for over a millennium, display potent anti-inflammatory effects. Additionally, acetophenones as a general class demonstrate anticancer, analgesic, antioxidant, cardioprotective, neuroprotective, and antidiabetic properties. Their distinctive odour makes them valuable in perfumes and cosmetics[206, 211] and they are often incorporated into sunscreens generating skin protection against harmful UV radiation.[212] Finally, both benzaldehydes and acetophenones are key building blocks in synthetic organic chemistry. As such access to these compounds is of particular interest to the synthetic community.

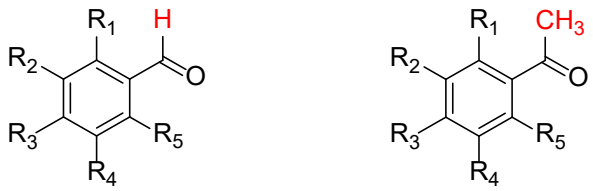

Figure 56. Structure of benzaldehyde derivatives and acetophenone derivatives

Figure 57. Top left: Almonds.[213] Top right: Hericium erinaceus.[200] Bottom Left: Genera Melicope.[214] Bottom right: Genera Acronychia.[215]

Despite extensive research on benzaldehydes and acetophenones, selective positioning of the aldehyde/ acetyl group between the 1,3-dioxygenated system remains relatively underexplored. Two such compound, 2-hydroxy-6-methoxybenzaldehyde (**20**) and 2-hydroxy-6-methxoyacetophenone (**21**), exemplify this rarity and are the focus of the investigation (Figure 58).

SciFinder lists over 1,000 synthetic routes involving compounds **20** and **21** with 89% employing them as intermediates in the synthesis of other structures,[216] including indole derivatives used in UV-detecting devices, and numerous biologically and pharmaceutically significant scaffolds.[86,217-220,203, 221-225,226,227] Notably, these compounds have been explored for therapeutic applications such as progesterone receptor modulators[228] and treatments for gastric cancer[229].

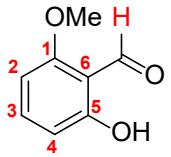

2-hydroxy-6-methoxybenzaldehyde
20

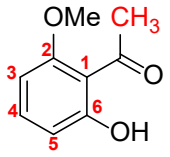

2-hydroxy-6-methoxyacetophenone
21

Figure 58. The structure of 2-hydroxy-6-methoxybenzaldehyde (**20**) and 2-hydroxy-6-methoxyacetophenone (**21**).

However, existing synthetic methods starting from simple reagents often lack regioselectivity, involve multiple steps with strong acids and bases, or omit yield analysis.[230-233] Alternative approaches with more complexed starting material often prepared using strong acids or bases, are costly to obtain.[234-236] Additionally, their commercial availability is still associated with high prices.[237] In Chapter 3 and Chapter 4, we will introduce literature synthesis and novel methodologies for the sustainable and cost-effective synthesis of these two compounds.

Chapter 3

Synthesis of 2-hydroxy-6-methoxybenzaldehyde (20)

3.1 Synthetic analysis of 2-hydroxy-6-methoxybenzaldehyde (20)

Preparation of **20** began with retrosynthetic analysis guided by target-oriented methods as detailed in Sectio 1.3. In principle, the target can either be synthesized by formylation of 3-methoxyphenol (**22**) (Scheme 17-A1) or methylation of 2,6-dihydroxybenzaldehyde (**20**) (Scheme 17-A2) after formylation of resorcinol (**23**) (although this imposes potential selectivity concerns). Two literature references follow such routes; Schemes 17B[238] and 17C[232]. Scheme 17B involves using *n*-BuLi (4 equivalents excess) to perform a directed lithiation at the position *ortho* to both the hydroxyl and methoxy groups on the aromatic ring, with *N*-methylformanilide (**24**) serving as the formylation agent. This reaction requires careful temperature control during base addition and subsequent work-up with the need for strong acids to neutralize any excess base. According to the literature, this method achieved a yield of 61%. On the other hand, Scheme 17C incorporates the desired formylation step as part of a longer, five-step synthesis sequence to produce the starting material, but lacks a reported yield. The harsh conditions and the need for extensive column purification in this process are unsurprising, as both hydroxyl and methoxy groups are known to be *ortho*- and *para*-directing in electrophilic aromatic substitution reactions. Although, position 1 (3-methoxyphenol (**22**), Scheme 17-A1) is sterically hindered, formylation at positions 3 and 5 would be proposed without other limiting factors. Since both retrosynthetic disconnections involve formylation steps, the synthesis was designed around an ortho-directed formylation strategy.

Retrosynthesis analysis

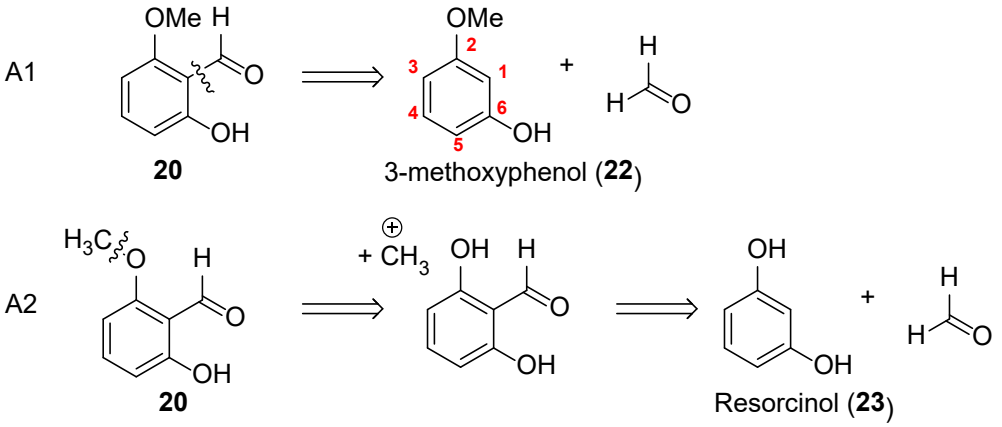

Literature synthesis

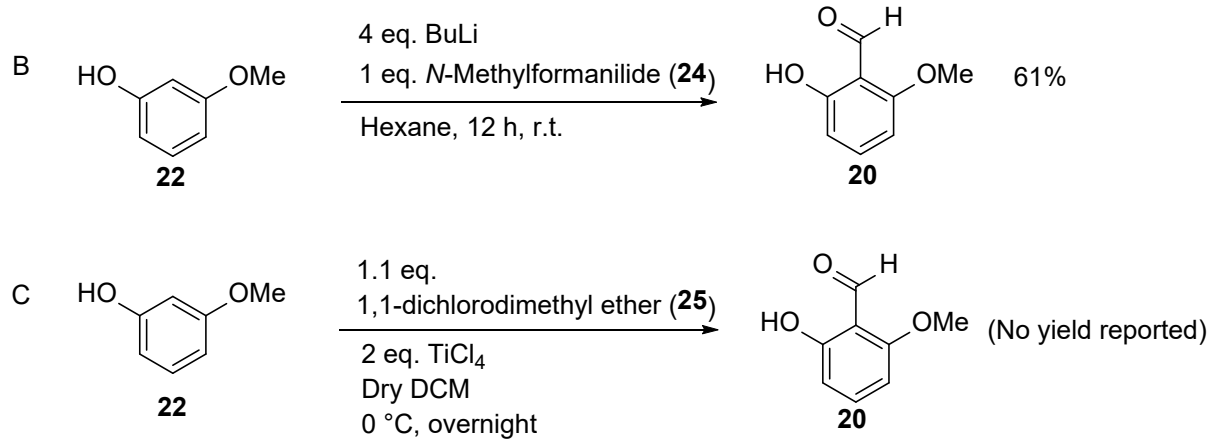

Scheme 17. A. Retrosynthesis of 2-hydroxy-6-methxoybenzaldehyde (**22**). B. Literature synthesis of 2-hydroxy-6-methxoybenzaldehyde (**23**) using *n*-butyl lithium and *N*-methylformanilide (**24**).[238] C. Literature synthesis of 2-hydroxy-6-methxoybenzaldehyde using 1,1-dichloridimethyl ether (**25**) and 2 eq. $TiCl_4$.[232]

There are several well documented formylation of aromatic compounds that possess electron donating group such as phenols, for example the Gattermann-Koch reaction, Reimer-Tiemann reaction,[239] Vilsmeier-Haack reaction,[240] and Duff reaction.[241] These methodologies often rely on relatively harsh conditions or generate poor selectivity for the target, despite continued development and optimization refinement over the years (literature examples given in Scheme 18).[242] In contrast, the Casnati-Skattebøl reaction provides a more environmentally friendly approach while achieving selective *ortho*-formylation using an interesting $MgCl_2$-Et_3N base system (Scheme 19).[243, 244] This reaction is typically conducted with paraformaldehyde and phenol

substrates in tetrahydrofuran or acetonitrile, avoiding the use of corrosive acids and bases or carcinogenic metal complexing agents.[244]

Vilsmeier-Haack formylation

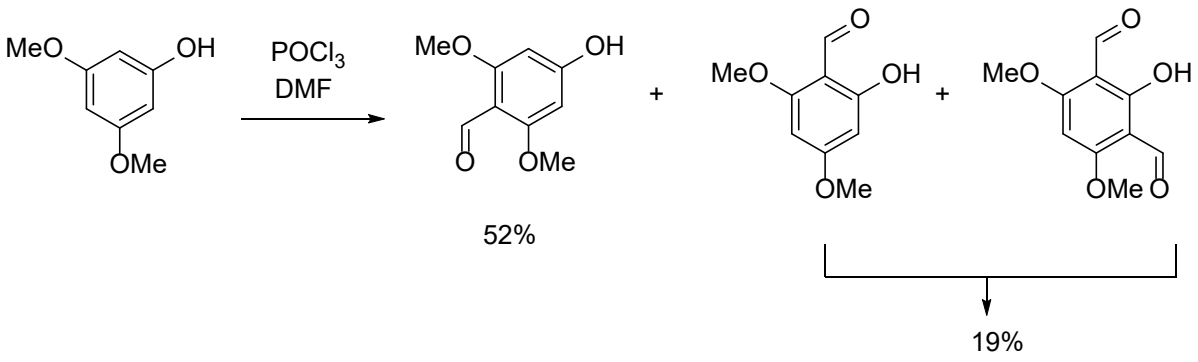

Scheme 18. Literature examples of Vilsmeier Haack formylation of phenol derivatives.

Reaction scheme

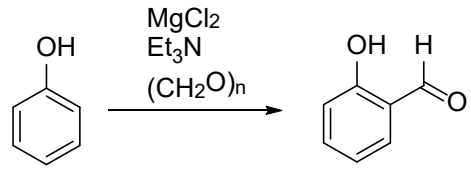

Proposed mechanism

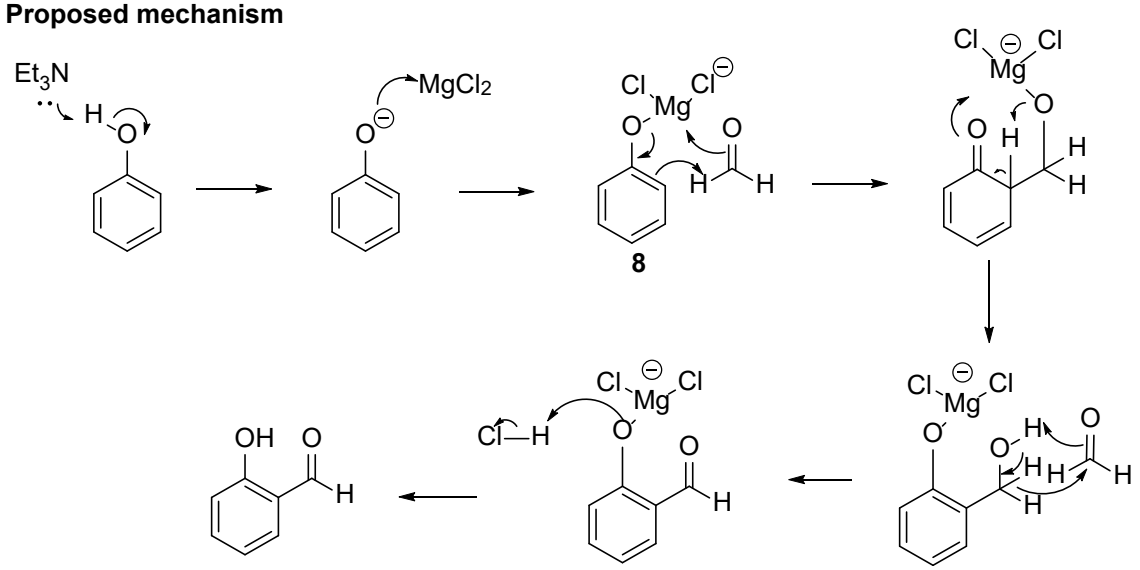

Scheme 19. Reactions scheme and proposed mechanism of Casnati-Skattebøl reaction.

This $MgCl_2$-Et_3N system has been successfully applied to various reactions, including acylation of malonates, α-carboxylation of ketones and Dickmann-type cyclisation.[244] The formation of a reactive phenoxide species in the presence of $MgCl_2$ facilitates *ortho*-selective formylation as illustrated in the proposed mechanism (Scheme 19). For phenol substrates bearing alkyl, alkoxy and halogen substituents at the 2- or 4-positions, good to excellent yields have been achieved (Scheme 20 and Table 26).[245]

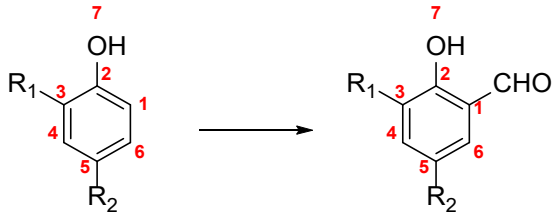

Scheme 20. Formylation of 2 and/or 4 substituted phenols.

Table 26. R_1, R_2 groups and yields of Scheme 20.[245]

Entry	R_1	R_2	Yield
1	F	H	80%
2	Cl	H	87%
3	CH_3	H	99%
4	F	H	85%
5	H	Br	91%
6	H	OCH_3	87%
7	H	CO_2CH_3	88%
8	*tert*-Bu	*tert*-Bu	84%
9	CH_3	CH_3	90%

The proposed synthetic route was developed base on the findings of Akselsen *et al*. 2009 who extended this *ortho*-formylation methodology to a collection of 15 mono-protected resorcinol derivatives (Table 27) bearing chloro- or bromo- or methoxy- substituents adjacent to an electron donating group.[246]

Table 27. Schemes and yields of formylation of 15 mono-protected resorcinol derivatives.

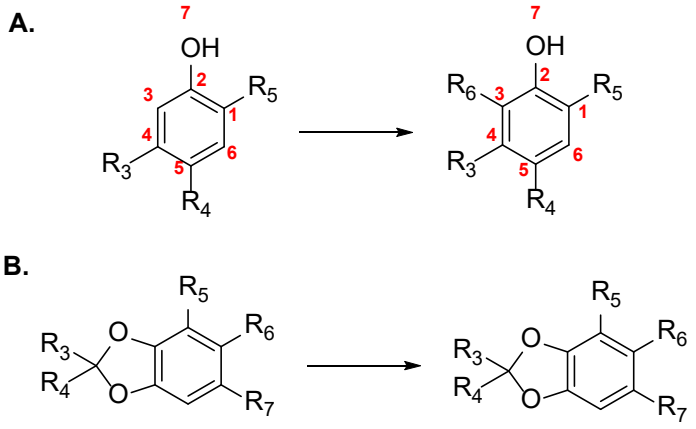

Entry	R_3	R_4	R_5	R_6	R_7	Yield
Scheme A						
1	OMe	H	H →CHO	H	/	92%
2	OBn	H	H →CHO	H	/	88%
3	OTBS	H	H →CHO	H	/	80%
4	OTDS	H	H →CHO	H	/	88%
5	OMe	Cl	H →CHO	H	/	94%
6	OBn	Cl	H →CHO	H	/	85%
7	OTBS	Cl	H →CHO	H	/	60%
8	OTBS	Cl	H →CHO	H	/	73%
9	OMe	Br	H →CHO	H	/	90%
10	OTBS	Br	H →CHO	H	/	73%
11	OTBS	H	Br	H →CHO	/	85%
12	OMe	H	H →CHO	OMe	/	11%
Scheme B						
13	H	H	OH	H →CHO	H	97%
14	H	H	H	OH	H →CHO	45%
15	CH_3	CH_3	OH	H →CHO	H	82%

The 2-hydroxy-4-methoxybenzaldehyde (**26**) was synthesized from 3-methoxyphenol (**22**) (Table 27 Entry 1 and Scheme 21A), as the *ortho*-position is less sterically hindered. This was verified prior to the target synthesis to confirm the reported *ortho*-selectivity and the product structure (Section 3.2.2). To access formylation at the 2-position, a blocking bromo- or chloro- group was employed as depicted in Scheme 21B. Therefore, based upon the literature synthesis, a three-step process was proposed involving: regioselective halogenation of 3-methoxyphenol at position 4, formylation by Casnati-Skattebøl reaction at position 2 and finally dehalogenation to afford the target 2-hydroxy-6-methoxybenzaldehyde (**20**) (Scheme 22). The syntheses will be illustrated in this order in Section 3.2.

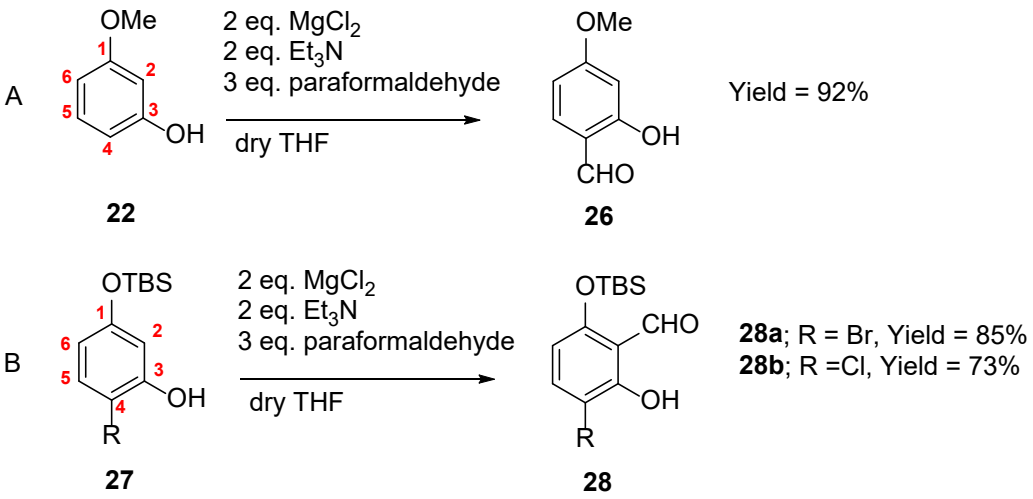

Scheme 21. Formylation of mono-protected resorcinol derivatives.

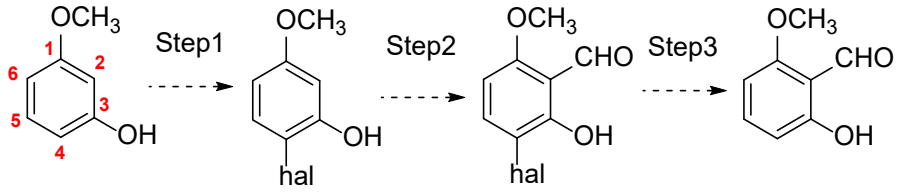

Scheme 22. Proposed synthesis of 2-hydroxy-6-methoxybenzaldehyde (**20**).

3.2 Synthesis of 2-hydroxy-6-methoxybenzaldehyde (21) via brominated 3-methoxyphenol (29).

3.2.1 Bromination of 3-methoxyphenol (22)

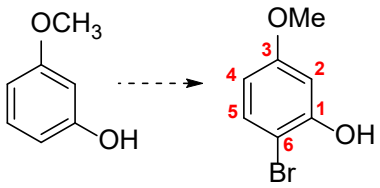

22 **29**

Scheme 23. Proposed synthesis of bromination of 3-methoxyphenol (**22**).

As proposed in Scheme 22, the first step of the proposed synthesis is the regioselective halogenation of 3-methoxyphenol (**22**) at position 6 (Scheme 23). Halogens are broadly used in organic synthesis as temporarily masking groups to assist regioselective synthesis. For this synthesis the choice of the halogenating agent required consideration of reactivity of halogenation and dehalogenation. The investigation was initiated with bromination, as the C–Br bond is generally more labile than the C–Cl bond, based on bond dissociation energies (C–Br: 280 kJ mol^{-1}; C–Cl: 339 kJ mol^{-1})[247]. However, this trend may vary depending on the substrate context.[248] Brominating agents are either in liquid (e.g. Br_2) or solid forms (e.g. *N*-bromosuccinimides). The more flammable and toxic liquid form is considerably less favourable than the solids. Today, brominating agents such as *N*-bromosuccinimides (NBS **30**), 1,3-dibormo-5,5-dimethylhydantoin (DBDMH **31**) are commonly employed as reagents of choice.[249] The rate of bromination can be hard to control, this can result in the formation of mono- and multi-substituted bromination compounds often generated as crude mixtures. In addition, electron donating substituents like hydroxy and methoxy groups are both *ortho*- and *para*-directing leading to various regioisomers. The addition of a catalyst is one of the common approaches to gaining better control over regioselectivity in these reactions. Catalysts such as PIDA-$AlBr_3$,[250] KBr with ZnAl-BrO_3^-,[251] *p*-toluenesulfonic acid,[252] have been reported to perform bromination reactions with higher selectivity. When the *para* position is substituted, the *ortho*-brominated compound is the dominate

product. The *para*-directed bromination occurs when this position is reactive for electrophilic aromatic substituents. In summary, the literature suggested that, in the presence of strong acids, bromination is more *para*-directing, and the addition of a strong, basic aliphatic amine is helpful in neutralizing the liberated hydrogen bromide, affording 60% mono *ortho*- directed products (Scheme 24).[253]

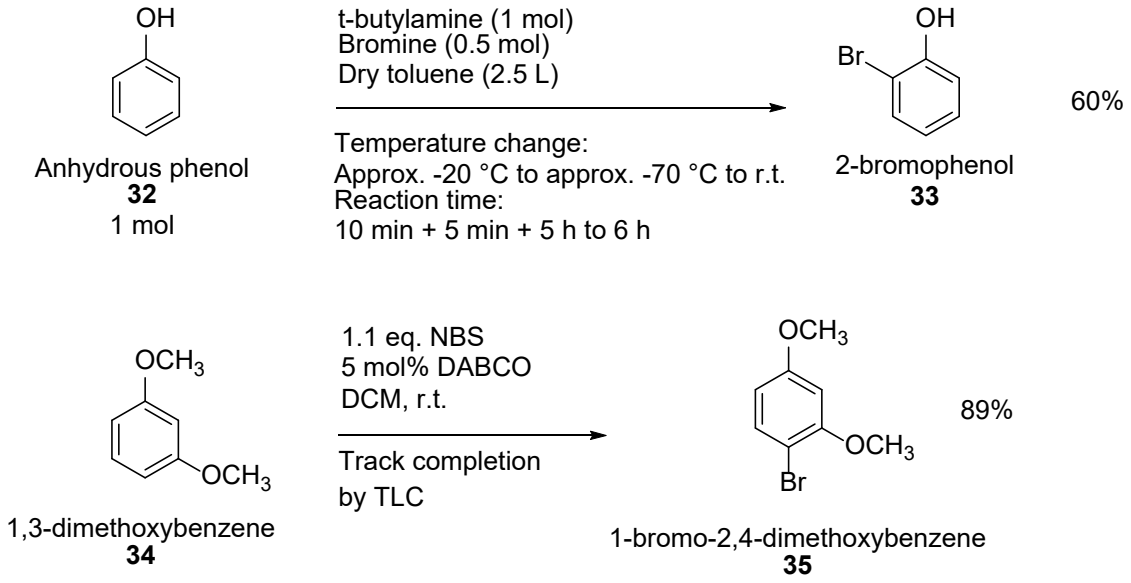

Scheme 24. Literature synthesis of *ortho*-selected bromination using *t*-butylamine and DABCO.[253, 254]

However, in the absence of aliphatic amine, 2-bromophenol (**29**) was obtained in 74.5% (GC yield) with 1 equivalent of phenol (**32**) and 1 equivalent of NBS (**30**) in literature (Scheme 25).[255] Hence, the initial test of bromination was performed without any catalyst for 3-methoxyphenol (Table 28).

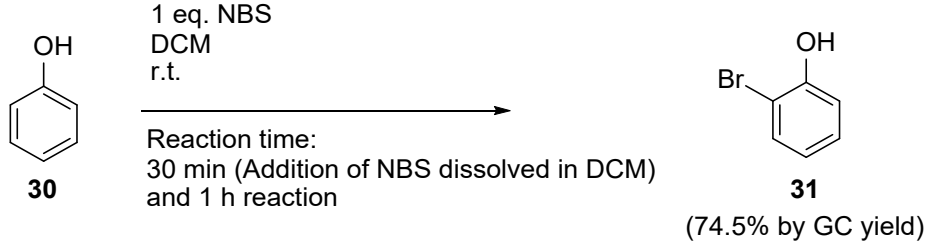

Scheme 25. Literature reaction scheme.[255]

For the initial attempt (Table 28), NBS (**30**) was added in portions (over 4 h) to avoid over-bromination at room temperature. The compound with the target mass was isolated for structural verification. As no suitable crystals were obtained for X-ray analysis, the compound was

characterized by comparing its analytical data (NMR spectroscopy, mass spectroscopy) with literature values before optimizing the reaction.[256] This was further confirmed by the X-ray crystal structure of the subsequent compound (Section 3.2.2). While the total area% of the target compound in the GC-MS showed a low selectivity of 14.91% for Entry 1, temperature and reaction time were adjusted to observe the consequential effects (Entry 2 – Entry 5). Room temperature was used in the following tests since results from Entry 4 and Entry 5 were shown to be approximately the same. A decreased reaction time did not influence the target selectivity as compared by Entry 1 and Entry 5, so 1.5 h reaction time was applied for subsequent reactions. When the scale of the reaction was reduced from 100 mol to 10 mmol (Entry 6), the bromination gave a slight decrease towards the target compound. The dropwise addition of the NBS (**30**) as an acetonitrile solution (Entry 7) did not yield any enhancement either. As room temperature conditions are more favourable than other temperatures, Entry 5 was deemed to be the optimum obtained for this test. However, the only difference between Entry 3 and Entry 5 is the rate of solid addition of NBS, while the selectivity varied significantly (Figure 59). The double brominated products were observed while starting material was still present.

Table 28. Bromination of 3-methoxyphenol (**22**).

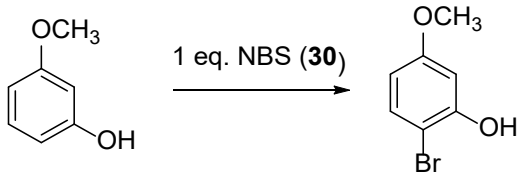

22 **29**

Entry	Scale/ mmol	NBS (1 eq.)	Solvent, concentration	Temp.	Time/ h	GC-Ms Total area % of target
1	100	portion wise	DCM, 0.5 M	r.t.	4	14.91
2	100	portion wise	DCM, 0.5 M	0 °C – r.t.	4	31.59
3	100	portion wise	DCM, 0.5 M	r.t.	1.5	33.73
4	100	portion wise	DCM, 0.5 M	0 °C	1.5	39.23
5	100	Approx. 4 portions	DCM, 0.4 M	r.t.	1.5	39.15
6	10	One portion	DCM, 0.5 M	r.t.	1.5	32.10
7	100	Dissolved in MeCN	MeCN, 0.4 M	r.t.	1.5	37.93

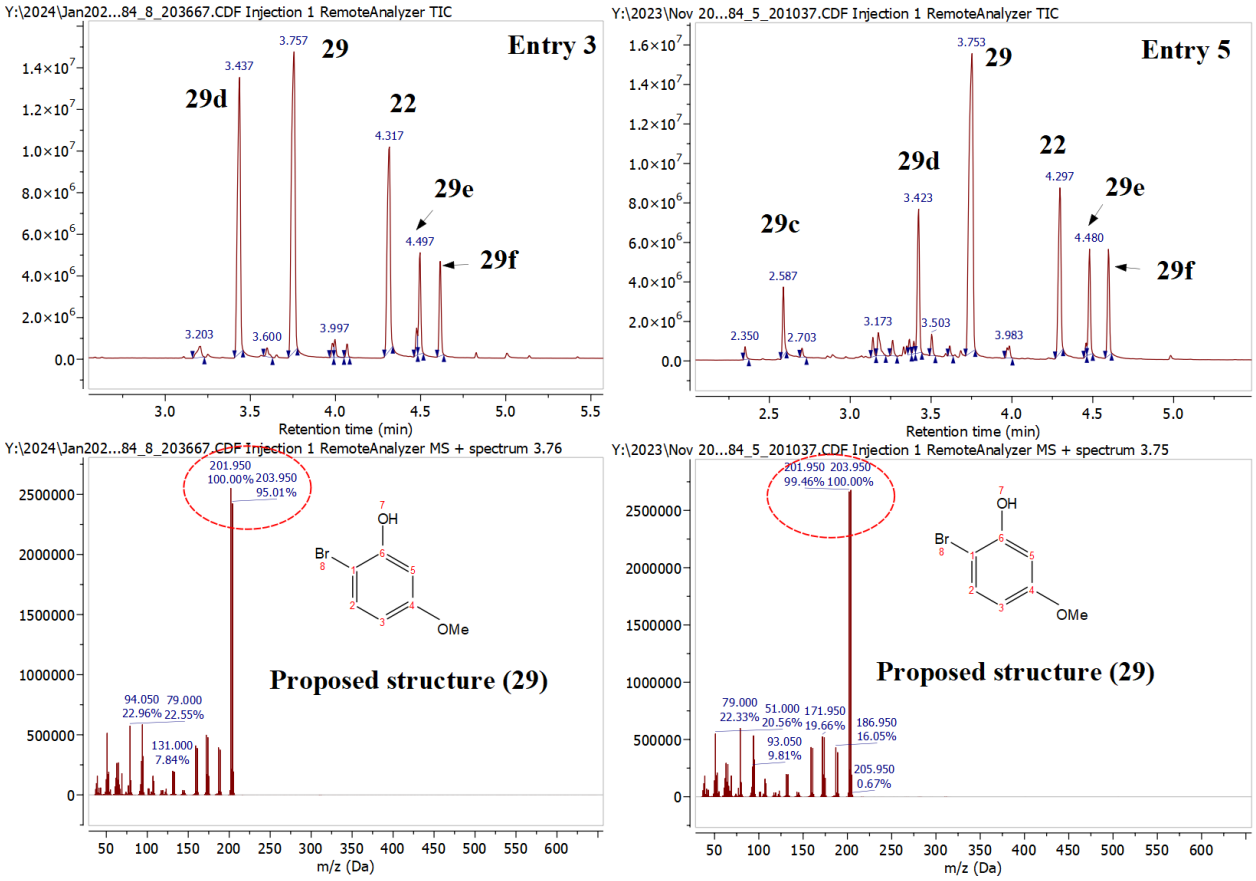

Figure 59. A. The mass spectrum of Entry 3 and Entry 5 of Table 28.

Table 29. The proposed structures at various retention time in Figure 59 and comparisons of Total area% of these compounds of using conditions in Entry 3 and Entry 5 of Table 28.

Proposed structure	R_t/ min	Total area% of the proposed structure Entry 3, Figure 60	Total area% of the proposed structure Entry 5, Figure 60
Regioisomers of the target (**29c**)	2.6	4.30	0
Regioisomers of the target (**29d**)	3.4	25.96	10.68
Target (**29**)	3.8	33.73	39.15
Starting material (**22**)	4.3	20.70	15.77
Double brominated compound (**29e**)	4.5	6.81	7.66
Double brominated compound (**29f**)	4.6	5.95	7.86

In summary, given the difficulty found in balancing starting material consumption and the formation of over-brominated compounds, exploring additional factors is likely crucial to achieving selective mono-bromination.

Optimization by Electronic structure calculations and visible light analysis

In Section 1.4 a theoretical framework was used to predict the favoured site of attack by calculating the overall charge distribution and the HOMO coefficients of 3-methoxyphenol (**22**).[60] The energy changes arising from the overlap of orbitals between two reactants are expressed using the Klopman-Salem equation (Equation 5). This equation models the energy change that occurs when orbitals of one reactant overlap with those of another. Although the equation includes three terms, the first term primarily accounts for bond breaking and forming and is typically similar for different regioisomers. The second term relates to the overall charge distribution, while the third term pertains to the HOMO coefficients. For electrophilic aromatic substitution of phenols, term 3 is more significant than term 2.[60] As such these derived values can be used to aid analysis of targeted mono-bromination.

For the target synthesis (Scheme 26), the experimental GC-MS results (Total area %, Tables 30 and 31) were compared with the computed predictions for validation. Some variables that can complicate the practical results were eliminated prior to calculations. Firstly, temperature which was fixed at room temperature and portion wise addition was neglected as these did not show significant influence in Table 29. Additionally, halogenation can be induced photochemically or by conventional heating.[252, 257] Potentially leading to over-brominated compounds and unreacted starting material which would complicate the assessment based upon electronic structure calculations. As a first step, the chance of photochemical activation was eliminated by shielding the reaction flask with aluminum foil, as reported in the literature[111,258]. The result without light is shown in Table 30 Entry 2 (Cf Table 29 Entry 1), where target compound has a higher total area% (38.45 > 14.91), potentially reducing other side products. Later tests were also conducted in the absence of light.

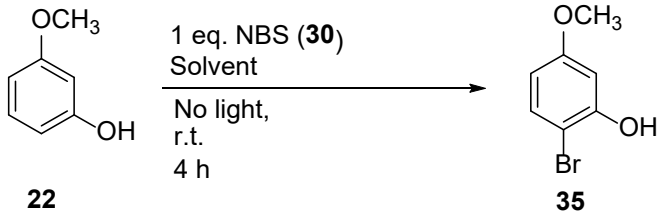

22 **35**

Scheme 26. The synthetic scheme used to generate the experimental results for comparison with computational predictions (Tables 30 and 31). All reactions were performed on a 10 mmol scale.

Table 30. Comparisons of regioselectivity predicted by Atomic charge distribution (AC) and highest occupied molecular orbital coefficients (HOMO coefficients) (Columns listing HF/3-21G calculation results) with experimental outcomes (column recording GC-MS data). Geometry optimisations of these compounds were carried out at the HF/3-21G model chemistry using the SMD solvation model where solvent is applied. A higher absolute value at position 6 comparing to position 4 of either AC or MOC is highlighted by grey background. The GC-MS column recorded the experimental results to compare with estimated data.

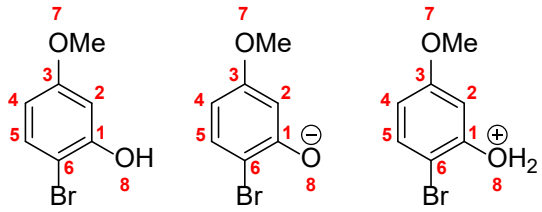

29 **29a** **29b**

Entry	HF/3-21G with SMD solvation model applied for solvent listed						GC-MS
	Reaction medium, molecule	AC or MOC	4 (*ortho* to -OMe)	6 (*ortho* to -OH)	5 (*para* to both)	2 (*ortho* to both)	Total area % of target
1	Gas, (**8**)	AC	-0.305	-0.272	-0.211	-0.317	N/A
		HOMO $2p_z$	-0.23170	0.23675	0.00498	-0.00762	
		HOMO $3p_z$	-0.2917	0.30353	0.00332	-0.01306	
2	DCM, (**8**)	AC	-0.303	-0.317	-0.246	-0.301	38.45
		HOMO $2p_z$	-0.23177	0.23310	0.00101	-0.00216	
		HOMO $3p_z$	-0.29472	0.30161	-0.00150	-0.00571	
3	MeOH, (**8**)	AC	-0.303	-0.298	-0.248	-0.321	27.12
		HOMO $2p_z$	0.23413	-0.22877	0.00565	-0.00696	
		HOMO $3p_z$	0.29621	-0.29419	0.00962	-0.00640	
4	MeCN, (**8**)	AC	-0.322	-0.338	-0.240	-0.342	28.06
		HOMO $2p_z$	-0.23123	0.23291	0.00132	-0.00262	
		HOMO $3p_z$	-0.29455	0.30183	-0.00111	-0.00630	
5	Toluene, (**8**)	AC	-0.274	-0.270	-0.247	-0.277	55.70
		HOMO $2p_z$	-0.23079	0.23579	0.00482	-0.00744	
		HOMO $3p_z$	-0.29237	0.30366	0.00315	-0.01274	
6	Toluene, (**8B**)*	AC	-0.374	-0.370	-0.370	-0.392	22.37
		HOMO $2p_z$	0.20651	-0.17940	0.02627	-0.17367	
		HOMO $3p_z$	0.30666	-0.29006	0.03061	-0.28126	

7	Toluene, (**8C**)**	AC	-0.267	-0.256	-0.223	-0.256	78.88
		HOMO $2p_z$	-0.19848	**0.24789**	0.04444	-0.08014	
		HOMO $3p_z$	0.04459	**0.30378**	0.04920	-0.11353	

* 10 mol% diisopropylamine was used. ** 10 mol% of *p*-toluenesulfonic acid was used. Other reaction conditions are given in Scheme 26.

Table 31. Computed values of atomic charge distribution (AC) and molecular orbital coefficients (MOC). Geometry optimisations of these compounds were carried out at the AM1/3-21G model chemistry using the SMD solvation model where solvent is applied. A higher absolute value at position 6 comparing to position 4 of either AC or MOC is highlighted by grey background. The GC-MS column recorded the experimental results to compare with estimated data.

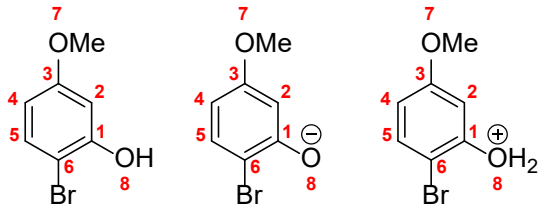

Entry	AM1/3-21G with SMD solvation model applied for solvent listed						GC-MS
	Reaction medium, molecule	AC or MOC	5 (*ortho* to -OMe)	6 (*ortho* to -OH)	5 (*para* to both)	2 (*ortho* to both)	Total area % of target
1	Gas, **(8)**	AC	-0.191	-0.192	-0.067	0.112	N/A
		HOMO $1p_z$	0.50019	-0.48239	0.02352	-0.02581	
2	DCM, **(8)**	AC	-0.217	-0.260	-0.072	-0.256	38.45
		HOMO $1p_z$	0.50490	-0.47167	0.03918	-0.01605	
3	MeOH, **(8)**	AC	-0.216	-0.246	-0.075	-0.251	27.12
		HOMO $1p_z$	0.50994	-0.45594	0.05937	-0.07109	
4	MeCN, **(8)**	AC	-0.221	-0.262	-0.074	-0.260	28.06
		HOMO $1p_z$	0.50460	-0.47126	0.03919	-0.04616	
5	Toluene, **(8)**	AC	-0.205	-0.206	-0.072	0.111	55.70
		HOMO $1p_z$	0.50093	-0.47941	0.02728	-0.03043	
6	Toluene, **(8B)** *	AC	0.361	-0.375	-0.050	-0.424	22.37
		HOMO $1p_z$	0.44556	-0.41182	0.05139	-0.40522	
7	Toluene, **(8C)** **	AC	-0.164	-0.125	-0.064	-0.181	78.88
		HOMO $1p_z$	0.22468	**-0.52855**	-0.28444	0.41090	

*10 mol% diisopropylamine was used for base. ** 10 mol% *p*-toluenesulfonic acid was used as acid. Other reaction conditions are given in Scheme 2.

Another reaction parameter that can be computed is the solvent medium. Calculations were carried out with various solvents using SMD solvation model through either Hartree-Fock (HF) approximation or semi-empirical Austin-model 1 (AM1) method in Gaussian 16 (Table 30 and 31). Both atomic charge distribution (AC) and highest occupied molecular orbital coefficients (HOMO coefficients) were recorded. Despite the potential lack of precision in these methods, they facilitate quick evaluation of the screened conditions and are useful for indicating trends. Entry 1 of Table 30 and 31 are referential calculations for gaseous phase reaction. Considering the *ortho*-selectivity of both hydroxy and methoxy groups, position 4 is the most competitive bromination position compared to position 6 in general (Figure 60) and this is consistent with the experimentally derived results.

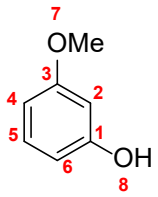

22

Figure 60. Labelled positions of 3-methoxyphenol (**22**).

The HF/3-21G model (Table 30, Entry 2, 4, 5) showed higher absolute values of either HOMO coefficients or both AC and HOMO coefficients at position 6 over position 4, Entry 5 showed more significantly higher values of HOMO coefficients than the other two, and this correlated with GC-MS total area%. Accordingly, toluene was selected as the solvent for Entries 6 and 7 to investigate the effect of adding either diisopropylamine or *p*-toluenesulfonic acid. In Entry 7 the HOMO coefficients of the acid catalysed bromination are significantly higher than for Entry 5, this also equates with the highest GC-MS total area% of all the tests undertaken. For AM1/3-21G model Entry 2, 4, 6 (Table 31) had a higher AC at position 6 than position 4 for compound **29**, Entry 7 had higher HOMO coefficient at position 6 than 4 for species **29b**. In summary, when the HOMO coefficient is significantly higher, the computed result tends to be better at predicting the experimental results. The HOMO coefficient is more dominant than the overall atomic distribution for this regioselective bromination of 3-methoxyphenol (**22**). The established scheme is shown by Scheme 27.

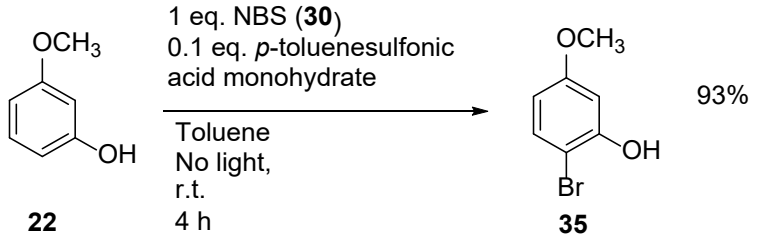

Scheme 27. The established regioselective bromination of 3-methoxyphenol (10 mmol scale). A 93% yield was determined by ^{1}H NMR spectroscopy as explained in Section 3.5 Experimental procedure.

One aspect worth noting is that achieve an improved yield of the final compound **20**, purification at this stage is not recommended. The yield of **29** was significantly reduced on purification (estimated yield > isolated yield, 93% > 66%). Secondly, repetitive separation by flush column chromatography (Hexane: EtOAc = 55:1 to 54:1) was found to be the best isolation method for **29** which is very time consuming. Since side products have no observed effect on the target synthesis, crude material was carried through to the next step and the yield estimated by ^{1}H NMR spectroscopy was recorded. For later syntheses, crystal structures were obtained to confirm the structure of compounds.

3.2.2 Formylation of 2-bromo-5-methoxyphenol (29)

For this section, the proposal regarding *ortho*-directed formylation of 2-bromo-5-methoxyphenol (**29**) using the Casnati-Skattebøl formylation method was tested. To gain the optimum efficacy of the reaction, literature conditions were reviewed as shown in Table 32, Entry 1 and 2 with 3-methoxyphenol (**22**, Table 32, Scheme A). A crystal structure was obtained for **26** in addition to other analysis data given in Section 3.4 (Experimental procedure) to confirm the regioselectivity of this process (Figure 61). A better yield of **26** was achieved by using 7 equivalents of paraformaldehyde (Table 32, Entry 2). Potentially due to loss of paraformaldehyde during condensation as observed by the buildup of white solids in the condenser (Figure 62). This condition successfully generated our desired target 3-bromo-2-hydroxy-6-methoxybenzaldehyde (**36**) in 82% yield as estimated by ^{1}H NMR spectroscopy with an internal standard and was used directly for the next step for optimum yield estimation. A small sample of the crude material was purified to obtain the crystal structure as shown by Figure 63.

Table 32. Screened literature conditions of Casnati-Skattebøl formylation using 3-methoxyphenol (**22**) for Entry 1 and 2 and application of the better methodology to **29** for Entry 3. Scheme A. Synthesise of 2-hydroxy-4-motheoxybenzaldehyde (**26**). Scheme B. Synthesis of 3-bromo-2-hydroxy-6-methoxybenzaldehyde (**35**). All reactions were performed at reflux temperature over 17 h.

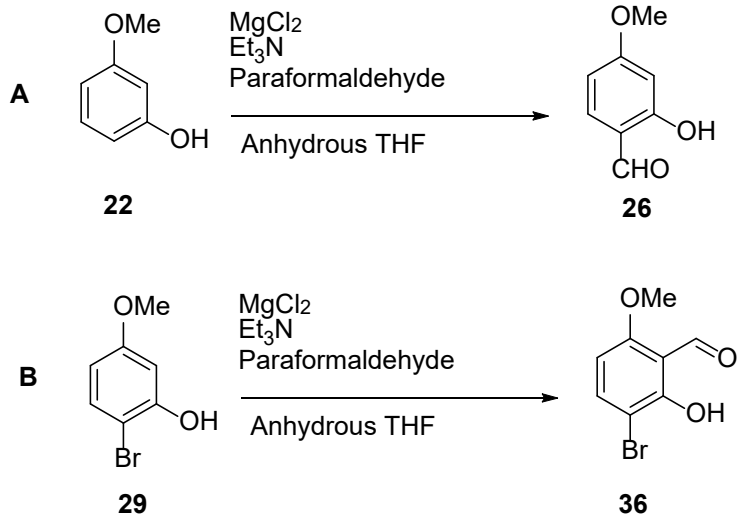

Entry	Substrate	Scale/ mmol	Eq. of Paraformaldehyde	Eq. of anhydrous $MgCl_2$	Eq. of Et_3N	Anhydrous THF/ mL	Yield*
1[246]	**22**	10	3	2	2	40	63
2[259]	**22**	10	7	1.5	3.8	40	82
3	**29**	10	7	1.5	3.8	40	72

*The yields were estimated by ^{1}H NMR spectrosopy using the internal standard 3-(trimethylsilyl)-1-propanesulfonic acid sodium salt (**8**) using methodology introduced in Section 2.4 Experimental procedure (Genera information, calculations of estimated yield by NMR).

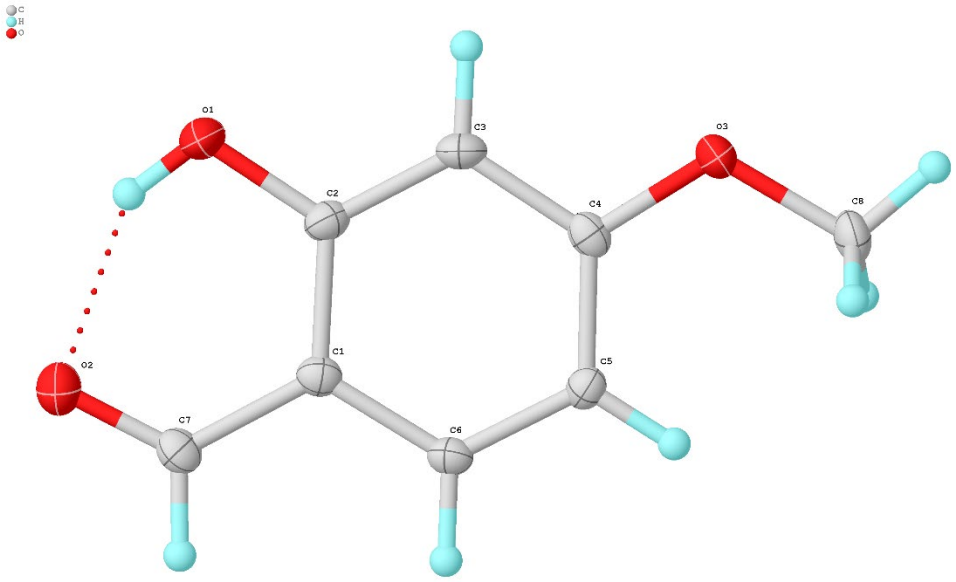

Figure 61. Crystal structure of 2-hydroxy-4-methoxyacetopheone (**26).**

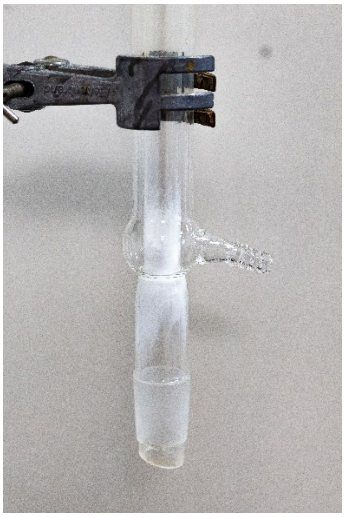

Figure 62. Paraformaldehyde subliming in the reflux condenser.

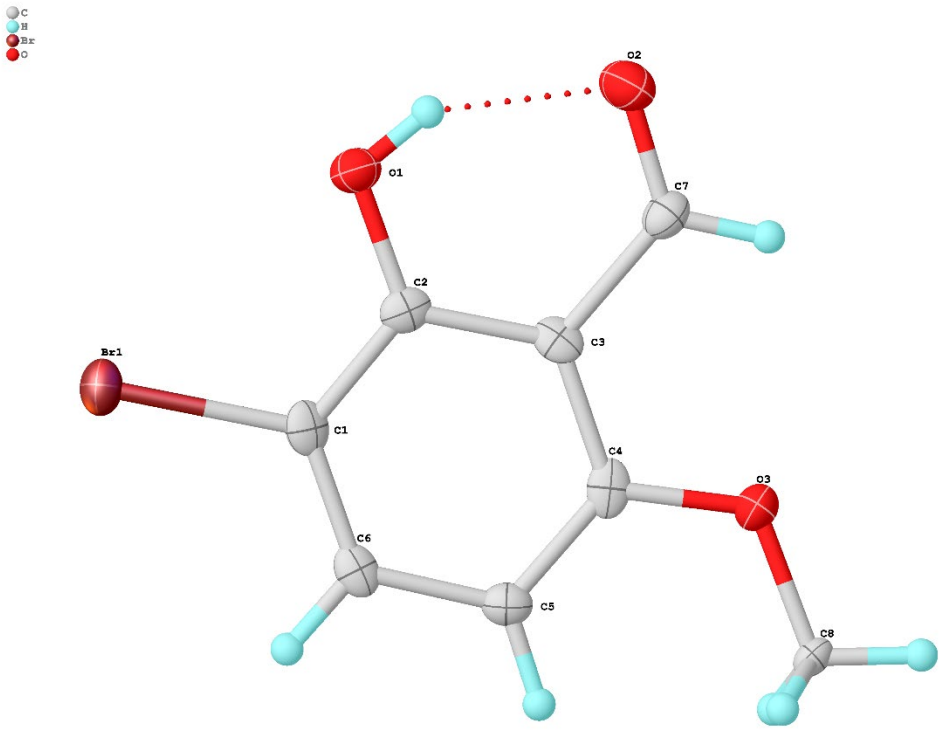

Figure 63. The crystal structure of 3-bromo-2-hydroxy-6-methoxybenzaldehyde (**36**).

3.3.3 De-bromination of 3-bromo-2-hydroxy-6-methxoybenzaldehyde (20)

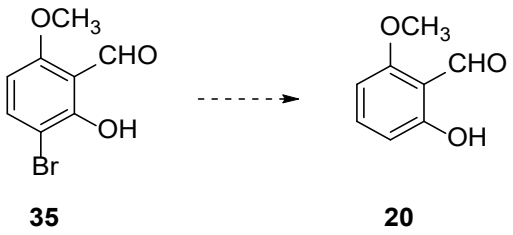

35 **20**

Scheme 28. Proposed Scheme of debromination.

The final step of the proposed synthesis (Scheme 28) is to perform a debromination of compound **35** to afford the target product 2-hydroxy-6-methoxybenzaldehyde (**20**). This type of dehalogenation is often performed by metal catalyst in the presence of various sources of hydrogen.[260-262] Commercially available Pd/C offers a convenient synthesis approach since minimal waste is produced in this process as the catalyst can be filtered and potentially recycled.

When using hydrogen gas as the hydride source, simple filtration can facilitate isolation of the product in the organic solute.

The selectivity and efficiency of the Pd/C catalyzed reaction can be significantly different using various commercial sources.[263] The process was tested with recommended catalysts from Johnson Matthey obtained from their extensive research on Pd/C catalyst applications. These catalysts were:

A. Palladium on activated carbon paste (5 wt.%), Lot Number DLV0053

B. Palladium on activated charcoal paste (20 wt.%), Lot Number DLV0164

Initially the reactions were tested with Pd/C(**A**) in ethanol at room temperature (Table 33, Entry 1 and 2). While side products were discovered, the target molecular mass (Figure 64) was identified in the chromatograph at R_t = 3.72 min, m/z 152 via GC-MS analysis (Table 34). This structure of the material was confirmed by a single-crystal X-ray diffraction analysis of the isolated material (Figure 65). One of the major by-product peaks corresponded to a m/z of 138 and was found at R_t = 3.60 min for both attempts of the reaction. The predicted structure of this side product is 2,6-dihydroxybenzaldehyde (**37**) indicating demethylation. Potentially after initial debromination, the formation of hydrogen bromide leads to the demethylation of the methoxy substituent to form compound **37** (Scheme 29). The formation of compound **38** (m/z 275) is proposed in Scheme 30 under a reducing environment as a hydride transfer to the hemi-acetal. To eliminate the formation of these two indicated by-products, the solvent was changed to THF and 1 equivalent of Et_3N was added to help trap the liberated hydrogen bromide (Table 33 Entry 3, Figure 66).

Table 33. Reaction conditions of synthesizing **6**. Pd/C: **A**. Palladium on activated carbon paste (5 wt.%), Lot Number DLV0053.

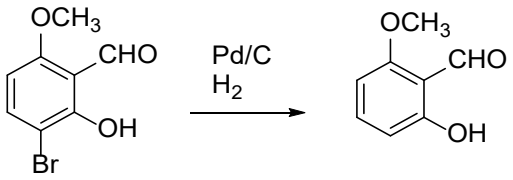

36 **20**

Entry	Scale/ mmol	Solvent (volume = 25 mL)	Pd/C	Temp.	Time	R_t/ min	Total area% of target m/z in GC	Major m/z
1	10	EtOH	Approx. 0.15 g	r.t.	48 h	3.70	12.63	138

2	10	EtOH	Approx. 0.15 g	r.t.	12 h	/	0	138, 275
3*	1.3	THF	Approx. 0.15 g	r.t.	12 h	3.73	15.12	152, 154, 217
4	1.3	THF	Approx. 0.15 g	r.t.	1 h	/	0	Starting material
5	1.3	EtOAc	Approx. 0.15 g	r.t.	1 h	/	0	Starting material
6	1.3	Acetone	Approx. 0.15 g	r.t.	1 h	/	0	Starting material
7	1.3	THF	Approx. 0.15 g	r.t.	3 h	/	0	Starting material
8	1.3	THF	Approx. 0.15 g	r.t.	4 h	/	0	Starting material
9	1.3	THF	Approx. 0.15 g	r.t.	5 h	/	0	Starting material
10	1.3	THF	Approx. 0.15 g	40℃	4 h	/	0	Starting material
11	1.3	THF	Approx. 0.15 g	40℃	12 h	/	0	Starting material
12	1.3	THF	0.70 g	40℃	5 h	/	0	152, 220, 217
13	1.3	THF	0.85 g	r.t.	5 h	3.74	13.10	152
14	1.3	THF	1.70 g	r.t.	5 h	3.72	70.45	152
15	1.3	THF	1.70 g	r.t.	10 h	3.72	41.56	152

* 1 Eq. triethylamine was added.

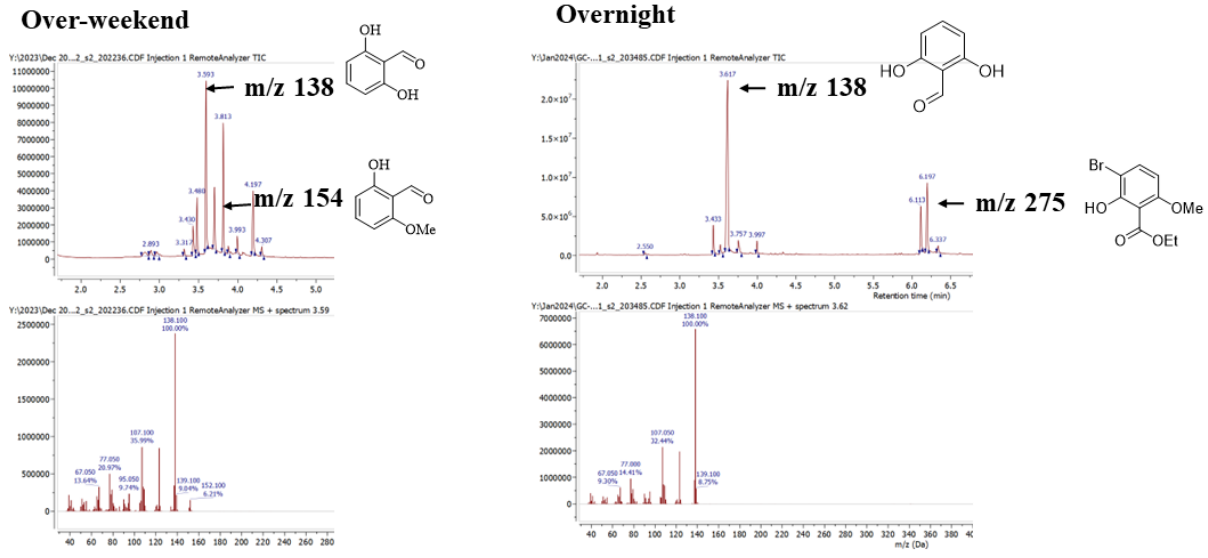

Figure 64. GC-MS spectrum of reaction in Table 29, Entry 1 and Entry 2.

Table 34. Proposed structures of m/z identified from GC-MS spectra analysed in Table 33.

Compound label	Proposed structure	R_t/min	m/z (GC-MS peak)	m/z (ChemDraw)
37	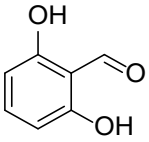	3.60	138	138.0317 (100.0%), 139.0350 (7.6%)
20	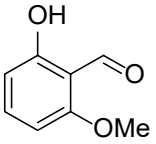	3.72	152	152.0473 (100.0%), 153.0507 (8.7%)
38	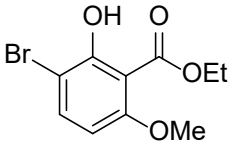	6.17	274	273.9841 (100.0%), 275.9820 (97.3%), 274.9874 (10.8%), 276.9854 (10.5%)
39	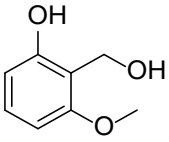	4.22	**154**, 205, 220	154.0630 (100.0%), 155.0663 (8.7%)
40	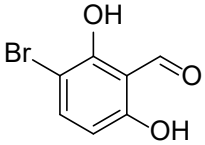	5.28	217	215.9422 (100.0%), 217.9402 (97.3%), 216.9456 (7.6%), 218.9435 (7.4%)

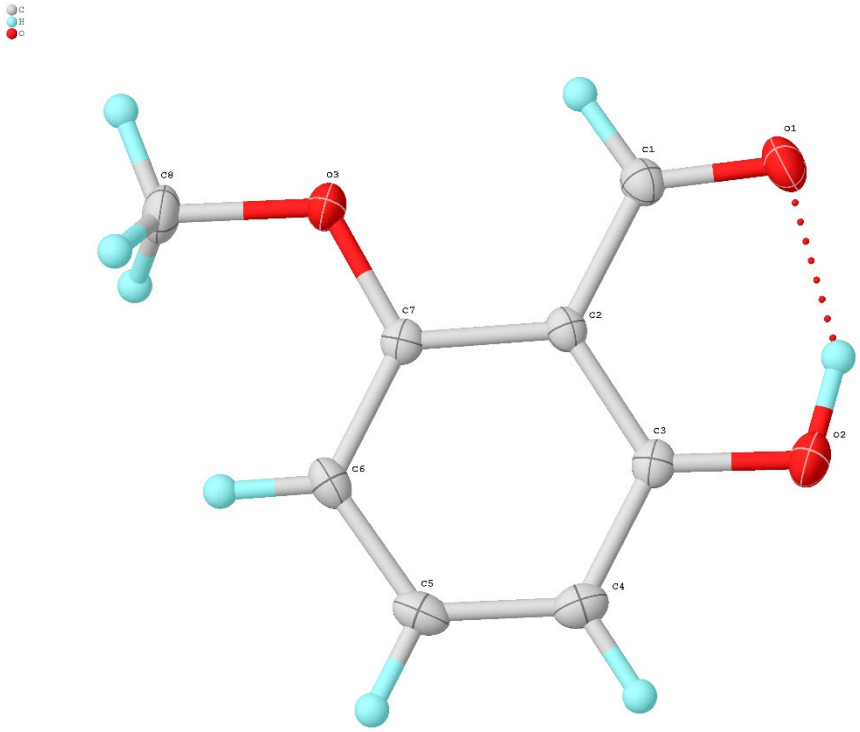

Figure 65. Crystal structure of isolated **20**.

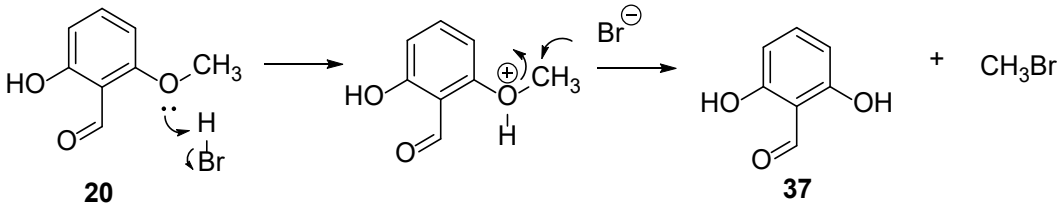

Scheme 29. Proposed scheme for the formation of side product **37**.

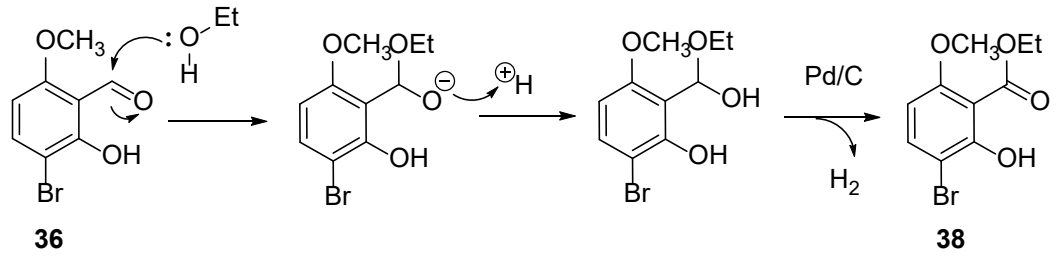

Scheme 30. Proposed mechanism of forming side product **38** from **36** in a reducing environment as a hydride transfer process for the hemi-acetal.

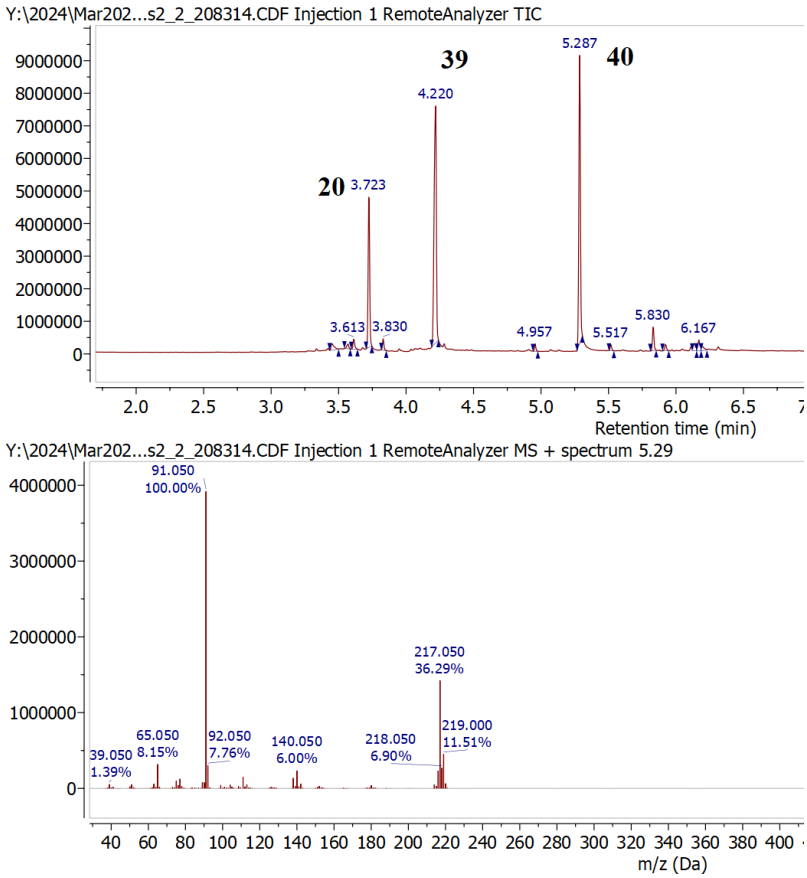

Figure 66. GC-MS of Table 33 Entry 3 after the completion of the 12 h reaction.

Under the modified condition, the formation of compound **38** (m/z 274) was eliminated. However, in addition to the target material with m/z 152, there appeared two new side product peaks which were assigned as 2-(hydroxymethyl)-3-methoxyphenol (**39**) with m/z 154 and 3-bromo-2,6-dihydroxybenzaldehyde (**40**) with m/z 217 (Table 30). This was noted as arising from the competing rate of demethylation and aldehyde reduction upon addition of triethylamine. Next, the reaction optimization focused on reaction time, solvent and reaction temperature instead of doping the reaction with the triethylamine. However, all attempts yielded predominantly starting material maintaining the amount of Pd/C (Entry 4-11, Table 33) with the reaction time indicated in the table. It was noted that the outcome as shown by GC-MS changed when higher amounts of Pd/C were used (Entry 12). In addition, it was observed that the peak area of the target was not reduced under room temperature conditions with higher equivalent weights of the 5 wt.% palladium on carbon (Entry 13). Hence, increased equivalents of the 5 wt.% palladium on carbon was tested (Entry 14) and this provided the best selectivity for our target whilst ensuring complete consumption of the

starting material (Entry 12, 13, 14) (Figure 67, 68). A similar set of tests were performed with a corresponding higher loading 20 wt.% palladium on charcoal where Entry 1, 3, 5 achieved the optimum yield of the target compound and Entry 3 was easier to purify (Table 35, Figure 69). The yield was estimated by ^{1}H NMR spectroscopy with an internal standard as 47%. Note at this stage catalyst **A** had been discontinued by Johnson Matthey, hence the yield was estimated with catalyst **B**.

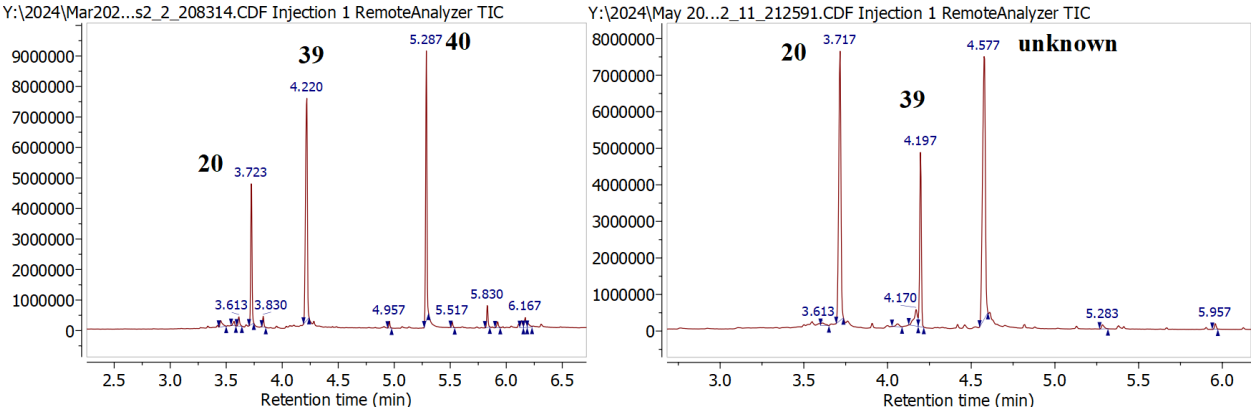

Figure 67. GC-MS of reaction in Table 29, Entry 12 (left) and Entry 13 (right).

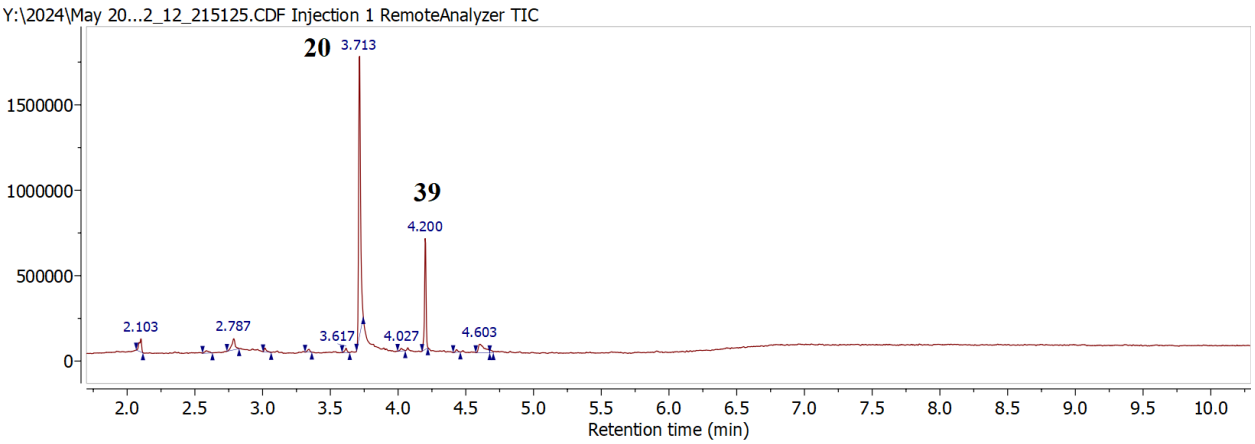

Figure 68. GC-MS of reaction in Table 29 Entry 14.

Table 35. Reaction conditions of synthesizing compound **20** in 5 hours. Pd/C: palladium on activated charcoal paste (20 wt.%), Lot Number DLV0164.

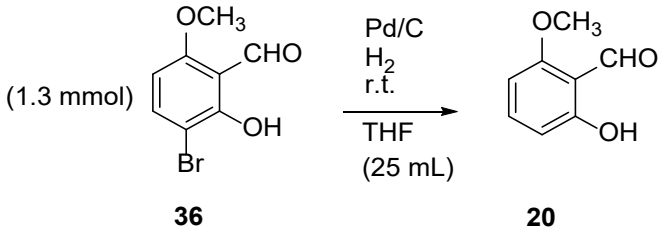

36 **20**

Entry	Pd/C	Time/ h	R_t/ min	Total area% of target compound in GC	Temp.
1	0.6 g	5	3.69	35.54	r.t.
2	0.8 g	5	3.69	31.04	r.t.
3	1.0 g	5	3.69	35.50	r.t.
4	1.2 g	5	3.69	35.54	r.t.
5	1.0 g	4	3.69	34.42	r.t.
6	1.0 g	6	3.70	33.84	r.t.

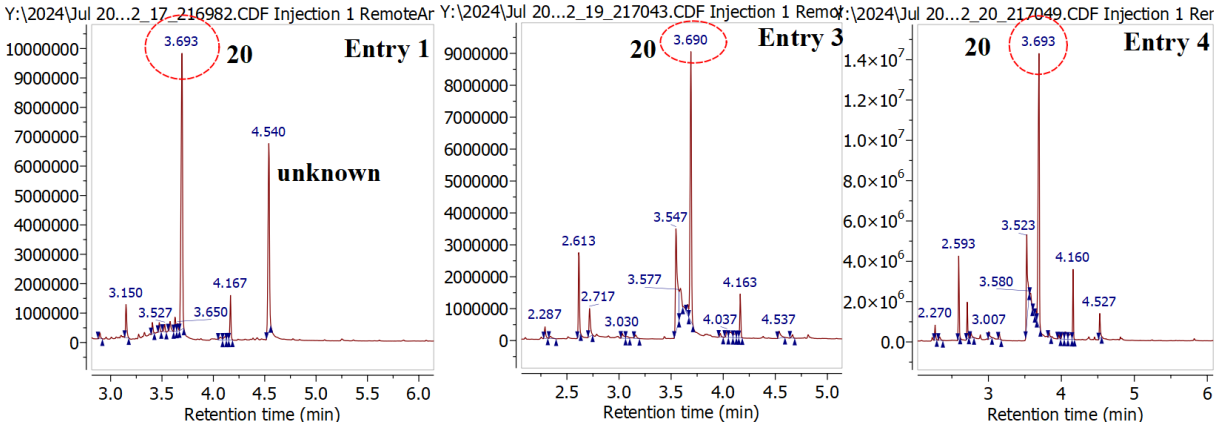

Figure 69. GC-MS of reaction to derive the target compound **20** in Table 35 Entry 1, 3, 4.

3.3 Conclusion for synthesis of 2-hydroxy-6-methxoybenzaldehyde (20) and proposed future work

Overall, the synthetic method for formylation at a sterically hindered position of 3-methxoyphenol (**22**) was established as shown in Scheme 31. Moderate to excellent yields were achieved for each step of the synthesis excluding the final dehalogenation.

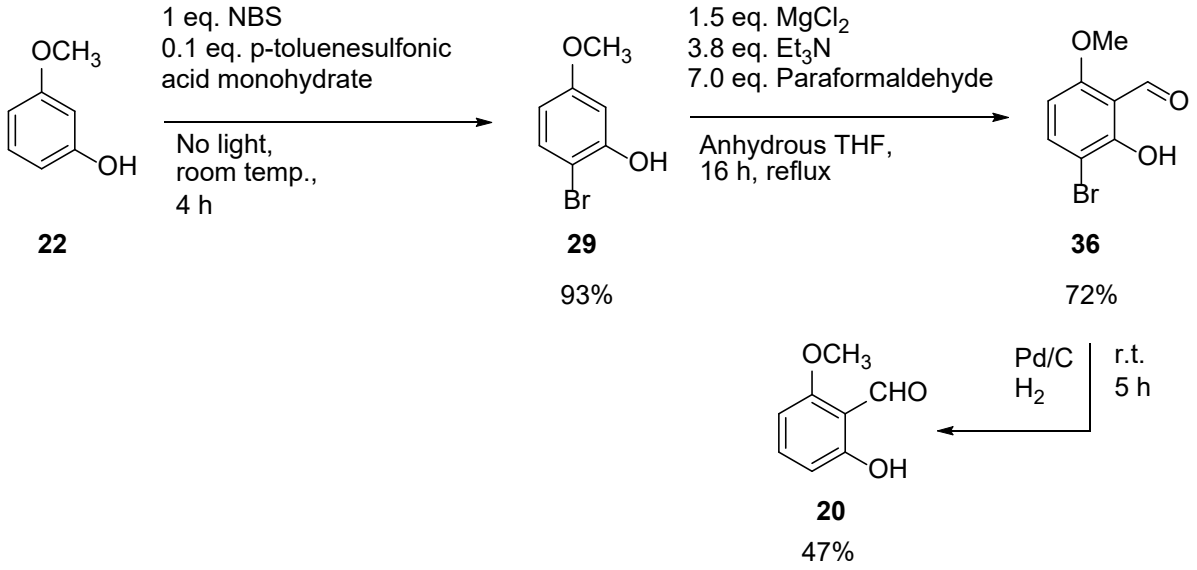

Scheme 31. The synthetic scheme of 2-hydroxy-6-methxoybenzaldehyde (**20**). The yields were estimated by ^{1}H NMR spectroscopy as explained in Section 3.5.

Step 1 involved a novel acid catalysed bromination of 3-methoxyphenol (**29**) under mild reaction conditions. The reaction was conducted in the absence of light to limit potential light-induced radical reactions and over-brominated side products. Toluene was selected as the optimal solvent to provide the best selectivity for the target compound, when 10% *p*-toluenesulfonic acid was added, the selectivity was increased further as analysed by total area% of GC-MS spectrum, achieving 93% yield of brominated product 2**9** from starting material **22**. Experimental analysis of this electrophilic aromatic substitution was compared with computed results by HF/3-21G or AM1 model chemistry using the SMD solvation model where solvent is applied. According to Klopman-Salem equation (Equation 5), the highest occupied molecular orbital (HOMO) coefficients were

more dominant than overall atomic charge distribution. For this simple reaction, HF/3-21G aligned better with experimental results while performing solvent screening tests, both models predicted the better selectivity at desired bromination position with HOMO coefficients. As many have mentioned, "*The quantitative aspects of calculations like this are not to be relied upon, but the directions in which changes in energy and polarization occur, and the ordering of energy levels are usually trustworthy*.".[60]

The Casnati-Skattebøl formylation method was successfully applied to next synthesize aldehyde **36** by *ortho*-directed formylation of compound **39** using a $MgCl_2$-Et_3N system in 72% yield. The previous bromination was necessary to assist this formylation at a sterically hindered position. Large excess of paraformaldehyde was used to compensate for the loss to the condenser during the reaction (sublimination).

The final debromination step was necessary to afford the target 2-hydroxy-6-methoxyphenol (**20**) in 47% yield. Compound **36** has multiple reactive functionalities. Besides Pd/C and hydrogen reagents, additional reagents such as triethylamine and ethanol yielded several side products. The conversion towards the target compound was improved by increased equivalents of Pd/C and reduced reaction time. When a different Pd/C source was used, the conversion towards the target compound varied. For proposed future work, the following options are provided for consideration:

- Prepare other catalysts.[264, 265,266-268]
- Explore γ-terpinene as an reductant.[269]
- Employ hydrogen produced by living microorganisms.[270]

Commercially available catalysts would be efficient to conduct the test, and the development of more environmentally friendly catalysts is also essential. Heterogeneous scavengers with the ability to consume side products would also be valuable.

The green chemistry metrics for this synthetic route, including atom economy and reaction mass efficiency are summarized in Table 36.

Table 36. Summary of Green metrics of **Scheme 30**. AE = atom economy, RME = reaction mass efficiency.

Step	**Yield**	**AE/%**	**RME/%**
1	93	41	38
2	72	54	39
3	47	45	21

3.4 Experimental procedure

For General Information please refer to Section 2.4.

2-bromo-5-methoxyphenol (29)[256]

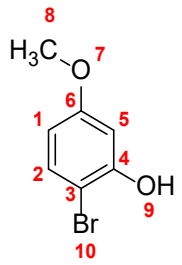

Chemical Formula: $C_7H_7BrO_2$
Exact Mass: 201.96

To a solution of 3-methoxyphenol (**22**) (1.24 g, 10 mmol) in toluene (100 mL) was added *p*-toluenesulfonic acid monohydrate (0.19 g, 1 mmol). The reaction flask was covered with aluminium foil to prevent light ingress. A sample of *N*-bromosuccinimide (1.78 g, 10 mmol) was first ground using a pestle and mortar to avoid small chunks and the fine powder charged to the reaction solution and stirred at room temperature for 4 h to afford the title compound, 2-bromo-5-methoxyphenol (**29**). The crude product was used directly in the subsequent formylation step, as the side products showed no observable impact on the target reaction. Purification at this stage was avoided due to the difficulty in separating over-brominated species and the time-intensive nature of the process. For analytical purposes, a pure sample (cream-white solid) was obtained via flush column chromatography. (1.35 g, 66%) (Hexane: EtOAc = 55:1 to 54:1), R_f = 0.54 (Hexane:EtOAc = 3:1).

Estimated yield by ^{1}H NMR spectroscopy: 93%.

^{1}H NMR (599 MHz, $CDCl_3$) δ/ppm 7.30 (d, *J* = 8.9 Hz, 1H, H2), 6.59 (d, *J* = 2.9 Hz, 1H, H5), 6.40 (dd, *J* = 8.9, 2.9 Hz, 1H, H1), 5.47 (s, 1H, H9), 3.76 (s, 3H, H8).

^{1}H NMR (400 MHz, DMSO) δ/ppm 10.21 (s, 1H), 7.33 (d, *J* = 8.8 Hz, 1H), 6.53 (d, *J* = 2.8 Hz, 1H), 6.36 (dd, *J* = 8.8, 2.8 Hz, 1H), 3.69 (s, 3H).

^{13}C NMR (151 MHz, $CDCl_3$) δ/ppm 160.57 (C6), 152.97 (C4), 131.92 (C2), 108.41 (C1), 101.63 (C5), 100.86 (C3), 55.51 (C8).

^{13}C NMR (101 MHz, DMSO) δ/ppm 160.13, 155.21, 133.32, 106.81, 102.84, 100.61, 55.66, 40.60, 40.24.

IR (neat) ν = 3424 (b, OH) 1452 (s) 1395 (s) 1288 (s, CO)1214 (s, CO).

LC-MS: R_t = 2.11 min, m/z 202.80 (100%) 204.89 $[M+H]^+$; HR-MS calculated for $C_7H_8BrO_2$ 202.9708, found 202.9719 (Δ = 1.1 mDa; 5.4 ppm).

Melting point: 39.4 – 41.4 ℃ (Hexane: EtOAc = 54:1), literature 38 °C (DCM:isohexane = 2:1)[271].

2-hydroxy-4-methoxyacetophenone (26)[259]

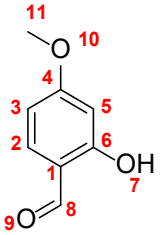

Chemical Formula: $C_8H_8O_3$
Exact Mass: 152.0473

Anhydrous magnesium chloride (1.43 g, 15 mmol) and paraformaldehyde (2.10 g, 70 mmol) were added to a two neck round bottom flask and further dried by heating with a heat gun under Schlenk line until the material became free flowing (around 30 seconds). To the flask was added anhydrous triethylamine (5.3 mL, 38 mmol) and 3-methoxyphenol (**22**) (1.24 g, 10 mmol) in anhydrous THF (40 mL). The mixture was heated to reflux for 17 hours – (CARE! carcinogenic chloroalkyl ether by-products may be formed, and monomeric formaldehyde is very volatile) – after which the reaction was quenched via the slow addition of HCl (1 M, 50 mL). The reaction was extracted with ethyl acetate (2 × 80 mL), dried over anhydrous Na_2SO_4 and the solvent removed in vacuo to yield an orange-red oil.[259]

Mass of yielded compounds without purification: 1.68 g.
Estimated yield by ^{1}H NMR spectroscopy: 82%.
^{1}H NMR (599 MHz, DMSO) δ/ppm 10.99 (s, 1H, H7), 9.98 (s, 1H, H8), 7.59 (d, *J* = 8.7 Hz, 1H, H2), 6.54 (dd, *J* = 8.7, 2.4 Hz, 1H, H3), 6.46 (d, *J* = 2.4 Hz, 1H, H5), 3.78 (s, 1H, H11).
^{1}H NMR (400 MHz, DMSO) δ/ppm 11.02 (s, 1H), 10.01 (s, 1H), 7.63 (d, *J* = 8.7 Hz, 1H), 6.57 (dd, *J* = 8.7, 2.4 Hz, 1H), 6.49 (d, *J* = 2.4 Hz, 1H), 3.82 (s, 3H).
^{13}C NMR (151 MHz, DMSO) δ/ppm 191.59 (C8), 166.39 (C4), 163.52 (C6), 132.69 (C2), 116.61 (C1), 107.87 (C3), 101.19 (C5), 56.60 (C11).
^{13}C NMR (101 MHz, DMSO) δ/ppm 191.63 (C8), 166.43 (C4), 163.55 (C6), 132.73 (C2), 116.65 (C1), 107.91 (C3), 101.23 (C5), 56.12 (C11).
IR (neat) ν = 2994 (b, OH) 1628 (s, C=O) 1583 (s, aromatic C-C) 1506 (s, aromatic C-C) 1442 (m) 1297 (s, CO) 1236 (s, CO) 1134 (s).
LC-MS: R_t = 2.12 min, m/z 153.08 $[M+H]^+$; HR-MS calculated for $C_8H_9O_3$ 153.0552, found 153.0540 (Δ = -1.2 mDa; -7.8 ppm).

Melting point: 36.7 – 39.3 °C, literature 39 – 41 °C[272].

The structure and connectivity were confirmed by single crystal X-ray crystallography, performed by Dr Toby Blundell of the Durham University X-Ray Crystallography Service and has the unique identifier of '23srv391'.

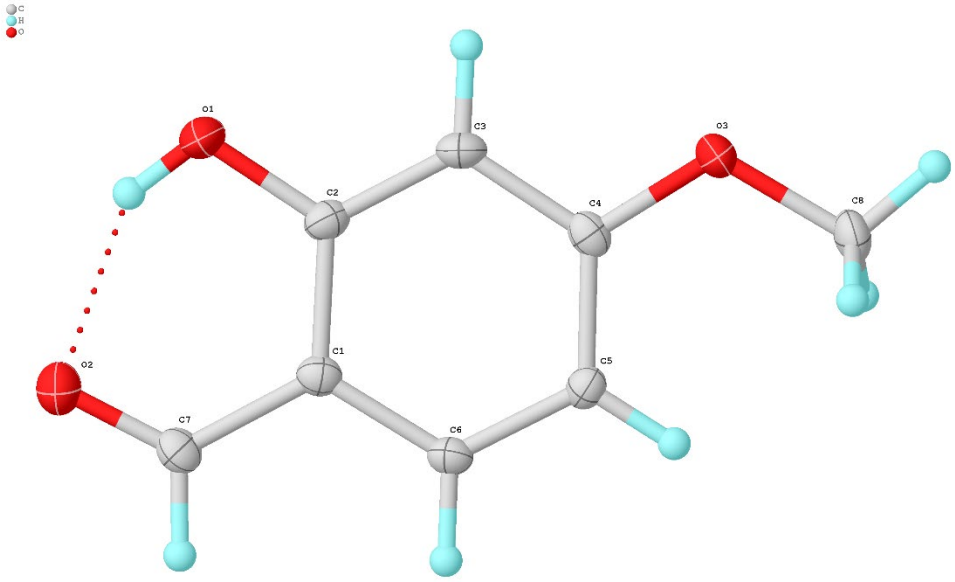

Space Group	$P2_1$
a/Å	3.8205(4)
b/Å	13.5590(13)
c/Å	6.7891(7)
α/°	90
β/°	94.826(4)
γ/°	90

3-bromo-2-hydroxy-6-methoxybenzaldehyde (36)[273]

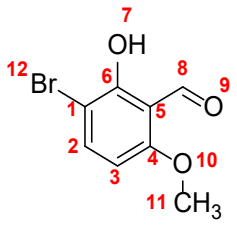

Chemical Formula: $C_8H_7BrO_3$
Exact Mass: 229.9579

Anhydrous magnesium chloride (1.43 g, 15 mmol) and paraformaldehyde (2.10 g, 70 mmol) were added to a two-neck round bottom flask further dried by heating with heat gun under Schlenk line until the material became free flowing (around 30 seconds). To the flask was added triethylamine (5.3 mL, 38 mmol) and crude mixture containing 2-bromo-5-methoxyphenol (**29**) (2.03 g, 10 mmol) in anhydrous THF (40 mL). The mixture was heated to reflux for 17 hours – (CARE! carcinogenic chloroalkyl ether by-products may be formed and monomeric formaldehyde is very volatile)) – after which the reaction was quenched via the slow addition of HCl (1 M, 50 mL). The reaction was extracted with ethyl acetate (2 × 80 mL), dried over anhydrous Na_2SO_4 and the solvent removed in vacuo to yield a yellow solid.

Mass of yielded product mixture without purification: 1.87 g.
Estimated yield by ^{1}H NMR spectroscopy: 72%.
R_f = 0.43 (Hexane:EtOAc = 3:1)
^{1}H NMR (599 MHz, DMSO) δ/ppm 12.41 (s, 1H, H7), 10.17 (s, 1H, H8), 7.80 (d, *J* = 9.0 Hz, 1H, H2), 6.62 (d, *J* = 9.0 Hz, 1H, H3), 3.87 (s, 3H, H11).
^{1}H NMR (400 MHz, DMSO) δ/ppm 12.44 (s, 1H), 10.20 (s, 1H), 7.83 (d, *J* = 9.0 Hz, 1H), 6.65 (d, *J* = 9.0 Hz, 1H), 3.90 (s, 3H).
^{13}C NMR (151 MHz, DMSO) δ/ppm 194.59 (C8), 162.20 (C4), 158.78 (C6), 141.56 (C2), 111.43 (C1), 104.56 (C3), 100.81 (C5), 56.99 (C11).
^{13}C NMR (101 MHz, DMSO) δ/ppm 194.63 (C8), 162.24 (C4), 158.82 (C6), 141.60 (C2), 111.47 (C1), 104.60 (C3), 100.85 (C5), 57.03 (C11).
^{1}H NMR (599 MHz, $CDCl_3$) δ/ppm 12.60 (s, 1H), 10.27 (s, 1H), 7.63 (d, *J* = 8.9 Hz, 1H), 6.34 (d, *J* = 8.9 Hz, 1H), 3.89 (s, 3H).

^{1}H NMR (400 MHz, $CDCl_3$) δ/ppm 12.64 (s, 1H), 10.30 (s, 1H), 7.67 (d, *J* = 8.9 Hz, 1H), 6.37 (d, *J* = 8.9 Hz, 1H), 3.92 (s, 3H).

^{13}C NMR (151 MHz, $CDCl_3$) δ/ppm 193.97 (C8), 161.81 (C4), 159.69 (C6), 140.87 (C2), 111.33 (C1), 102.50 (C3), 101.72 (C5), 56.08 (C11).

^{13}C NMR (101 MHz, $CDCl_3$) δ/ppm 194.00, 161.84, 159.72, 140.90, 111.37, 102.53, 101.75, 56.10.

IR (neat) ν = 2911 (s, OH) 1644 (s, C=O) 1599 (m, C-C aromatics) 1567 (m, C-C aromatics) 1426 (s) 1092 (s) 653 (b, C-Br)

LC-MS: R_t = 2.21 min, m/z 230.92 232.82 $[M+H]^+$; HR-MS calculated for $C_8H_8BrO_3$, found 230.9657 (Δ = -2.3 mDa; -10 ppm)

Melting point: 118.2 – 120.2 °C, literature 109-110 °C[273].

The structure and connectivity were confirmed by single crystal X-ray crystallography, performed by Dr Toby Blundell of the Durham University X-Ray Crystallography Service and has the unique identifier of '23srv405'.

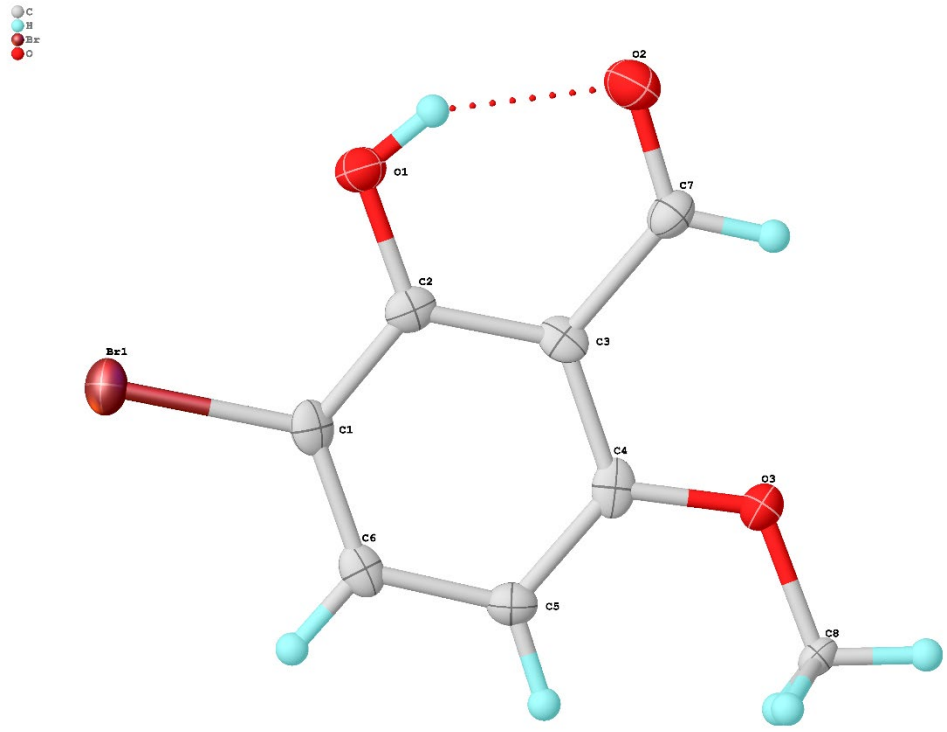

Space group	$P2_12_12_1$
a/Å	3.9120(5)
b/Å	13.1854(15)

c/Å	15.4895(18)
α/°	90
β/°	90
γ/°	90

2-methoxy-6-hydroxybenzaldehyde (20)[274]

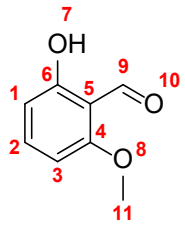

Chemical Formula: $C_8H_8O_3$
Exact Mass: 152.0473

To a solution of 3-bromo-2-hydroxy-6-methoxybenzaldehyde (**36**) (0.3 g, 1.3 mmol) in THF (20 mL) was added 20% Palladium on Charcoal Paste (1.0 g, from Johnson Matthey Lot Number DLV0164) and the reaction supplied with hydrogen gas (ballon) and stirred at room temperature for 5 h. The solution was filtered and concentrated in vacuo to obtain the crude oil which slowly solidified. The light-yellow solid was purified by column chromatography (Hexane:EtOAc = 43:2). Crystals were obtained from the same solvent mixture used for column purification by slow evaporation, R_f = 0.72 (Hexane:EtOAc = 3:1).

Mass of yielded product mixture without purification: 0.25 g.
Estimated yield by ^{1}H NMR spectroscopy: 47%.
^{1}H NMR (599 MHz, DMSO) δ/ppm 11.73 (s, 1H, H7), 10.23 (d, *J* = 0.6 Hz, 1H, H9), 7.49 (t, *J* = 8.4 Hz, 1H, H2), 6.57 (dd, *J* = 8.4, 0.8 Hz, 1H, H1), 6.48 (dt, *J* = 8.4, 0.8 Hz, 1H, H3), 3.84 (s, 3H, H11).
^{1}H NMR (400 MHz, DMSO) δ/ppm 11.77 (s, 1H, H7), 10.26 (d, *J* = 0.7 Hz, 1H, H9), 7.53 (t, *J* = 8.4 Hz, 1H, H2), 6.61 (dd, *J* = 8.4, 0.7 Hz, 1H, H1), 6.52 (dt, *J* = 8.4, 0.7 Hz, 1H, H3), 3.88 (s, 3H, H11).
^{13}C NMR (151 MHz, DMSO) δ/ppm 194.34 (C9), 162.84 (C5), 162.65 (C4), 139.35 (C2), 110.82 (C6), 109.59 (C3), 102.55 (C1), 56.60 (C11).
^{13}C NMR (101 MHz, DMSO) δ/ppm 194.37 (C9), 162.87 (C5), 162.68 (C4), 139.38 (C2), 110.86 (C6), 109.62 (C3), 102.59 (C1), 56.63 (C11).
IR (neat) ν = 2952 (br, OH) 1613 (s) 1578 (m, aromatic C-C) 1443 (m, aromatic C-C) 1307 (s, C-O) 1236 (s, C-O).
LC-MS: R_t = 2.16 min, m/z 152.93 $[M+H]^+$; HR-MS calculated for $C_8H_9O_3^+$ 153.0552, found 153.0558 (Δ = 0.6 mDa; 3.9 ppm).

Melting point: 73.5 – 75.5 °C, literature 73.5 – 74.5 °C[274].

The structure and connectivity were confirmed by single crystal X-ray crystallography, performed by Dr Toby Blundell of the Durham University X-Ray Crystallography Service and has the unique identifier of '24srv127'.

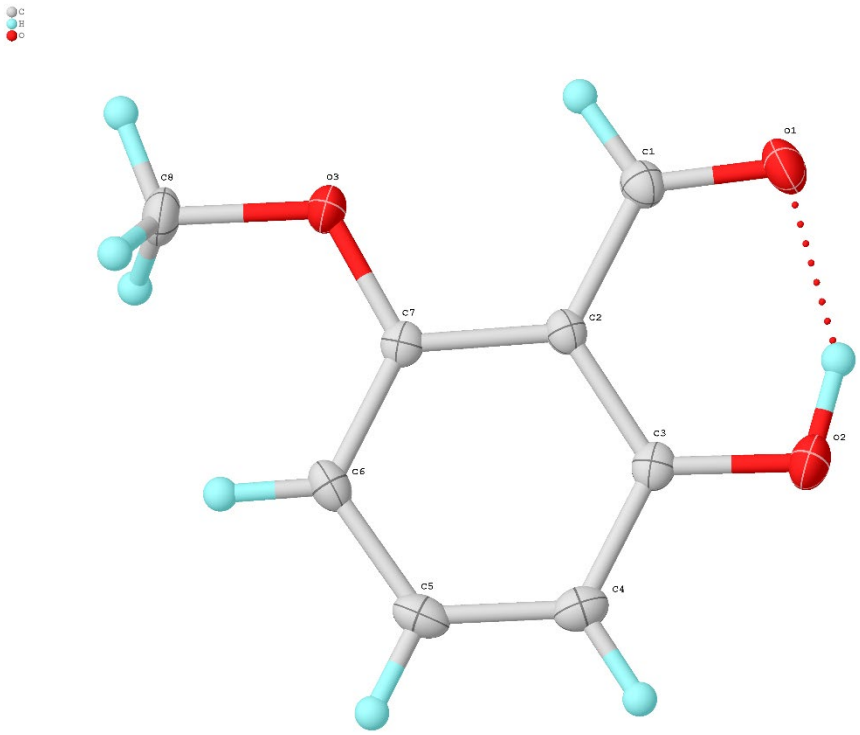

Space group	$P2_1/n$
a/Å	9.2835(6)
b/Å	6.7059(5)
c/Å	11.3165(8)
α/°	90
β/°	94.377(2)
γ/°	90

Chapter 4

Synthesis of 2-hydroxy-6-methoxyacetophenone

4.1 Retrosynthetic analysis of 2-hydroxy-6-methoxyacetophenone (21)

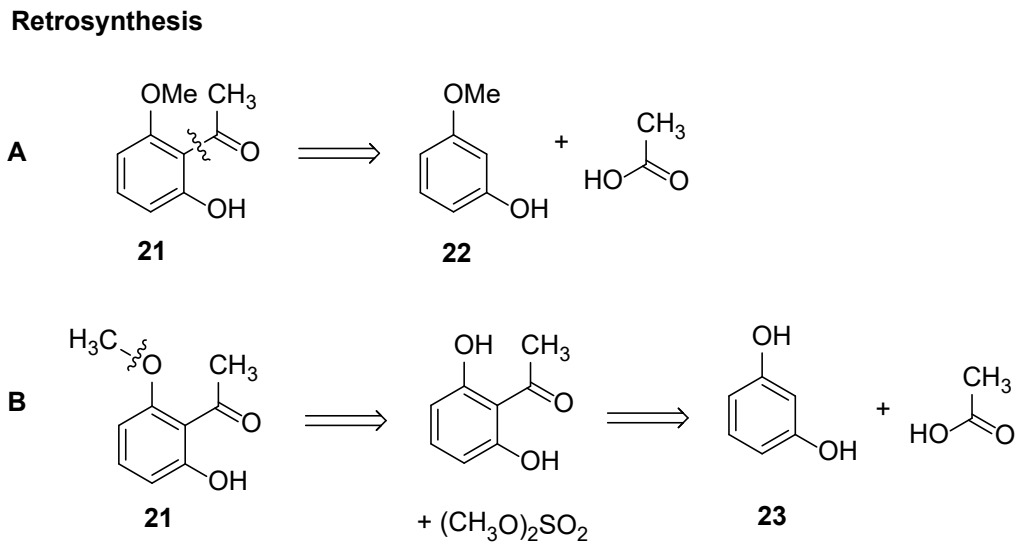

Scheme 32. Retrosynthetic disconnection for 2-hydroxy-6-methoxyacetophenone (**21**).

In addition to 2-hydroxy-6-methoxybenzaldehyde (**20**) the acetophenone derivative (**21**) was the other compound of interest Scheme 32. Scheme 32A involves an acylation reaction, commonly carried out through Friedel–Crafts acylation or a two-step approach involving *O*-acylation (Scheme 33, B-1) followed by Fries rearrangement (Scheme 33, B-2).[275] When starting from 3-methoxyphenol (**22**), the hydroxy and methoxy groups are *ortho*- and *para*-directing, acylation of 3-methoxyphenol (**22**) yields compounds **41a** (27%) and **41b** (25%) as demonstrated by Olah in

1963 using acetic acid as the acylating agent (Scheme 34)[275]. Additionally, the diketone **41c** is formed (no yield was reported in the literature); however, the target compound **41** is not obtained.[275]

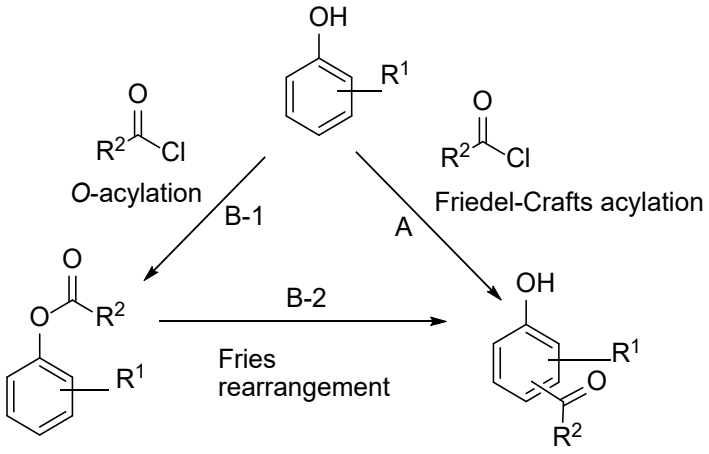

Scheme 33. Acylation by Friedel-Crafts acylation or *O*-acylation and Fries rearrangement.[276]

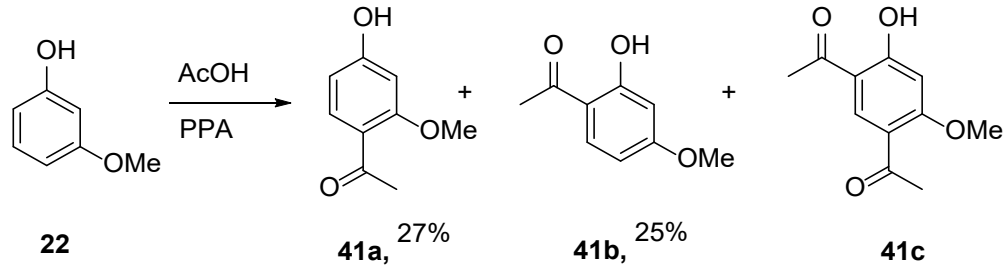

Scheme 34. Acylation of 3-methxoyphenol (**22**) by acetic acid and polyphosphoric acid (PPA).[275]

This acylation was tested with Eaton's reagent, replacing the polyphosphoric acid (PPA) as shown in Scheme 35. Eaton's reagent is a liquid formulation containing 7.7 wt.% phosphorus pentoxide in methanesulfonic acid, it is easier to handle than PPA, which typically exists as a very sticky gel. The experiment results (Table 37) aligned with those previously reported in the literature, producing two regioisomers of singly acylated compounds, a di-acylated compound, and an unidentified peak in GC-MS spectrum. Additionally, the compounds' structures were further analysed using 2D NMR spectroscopy (Section 4.5.0).

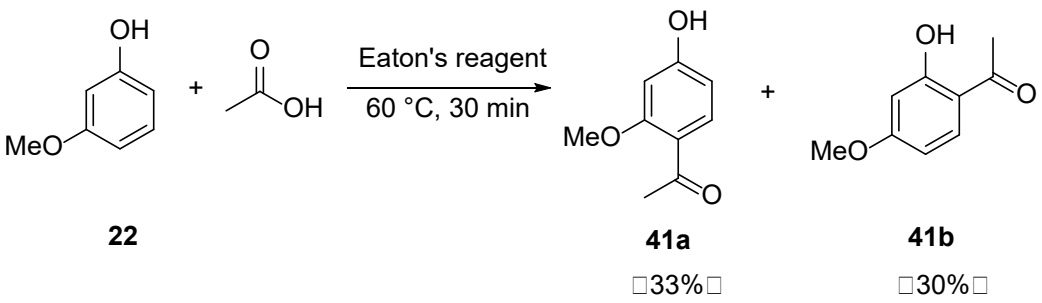

22 **41a** **41b**

□33%□ □30%□

Scheme 35. 3-methoxyphenol (**22**) (10 mmol) and 1.5 eq. of acetic acid stirred in Eaton's reagent (10 g) at 60 °C for 30 min.

Table 37. GC-MS summaries of Scheme 34.

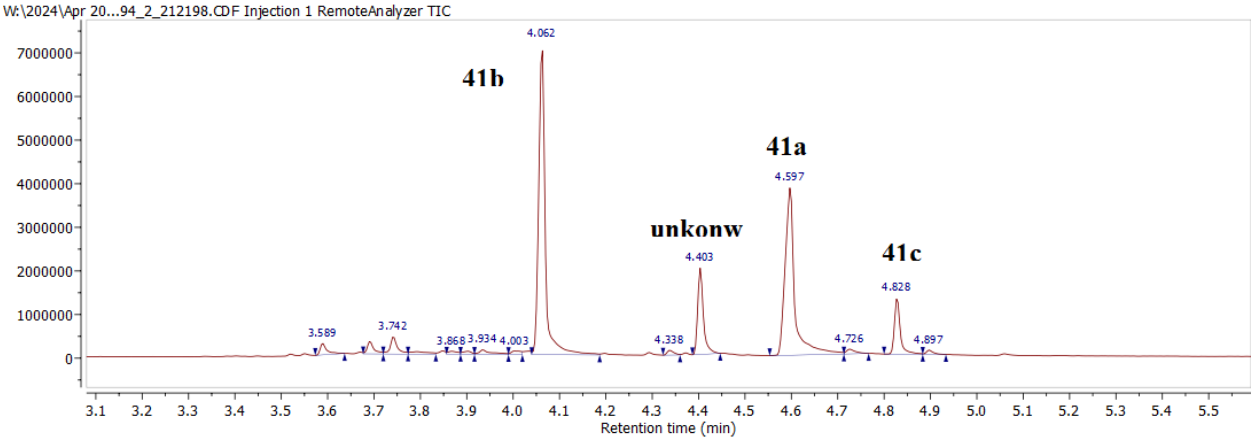

Entry	R_t/ min	m/z	Total area%	Proposed molecule
1	4.06	166.05	40.41	**41b**
2	4.40	202	9.70	unknown
3	4.60	166.05	31.90	**41a**
4	4.83	208.05	6.48	**41c**

Alternatively, halogenated 3-methoxyphenol (**22**) as described previously in Chapter 3 was used as the starting material. This reaction between 2-bromo-5-methoxyphenol (**29**) and acetic acid in Eaton's reagent did not yield the target compound (m/z 200.62) (Scheme 36). Instead, numerous side products were observed (Table 38). The major peaks identified from the mass spectrum exhibited m/z values of 243.95 and 245.95, suggesting the formation of mono acylated 2-bromo-5-methoxyphenol. The bromo group seemingly did not act as a sufficient blocking and deactivating group to facilitate selective acylation under these acidic conditions compared to the mild base system for formylation.

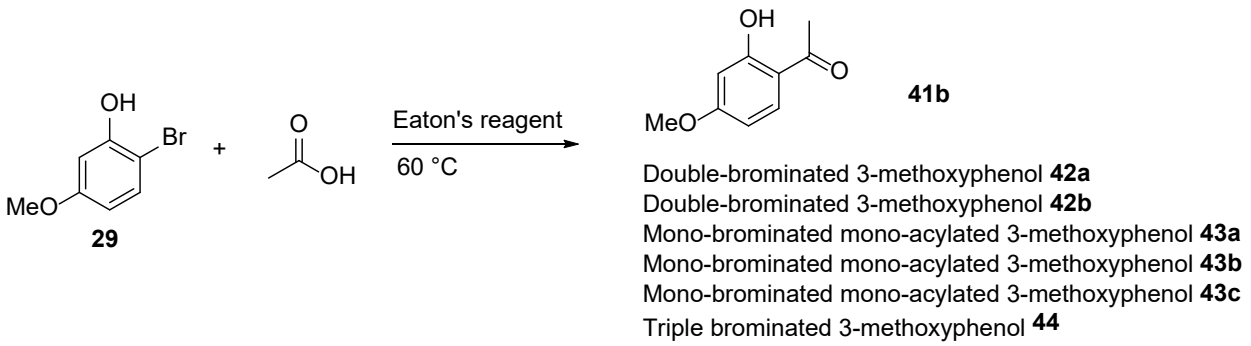

Scheme 36. Acylation of 5 mmol 2-bromo-5-methoxyphenol (**29**) using 1.5 eq. of acetic acid and 5 g Eaton's reagent at 60 °C for 2 h.

Table 38. GC-MS analysis of Scheme 36.

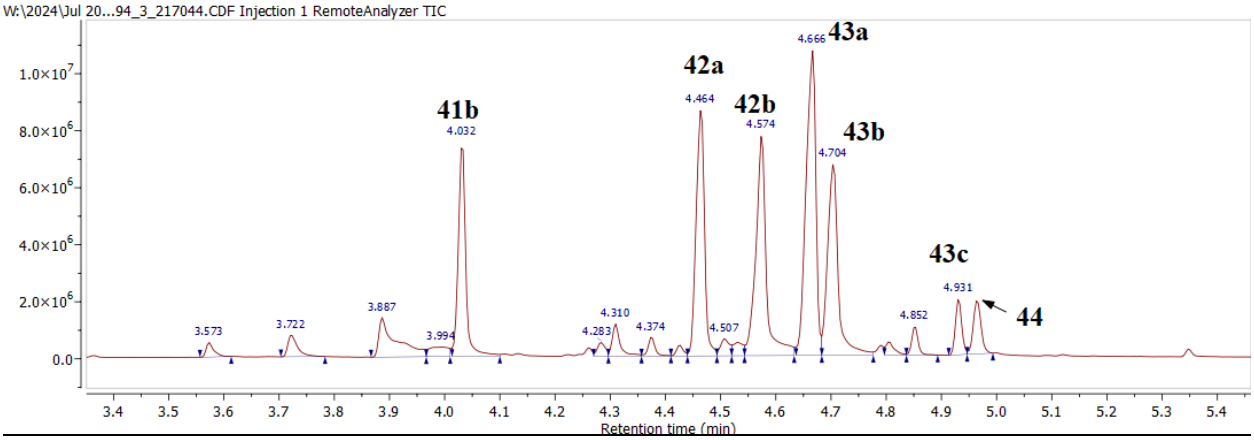

R_t/ min	Indicative m/z	Total area%	Proposed molecule
4.03	166.05	11.25	**41b**
4.47	279.85, 281.90, 283.90	14.70	Double-brominated 3-methoxyphenol (**42a**)
4.57	279.90, 281.90, 283.90	16.34	Double-brominated 3-methoxyphenol (**42b**)
4.67	243.95, 245.95	21.19	Mono-brominated mono-acylated 3-methoxyphenol (**43a**)
4.70	243.95, 245.95	14.39	Mono-brominated mono-acylated 3-methoxyphenol (**43b**)
4.93	244.00, 245.95	2.50	Mono-brominated mono-acylated 3-methoxyphenol (**43c**)
4.96	357.80, 359.80, 361.80, 363.80	2.95	Triple brominated 3-methoxyphenol (**44**)

Other alternative acylation methods such as the Hoesch Reaction for multi-hydroxyphenols in the presence of acids and Lewis acids[277] were not deemed viable. These methodologies often require toxic and corrosive reagents and are less suitable for efficient sustainable synthesis of compound **21**.

The alternative retrosynthetic scheme (Scheme 32B) is more widely explored in the literature as exemplified by Scheme 37, A and B. However, the reported selectivity for synthesizing 2,6-dihydroxyacetophenone (**21**) in these methods is relatively low. Alternatively, 2,6-dihydroxyacetophenone (**21**) can be synthesized from 7-hydroxy-4-methylcoumarin (**45**) (Scheme 37C). This approach requires an extremely high temperature (160 °C) for the Fries rearrangement of 4-methyl-2-oxo-2*H*-chromen-7-yl acetate (**46**). In addition, Scheme 37C was tested under acidic condition using Eaton's reagent as the promotor which yielded 4-methyl-2-oxo-2*H*-chromen-7-yl acetate (**48**) (Table 39). This scheme did not achieve complete consumption of starting materials (Table 39 and 40).

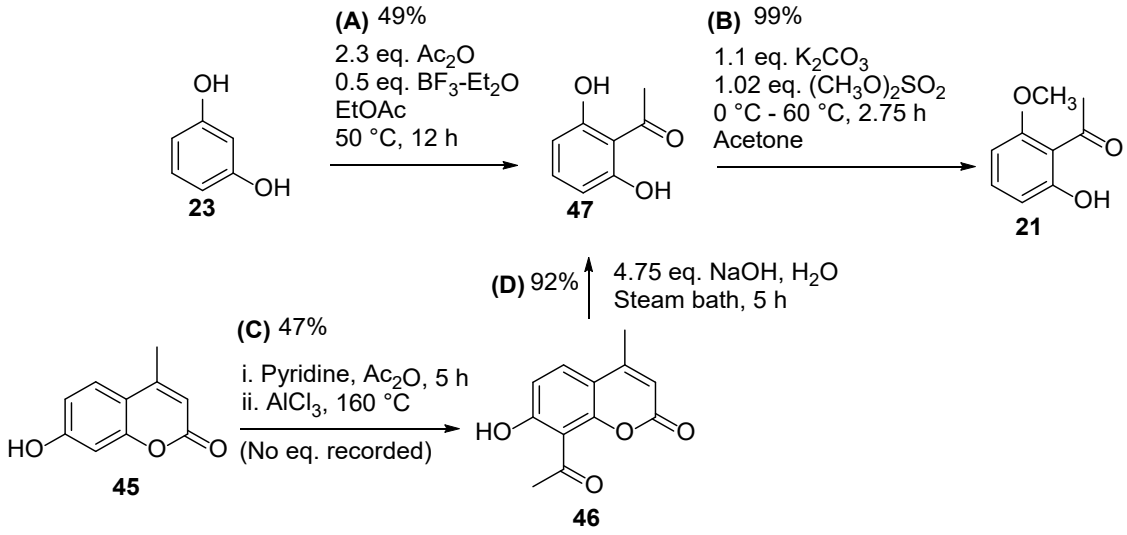

Scheme 37. Literature syntheses: (A) Syntheses of 2,6-dihydroxyacetophenone (**23**).[278, 279] (B) Methylation of 2,6-dihydroxyacetophenone (**47**).[280] (C) Acylation of 7-hydroxy-4-methylcoumarin (**45**).[281] (D) Reduction of **46** [282]

Table 39. Reaction conditions tested for acylation of 7-hydroxy-4-methylcoumarin (**45**).

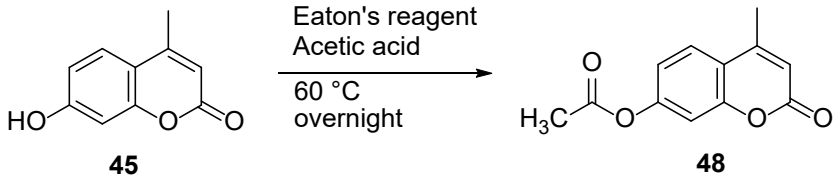

Entry	Scale/ mmol	Equivalent of acetic acid	Mass of Eaton's reagent /g	Temp. /°C	R_t of GC-MS /min	m/z
1	10	1.5	10	60	5.35 5.39 5.57	218.05 176.05 218.05

2	10	1.5	10	80	5.34	218.05
					5.38	176.05
					5.57	218.05
3	5	1.5	5	100	5.40	176.05
4	5	2	5	108	5.38	302.10

Table 40. GC-MS Spectrum of Entry 1 Table 39.

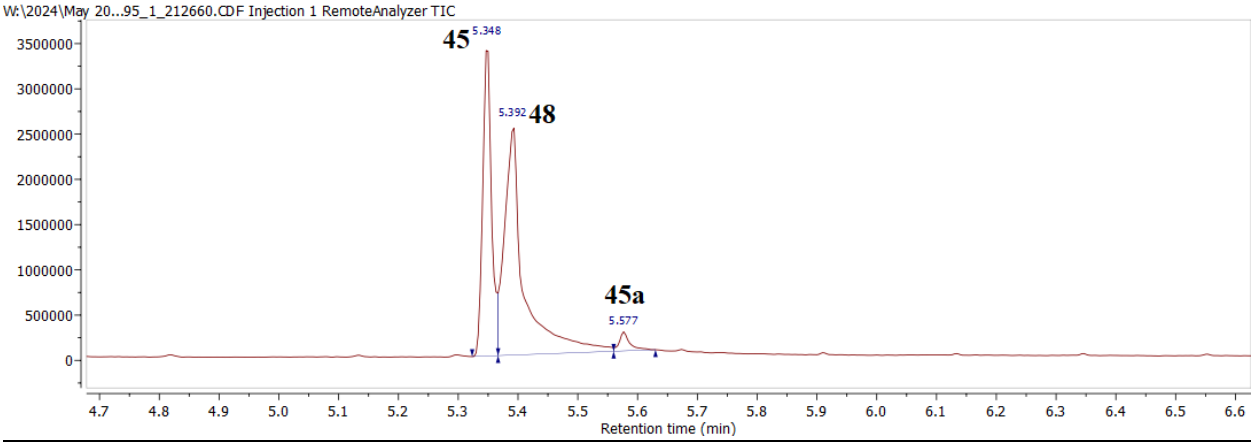

R_t/ min	m/z	Total area%	Proposed molecule
5.35	218.05	37.24	**48**
5.39	176.05	60.06	**45**
5.58	218.05	2.70	Regioisomers of **48 (45a)**

In addition, a flow process has been reported in the literature which achieved an excellent yield of the target compound, exceeding those documented in earlier studies (Scheme 38). This sequence started from cyclohexane-1,3-dione (**54**) which was converted to the target compound via 2-acetylcyclohexane-1,3-dione (**49**), either in batch or flow systems. The integrated process fits well with automation principles; however, the primary limitation of this process is the high cost of the microwave and flow reactors and scaling potential of filtering columns. In addition, the iodine reagent is a non-renewable resource and requires additional treatment to avoid forming halogenated by-products. Other reagents like polystyrene-bound dimethylaminopyridine (PS-DMAP, £101/5 g)[283] are costly.

Synthesis of 2-hydroxy-6-methoxyacetophenone from cyclohexane-1,3-dione

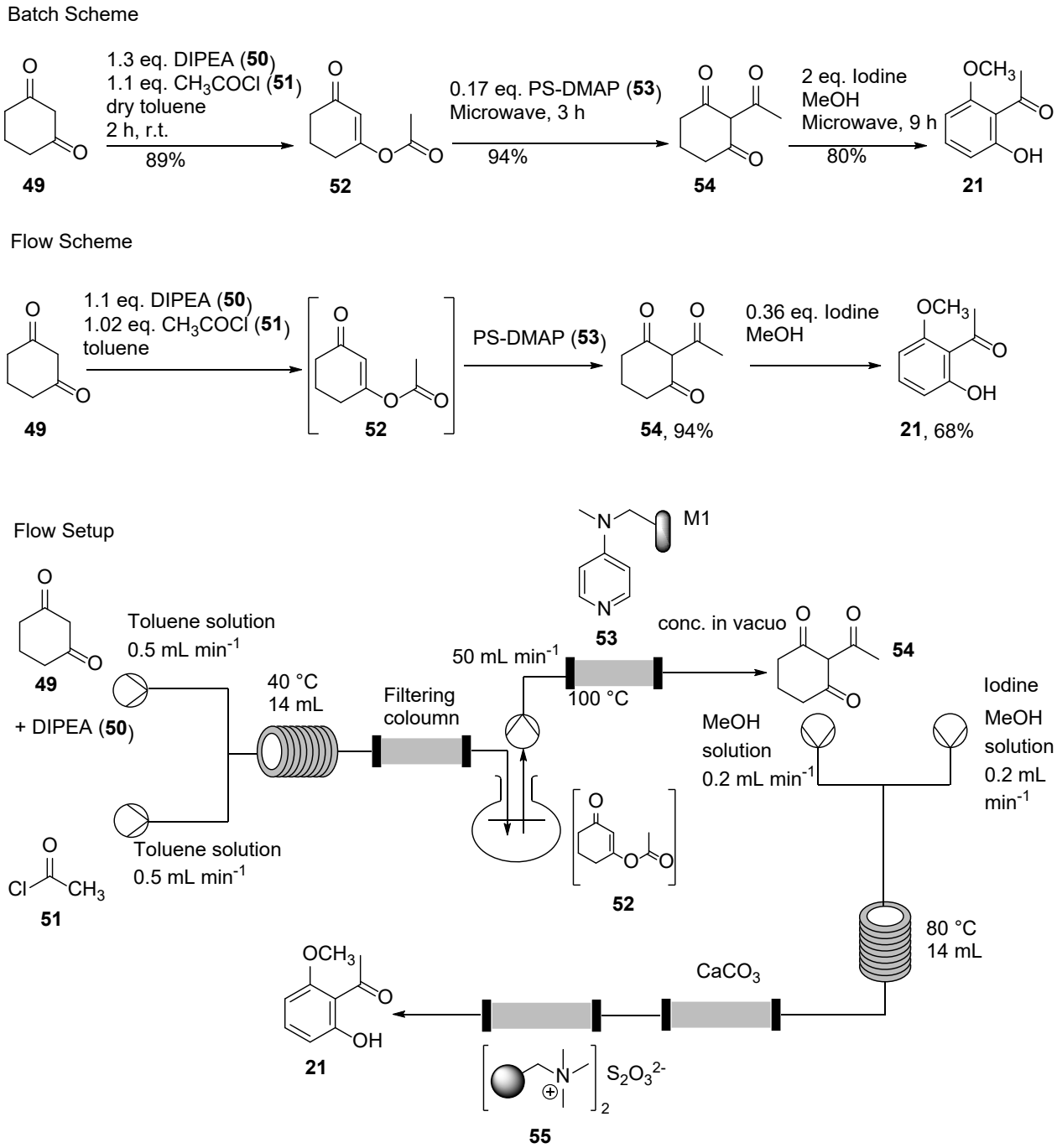

Scheme 38. The batch process and flow process of converting cyclohexane-1,3-dione (**49**) to 2-hydroxy-6-methoxyacetophenone (**21**). DIPEA: *N*,*N*-diisopropylethylamine, PS-DMAP: polystyrene-bound dimethylaminopyridine.[218]

4.2 Acylation of 3-methoxyphenol (22) using $MgCl_2$-Et_3N system

Given the limitations of traditional approaches and the lack of literature precedent, an initial synthetic strategy following methodology developed in Chapter 3 was proposed, employing a $MgCl_2$-Et_3N combination. However, this soft base system was not effective for *ortho*-directed acylation using ethanal (Scheme 39), as only starting material was observed in the reaction mixture. The proposed mechanism for previous reaction does not fit this process.

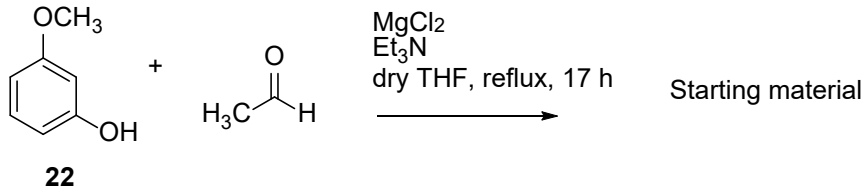

22

Scheme 39. The mild-base system catalyzed reaction where a solution of 3-methoxyphenol (**22**) (10 mmol), 1.5 equivalent anhydrous magnesium dichloride, 3.8 equivalent triethylamine, 7 equivalent of ethanal in dry THF (80 mL) was refluxed for 17 h.

4.3 Alternative Synthesis of 2-hydroxy-6-methoxyacetophenone (21) via ozonolysis

Synthetic plan

In addition to achieving the regioselective acyl group insertion via electrophilic aromatic substitution, we explored functional group interconversion as a strategy to introduce the acyl group onto the aromatic ring (Scheme 40A). Ozonolysis of alkene substrates offers a pathway to generate the desired carbonyl group of compound **7**. Traditionally, alkene substrates react with ozone to form an unstable cyclic primary ozonide which subsequently rearranges into a more stable ozonide via the Criegee intermediate (Scheme 40, B1 to B3). However, one of the notable drawbacks is the use of toxic reductants such as dimethyl sulfide (Me_2S), during the workup. These reagents often result in highly disagreeable smell and complicated purifications (Scheme 40, B4).

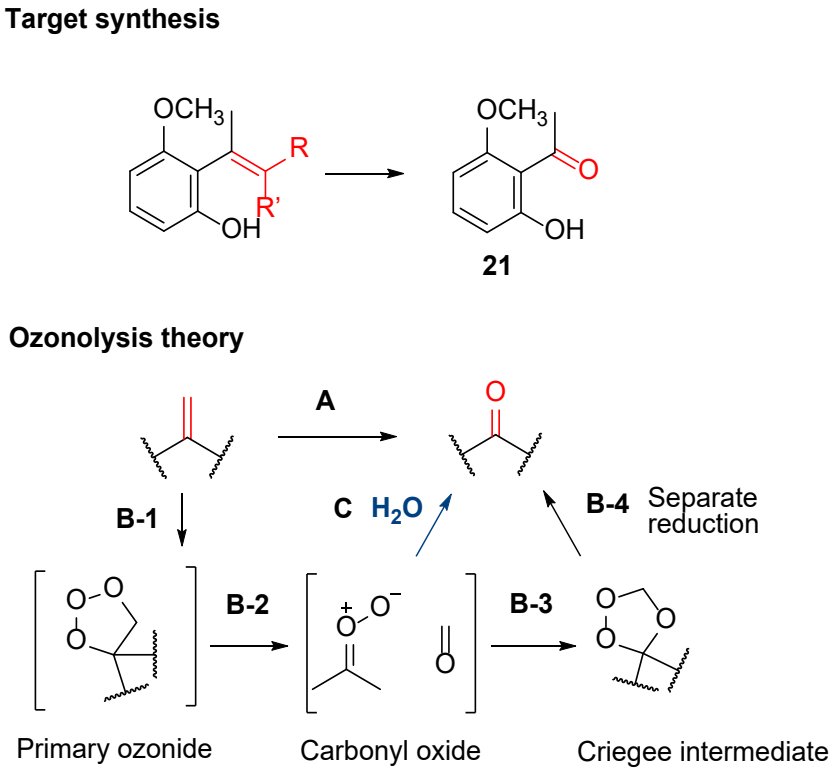

Scheme 40. The scheme to generate carbonyl substrate from alkene functional group via ozonolysis reaction.

In 2008, Schiaffo and Dussault addressed these challenges by developing a preparative scale method for direct aldehyde formation through alkene ozonolysis without relying on unfavourable reductants.[284] Instead, they employed water as a cosolvent, trapping the carbonyl oxide in the solution phase upon its formation (Scheme 40C). To synthesise the target, the required alkene starting material could be the coumarin derivative, namely, 5-methoxy-4-methylcoumarin (**56**), as shown by the mechanism in Scheme 41. The preparation of this starting material is therefore crucial for the proposed ozonolysis. The synthesis plan is thus described in two sections, firstly preparation of 5-methoxy4-methylcoumairn (**56**) and secondly synthesis of 2-hydroxy-6-methoxyacetophenone (**21**) via ozonolysis.

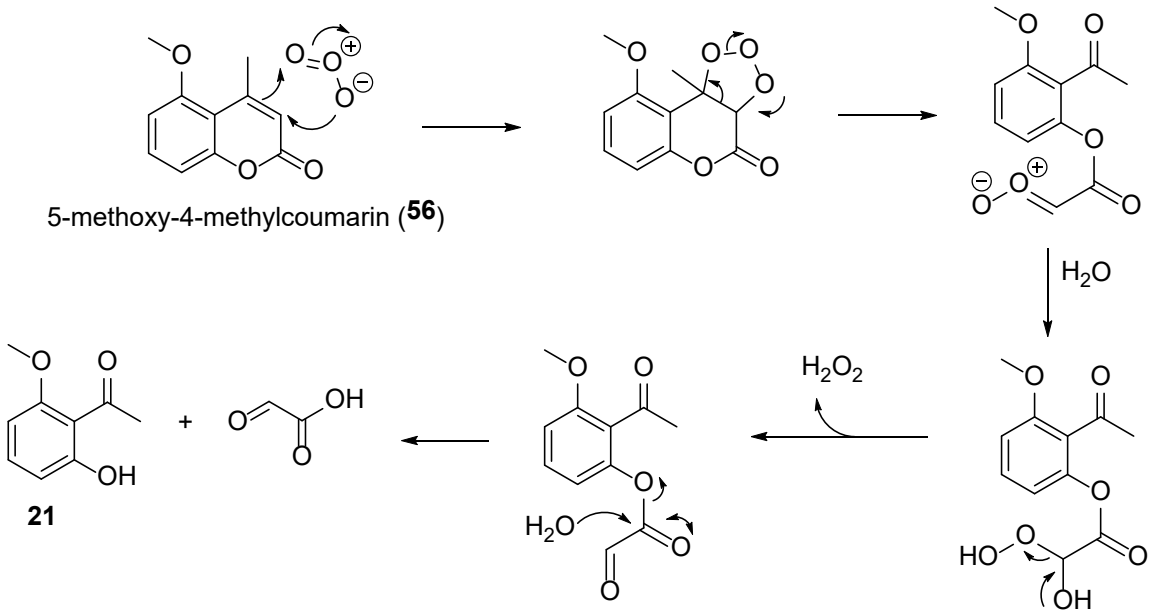

Scheme 41. Proposed mechanism of ozonolysis of 5-methoxy-4-methylcoumarin (**56**).

Coumarin preparation

Coumarin compounds are widespread in nature and are renowned for their diverse biological activities and therapeutic applications.[285] One the most famous examples is warfarin, a widely used anticoagulant that prevent blood clots (Figure 70). Due to the expensive and time-intensive process of isolating these substrates from natural sources, significant efforts have been made to develop new synthetic methodologies. The most common strategies for preparing coumarin substrates involve a variety of condensations reactions, such as the Knoevenagel reaction and the Pechmann

condensation with precursors such as benzaldehydes, phenols, and acetophenones.[285] Scheme 42A illustrates syntheses of coumarins from benzaldehyde and ester substrates. Alternatively, Scheme 42B presented the condensation of resorcinol substrates and 1,3-diketone derivatives. Finally, Scheme 42C presents the formation of coumarin derivatives from acetophenones and 1,3-diketones.

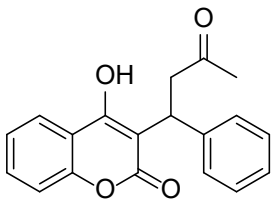

Figure 70. Warfarin structure.

Despite the variety of different syntheses reported none of these methods were suitable for preparing our specific coumarin derivative **56**. The position of the reactive sites of starting materials is one of the prohibitive reasons. As depicted in Scheme 43, for resorcinol (**23**) and 3-methoxyphenol (**22**), an attack at position 9 is more favourable than the more sterically hindered 2 position. This is supported by computational analysis presented in Chapter 3.2.1, Table 26, 27 and is corroborated by experimental results documented in the literature.[286] Acetophenone substrates, when reacted with *α*,*β*-diketones or *α*,*β*-dicyanides, tend to produce undesired substituents at position 4, as illustrated in Scheme 42C. A retrosynthesis of 5-methoxy-4-methylcoumarin (**56**) is presented in Scheme 44. The first pathway involves intramolecular cyclisation of **59**, where **59** is derived from a ketone-ester condensation of 2-methoxyacetophenone (**57**) followed by the hydrolysis of **58**. The second disconnection focuses on preparing compound **56** via the methylation of the hydroxy group in compound **61.** Compound **61** is derived from oxidation of compound **60**. Compound **60** is readily accessed in our laboratory, synthesised from 1,3-cyclohexanedione (**49**) and ethyl acetoacetate using a base catalyst. Herein, the remainder of this chapter will first describe the preparation of 5-methoxy-4-methylcoumarin (**56**) and then the detail of ozonolysis of this coumarin substrate.

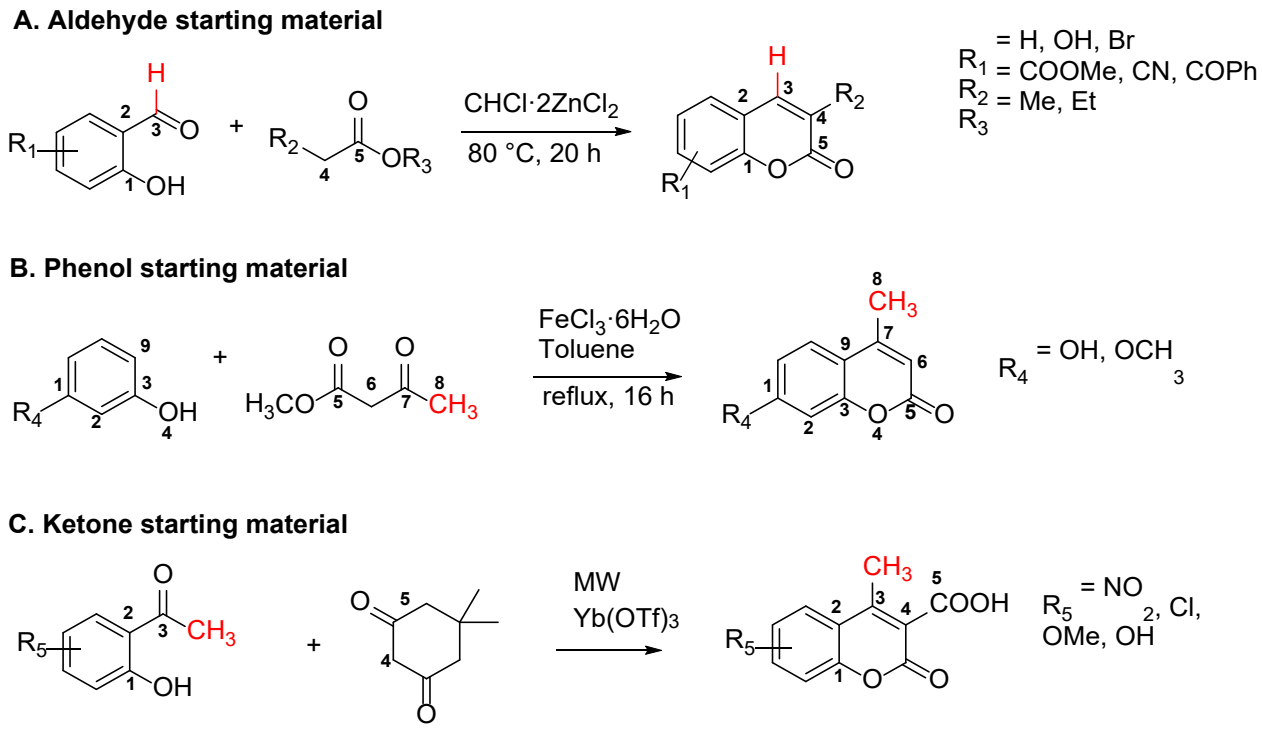

Scheme 42. Examples of coumarin substrates syntheses from benzaldehydes, phenols and acetophenones.

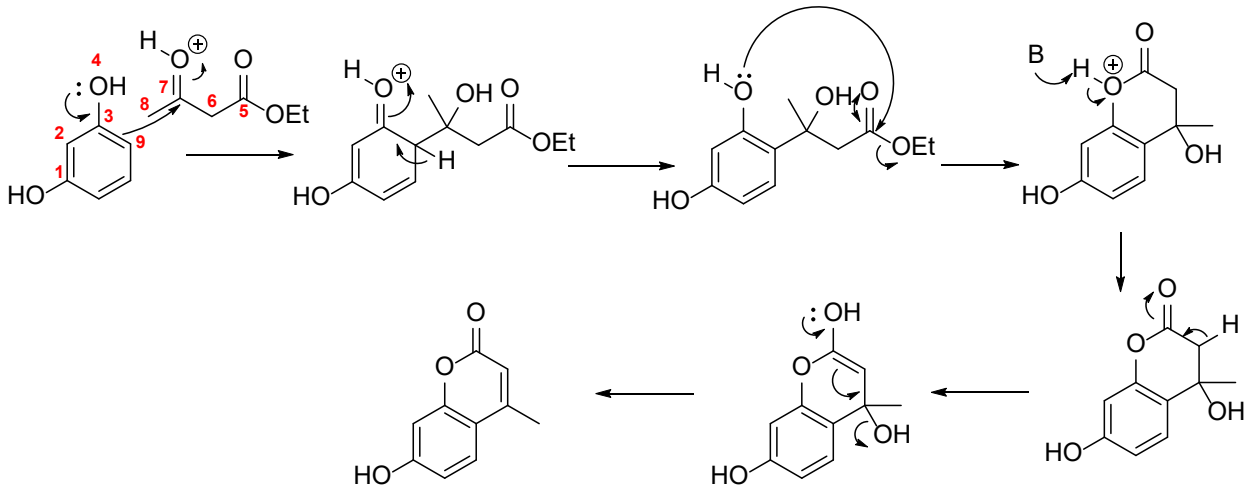

Scheme 43. Proposed mechanism of the Pechmann condensation.[287]

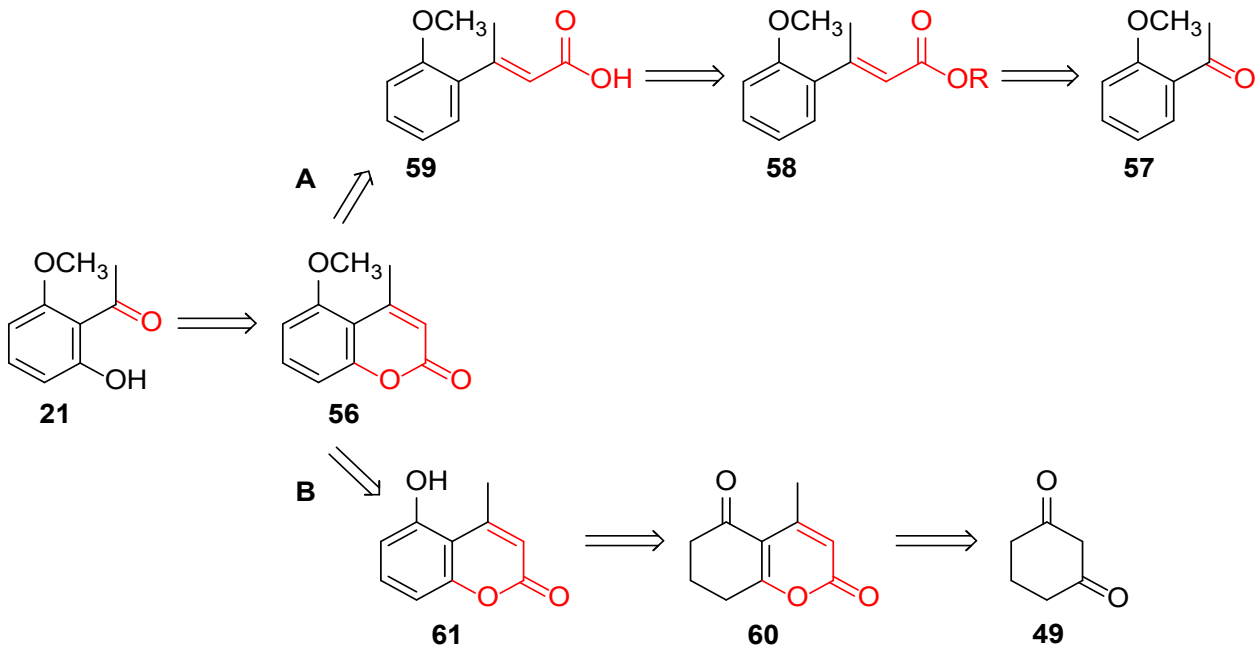

Scheme 44. Retrosynthesis of target molecule **21**.

4.3.1 Route 1 preparation of 5-methoxy-4-methylcoumarin

The first preparation scheme is a biosynthesis inspired approach for coumarin synthesis, further explored in the organic preparation of coumarin derivatives (Scheme 45A and 45B).[288, 289] Both conversions utilised light as a source of chemical energy to promote the *E* to *Z* isomerization of the phenylpropanoid derivatives, which subsequently form coumarin derivatives by intramolecular cyclisation as a sequential two-step process. Since the literature synthesis did not incorporate substituents at position 3 of the phenylpropanoid derivative, this compound was initially prepared from 2-methoxyacetophenone (**57**) (Scheme 46, 47).[290] A customized designed photoreactor was used to conduct this reaction (Figure 71 and 72). The process was initially tested following the literature scheme using riboflavin (**62**) as the photocatalyst, but this catalyst had poor solubility in acetonitrile and methanol mixtures. To increase solubility of the catalyst, the riboflavin (**62**) was converted into its tetraacetate **63** (Scheme 48). The photosynthesis reaction of substrate yielded compounds **59a** and **64** (Scheme 49).

A Biosynthesis of coumarin

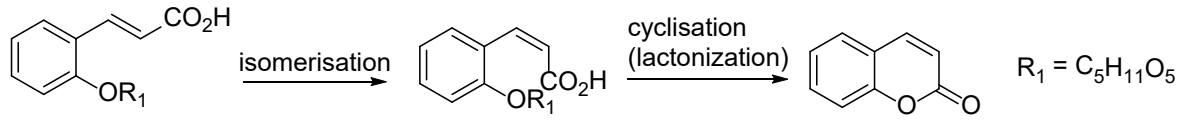

B Organic photosynthesis of some coumarin substrates

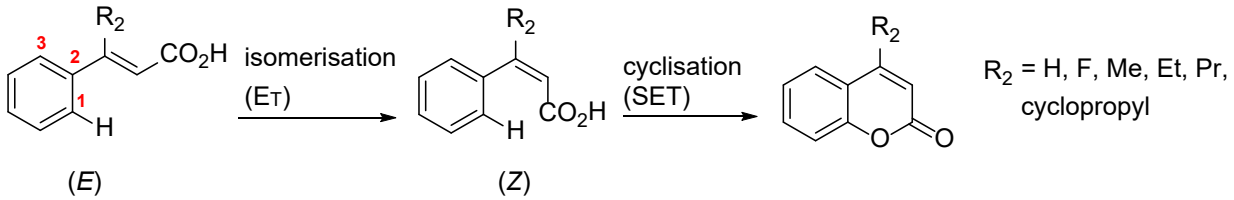

Scheme 45. Coumarin synthesis via intramolecular cyclisation of phenylpropanoid.

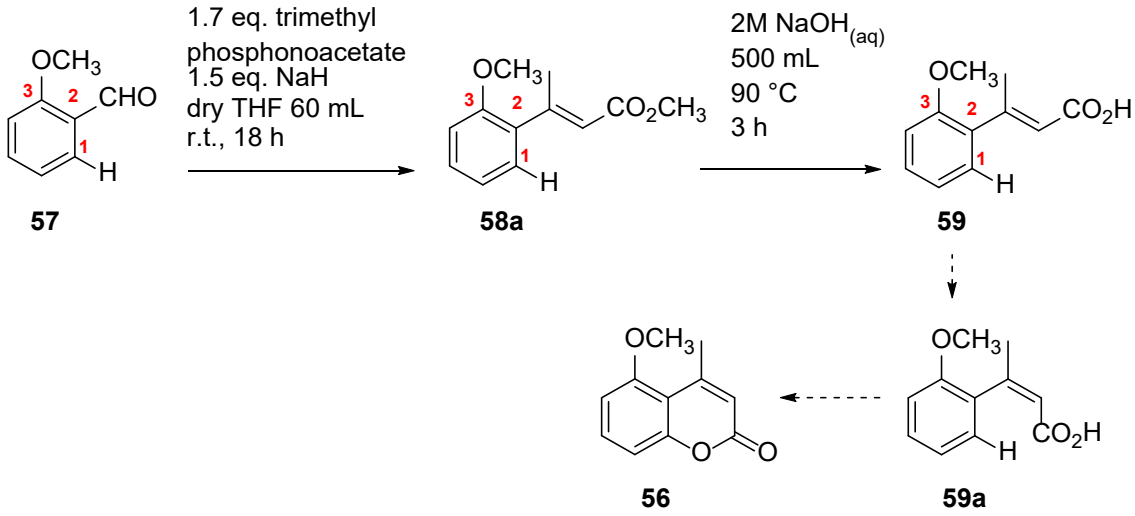

Scheme 46. The preparation of phenolpropanoid derivative and proposed target synthesis for **56**.

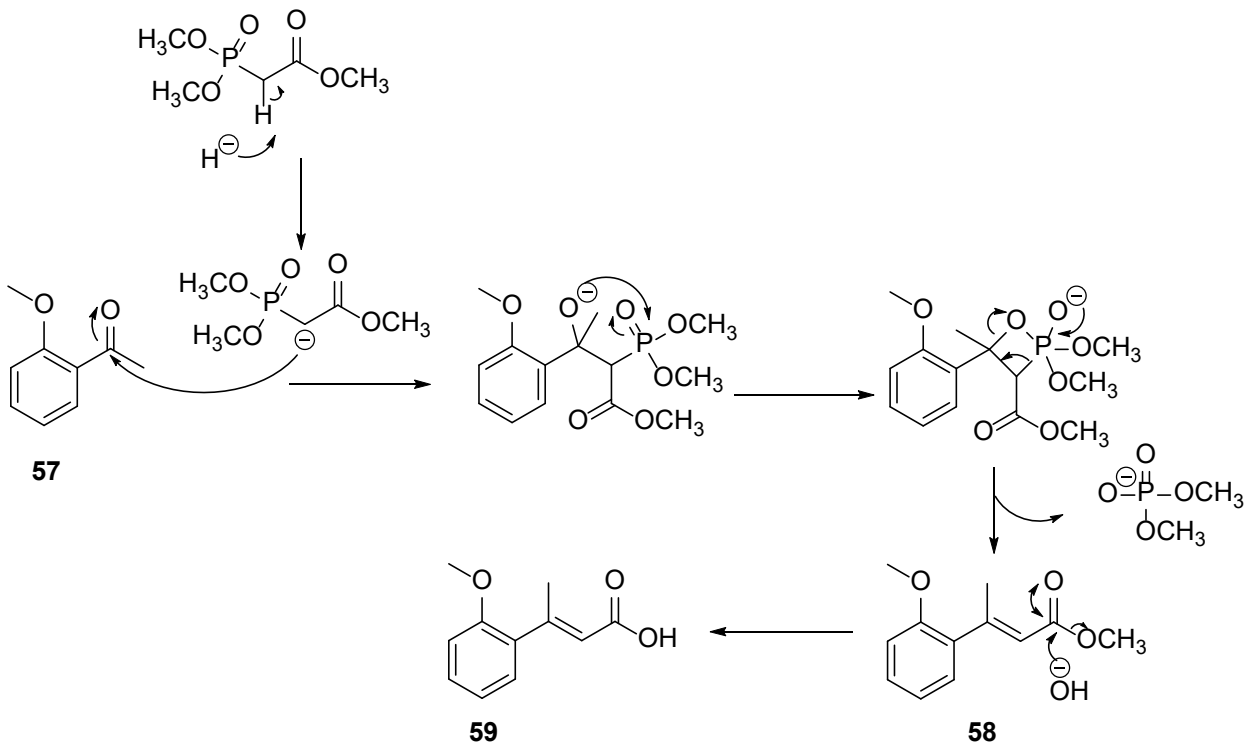

Scheme 47. Proposed mechanism for synthesis of (*E*)-3-(2-methoxyphenyl)but-2-enoic acid (**59**).

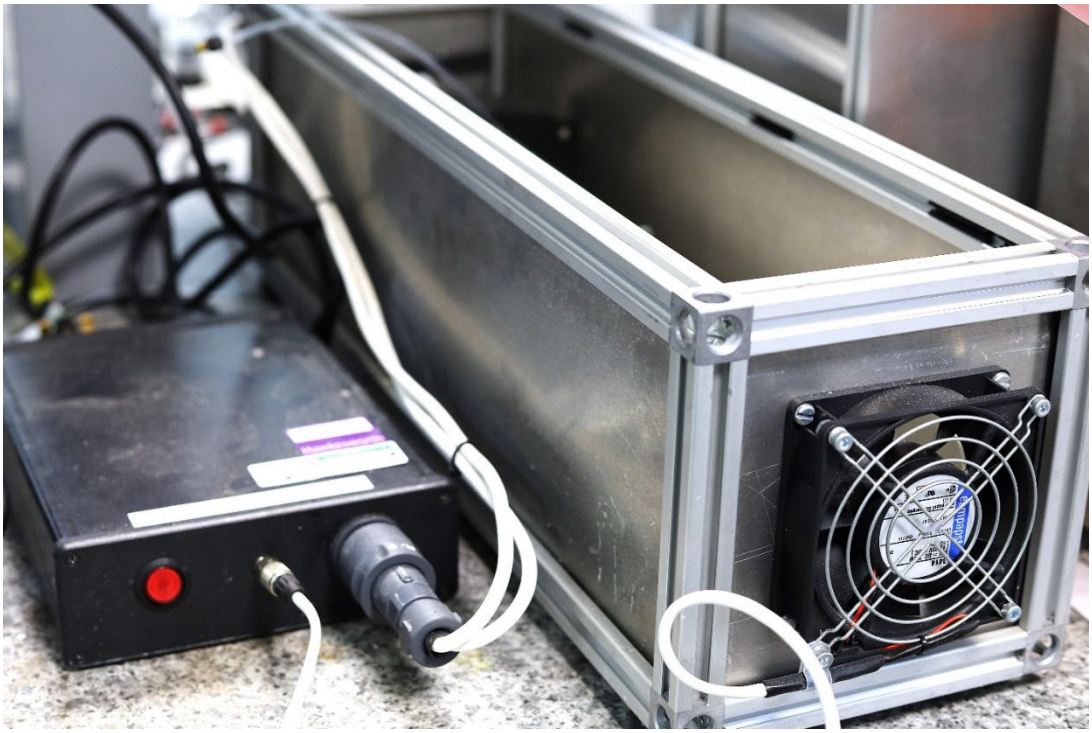

Figure 71.Customized design of photoreactor.

Figure 72. Interior look of the customised design of the photoreactor.

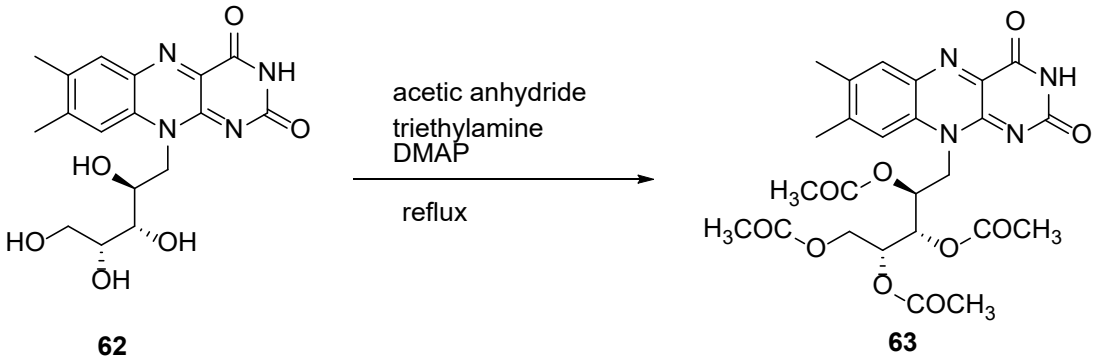

62 **63**

Scheme 48. Conversion of riboflavin into riboflavin tetraacetate (**63**).

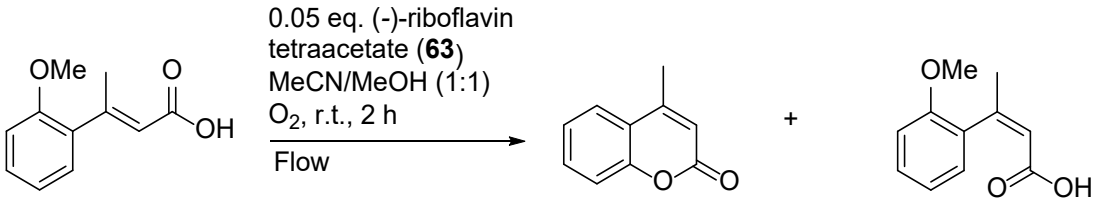

59 **64** **59a**

Scheme 49. Conversion of (*E*)-3-(2-methoxyphenyl)but-2-enoic acid (**59**) by (-)-riboflavin tetraacetate (**63**) catalyzed photosynthesis.

The NMR data of **64** is given in Figure 73. The ^{1}H NMR spectroscopy, crystal structure, and computed optimized structure of **59a** are shown in Figures 74 and 75. While 4-methyl coumarin **64** was formed, the target compound was not observed.

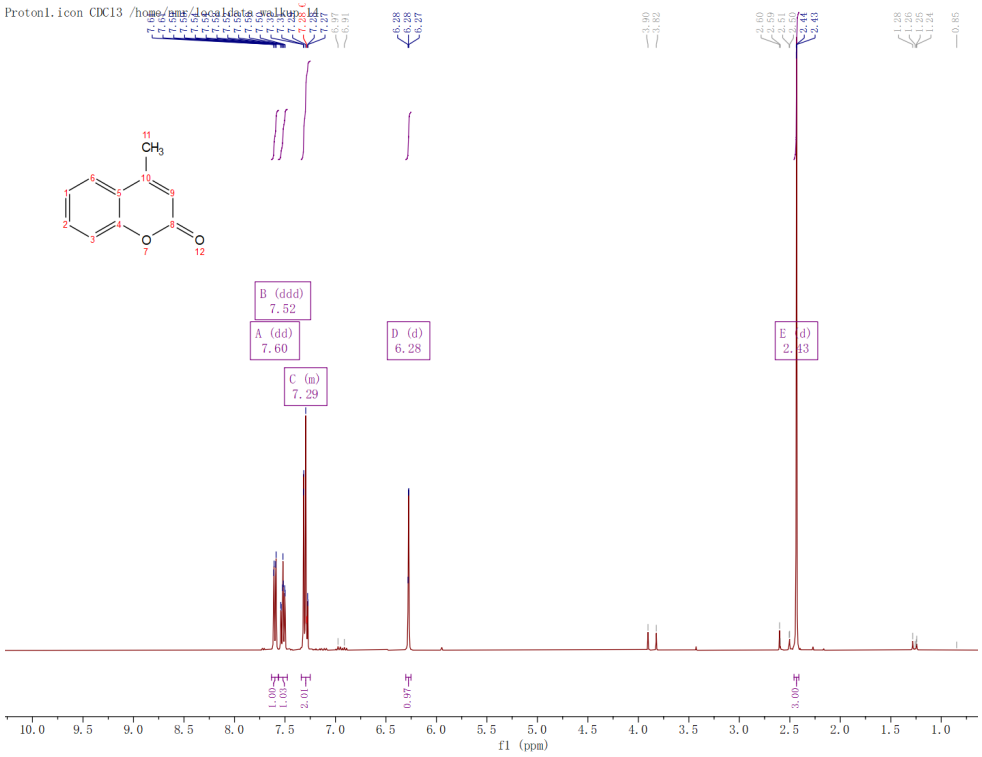

Figure 73. ^{1}H NMR spectroscopic analysis for proposed 4-methylcoumarin (**64**).

A mechanism resembling the biosynthetic pathway (Scheme 45A) was proposed, in which the methoxy group participates in intramolecular cyclisation. As noted in the literature discussed earlier, the other study employing photosynthesis to produce coumarin derivatives[288] also has a hydrogen atom at the position occupied by the methoxy group (position 3, Scheme 45B). This 1,3-dihydrogen attached structure potentially attributes to the selectivity of the intramolecular cyclisation.[291] Upon reviewing the second catalyst system (Scheme 50), LC-MS analysis of the crude mixture revealed the formation of the *cis* isomer with a retention time (R_t) of 2.42 minutes (Figure 76). However, neither catalyst system afforded the desired target molecule **56**. Additionally, 2-methoxyacetophenone (**57**), when used as a starting material in this approach, is significantly more expensive than cyclohexane-1,3-dione (**49**), as utilised in route B (Scheme 44). Therefore, to align with green and efficient synthesis principles and considering time constraints, the second option (Route B) was explored further as presented in Scheme 44.

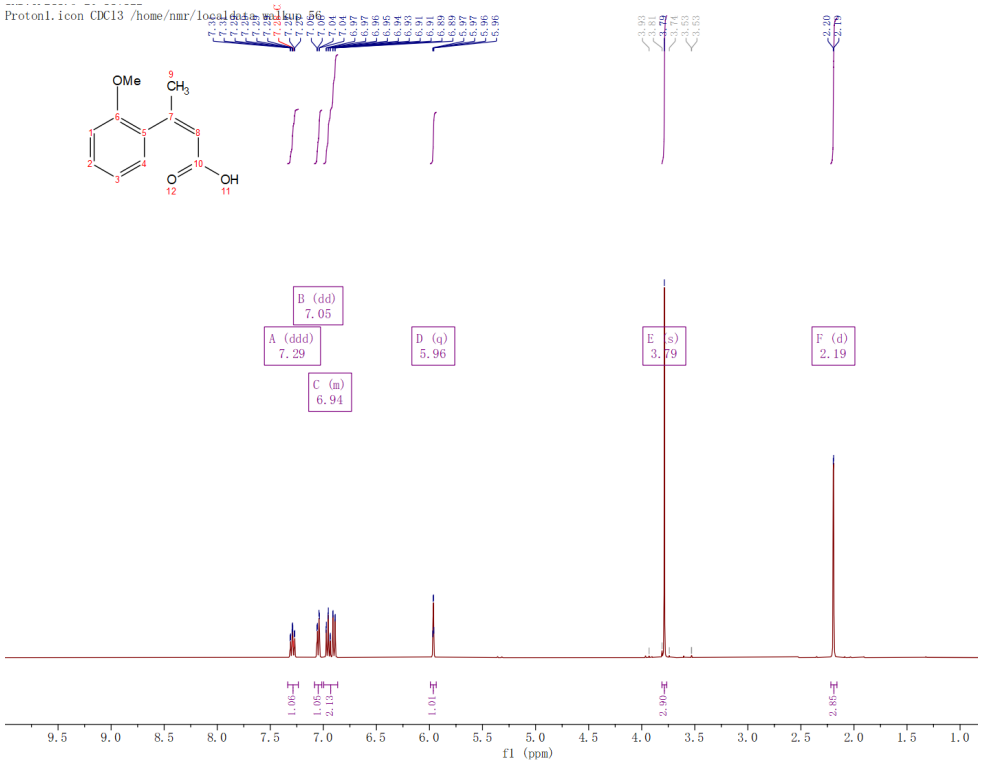

Figure 74. ^{1}H NMR spectroscopic analysis for (*Z*)-3-(2-methoxyphenyl)but-2-enoic acid (**59a**).

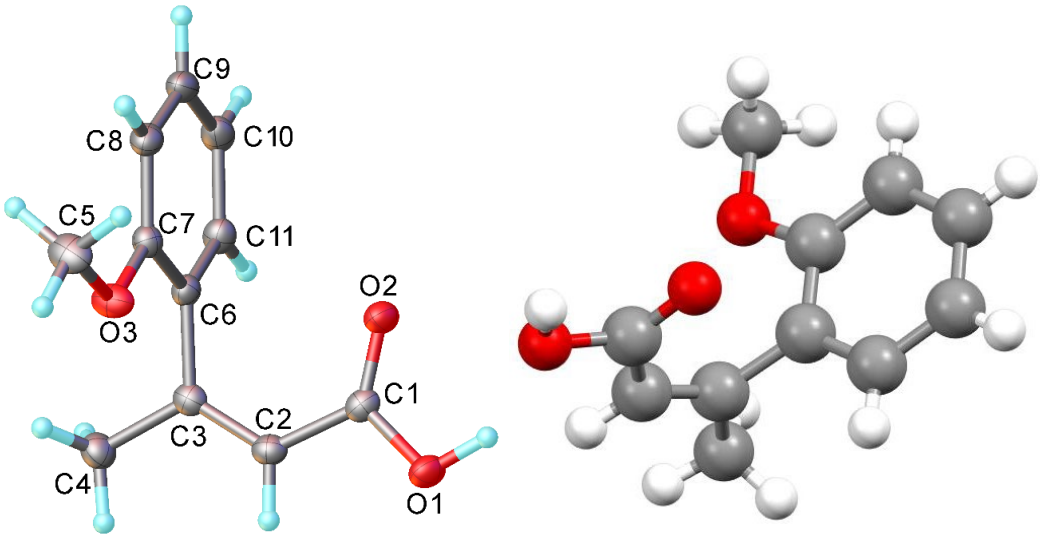

Figure 75. Left, Crystal structure of (*Z*)-3-(2-methoxyphenyl)but-2-enoic acid (**59a**). Right, geometry optimized structure **59a** as given by Gaussian 16.

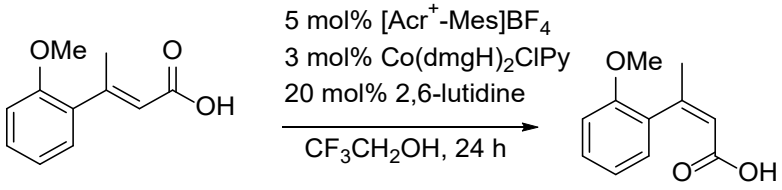

Scheme 50. Alternative photocatalysis scheme.

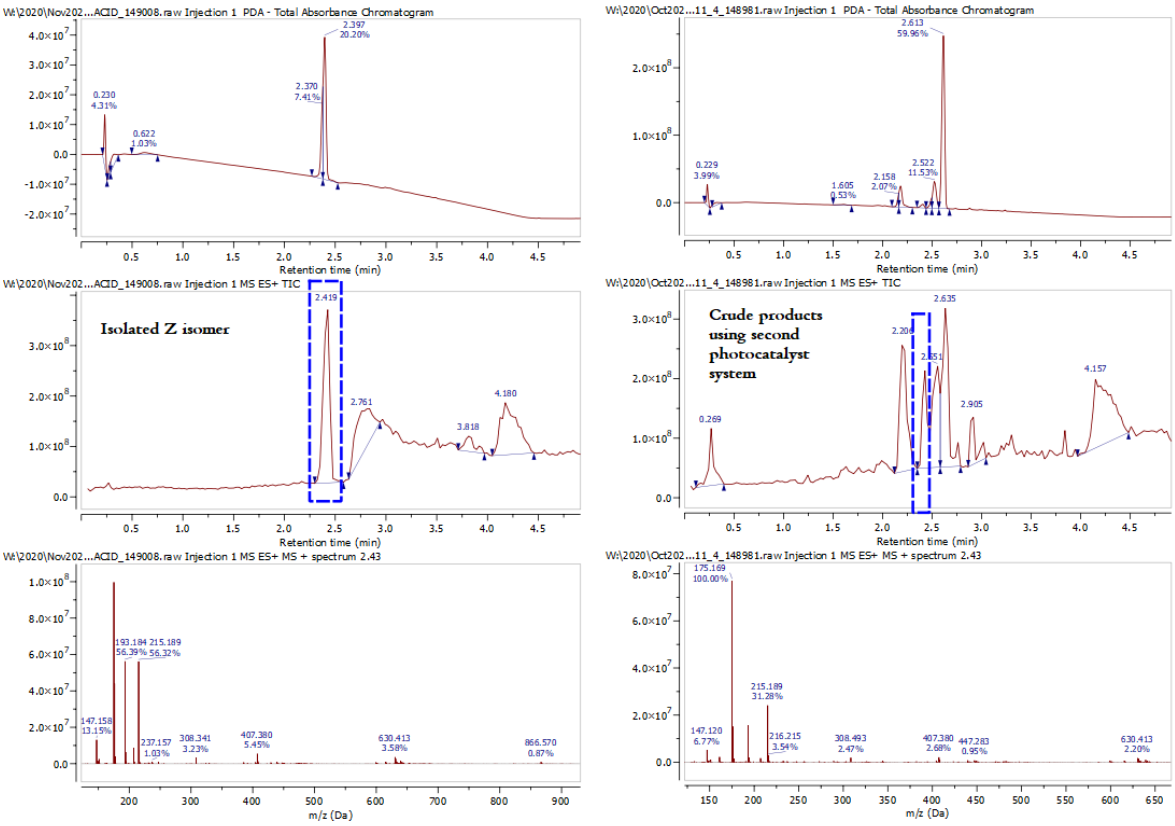

Figure 76. LC-MS comparison of isolated (*Z*)-3-(2-methoxyphenyl)but-2-enoic acid (**59a**) and crude products of Scheme 49.

4.3.2 Preparation of 5-methoxy-4-methylcouamrin from 4-methyl-7,8-dihydro-2*H*-chromene-2,5(6*H*)-dione (17)

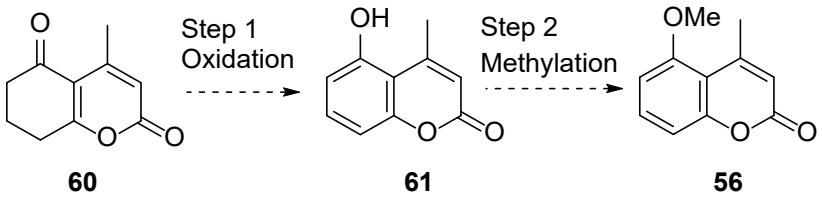

Scheme 51. Planned synthesis of 5-methoxy-4-methyl coumarin (**56**).

The second preparation was a novel synthesis with two proposed steps, firstly forming 5-hydroxy-4-methylcoumarin (**61**) from oxidation of 4-methyl-7,8-dihydro-2*H*-chromene-2,5(6*H*)-dione (**60**) and secondly *O*-methylation of 5-hydroxy-4-methylcoumarin (**61**) can yield 5-methoxy-4-methylcoumarin (**56**) in principle (Scheme 51).

(i) Method 1, by oxidizing agents

The first oxidation was trialed using 2,3-dichloro-5,6-dicyano-1,4-benzoquinone (DDQ; **65**). This oxidant has been successfully employed by Brady *et al*. in 1984 to synthesize 3,6,8-substituted coumarins from 3-substituted-5,6,7,8-tetrahydrocoumarins (Scheme 52).[292] The proposed hydride transfer mechanism is a consecutive process of transferring protons, starting from DDQ (**65**) and forming semiquinone (**65a**) and DDQ-H_2 (**65b**) in order (Scheme 53). The use of DDQ (**65**) is an eco-friendlier oxidant compared to many other inorganic oxidants which are more toxic and expensive in general.[293] Examples in the literature have also shown it can be coupled with other oxidant for improved efficiency, stability and reduced toxicity (e.g. bleach and oxygen). Herein, super stoichiometric quantity of DDQ (**65**) was tested for this dehydrogenation process as shown by Table 41.

Initially, the proposition was tested using 1,4-dioxane[294], 3 equivalents of DDQ (**65**) and acid catalysts under conventional heating to explore the conversion of the starting material. The reaction conditions are listed in Table 41, Entry 1-4 and GC-MS analysis are in Table 42, Entry 1-4. The ratio of 4-hydroxy-5-methylcoumarin (**61**) in the crude mixture was approximated using the total area% of GC-MS for initial screening of the various reaction conditions.

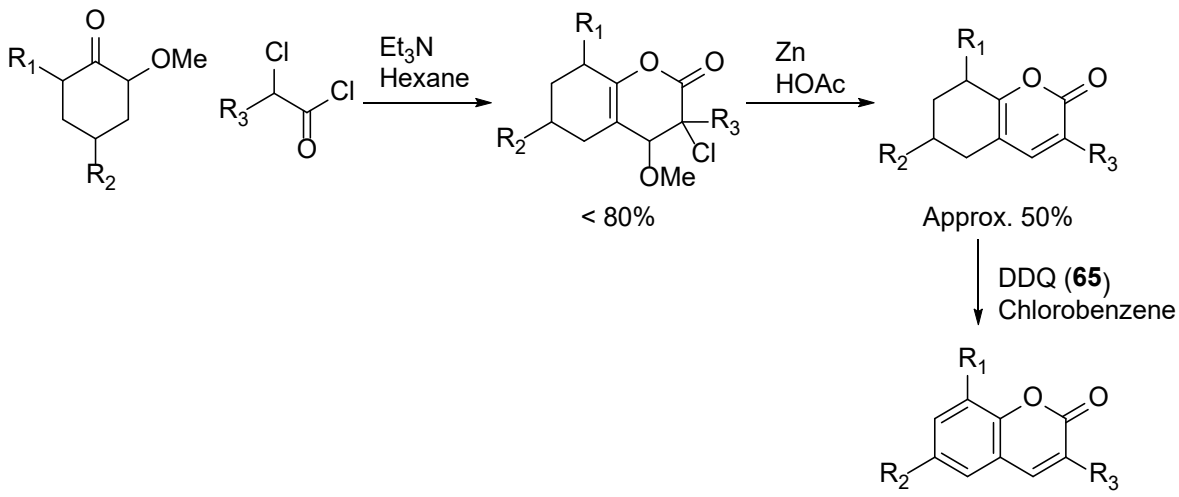

Scheme 52. Literature synthesis of coumarin substrates via oxidation step.

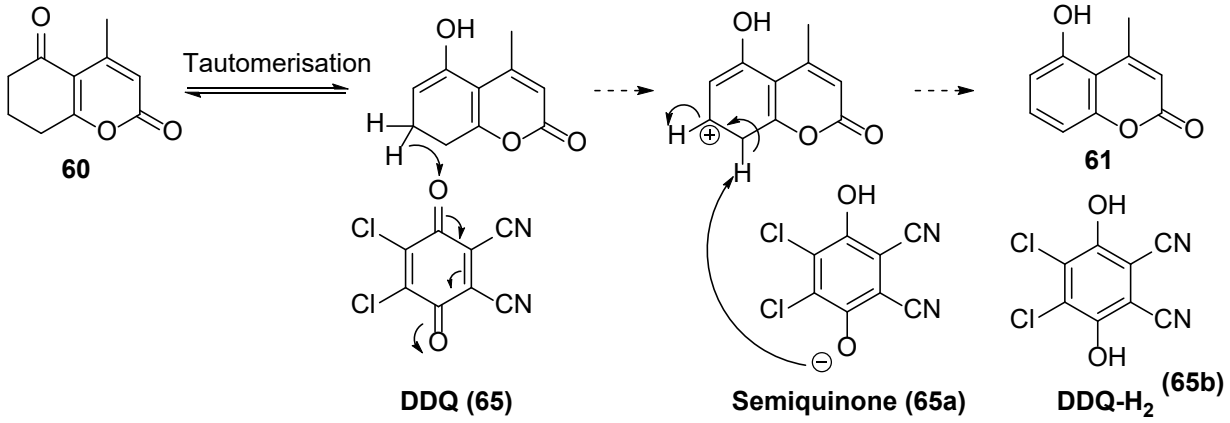

Scheme 53. Proposed mechanism for oxidation of 4-methyl-7,8-dihydro-2*H*-chromene-2,5(6*H*)-dione (**60**) by DDQ (**65**) and the three oxidation states, quinone, semiquinone (one-electron-reduced), and hydroquinone (two-electron-reduced).

The retention time of **61** was obtained from the purified and fully characterized material. Note that the peak at retention time (R_t) between 4.68 – 4.71 min with m/z 178.05 was the starting material and R_t at between 5.30 – 5.37 min with m/z 176.00 relates to the target structure **61**. The best conversion of **61** achieved was given by Entry 2 where BF_3•OEt_2 was used as the additive under conventional heating (Table 42). To employ greater energy beyond the reflux temperature of dioxane, a microwave reactor was used to induce super-heated conditions. The better conversion of the **61** was achieved without additives this time (Entry 5 vs Entry 6, Table 41 and 42) but a longer reaction time led to no product peak at the usual retention time (Entry 7, Table 41 and 42).

Table 41. Rection conditions of dehydrogenation test with super stoichiometric quantity of DDQ (**65**). RXN Time = Reaction Time

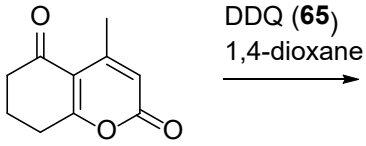

60

Entry	Scale/ mmol	Equivalent of DDQ	Solvent 1,4-dioxane	Additives	RXN Time	Temperature/°C
Conventional heating						
1	10	3	20 mL	/	24 h	Reflux
2	10	3	20 mL	0.2 eq. BF_3•OEt_2	24 h	Reflux
3	5	3	10 mL	0.2 eq. PTSA•H_2O	24 h	Reflux
4	5	3	10 mL	0.2 eq. Acetic acid	24 h	Reflux
Microwave						
5	5	3	10 mL	/	1 h	150
6	5	3	10 mL	0.2 eq. BF_3•OEt_2	1 h	150
7	5	3	10 mL	/	4 h	150

Table 42. Total area% of GC-MS analysis of proposed starting material m/z and product m/z of reaction conditions in Table 41.

Entry	R_t = 4.68 – 4.71 min, m/z 178.05	R_t = 5.30 – 5.37 min, m/z 176.05
	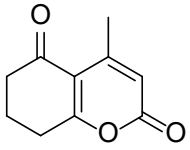	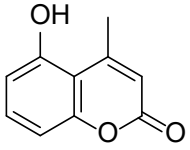
	60	**61**
Conventional heating		
1	26	9
2	30	10 (10.4)
3	16	5
4	24	10 (9.5)
Microwave		
5	44	26
6	30	12
7	/	/

Due to the encountered low conversions, the proposed reaction was analysed (Scheme 54, Figure 77). In its neutral state, the keto tautomer is more stable than its corresponding enol form.[295] If tautomerization to achieve the enol form is the rate determining step to generate the product then

the lack of efficiency for the reaction would be explained by the low concentration of the enol tautomer under the above reaction conditions. In the excited state, the enol radical is more stable than its corresponding keto tautomer since it is the lower energy tautomer, achieving the desired intermediate for proposed oxidation (Figure 77). Evidentially, researchers have shown that under photo-excited conditions, 1-tetralone (**66**) was successfully converted to α-naphthol (**67**) via one-step oxidation synthesis (Scheme 55 and 56).[296] The energies of electronic structure of our starting material (**60**) and target compound (**61**) were estimated. The AM1 method performed using Gaussian 16 was chosen for its balanced efficiency and accuracy as explained in the literature.[297] The energy computed for the neutral keto form was -0.16 eV which is more stable than the enol form at 0.23 eV, in the excited state the keto form is less stable (9.12 eV) than the enol form (8.00 eV) (Figure 74). These values agree with conclusions drawn from other literature studies[296] and account for the potential reason for the low conversion in our reaction. In addition, other oxidants were tested for comparisons including oxone, DMSO, Mn_2O and trimethyl oxoacetate, none of these produced the target as analyzed by LC-MS under conventional heating. Conventionally, photochemical reactors are used to generate enol radicals through the application of photoredox catalysts. The proposed scheme for this reaction is shown in Scheme 54B.

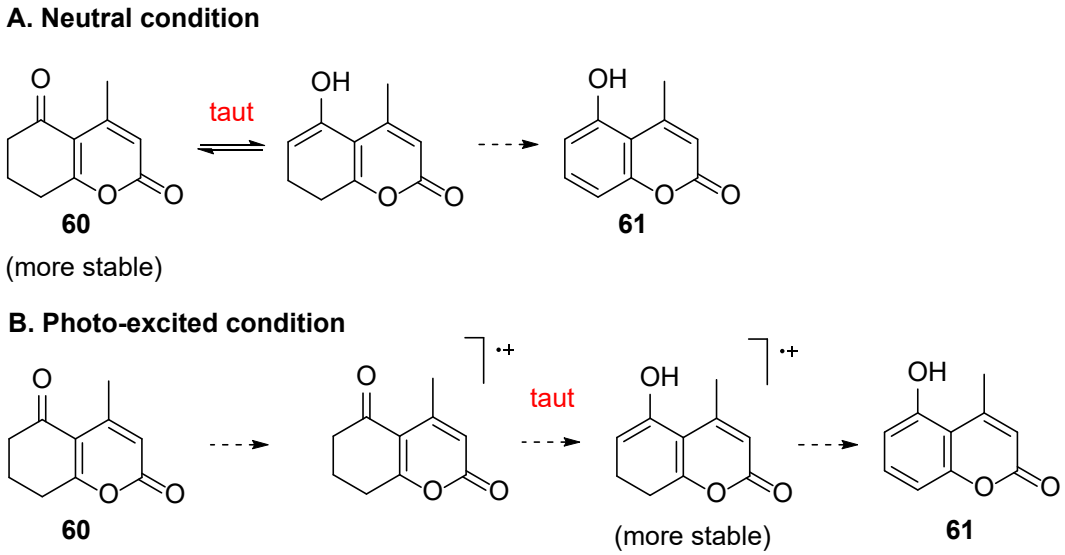

Scheme 54. Proposed reaction of oxidising **60** under neutral or excited conditions. The stability of two tautomer are analysed in Figure 77.

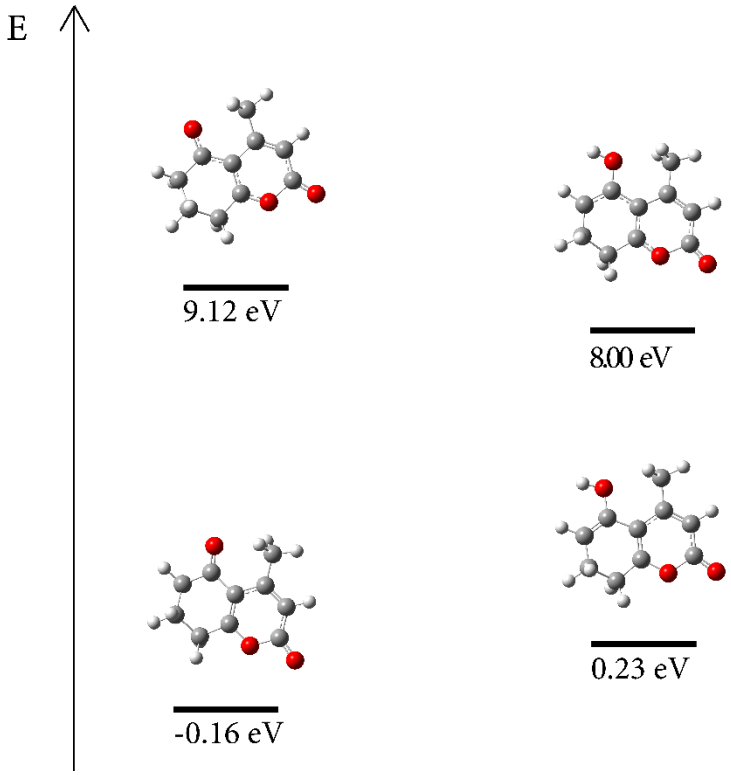

Figure 77. Energy plot of gaseous enol and keto tautomer at neutral and radical state. At neutral state, energy of keto form = -0.16 eV, energy of enol form = 0.23 eV. At excited state, energy of keto form = 9.12 eV, energy of enol form = 8.00 eV.

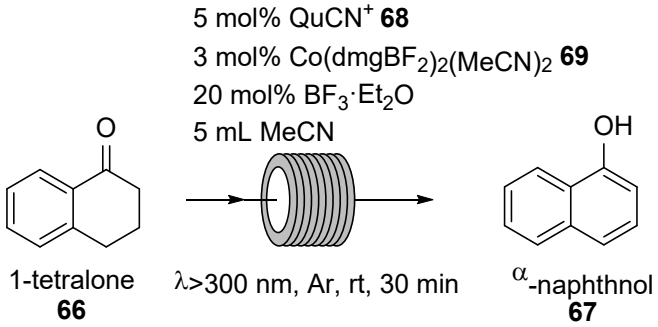

Scheme 55. The photocatalytic conversion of 1-tetralone (**66**) to *α*-naphthols (**67**).[296]

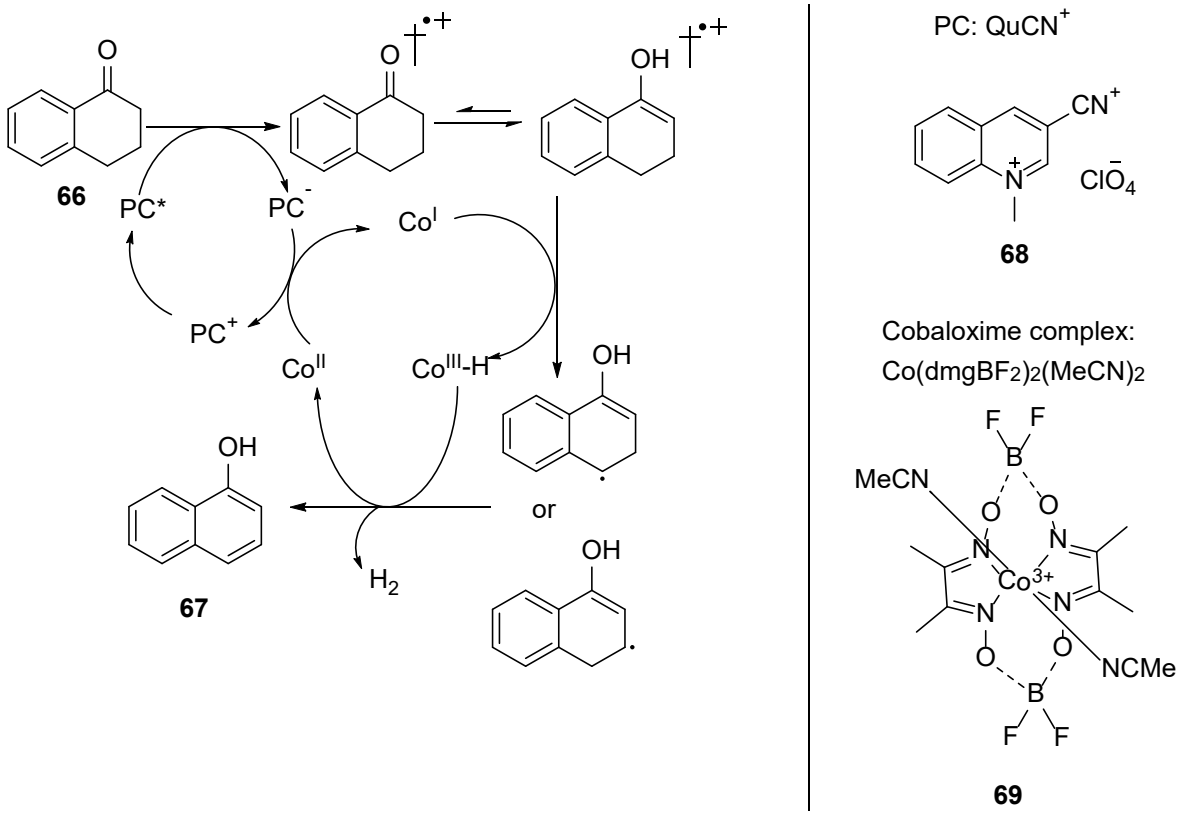

Scheme 56. Mechanism for photocatalytic dehydrogenation of 1-tetralone (**66**) to α-naphthols (**67**).[296]

There are two values used to help select catalysts. Firstly, the one-electron oxidative potential of the substrate (E_{ox}) and reduction potential of the excited catalyst (E^*_{red}).[298] According to Equation 15 the E^*_{red} of the photoredox catalyst needs to be more positive than E_{ox} to obtain a negative value of the Gibbs free energy (ΔG_{PET}), i.e. to ensure the reaction is feasible.

$$\Delta G_{PET} = -F\{[E_{red}(Cat/Cat^{\bullet+}) + E_{0,0}] - E_{ox}(Sub^{\bullet+}/Sub)\}$$
$$= -F[E^*_{red}(Cat^*/Cat^{\bullet+}) - E_{ox}(Sub^{\bullet+}/Sub)]$$

Equation 15. The Gibbs energy of photoinduced energy transfer involving reduction of excited catalyst (Cat^*) and reduction of ground state substrate (sub). ΔG_{EPT}: Gibbs free energy of photoinduced electron transfer. F: Fraday's constant (23.061 kcal $V^{-1}mol^{-1}$). $E_{red}(Cat/Cat^{\bullet+})$: Ground state reduction potential of the catalyst. $E_{0,0}$ ($E^{S1}_{0,0}$ *or* $E^{T1}_{0,0}$): excited state energy (Excited State Energy of the First Singlet, Excited State S_1 / Excited State Energy of the First Triplet Excited State T_1.). E_{ox} ($Sub^{\bullet+}/Sub$): Ground state oxidation potential of the substrate. $E^*_{red}(Cat^*/Cat^{\bullet+})$: The excited state potential of the catalyst.

The values are commonly measured by cyclic voltammetry when the electron-transfer process is reversible. For non-reversible reactions, pulse radiolysis is seen as the only accurate spectroscopic technique for measurement.[297, 299] Keto-enol tautomerisation is a reversible process, in principle the electron transfer process can therefore be measured by cyclic voltammetry, but this is not currently available in the department. Alternatively, computational analysis can be a helpful tool for designing molecules with the desired redox potentials[300, 301] while the calculated estimations still have inaccuracies.[297,178,179] To overcome this problem, literature reference combined with calculation predictions was used to select our photoredox catalysts which will be explained below. The first combination was 3-cyano-1-methylquionolinium perchlorate ($QuCN^+$; **68**) and the cobaloxime complex **69**, the second choice was DDQ (**65**). The reactor set up will be explained first followed by the catalyst(s) selection and then the reaction conditions employed.

The UV150 photochemical reactor was assembled with a Vapourtec E series (Figure 78). The peristaltic pump provides the stream of reaction mixture to the photochemical reactor at the prescribed flow rate. Two types of light source were used: high power LED at 365 nm (Figure 79) and a medium pressure mercury lamp with broad radiant output from 220 nm to 600 nm (Figure 80). For the rest part of the thesis, these systems will be abbreviated as ‘LED’ and ‘mercury lamp’.

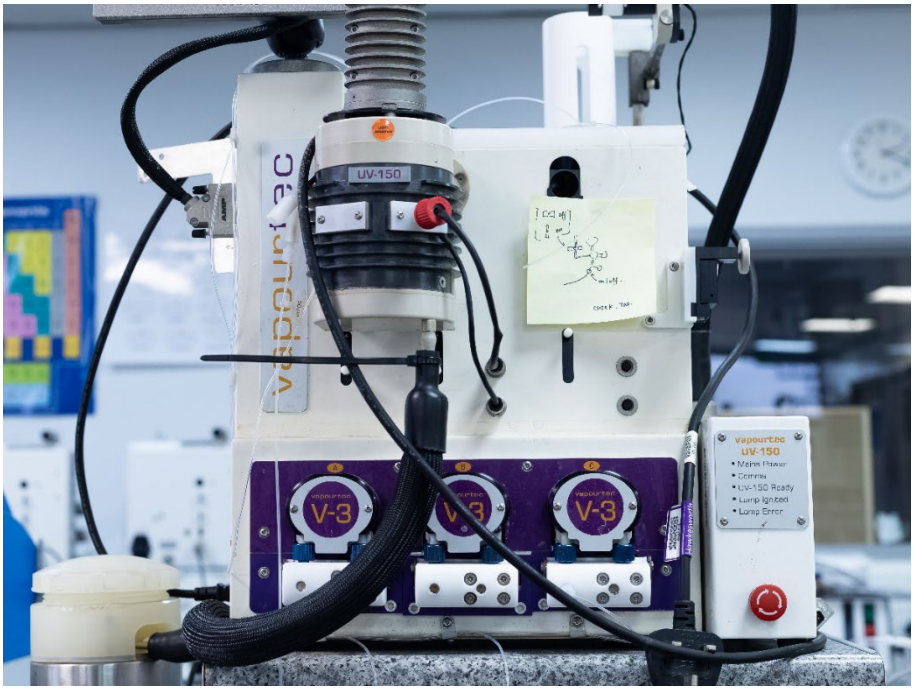

Figure 78. The Vapourtec UV150 photochemical reactor used in experimentation.

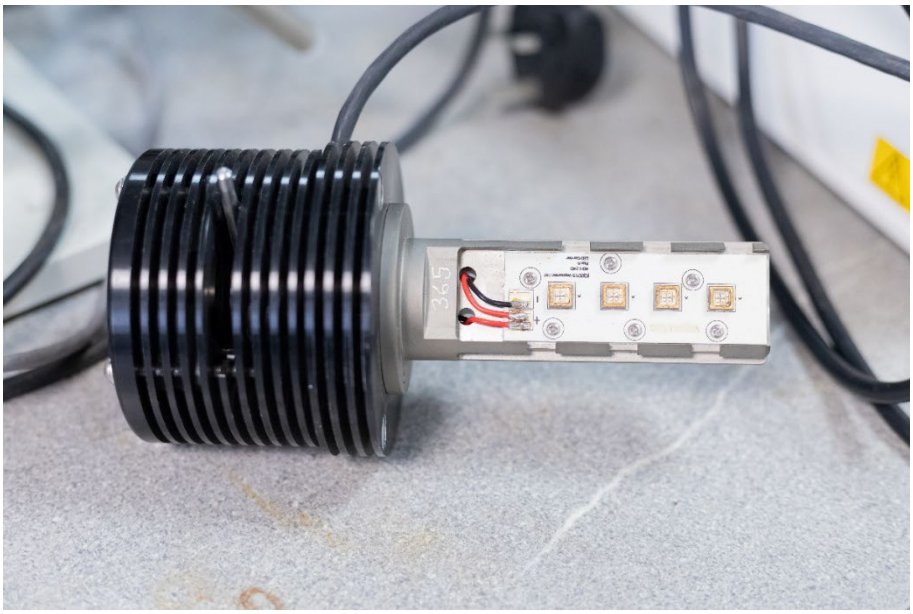

Figure 79. High power LED at 365 nm.

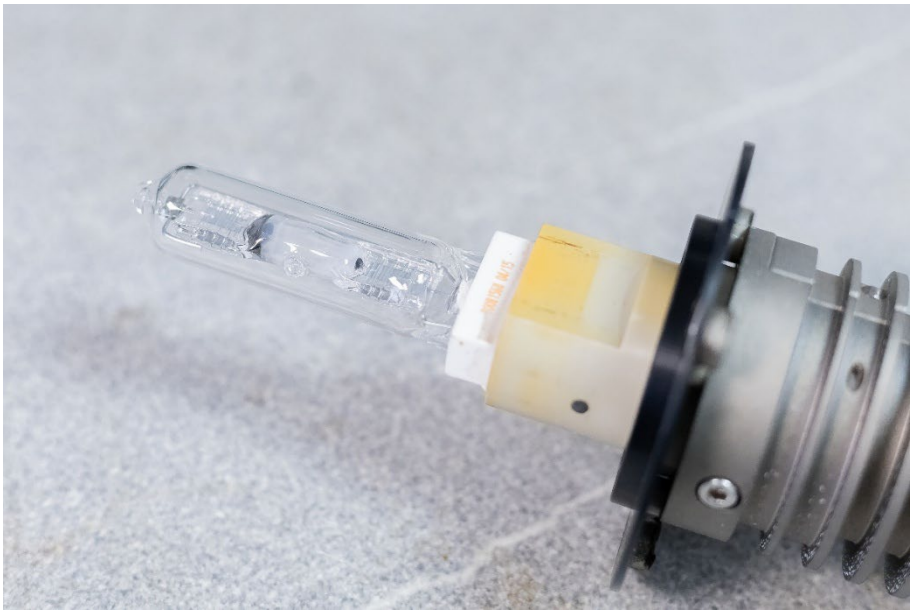

Figure 80. Medium pressure mercury lamp with broad radiant output from 220 nm to 600 nm.

Redox catalysts 1: ($QuCN^+$) and and cobaloxime complex

The $QuCN^+$ **68** and cobalxime complex **69** dual catalyst system was discovered in the work of He *et al*. published in 2019 where they reported the photocatalytic dehydrogenation of 1-tetralone (**66**) to α-naphthol (**67**) (Scheme 55).[296] While various cobaloxime complexes (**69**, **69a**, etc.) have been reported (Figure 81), **69a** was selected for this study due to its straightforward synthesis from readily available starting materials, facilitating a rapid evaluation of the method.

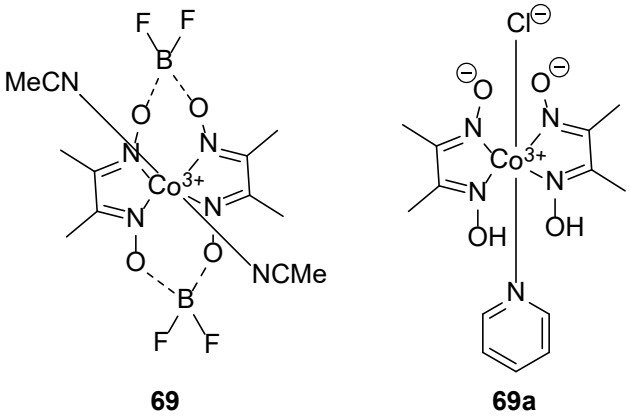

Figure 81. Structure of cobalxime complex 69 and 69a.

In this dual catalyst system, $QuCN^+$ **68** is responsible for generating the enol radical cation and the cobalxime complex then captures the proton eliminated from the enol to afford the α-naphthols (Scheme 55). As previously discussed, (Equation 15), the excited-state reduction potential of $QuCN^+$ **68** (2.72 V vs. SCE) needs to be higher than the one-electron oxidation potential of 1-tetralone (**66**) (2.51 V vs. SCE) reported in literature. Since computational methods have uncertain inaccuracies,[297] the calculated oxidative potential of **60** was not used as reference for reagent screening purposes. Literature studies have shown a strong linear relationship between HOMO energy and oxidative potential.[297, 302] This can be explained by the mechanism of oxidation and reduction where oxidation removes electrons from HOMO, while reduction adds electrons to LUMO; thus, redox potentials are closely related to the HOMO and LUMO energy levels.[303] To select screening catalyst for this reaction, HOMO energies were computed using Gaussian 16 for three model chemistries, namely AM1, HF/3-21G, and B3LYP/6-31G(d) (Table 43). The HOMO energy of 1-tetralone (**66**) is calculated as slightly lower than **60**, indicating that the HOMO-LUMO energy gap of **60** and the photocatalyst is reasonable for screening tests.

Table 43. HOMO energy estimations were computed by Gaussian 16. Values were reported in atomic units (a.u.). The atomic units multiplied by 27.2114 provide energy in electron volts (eV). Geometry optimisations of these compounds were carried out at AM1, HF/3-21G, and B3LYP/6-31G(d) model chemistry using default solvation model of acetonitrile.

Chemistry model	HOMO energy of 1-tetralone (**66**)		HOMO energy of **60**	
	In a.u.	In eV	In a.u.	In eV
AM1	- 0.35677	- 9.71	- 0.35352	- 9.62
HF/3-21G	- 0.34274	- 9.33	- 0.33691	- 9.17
B3LYP/6-31G(d)	- 0.24726	- 6.73	- 0.24153	- 6.57

The reaction was initially tested at 0.2 mmol scale with 5 mol% of $QuCN^+$ (**68**), 3 mol% $Co(dmgH)_2pyCl$ (**69a**) and 5 mL of acetonitrile at room temperature as shown in Table 40, Entry 1. The resultant GC-MS analysis did not provide any evidence of the target molecular ion peak only for the starting material. Since the LED source only provides a specific wavelength at 365 nm, this light source was swapped for the mercury lamp which offers a broader wavelength range for potential activation. While the temperature was controlled at around 30 - 40℃, again no molecular ion peak was observed for **61**. The conditions in Entry 4 were also applied for *α*-naphthol (substrate used in literature) for a test run and successfully afforded the target compound. The dehydrogenation of another test compound 3-isobutyl-5,6-dihydropyrazin-2(1*H*)-one (**70**) however was not successful via this photochemical synthesis.

Table 44. The flow set up and reaction conditions using photocatalysts of $QuCN^+$ (**68**) and $Co(dmgH)_2pyCl$ (**69a**).

Flow chart

Starting material (0.2 mmol)
$QuCN^+$ (0.01 mmol)
$Co(dmgH)_2pyCl$ (0.006 mmol)
MeCN (5 mL)
Conc. 0.04 M (w.r.t. starting material)

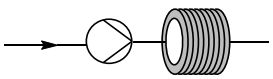

q = 0.333 μL min^{-1}
λ > 300 nm

Structure of starting materials

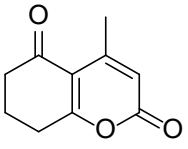

60

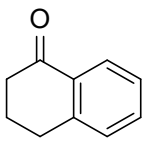

66

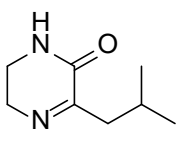

70

Entry	Compound	Temperature	Light source	Degassed with nitrogen balloon	Target compound
1	**60**	r.t.	LED	No	No
2	**60**	64 - 40℃	Mercury lamp	No	No
3	**60**	30 - 40℃	Mercury lamp	No	No
4	**60**	30˚- 40℃	Mercury lamp	Yes	No
5	**66**	31˚- 34℃	Mercury lamp	Yes	Yes
6	**70**	30 - 40℃	Mercury lamp	Yes	No

Redox catalyst 2: DDQ (65)

DDQ (**65**) was known in the literature to perform dehydrogenation of hydroaromatic compounds.[293] The reductive potential of DDQ (**65**) (E_{red}* = 3.18 V *vs*. SCE)[304] is higher than $QuCN^+$ (**68**), (E_{red}* = 2.72 V *vs*. SCE)[305]. This is important because 1-tetralone (**66**) and potentially the starting material possess a high one-electron oxidative potential and E_{red}* needs to be more positive than E_{ox}. The cobaloxime complex **69a** was used as the hydrogen sequestering agent with $QuCN^+$ (**68**) in previous experiment, while DDQ (**65**) can accept hydrogens itself, thus this single catalyst system was used. The reaction conditions are reported in Table 45. No target compounds were identified by GC-MS analysis, only starting material was observed.

Table 45. Reaction conditions of flow synthesis using DDQ (**65**) as the catalyst.

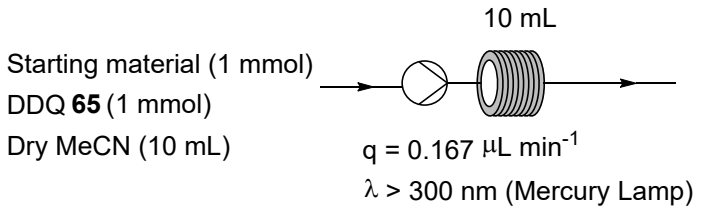

Entry	Scale/ mmol	Eq. of DDQ	Eq. of $BF_3{\cdot}OEt_2$	Solvent	Degas	Target GC-MS peak
1	1	0.1	0.2	MeCN, 3 mL	/	No
2	1	1	/	Dry MeCN 10 mL	Yes	No

(ii) Oxidation via chlorination

An alternative method would be to install a halo group on compound **60** to form, for example, **71** (Scheme 57). From **71** an elimination mechanism and tautomerisation give the aromatic product **56**. A conceived process using the chlorinating agent, 1,3-dichloro-5,5-dimethylhydantoin (**72**) and base 1,8-diazabicyclo(5.4.0)undec-7-ene (**73**) is shown.

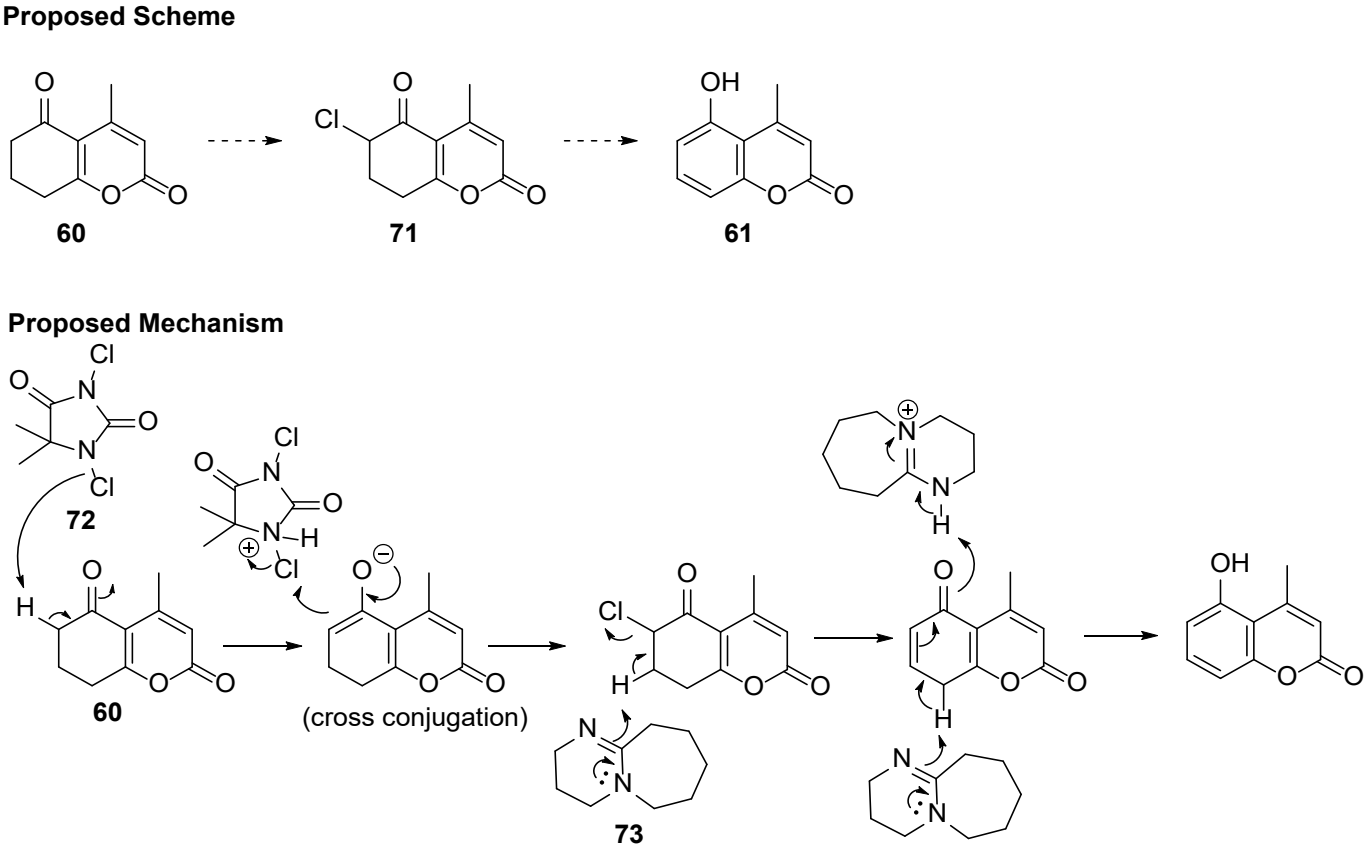

Scheme 57. The proposed oxidation pathway via chlorination of **60** and de-hydrochlorination of **71**.

As outlined in Chapter 2, halogenation is achieved through various halogenating agents, often in the presence of an acid or base to ensure regioselectivity. Initially **71a** was synthesized (Scheme 58) using *N*-bromosuccinimide **30** (NBS) following the procedure previously developed for a pyrazine synthesis project (Scheme 59 and Figure 82).[306] This process involved two key steps, attaching the bromine to the substrate and then eliminating hydrogen bromide using a base. However, in addition to generating compound **71a,** poly-brominated side products **71b** were also produced. These required an additional step to yield 5-hydroxy-4-methylcouamrin (**61**), reducing process efficiency and resulting in an overall reaction yield of less than 60%. While exploring the

conditions for coumarin substrates, additional optimisation was performed exploring the equivalents of *N*-bromosuccinimide **30** (NBS) and solvent in order to drive the reaction to completion (Table 46). For 1.2 equivalents of NBS (**30**), more starting material remained (indicated by Total area% of GC-MS analysis) compared to other entries. When the starting material was minimised (Table 46 Entry 4), the total area% of over-brominated compounds increased as the equivalents of NBS (**30**) was increased. Figure 83 gave the retention time of the targeting molecular ion peaks. The reaction conditions were optimised to increase the yield by modifying the halogenating agent, minimising side-product formation, and implementing flow reactors to enhance the space-time-yield.

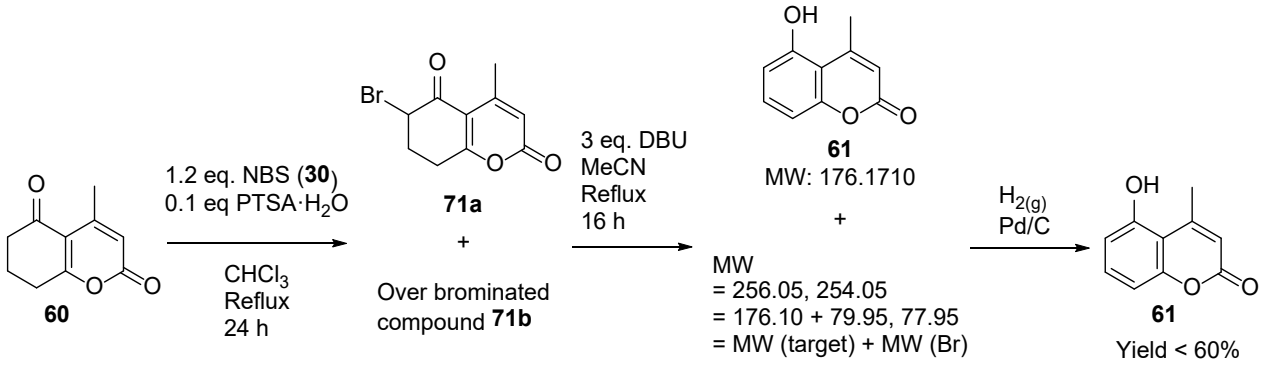

Scheme 58. The reaction scheme of converting **60** to **61** via **71a**.

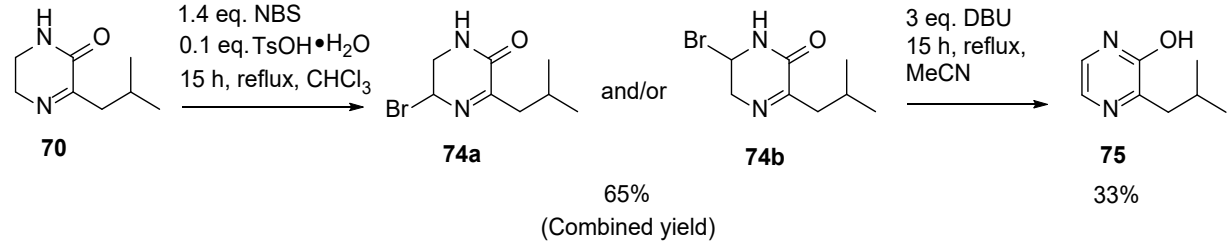

Scheme 59. The bromination and de-hydrobromination process to synthesize 2-isobutyl-3-hydroxypyrazine (**75**).

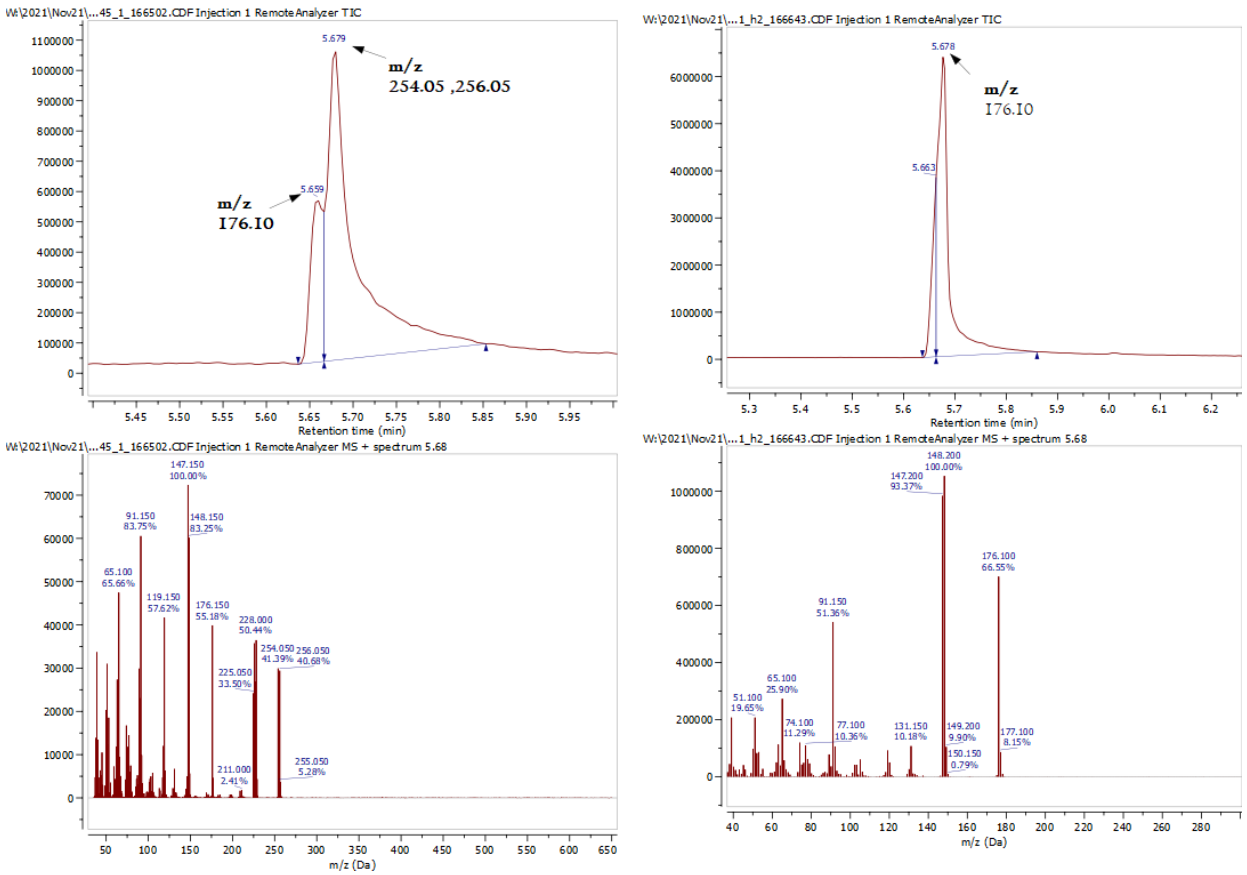

Figure 82. The GC-MS analysis before and after debromination of Scheme 59.

Table 46. The reaction results of 6-bromo-4-methyl-7,8-dihydro-2*H*-chromene-2,5(6*H*)-dione (**76**) preparation.

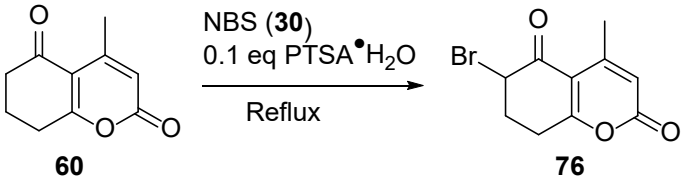

Entry	Scale/ mmol	Eq. of NBS	Solvent	Time/h	Total area% of **60** in GC	Total area% of **76** in GC	Total area% of over-brominated compound
1	10	1.2	CH_2Cl_2	40	21.15	63.34	7.79
2	10	1.3	CH_2Cl_2	40	5.93	60.15	24.92
3	10	1.4	CH_2Cl_2	40	7.52	58.34	31.64
4	50	1.4	$CHCl_3$	16	1.96	57.84	28.71

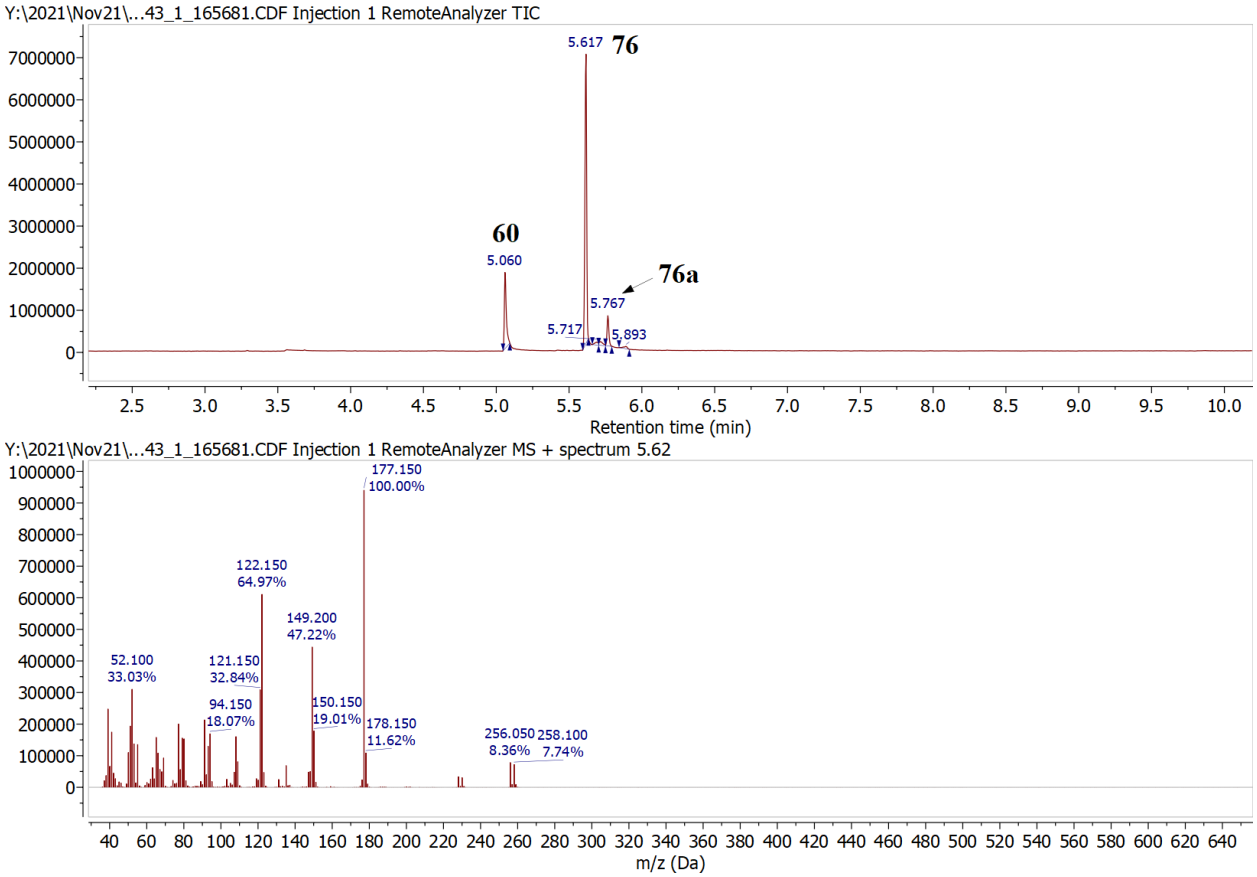

Figure 83. The retention time of the compounds compared in Table 10. Starting material (**60**) R_t = 5.06 min, m/z 178.15; Target (**76**) R_t = 5.62 min, m/z 256.05, 257.05; Over-brominated compound (**76a**) R_t = 5.77 min, m/z 256.10, 258.05.

Firstly, to balance the desire for complete consumption of the starting material but to prevent the over-brominated side products, chlorination was tested. As mentioned previously in Section 3.2.1, C-Cl bond is generally less labile than C-Br bond based on bond dissociation energies (C–Cl: 339 kJ mol^{-1}; C–Br: 280 kJ mol^{-1}).[247] In addition to *N*-chlorosuccinimide (NCS; **77**), two other chlorinating agents were also tested. These were 1,3-dichloro-5,5-dimethylhydantoin (DCDMH; **72**) and trichloroisocyanuric acid (TCCA; **78**) (Figure 84).

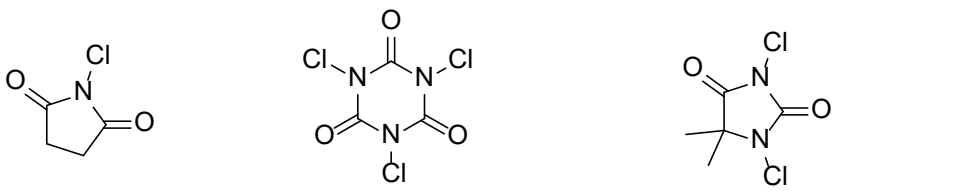

N-chlorosuccinimide (NCS) **77** | Trichloroisocyanuric acid (TCCA) **78** | 1,3-Dichloro-5,5-dimethylhydantoin (DCDMH) **72**

Figure 84. Structures of tested chlorinating agents.

N-chlorosuccinimide (NCS, 77)

The initial set of conditions tested *N*-chlorosuccinimide (NCS, **77**) in the presence of an acid catalyst (Table 47). When *p*-toluenesulfonic acid monohydrate (PTSA•H_2O) was employed, an optimal balance between starting material consumption and target production was achieved under the conditions of Entry 2 Table 47 as confirmed by the GC-MS Total area%. The structure of the product **71** was confirmed along with acquisition of its crystal structure provided in Table 47. Other side products are mainly regioisomer, over-chlorinated material (**71c**, **71d**) and **61** as illustrated by an example in Figure 85 and Table 48. Although compound **61** is the desired product of proposed oxidation of **60**, this was not obtained with a good yield**.** Subsequently, *p*-toluenesulfonic acid monohydrate was replaced with a heterogeneous solid acid catalyst (QP-SA) to simplify extraction and better align with the general principles of green synthesis. However, this approach resulted in incomplete conversion of starting materials (Table 47 Entry 5-7). For this reason, the best reaction condition developed remained Entry 2 Table 47.

Table 47. The set of reaction conditions using *N*-chlorosuccinimide (NCS; **77**) as chlorinating agent. PTSA•H_2O, *p*-toluenesulfonic acid monohydrate. From analysis of isolated material, **60** was identified with peak at R_t = 4.72 – 4.75 (m/z 178.10) and **71** at R_t = 5.20 (m/z 212.00, 214.00),

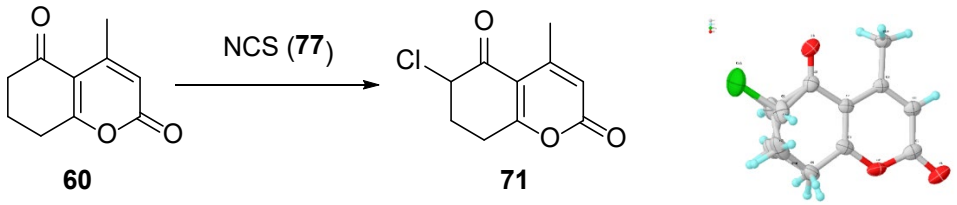

60 **71**

NCS & PTSA•H_2O

Entry	Scale / mmol	Eq. of NCS	Eq. of PTSA •H_2O	Temp./ °C	RXN time	Solvent, 50 mL	GC-MS Total area% (60)	GC-MS Total area% (71)
1	50	1.4	0.1	62 (reflux)	overnight	$CHCl_3$	4.71	58.45
2	50	1.2	0.1	62 (reflux)	overnight	$CHCl_3$	0.70	70.93
3	50	1.1	0.1	62 (reflux)	overnight	$CHCl_3$	8.53	65.73
4	50	1	0.1	62 (reflux)	overnight	$CHCl_3$	13.95	27.57
NCS & QP-SA								
Entry	Scale	Equiv. of NCS	Mass of QP-SA/g	Temp.	RXN time	Solvent	GC-MS Total area% (60)	GC-MS Total area% (71)
5	10	1.05	1 → 3→8	r.t.	overnight	EtOAc (0.5 M)	38.00	35.08
6	10	1.05	8	r.t.	overnight	EtOAc (0.5 M)	32.01	26.76
7	50	1.05	5	reflux	17 h	$CHCl_3$ (1 M)	31.87	36.99

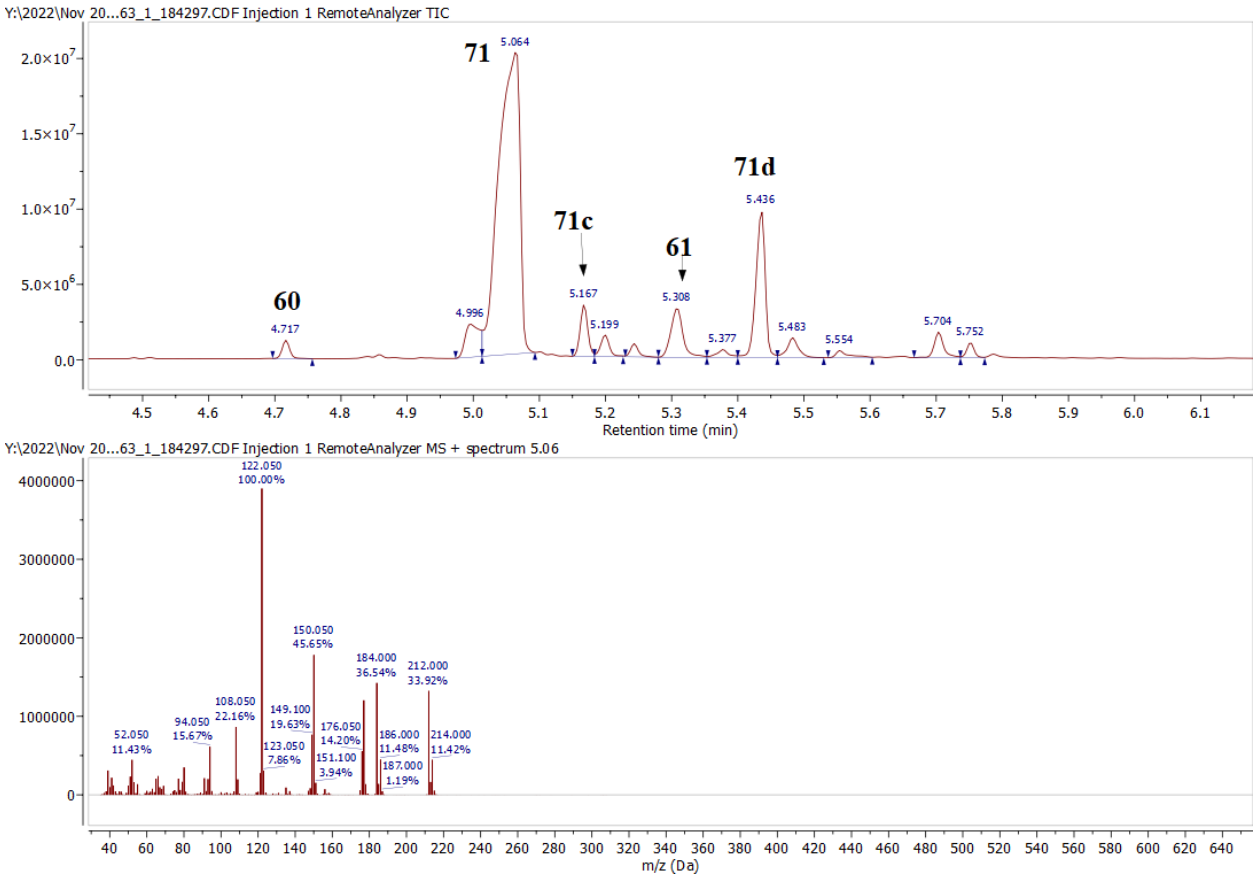

Figure 85. GC-MS analysis of reaction in Table 47 Entry1.

Table 48. Proposed structures of the crude mixture of reaction in Table 47 Entry1.

Compound label	Proposed structure	R_t/min	m/z (GC-MS peak)	m/z (ChemDraw)
60 (Starting material)	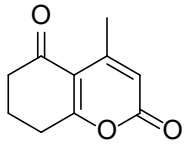	4.72	178	178.0630 (100.0%), 179.0663 (10.8%)
71 (Target)	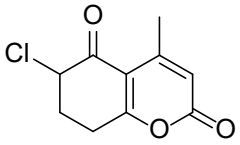	5.06	212, 214	212.0240 (100.0%), 214.0211 (32.0%), 213.0274 (10.8%), 215.0244 (3.5%)
71c	Regioisomer of **71**	5.17	212, 214	212.0240 (100.0%), 214.0211 (32.0%), 213.0274 (10.8%), 215.0244 (3.5%)
61	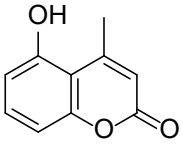	5.31	176	176.0473 (100.0%), 177.0507 (10.8%)
71d	Double chlorinated **60**	5.44	246, 248	245.9850 (100.0%), 247.9821 (63.9%), 246.9884 (10.8%), 249.9791 (10.2%), 248.9855 (6.9%), 250.9825 (1.1%)

1,3-dichloro-5,5-dimethylhydantoin (DCDMH; 72)

In addition to conducting the reaction under standard batch conditions, flow reactors were considered to improve the space-time-yield of the chlorination process. Although *N*-chlorosuccinimide (NCS; **77**) showed good conversion, its low solubility in chloroform at room temperature posed challenges for translation of the process into a continuous flow sequence. To ensure a homogeneous reaction mixture suitable for a flow reactor, the chlorination process was tested with another reagent, DCDMH **72** in ethyl acetate. Prior to adaptation to flow, the reaction was first assessed in batch to allow direct comparison with previous data. The desired product was successfully synthesized using DCDMH **72** (Scheme 60), however repeated experiments showed inconsistent conversion as the peak area in GC-MS spectra of starting material varied (**60**)

significantly (Figure 86). Analysis of GC-MS revealed that the decomposition of an aged DCDMH **72** batch contributed to this variability (Figure 86 and 87). Upon initial decomposition of DCDMH **72**, less overchlorinated products were produced (Figure 86), then many other side products were produced (Figure 87) Additionally, light-induced reactions may also induce inconsistent chlorination as discussed in section 3.2.1. Monitoring the reaction under light-free conditions improved product conversion and reduced over-chlorination, as shown in Figure 88.

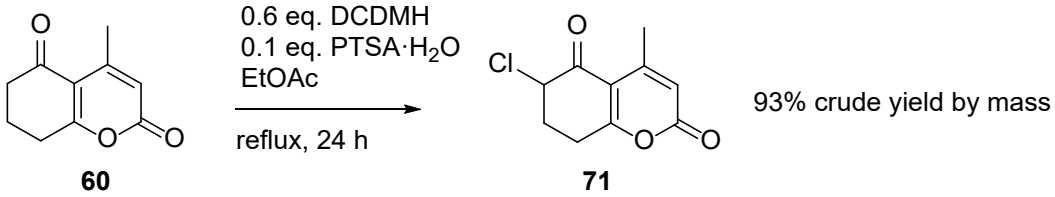

60 **71**

Scheme 60. Chlorination of **60** by DCDMH.

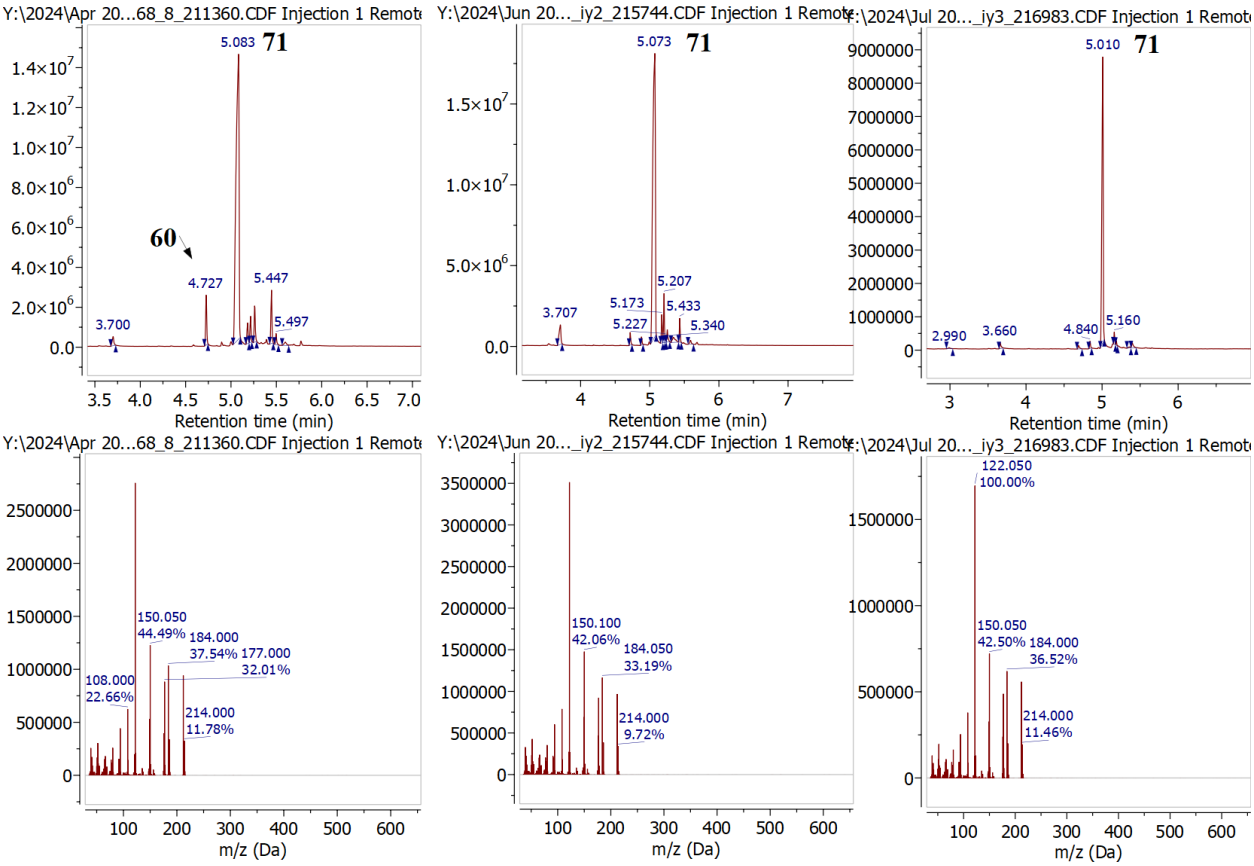

Figure 86. GC-MS comparisons of repeated chlorination with DCDMH under laboratory room lighting. Each spectra indicated the molecular ion peaks of starting material (**60**) and target molecule (**71**) of the crude mixture. The first spectra on the left showed a peak of **60** at R_t = 4.72, a lot less significant for the middle spectra and unable to detect any for the final one.

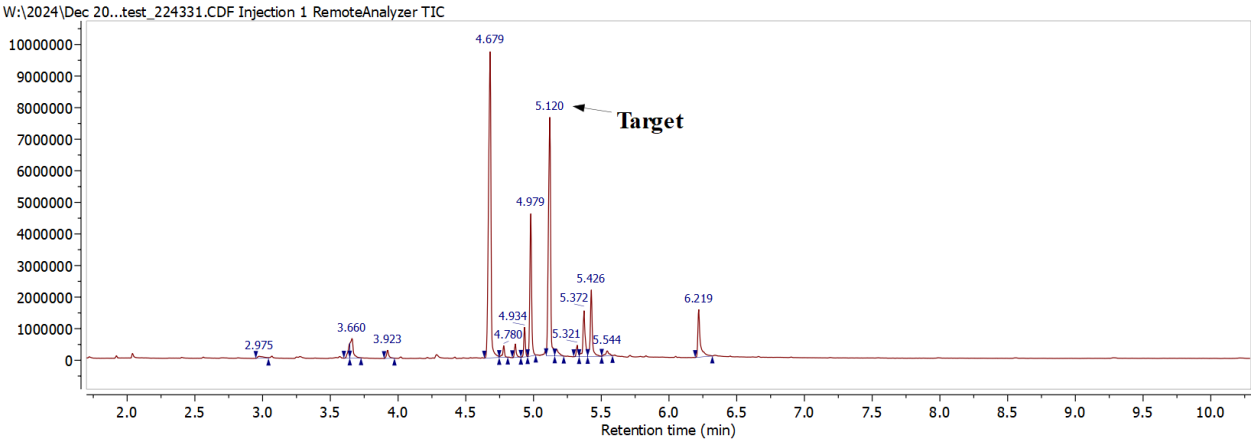

Figure 87. The GC-MS analysis of using decomposed DCDMH (**72**) to produce many other side products.

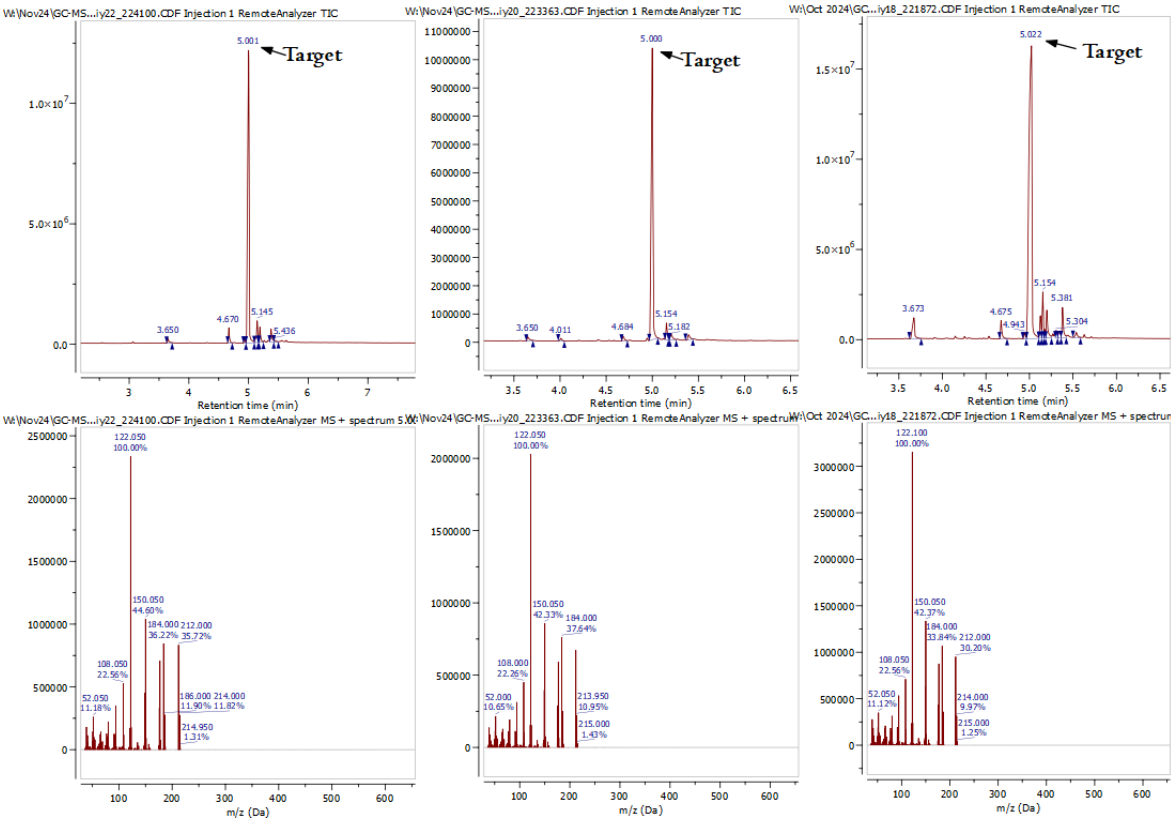

Figure 88. The GC-MS result comparisons of chlorination by DCDMH **72** under no light conditions.

Modification of dehydrochlorination and overall yield of oxidation in batch

In addition to the modification of the halogenation process, the subsequent elimination of hydrogen chloride was performed in ethyl acetate instead of acetonitrile (Scheme 61B), yielding excellent conversion to 5-hydroxy-4-methylcoumarin (**61**) consistently. An overall two-step yield of 81% (converting **60** to **61**) was achieved, where each step has conversions of >90% (Scheme 61). The presented yields were quantified using ^{1}H NMR spectroscopy with an internal standard, as calculated from Section 2.4 Experimental procedure (General information, calculations of estimated yield by ^{1}H NMR spectroscopy)

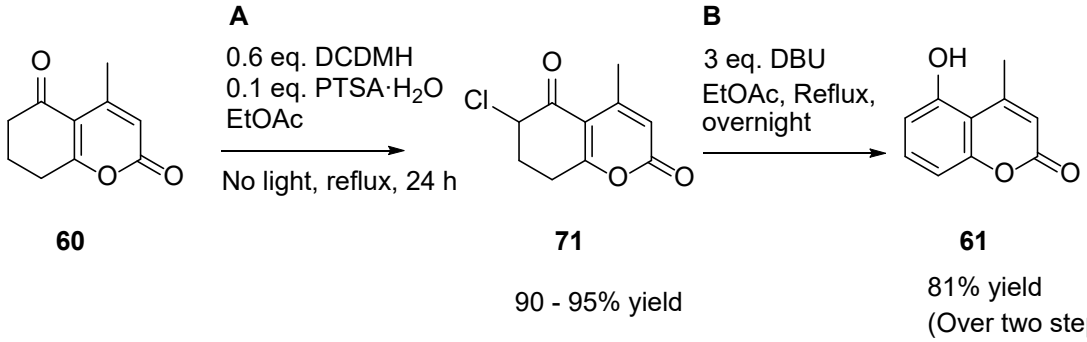

Scheme 61. Oxidation of 4-methyl-7,8-dihydro-2*H*-chromene-2,5(6*H*)-dione (**60**) via chlorination. The yields were estimated by ^{1}H NMR spectroscopy with the internal standard 3-(trimethylsilyl)-1-propanesulfonic acid sodium salt (**8**).

Adaptation of chlorination to a flow process

After optimisation of the batch chlorination reaction, another two processes using microwave irradiation and the use of flow reactors were attempted. Both systems are operatable at temperatures higher than the solvent's boiling point with potential to improve synthesis through primarily enhanced kinetics. Reaction conditions were tested using microwave irradiation with the additional benefit the microwave cavity excludes light. Reaction temperatures of 90 or 100 °C, with 0.6 or 0.7 equivalents of DCDMH **72** (Table 49) were run. While achieving the desired product, the reaction time was significantly reduced using the above conditions in Scheme 61A to 3 h or 1.5 h. However, some starting material remained as indicated by the peak with R_t = 4.7 min (Figure 89). Although using 0.7 equivalents of DCDMH **72** permitted 100% conversion (Table 49 Entry 4 and 8), DCDMH **72** was not completely soluble at 2.5 M concentration. Hence, flow

reactions were processed with conditions as: 0.6 equivalents of DCDMH **72** at 2.5 M (Table 49 Entry 2 and Entry 4). Since Entry 2 reported a higher total area% of the target compound, this condition was applied for further tests in flow.

Table 49. Microwave reaction conditions of 5 mmol starting material. Total area% of target molecule **71** of m/z 212.00, 214.00 at R_t = 5.04 min in GC-MS.

Entry	Eq. of DCDMH	Eq. of PTSA·H_2O	Temp.	Reaction time/ h	Solvent volume/ mL	Total area%[a]	Crude mass/ g	Crude yield/%
1	0.6	0.1	100	1.5	12	66.66	0.76	72
2	0.6	0.1	100	3	12	33.19	1.00	94
3	0.6	0.1	90	3	12	64.10	1.02	123
4	0.6	0.1	90	1.5	12	57.83	1.06	99
5	0.7	0.1	100	1.5	16	38.34	1.17	110
6	0.7	0.1	100	3	12	57.04	1.03	97
7	0.7	0.1	90	1.5	12	65.25	/	/
8	0.7	0.1	90	3	12	69.23	1.04	98

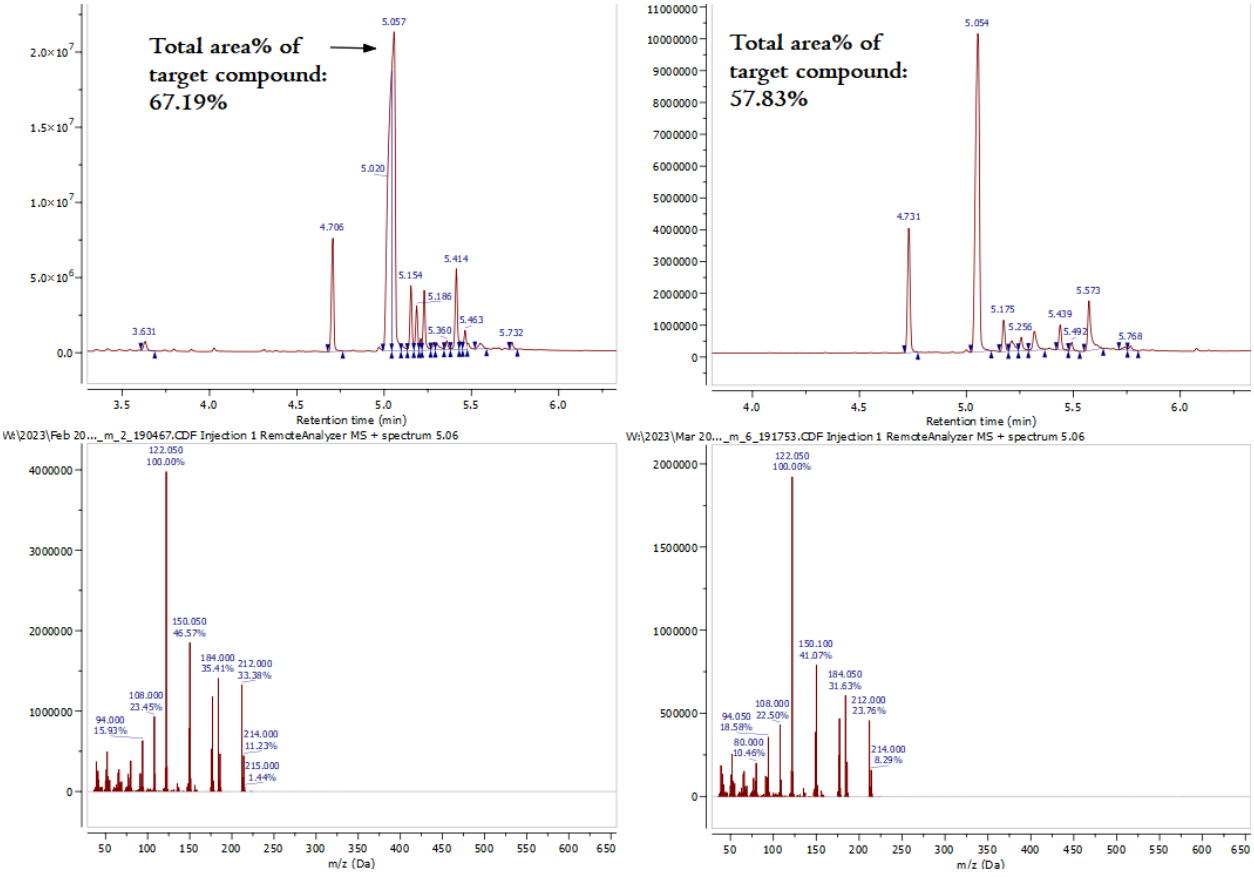

Figure 89. The GC-MS plot of compounds from Entry 2 (left) and Entry 4 (right) in Table 44.

The flow reactor was equipped with 3 peristaltic pumps (maximum flow rate: 10 mL/min per pump) (Figure 90). Pump A delivered the initial reaction mixture into the flow reactor at a rate of 0.33 mL min^{-1} which was set at a temperature of 100 °C. This solution was then combined with a stream of deionized water (0.267 mL min^{-1}) at room temperature, supplied by Pump B and combined at a Y-piece connector. Deionized water dissolved the hydantoin side products by introducing the water stream before the reactions reaches the back-pressure regulator (BPR), the risk of blockage in the flow reactor is reduced. A check valve (**C**) facilitated the forward flow of the reaction stream under pressure differences and was an integral part of the final flow setup, as illustrated in Figure 87. Additionally, the BPR (**D**) prevented gaseous flow by maintaining sufficient pressure, thereby regulating the reaction time. This was particularly important because the reaction temperature exceeded the boiling point of the solution being processed (Figure 90, **D**).

The flow reactions were tested at both 10 and 50 mmol scale resulting in excellent efficiency of product conversion as shown in Table 50 and Figure 91. For both scales, the total area% in GC-MS of compound **71** is higher than 65.66, the total area% by optimized batch reactions ($65.55 < 68.59 < 75.26$). The flow synthesis also showed better selectivity than the previous microwave reactions. Two of the potential reasons are the reduced reaction time and confined space in the reactor coil to limit light induced reactions. An extended flow reaction run was then monitored with fractional collection for steady state analysis as shown in Figure 92. This is hence a reliable process to scale in flow under beneficial conditions over the batch synthesis.

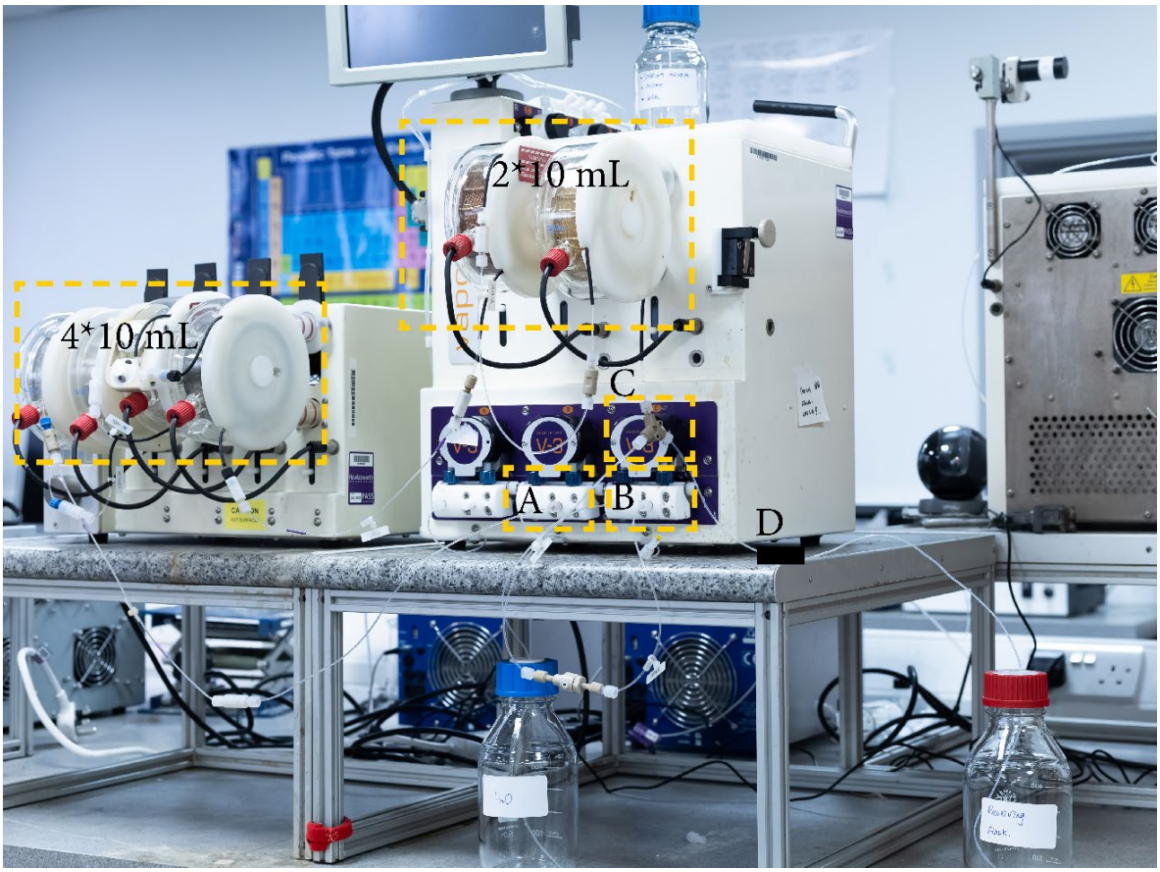

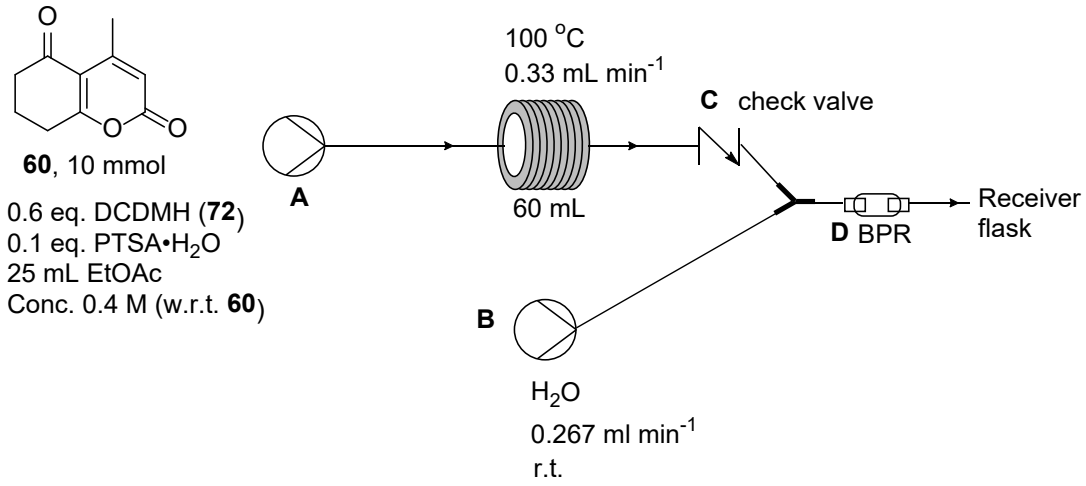

Figure 90. The Set up of flow reactors of chlorination by DCDMH (**72)** using 10 mmol starting material **60**. Reactors: The easy MedChem E-series with two standard coiled tubular reactors (10 mL); R4 reactor heater/ cooler module four standard coiled tubular reactors (10 mL). **A** and **B** pumps on easy-MedChem E-Series. **C** check valve. **D** Back pressure regulator.

Table 50. V = 60 mL, q = 0.333 mL min^{-1}, t = 180 min, temp. = 100 ℃

Scale/ mmol	Mass/ g	Crude yield/ %	Total area% by GC
10	2.09	98.6	75.26
50	11.10	104.7	68.59

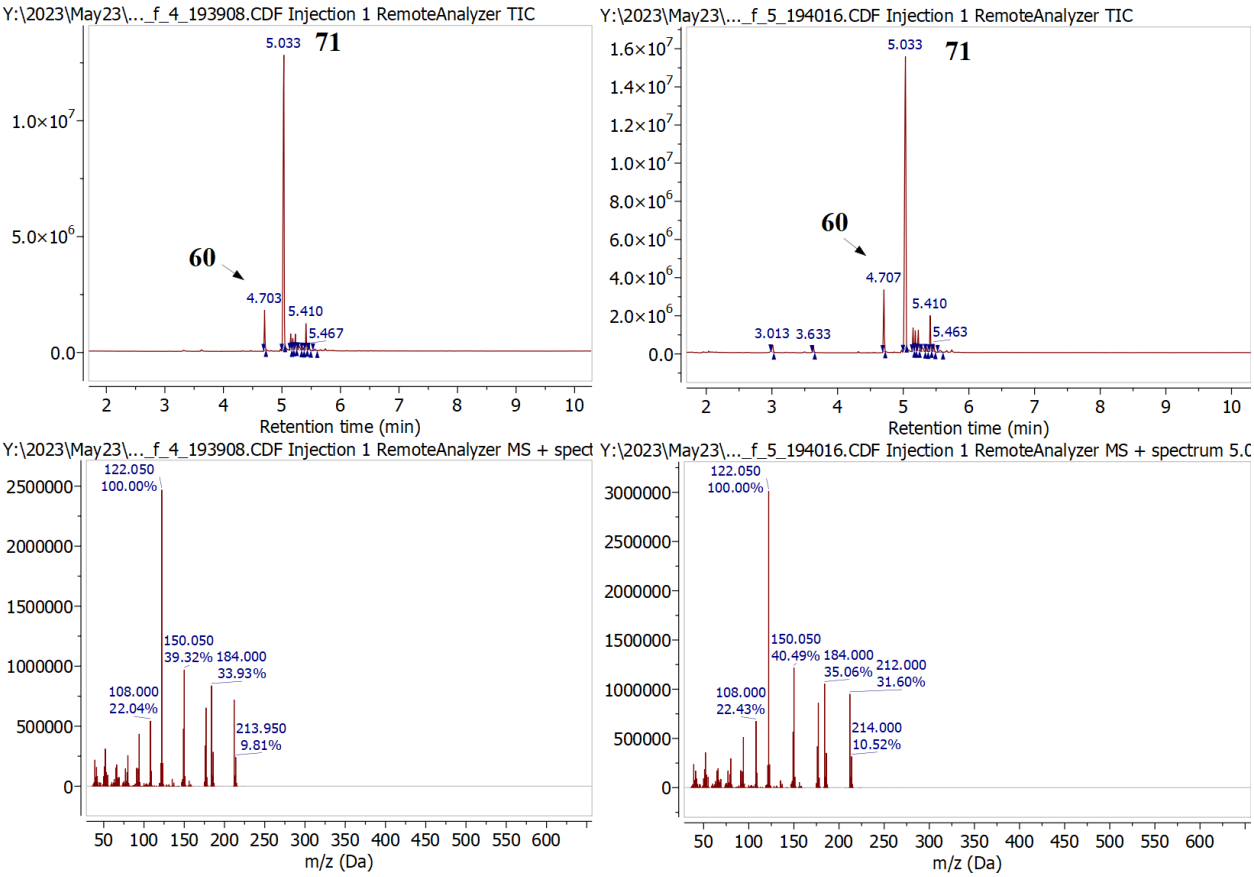

Figure 91. The GC-MS analysis of product conversion by flow.

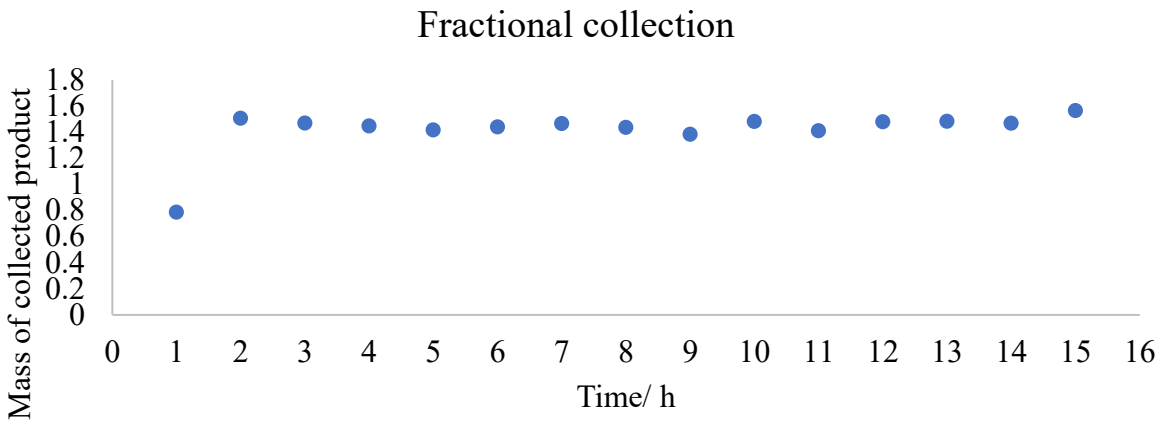

Figure 92. Steady state assessment of chlorination operated in flow reactors.

Chlorination by TCCA (78)

Trichloroisocyanuric acid (TCCA; **78**) was also investigated as a potential chlorinating agent, each equivalent of TCCA **78** provides three equivalents of chloro-electrophiles, this means its atom efficiency is very high per unit mass. The reaction conditions were initially optimised based upon the parameters of additive, reaction temperature, and conversions (Table 51, Entry 1-5).

Table 51. Rection concentration = 0.5 mmol mL^{-1}, reaction analysis based on GC-MS result. Total area% is the total area % given by GC-MS results in MestReNova. Compound **60**, R_t = 4.72 min, m/z 178.05; Compound **79**, R_t = 5.17 min, m/z 212.00, 214.00; Compound **80**, R_t = 5.47 min m/z 246.00, 248.00.

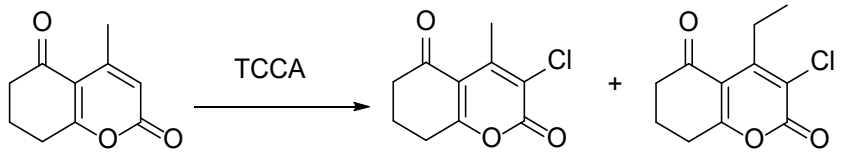

60 **79** **80**

Entry	Scale/ mmol	Equiv. of TCCA	RXN time/ h	RXN temp./ °C	Solvent	Total area% (**60**)	Total area% (**79**)	Total area% (**80**)
1	10	0.4	16	47	EtOAc	13.95	27.57	1.31
2[a]	10	0.4	16	47	EtOAc	22.40	39.00	5.12
3[b]	10	0.4	16	47	EtOAc	18.87	14.11	0.79
4	10	0.4	16	60	EtOAc	32.95	44.93	16.89
5	10	0.4	16	60	$CHCl_3$	51.69	37.05	5.77
6	10	0.5	2	47	EtOAc	8.91	14.43	4.73
7	10	0.6	3.5	47	EtOAc	9.09	58.70	24.29
8	10	0.7	3.5	47	EtOAc	2.08	57.93	28.40
9	10	0.8	3.5	47	EtOAc	/	62.98	26.18
10	10	1.0	3.5	47	EtOAc	/	57.92	26.24

[a]0.1 eq *p*-toluenesulfonic acid added. [b]0.6 eq. 2,2,6,6-Tetramethylpiperidinyloxy (TEMPO) added.

While complete conversions were observed for Entry 9 and 10, this was accompanied with significant over-chlorination that led to reduced yield of our target compounds. The structures of additional by-products which were isolated and crystallised are shown by Figure 90 These structures have different chlorinated positions than the target **71**. Two proposed mechanisms are postulated in Scheme 62 and 63. In this scenario, **79** was proposed with Scheme 62, where this is formed by a straightforward chlorination with TCCA. For

compound **80**, the light induced initiation can afford chlorine radical from TCCA (Scheme 63). The chlorine radical is conserved by abstracting hydrogen from the methyl group of coumarin substrates (**60**) (Scheme 63B). The coumarin radical **81** couples with another chlorine radical to terminate the reaction and form **82**. In addition, **82** can react further with TCCA to form **80** at another position (Scheme 63C).

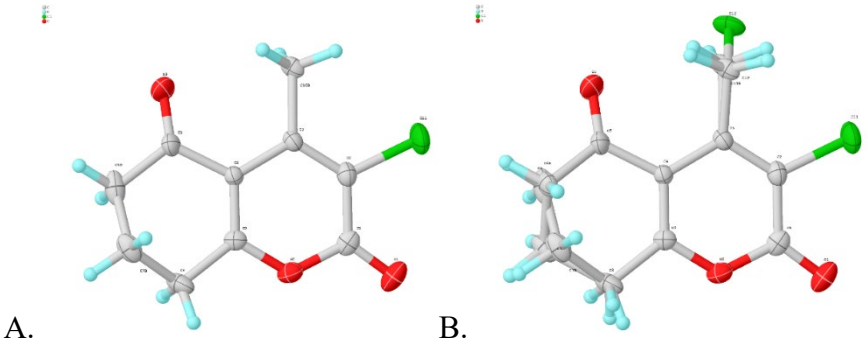

A. B.

Figure 93. Crystal structures of products A. **79** and B. **80** (Entry 6, Table 51) obtained by chlorination with TCCA.

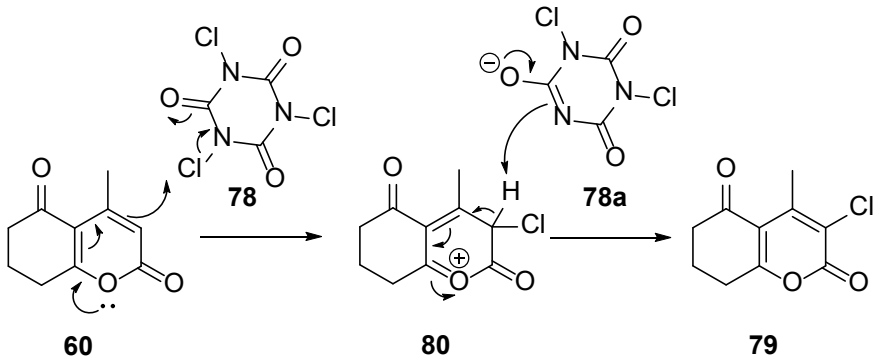

Scheme 62. Proposed reaction scheme of crystal **79**.

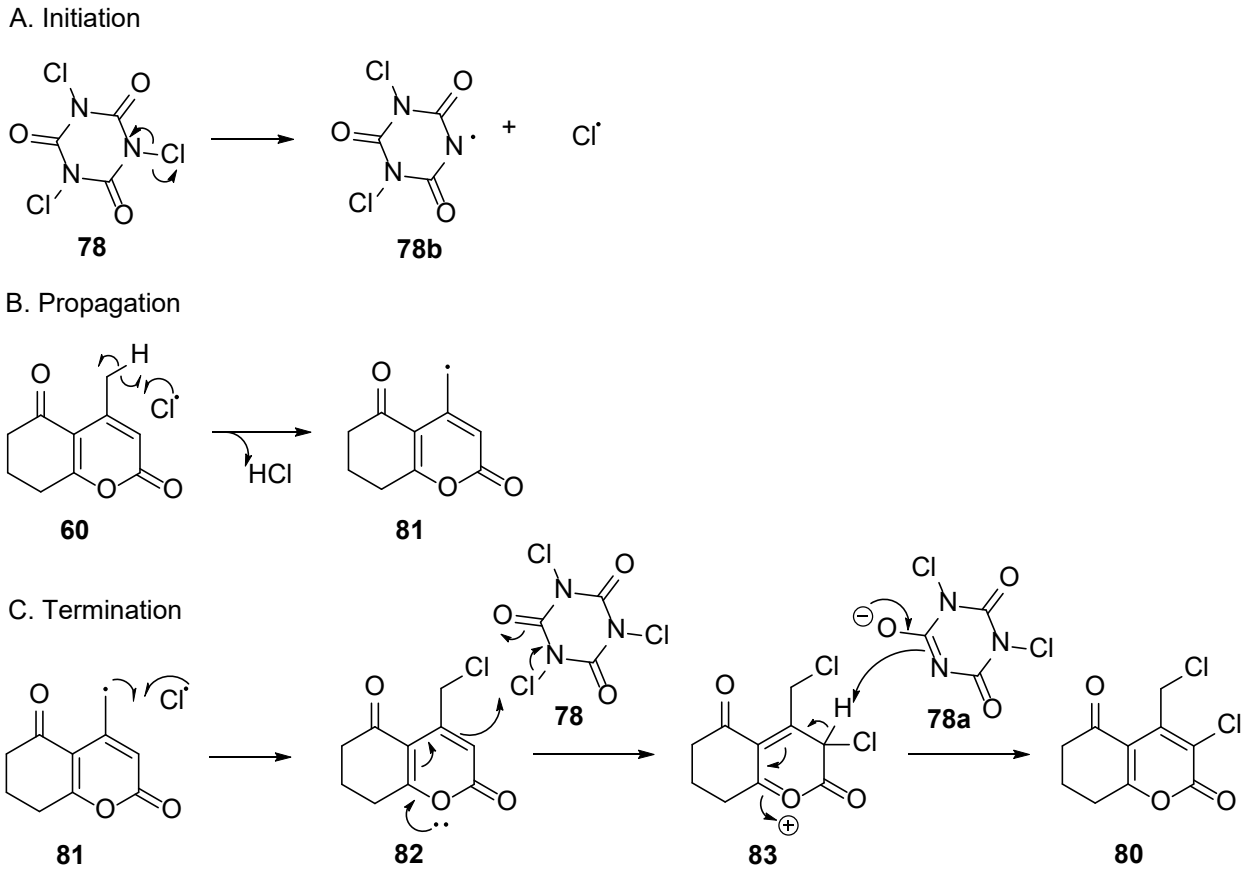

Scheme 63. Proposed reaction scheme of crystal **80**.

Conclusions on oxidation

In summary, the target compound **61** was successfully synthesized using a two-step process from **60**, firstly via chlorination (yielding **71**) and secondly through dehydrochlorination. The yield determined by quantified ^{1}H NMR spectroscopy was 81% over the two steps. In addition to the given conditions in batch, the chlorination reaction was successfully converted to flow in a significantly reduced residence time of 3 h (compared to 24 h in batch).

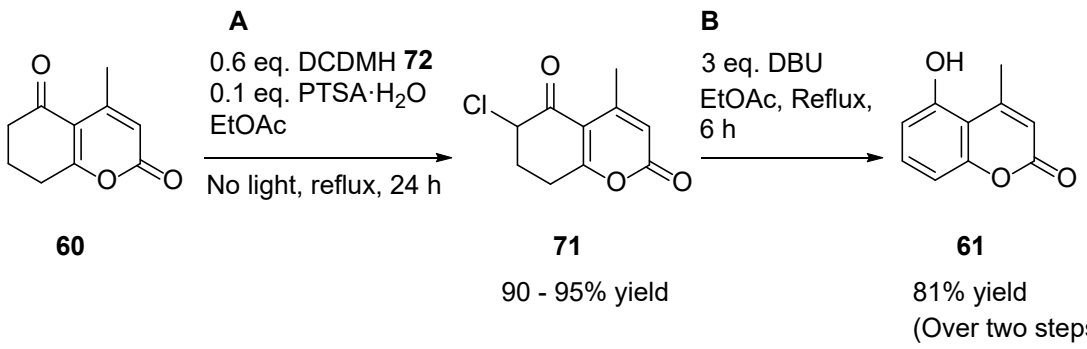

Scheme 64. Oxidation of 4-methyl-7,8-dihydro-2*H*-chromene-2,5(6*H*)-dione (**60**) via chlorination. The yields were determined by ^{1}H NMR spectroscopy with the internal standard 3-(trimethylsilyl)-1-propanesulfonic acid sodium salt (**8**) as calculated from Section 2.4 Experimental procedure (General information, calculations of estimated yield by ^{1}H NMR spectroscopy).

4.3.2.2 Methylation

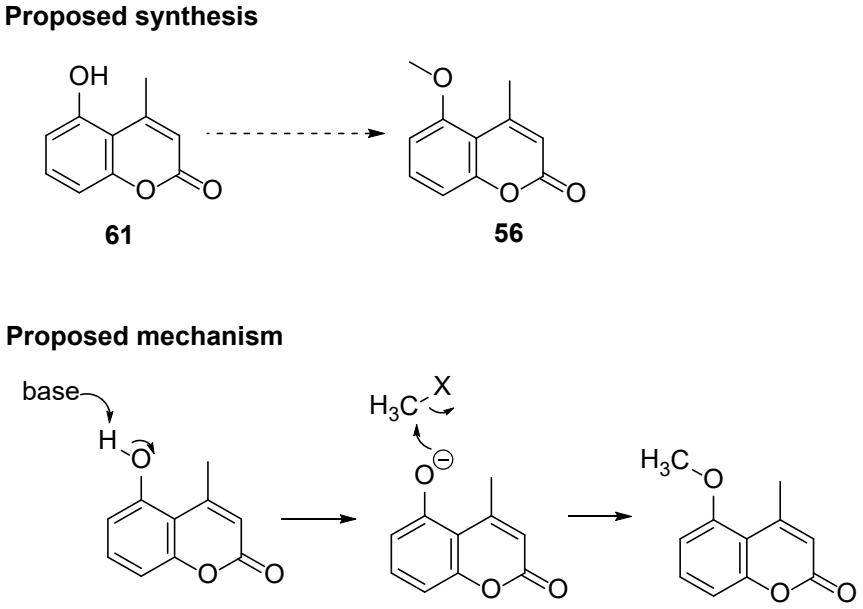

Scheme 65. Proposed synthesis and mechanism of methylation of 5-hydroxy-4-methylcoumarin (**56**).

The next required step in the synthesis of the target **56** was *O*-methylation of the hydroxy group (Scheme 65). Based on the acidity of the phenolic proton, the proposed mechanism begins with base-catalysed deprotonation, after which methylation occurs with a variety of methylating agents. Although in some cases, *C*-methylation and *O*-methylation are competitive, conditions could be monitored to make this process selective for the desired oxygen site of attack.[307-309] A survey of

the literature indicated a wide range of combinations of acids or bases with different methylating agents could achieve optimal efficiency and yields.[309-313] Indeed, well documented coumarin derivatives such as 4-methyl-7-hydroxycoumarin provided inspirations for the initial selection of reagents. Literature reports for this structure used base such as sodium hydroxide,[314] potassium carbonate,[315] 1,8-diazabicyclo[5.4.0]undec-7-ene,[316] with methylating agents of methyl halide,[315, 317] dimethyl sulfide,[318] dimethyl sulfate,[319] sodium *p*-toluenesulfonate[314]. Furthermore, additional reagents, such as phase transfer catalysts (PTC), can be used to facilitate the reaction as biphasic procesess.[320] This enables reactions under aqueous conditions where water is employed as a greener co-solvent. In addition, the option to use heterogeneous bases is available which can simplify work-up process, however it is often the case that homogeneous bases exhibit broader applicability across a more diverse set of substrates.

The test reactions were categorised based on the choice of base: either a heterogeneous base (Ambersep® 900 hydroxide form, pink solid insoluble in solvent, (Figure 94) or a homogeneous base (e.g., sodium hydroxide, sodium carbonate). The selection of methylating agent and the requirement for a PTC.

Figure 94. The heterogeneous base of Ambersep® 900 hydroxide form.

(i) Heterogeneous methylation

Polymer-supported reagents provide a highly efficient and environmentally friendly approach to preparing novel chemical compounds. Excess reactants and by-products can be trapped by these heterogeneous reagents, avoiding tedious separation steps. Products are isolated through straightforward filtration, and resin washing, ensuring optimal yields in multistep synthetic processes.[321, 322] The compound 2-alkyl-3-methoxypyrazines (**85**) was successfully synthesised in a previous project by this type of reaction using Ambersep® 900 hydroxide form (**86,** Figure 95) (Scheme 66).[306] This polymer supported base was therefore tested for the *O*-methylation of 5-hydroxy-4-methylcoumarin (**61**) (Scheme 67), with the reaction conditions being reported in Table 47.

Using the developed method for the pyrazine derivatives (**85**), the progress of the reaction was monitored via thin-layer chromatography (TLC). Completion of the deprotonation step was confirmed by the disappearance of the corresponding spots on the TLC plate (material immobilized by sequestration on the resin support). At this stage, methylating agent was added to the reaction mixture. Based on the group's previous work with coumarin substrates, dimethyl sulfate was selected. However, initial attempts conducted at room temperature failed to produce the desired product, as confirmed by gas chromatography-mass spectrometry (GC-MS) analysis which showed that the reactivity of pyrazine derivatives is different from coumarin derivatives (Table 52 Entry 1 and 2). Even when the temperature was raised to reflux for step 2, Entry 3 still no sign of product was found. Substituting THF for acetonitrile in step 2 afforded a side product, the proposed structure of this is shown in Figure 96. It is also worth noting that for this trial, a higher reaction temperature was used, because boiling points of acetonitrile is higher than THF (82 °C > 66 °C).

Reaction scheme

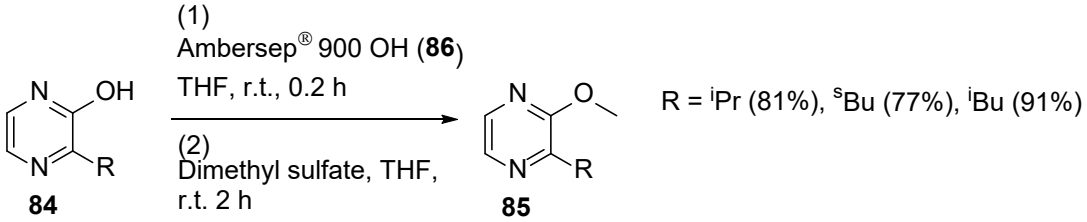

Proposed mechanism

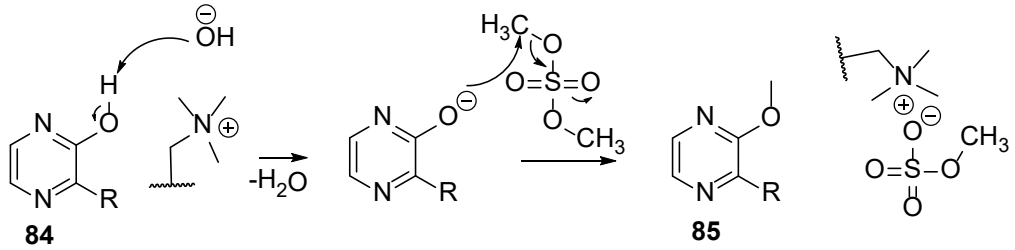

Scheme 66. Exemplary reaction employing Ambersep® 900 hydroxide (**86**) as the heterogeneous base in synthesizing 2-alkyl-3-methoxypyrazine derivatives (**85**).

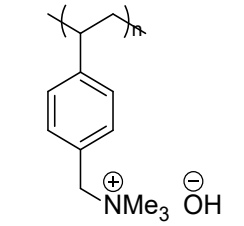

Figure 95. The structure of polymer supported reagent Ambersep® 900 hydroxide (**86**).

Proposed scheme

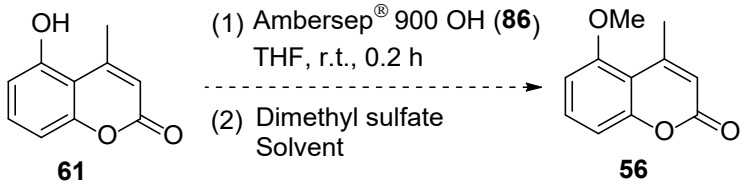

Scheme 67. Proposed scheme for heterogeneous methylation of 5-hydroxy-4-methylcoumarin (**56**).

Table 52. Reaction conditions for Scheme 66. NR = No Reaction.

Entry	Scale/ mmol	Ambersep® 900 OH form	Equiv. of $(MeO)_2SO_2$	Solvent	Temp.	Time	Crude yield/%
1	2.3	10 g	2.0	THF (30 ~ 50 mL)	r.t.	Overnight	NR
2	2.3	10 g	2.0	EtOAc (30 ~ 50 mL)	r.t.	Overnight	NR
3	2.3	10 g	2.0	THF (30 ~ 50 mL)	r.t. to reflux	Overnight	NR
4	2.3	10 g	2.0	Step 1: THF 30 mL Step 2: MeCN 20 mL	r.t. to reflux	Overnight	NR
5	2.8	4 g	1.25	Step 1: THF 30 mL Step 2: MeCN 20 mL	r.t. to reflux	Overnight	49%

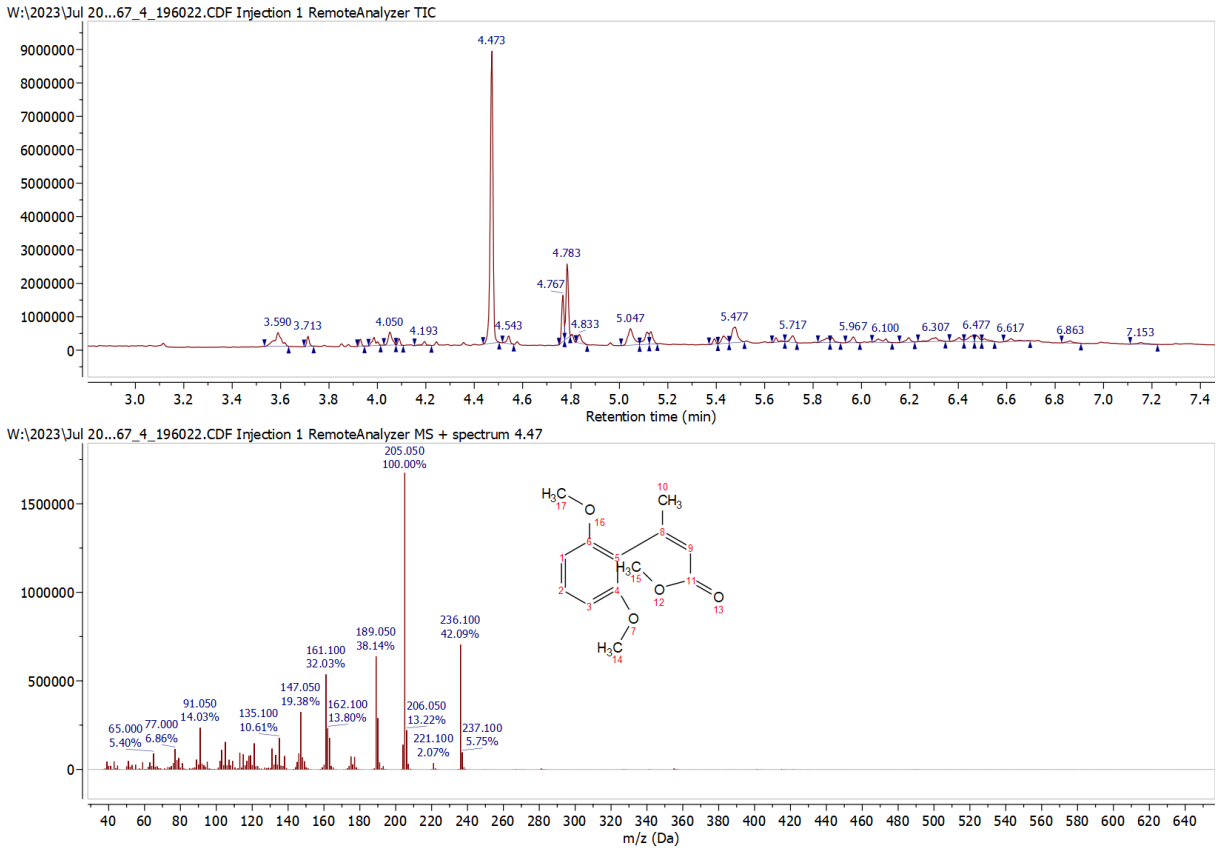

Figure 96. The GC-MS result and predicted structure of the side product by reaction conditions in Entry 4, Table 52. The sample was analysed after completion of the final work up procedure.

The formation of the side product in Figure 96 was potentially formed due to the formation of methoxide MeOH by reaction of excess Ambersep® 900 hydroxide form and dimethyl sulfate. This was then able to attack the 5-hydroxy-4-mehthylcoumarin (**61**) to afford the side product. As the equivalent of dimethyl sulfate and Ambersep® 900 hydroxide form (**86**) was reduced, the desired product was observed but with a crude yield of only 49% (Table 52 Entry 5, Figure 97). The GC-MS analysis confirmed the complete deprotonation of **61**. However, it was hypothesized that the starting material remained bound to the base, potentially hindering step 2 and contributing to the poor overall yield. Under these conditions, the reaction appeared to require extended reflux times for completion. Simultaneously, alternative methodologies were being explored, which yielded better results, so we moved on to explore these other methodologies.

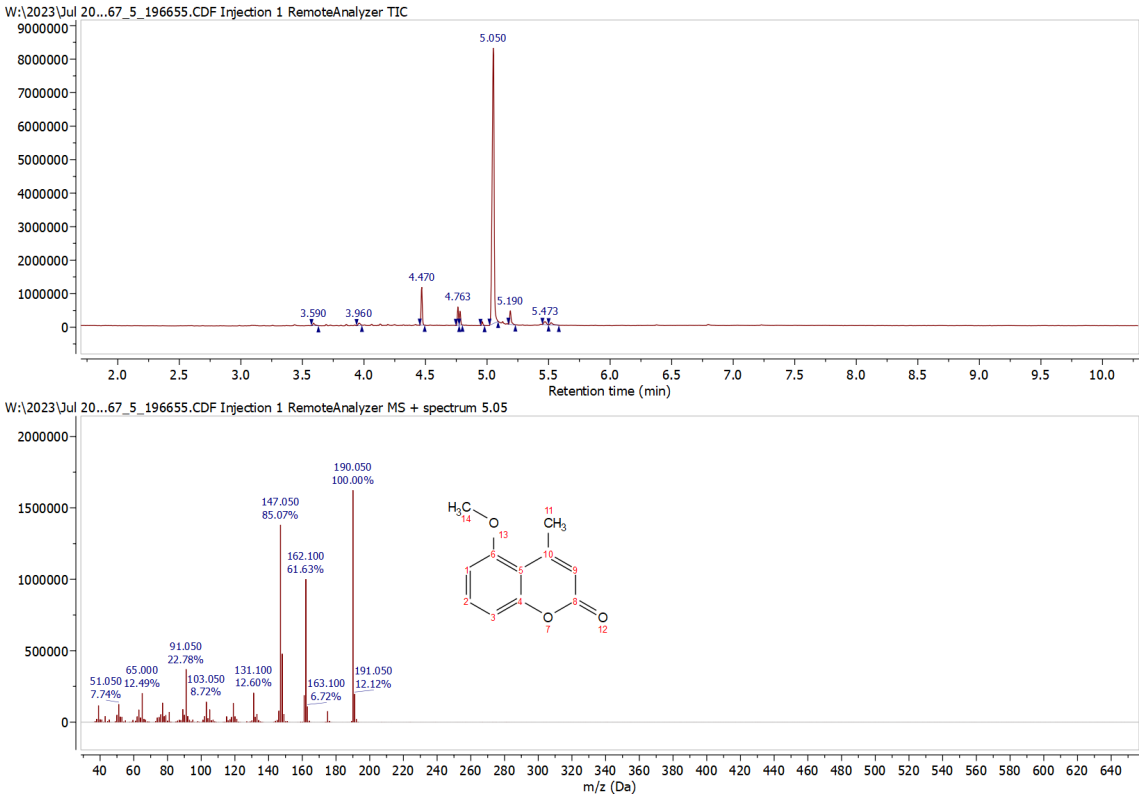

Figure 97. The GC-MS result for the reaction conditions in Entry 5 Table 52. The sample was analysed after completion of the final work up procedure. Target molecular mass was found at R_t = 5.05 min.

(ii) Homogeneous methylation

While the use of polymer-supported bases offers some environmental and user friendly benefits to the reaction process, other factors, such as reaction time, also influence the selection of a synthetic route. In this context, alternative base reagents—including sodium hydroxide, cesium carbonate, and sodium carbonate—were tested, as all three are widely employed in *O*-methylation syntheses.

a. Aqueous sodium hydroxide, phase transfer catalyst, and dimethyl sulfate

A literature source reported *O*-methylation with aqueous sodium hydroxide as base and tetrabutylammonium bromide as phase transfer catalyst (PTC) with more environmentally friendly methylating agent, dimethyl carbonate.[310] By using this base and the PTC, the reaction using dimethyl carbonate and dimethyl sulfate were compared (Table 53, Entry 1 and 2) (A large excess of dimethyl carbonate was suggested in the literature). The reaction using dimethyl sulfate afforded the target compound by GC-MS analysis (Table 54 Entry 2) while starting material remained the major peak for the process employing dimethyl carbonate. Reducing the equivalents of tetrabutylammonium bromide (the PTC) to 0.05 and 0 resulted in no sign of the product (Entry 3 and 4). A 41% isolated yield was achieved with 0.8 equivalents of PTC (Table 53, Entry 5). The GC-MS results of Entry 2 and Entry 5 are compared in Figure 98. In addition to the target 5-methoxy-4-methylcoumarin (**56**, R_f = 0.80 while Hex:EtOAc = 1:1), two other products at R_t = 3.30-3.36 and R_t = 4.46-4.47 were also found and are proposed as the compounds in Table 54, Entry 2 and Entry 3. The former structure was proposed as the by-product of tetrabutylammonium bromide, the latter from further analysis by ^{1}H NMR spectroscopy (Figure 99). Other side products were potentially over-chlorination compounds as suggested by Table 54, Entry 4, 5, 6 which can be carried through as impurities and separate upon achieving the final target compound. To improve the yield of **56** and simplify the purification of crude mixture later on, both reaction conditions and work up procedure were modified, the isolated yield of **56** slightly improved at 46%. For this trial, the temperature was raised to reflux (96 °C) as outlined in Entry 6 Table 53. Work up involved additional washing of using polymer supported reagent QP-SA (Figure 100) and Ambersep® 900 OH form (**86**) in ethyl acetate. The tributylamine peak (**87**) was removed by QP-SA wash, and the amount of **88** was reduced by Ambersep® 900 OH (**86**) wash (Figure 101). Recall that the same issue was encountered in part (i) with heterogeneous methylation, this is potentially caused by excess methylating agent which formed methanol. A reduced equivalent of

dimethyl sulfate, however, led to a notable reduction in the isolated yield (21%, Table 53 Entry 7). The best yield achieved was still given by Table 53 Entry 6.

Table 53. Reaction conditions of methylation of 5-hydroxy-4-methylcoumarin (**61**).

Entry	Scale/ mmol	Equiv. of NaOH	Equiv. of Bu_4NBr	Equiv. of $(MeO)_2SO_2$	H_2O/ mL	Temp.	Time	Yield/%
1[a]	10	2	0.5 eq.	16 eq. $CO(OCH_3)_2$	20	Approx. 85℃	overnight	/
2	10	2	0.5 eq.	2 eq.	20	Approx. 85℃	overnight	54 (crude)
3	10	2	0.05 eq.	2 eq.	20	Approx. 85℃	overnight	/
4	10	4	/	2 eq.	20	Approx. 85℃	overnight	/
5	10	2	0.8 eq.	2 eq.	20	82 ℃	~15 h	41 (isolated)
6[b]	10	2	0.8 eq.	2 eq.	20	97 ℃	~15 h	46[c] (isolated)
7[b]	10	2	0.8 eq.	1.25 eq.	20	97 ℃	~ 15 h	21%[c] (isolated)

[a]Dimethyl carbonate was used instead of dimethyl sulfate. [b]Additional work up by QP-SA and Ambersep® 900 OH form (**86**). [c]Additional work-up procedure was added to minimise side products.

Table 54. Proposed structures of methylation in Table 53.

Entry	**R_t/ min**	**m/z**	**Structure**
1 (target)	5.05	190.1	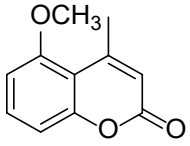 **56**
2	3.36/3.30	185.2	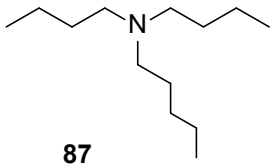 **87**
3	4.46	236.1	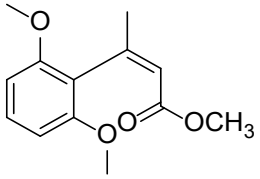 **88**

4	4.77	270.1	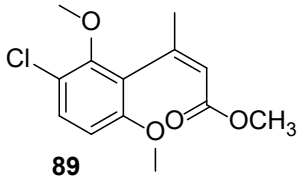 **89**
5	5.01	304	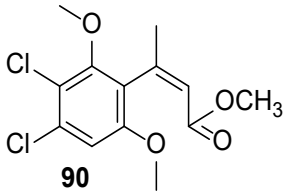 **90**
6	5.18	224	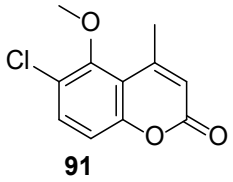 **91**

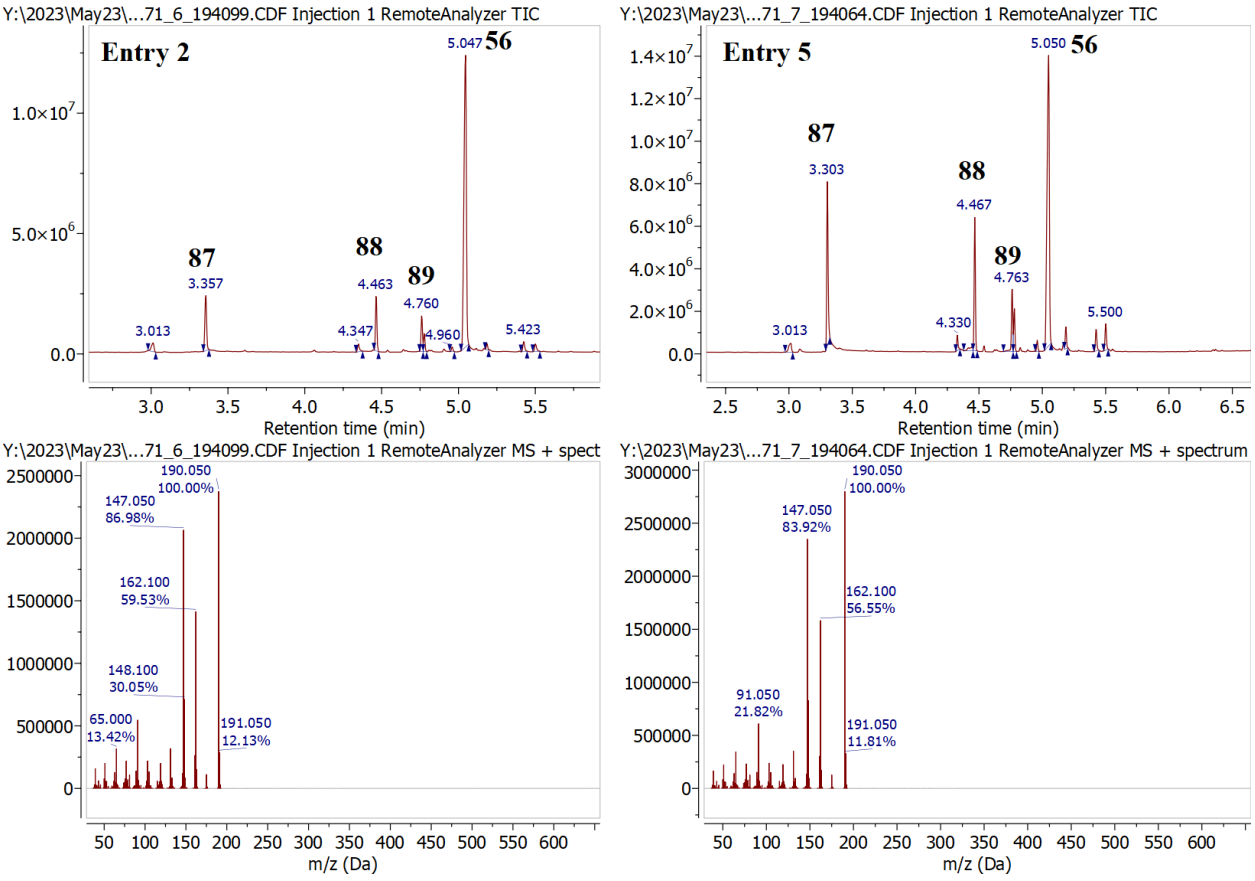

Figure 98. The GC-MS analysis of the reaction process in Entry 2 and Entry 5 of Table 53.

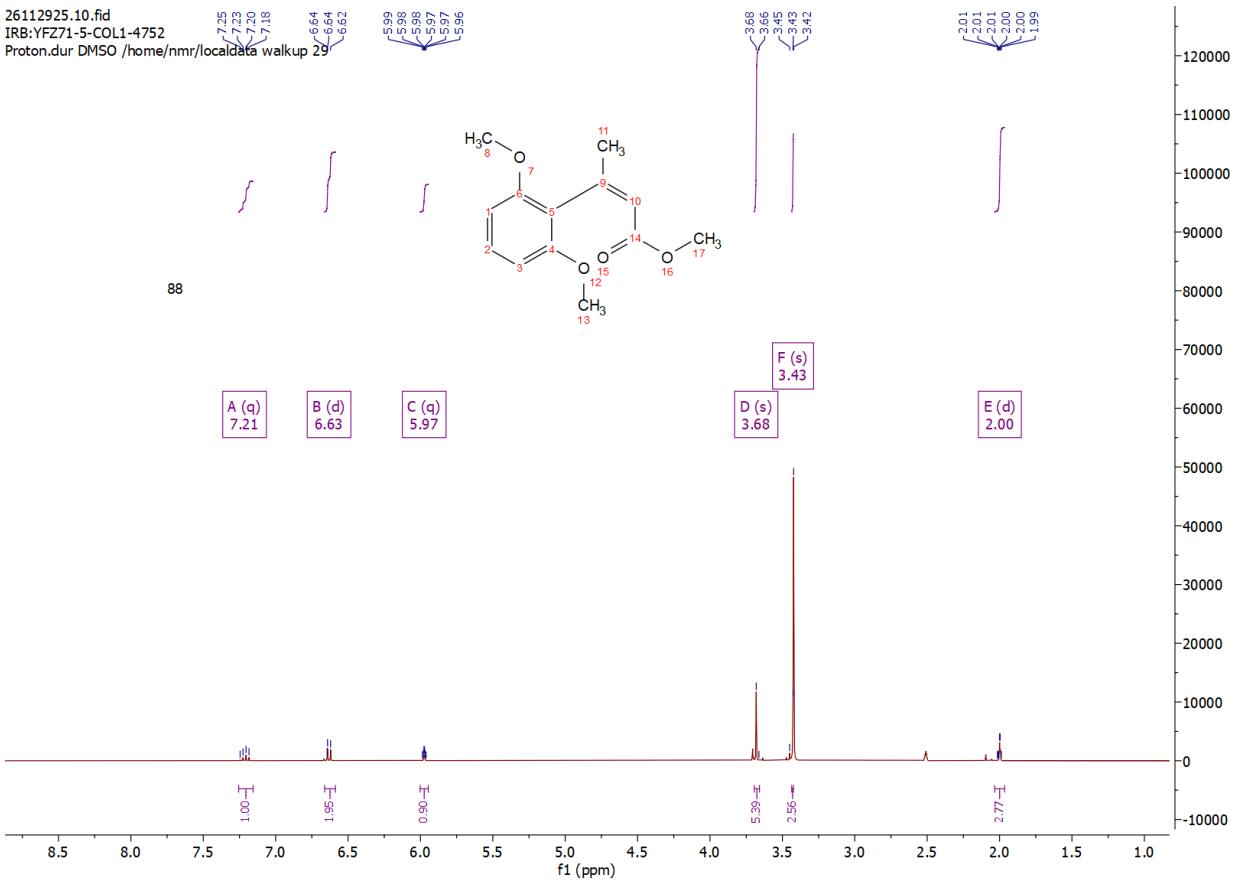

Figure 99. Proposed structure of isolated compound with Retention time 4.47 min and m/z of 236.1.

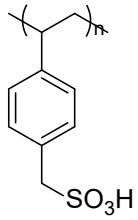

QP-SA
92

Figure 100. The structure of polymer supported reagent QP-SA (**92**).

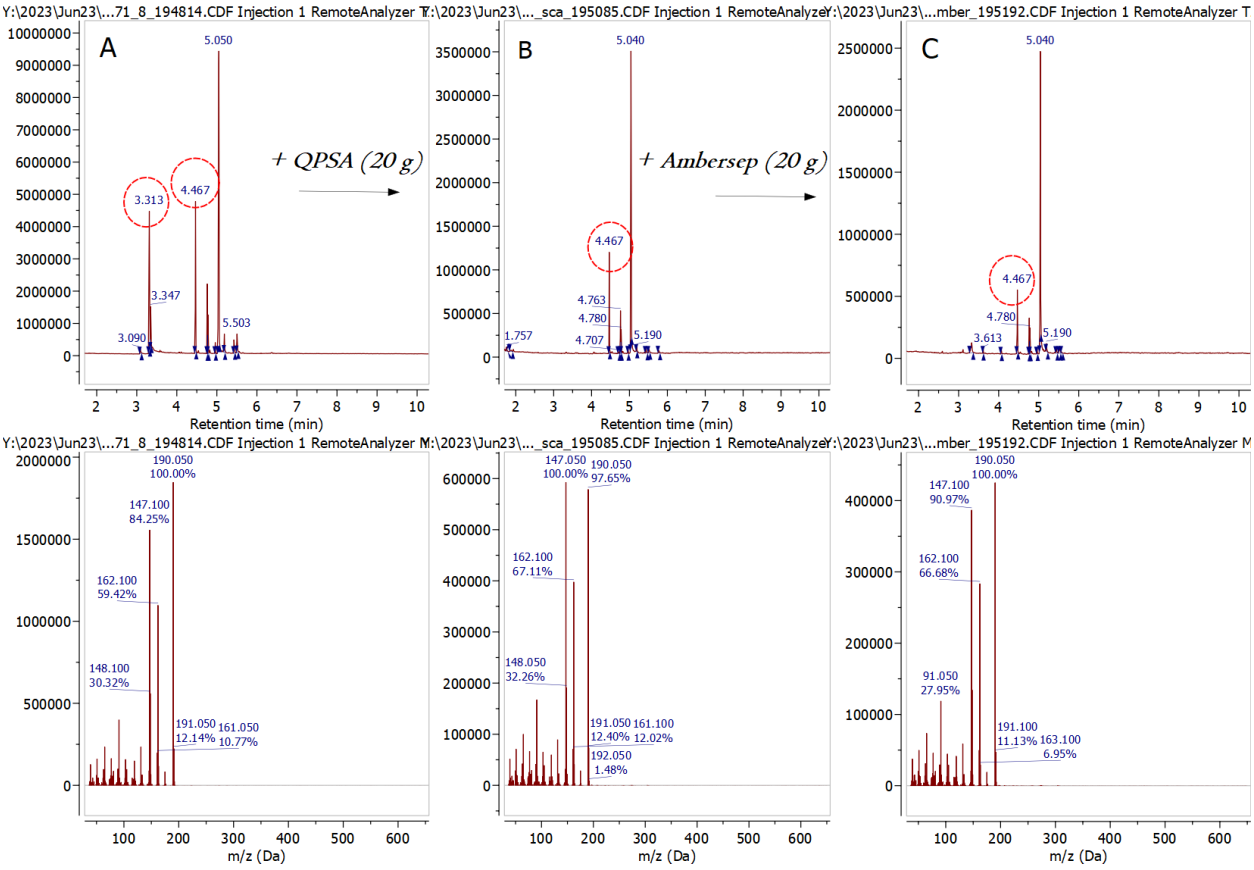

Figure 101. The evidence of reduced side products for crude compounds obtained from reaction conditions in Table 48, Entry 6. A. GC-MS of the crude material dissolved in ethyl acetate. B. Addition of QP-SA (20 g) resulted in vanished peak at R_t = 3.3 min (tributylamine) as shown by 8-2. C. Addition of Ambersep ® 900 OH form offered reduced total area% (from 17.32 to 11.11) of the peak at R_t = 4.47 min.

b. Potassium carbonate and dimethyl sulfate

In addition to the use of aqueous sodium hydroxide, cesium carbonate[323] and potassium carbonate[315] were also reported in literature for *O*-methylation of the coumarin substrates. As both carbonates are milder but offer a more nucleophilic hydroxide species due to counter ion coordination, these were also tested for this reaction. The crude yields employing dimethyl sulfate were compared for initial screening. With 1.2 equivalents of cesium carbonate, the crude yield of 5-methoxy-4-methylcoumarin (**61**) was 66% (Table 55 Entry 1), and 82% with 1.2 equivalents of potassium carbonate (Table 55 Entry 2). The potassium carbonate method was then further assessed with reduced and increased equivalents of reagents. Reduced potassium carbonate (0.6 equivalent) gave a lower yield with residual starting material being identified in the crude mixture

(Figure 102), and increased potassium carbonate (2.0 equivalents) afforded approximately the same result as 1.2 equivalents of potassium carbonate. Similarly, 1.35 and 1.5 equivalents of dimethyl sulfate did not show an improvement over 1.2 equivalents was determined. The optimal conditions using these reagents were thus given by Table 55 Entry 2, and the yield quantified by ^{1}H NMR spectroscopy estimation was 52% and 54% against an internal standard by using Equation from Section 2.4 Experimental procedure (General information, calculations of estimated yield by NMR) (Table 55, Entry 7 and 8).

Table 55. Methylation of 5-hydroxy-4-methylcoumarin (**61**) with cesium carbonate or potassium carbonate at 10 mmol scale using 20 mL of MeCN (concentration = 0.5 M, with respect to the starting material) under reflux condition for 16 h. [a]Crude yield by mass recovery. [b]Quantified yield by ^{1}H NMR spectroscopy analysis with an internal standard (**8**) calculated by Equation in Section 2.4, Experimental procedure.

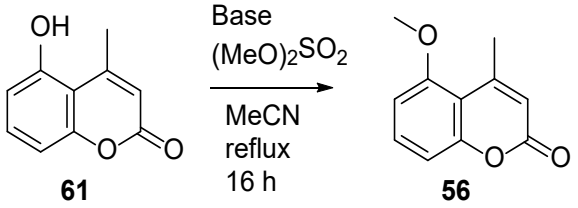

61 **56**

Entry	Eq. of K_2CO_3	Eq. of $(MeO)_2SO_2$	Yield/%
1	1.2 eq $CsCO_3$	1.25	66[a]
2	1.2	1.25	82[a]
3	0.6	1.25	45[a]
4	2.0	1.25	85[a]
5	1.2	1.35	79[a]
6	1.2	1.5	85[a]
7	1.2	1.25	52[b]
8	1.2	1.25	54[b]

Although the yield from the potassium carbonate method is only modest, it remains the best result among all the bases tested with dimethyl sulfate (Table 56). The study focused next on modifying other conditions to enhance the yield. Changing the solvent may have some influence on the result, but a key factor that can be quickly assessed is the choice of methylation agent. Since the ideal pairing of soft/hard nucleophiles and electrophiles can significantly impact the outcome, this was considered as electronic structure calculations can provide estimated results for comparison. Three other commonly used methylating agents were selected, namely, iodomethane, trimethyloxonium tetrafluoroborate, and methyl trifluoromethanesulfonate in addition to dimethyl sulfate. The results were recorded in Table 57 and 58.

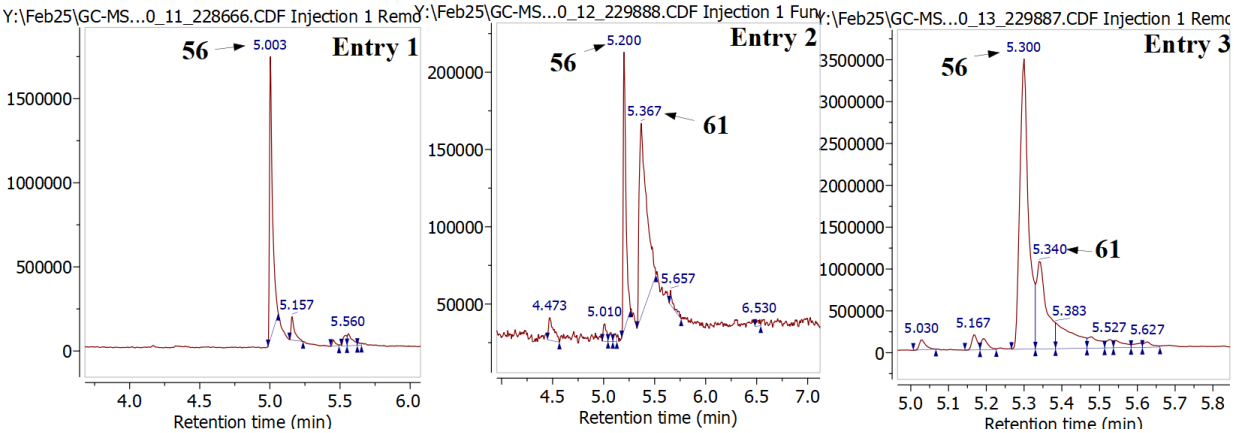

Figure 102. Plots of GC-MS for methylation reactions in Table 55 Entry 1-3.

Table 56. PTC = Phase transfer catalyst.

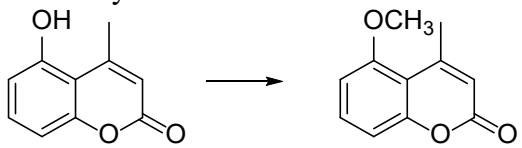

Entry	Scale/ mmol	Base (and PTC)	Eq. dimethyl sulfate	Solvent	Temp.	Time	Yield
1-step1	2.8	4 g Ambersep ® 900 OH	/	THF 30 mL	Room temp.	2 h	49% (Crude[a])
1-step2			1.25	MeCN 20 mL	Reflux	16 h	
2	10	2 eq. NaOH; 0.8 eq. Bu_4NBr	1.25	Water 20 mL	Reflux	16 h	46% (Isolated[b])
3	10	1.2 eq. K_2CO_3	1.25	MeCN 20 mL	Reflux	16 h	54 % (NMR[c])

[a]Crude yield by mass recovery. [b]Isolated yield. [c] ^1H NMR spectroscopic yield quantified using Equation given by Section 2.4 Experimental procedure.

Table 57. Atomic charge distribution (AC) and molecular orbital coefficients (MOC) of lowest unoccupied molecular orbitals (LUMO). Geometry optimisations of these compounds were carried out at the AM1 model chemistry using the SMD solvation model where solvent is applied.

	AM1/Gas*		**AM1/MeCN****	
	AC	**LUMO, $1P_z$**	**AC**	**LUMO,$1P_z$**
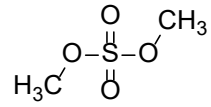 Dimethyl sulfate	-0.016	0.00961 -0.00961	-0.028	-0.00240, 0.00240

 Iodomethane	-0.382	0.63257	-0.373	0.64866
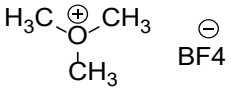 Trimethyloxonium tetrafluoroborate	-0.108	0.36890 -0.00014 -0.36833	-0.089 -0.090 -0.089	0.36834 -0.00013 -0.36779
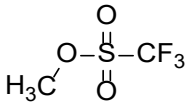 Methyl triflate	-0.031	-0.03927	-0.034	-0.003443

*No solvation model applied. **Acetonitrile was applied with SMD solvation model.

When AM1 modelling was applied, iodomethane had the largest absolute value of atomic charge distribution and lowest unoccupied molecular orbital coefficients (Table 57). Similar results were obtained with HF/3-21 model chemistry (Table58). Among the methylating agents tested for this reaction as shown by Table 59, iodomethane afforded our target compound **56** with an excellent yield of 86 - 100% as quantified by NMR with an internal standard (Entry 1). This is better than the 54% yield using dimethyl sulfate. The major molecular ion peaks by employing trimethyloxonium tetrafluoroborate and methyl trifluoromethanesulfonate was residual starting material (Entry 2 and Entry 3).

Table 58. Atomic charge distribution (AC) and molecular orbital coefficients (MOC) of lowest unoccupied molecular orbitals (LUMO). Geometry optimisations of these compounds were carried out at the HF/3-21G model chemistry using the SMD solvation model where solvent is applied.

	HF/3-21G/Gas*			**HF/3-21G/MeCN****		
	AC	**LUMO**		**AC**	**LUMO**	
		$2P_z$,	**$3P_z$**		**$2P_z$,**	**$3P_z$**
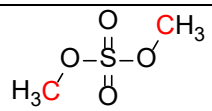 Dimethyl sulfate	-0.325	0.02114 -0.02114	0.07213 -0.07213	-0.340	0.01496	0.06140
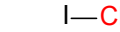 Iodomethane	-0.889	0.25132	0.74001	-0.882	0.25735	0.76091
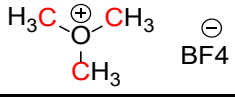	0.309 0.309	0.13665 -0.00004	0.46551 -0.00015	0.312 -0.312	0.13859 -0.00004	0.46791 -0.00016

Trimethyloxonium tetrafluoroborate	-0.309	-0.13639	-0.46466	-0.312	-0.13835	-0.46705
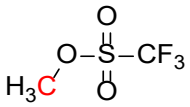 Methyl triflate	-0.320	-0.01362	-0.04112	-0.336	0.00514	0.00575

*No solvation model applied. **Acetonitrile was applied with SMD solvation model.

Table 59. Results comparisons using different methylating agents. Reaction conditions:10 mmol scale, 1.2 eq. of K_2CO_3, 20 mL of MeCN, refluxed over 16 h.

Entry	Methylating agent	Total area% of starting material	Total area% of target	Crude Mass/g	Yield
1	Iodomethane	0	97.57	0.51	86 - 100% (NMR[a])
2	Trimethyloxonium tetrafluoroborate	37.34	0	1.90	/
3	Methyl trifluoromethanesulfonate	63.12	0	1.38	/

[a]Estimated yield quantified by ^{1}H NMR spectroscopy using Equation in section 2.4 experimental procedure (General information, calculations of estimated yield by ^{1}H NMR spectroscopy).

c. Conclusions on methylation

In conclusion, the best yield (86 - 100%) was achieved using potassium carbonate for deprotonation and iodomethane as the methylating agent (Scheme 68). While using dimethyl sulfate and potassium carbonate, the yield was reduced to 54%. When PTC and sodium hydroxide were used, the highest isolated yield was only 46%. Heterogeneous base afforded our target compound in yields of 49%. From the computed result using AM1 model chemistry and HF/3-21g model chemistry, iodomethane was identified as best methylating agent for this coumarin substrate which proved to be experimentally validated.

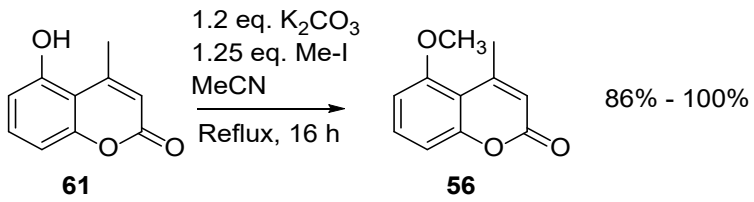

Scheme 68. The reaction scheme that achieved the best yield for methylation of 5-hydroxy-4-methylcoumarin (**56**).

4.3.3 Ozonolysis of 5-methoxy-4-methylcoumarin (56)

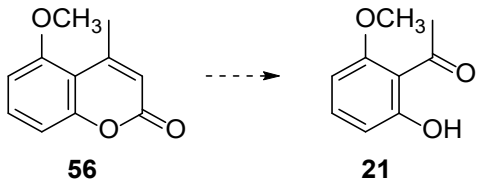

Scheme 69. Proposed ozonolysis of **56** to afford **21**.

As outlined at the start of this chapter, a two-step process was proposed for 2-hydroxy-6-methoxycoumarin (**21**) preparation. Having achieved the successful synthesis of 5-methoxy-4-methylcoumarin (**56**) we wished now to explore its ozonolysis. The set up of the reaction was constructed by providing oxygen from a gas cylinder, and comprised an ozone generator (Triogen, Figure 103), dreschel bottle and the reaction flask (Figure 104). A stream of 2% ozone in oxygen was generated and delivered to the reaction with the reacting solution being cooled to 0 °C. After the reaction was complete, water was added, and the organic phase was extracted using dichloromethane as in the literature.[284] This method was initially tested with two commercial chemicals (*E*)-prop-1-en-1-ylbenzene (**93**) and 7-hydroxy-4-methylcoumairn (**45**) (Table 60 Scheme A and B) where benzaldehyde (**94**) and 1-(2,4-dihydroxyphenyl)ethan-1-one (**95**) were successfully synthesized. These achieved 100% consumption of starting material within 20 and 30 minutes respectively (Table 60 Entry 1 and 2). By comparison our target substrate **21** synthesis achieved 100% consumption of the starting material in ~40 minutes (Table 60 Entry 3).

Figure 103. Ozone generator.

Reaction process:

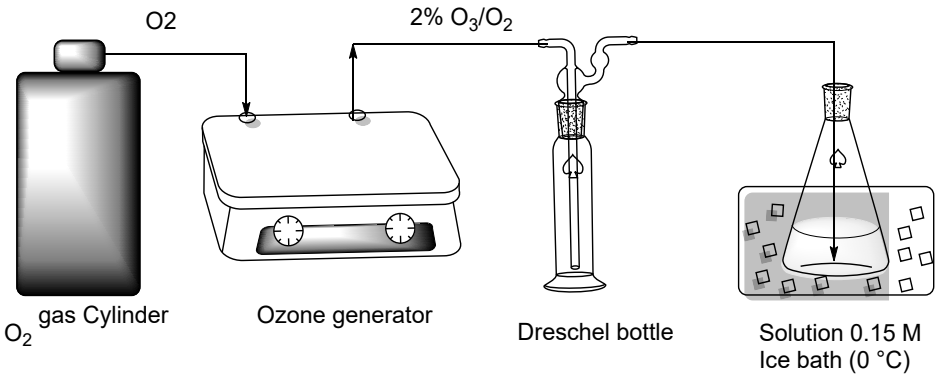

Figure 104. Set up for ozonolysis reaction. Ozone gas, generated by an ozone generator connected to an oxygen cylinder, is delivered to the reaction mixture via a dreschel bottle. The Dreschel bottle is installed to prevent backflow of the solution into the generator. The reaction vessel is cooled in an ice bath throughout the process.

Table 60. Reaction results of ozonolysis reactions at 3 mmol scale.

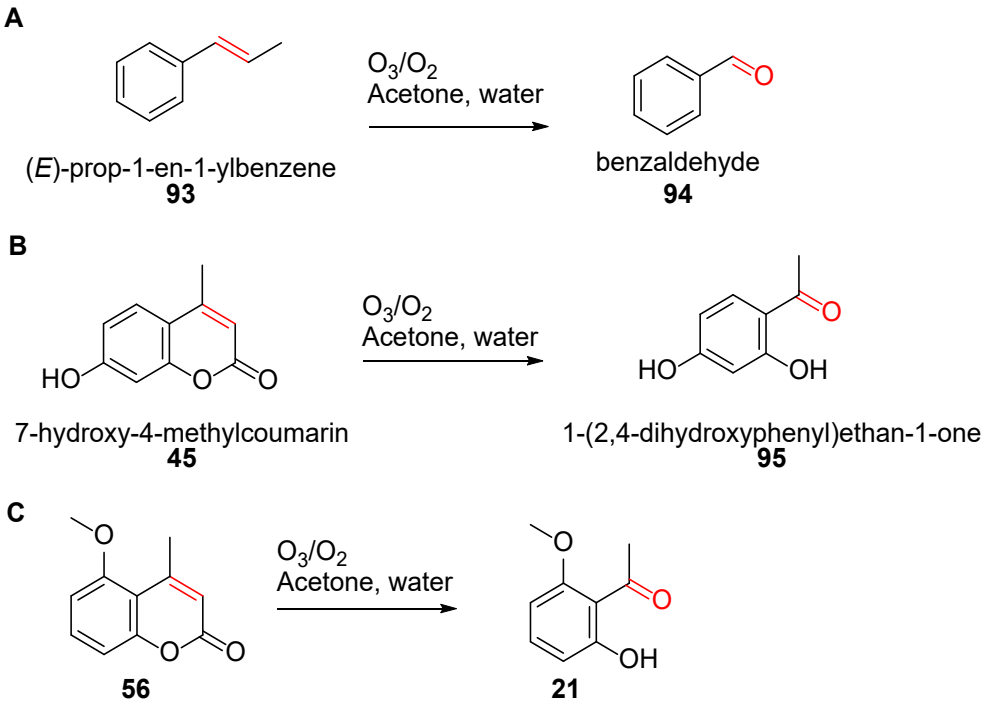

Entry	Reagent	Time/ min	Crude yield by DCM (2*50 mL) extraction/%	Yield by EtOAc (2*50 mL) extraction/%	Yield by EtOAc (2*100 mL) extraction/%
1	**93**	20	/	/	/
2	**45**	30	4 (Crude)*	99 (Crude)*	/
3	**45**	30	/	35 (NMR)**	/
4	**56**	40	/	41(Crude)*	83 (Crude)*
5	**56**	40	/	/	14 (NMR)**

*Crude yield. **Estimated yield by ^{1}H NMR spectroscopy using methodology in Section 2.4 Experimental procedure (General information, calculations of estimated yield by ^{1}H NMR spectroscopy).

For both coumarin compounds (**45** and **56**), the extraction solvent was changed to ethyl acetate for better extraction of these more polar products. Compound **7**, however, required more extraction solvents to achieve a higher crude yield. The extraction by DCM gave a higher yield for *trans*-β-methylstyrene (**94**), but less for 7-hydroxy-4-methylcoumarin (**45**) and 5-methoxy-4-methylcoumarin (**56**). Since these coumarin derived substrates are more polar than benzaldehyde, ethyl acetate was used for extraction and the crude yield of 1-(2,4-dihydroxyphenyl)ethan-1-one (**95**) was 99% (Table 60 Entry 2), this excess crude yield was due to the material not being fully dried of solvent. The target synthesis required even more solvent for effective extraction (Table 60

Entry 4). Although GC-MS showed the major peak as the targeted molecular ion, the estimated yields were significantly reduced to only 35% (Table 60 Entry 3) and 14% (Table 60 Entry 4). Two potential reasons contributed to these reduced yields. Firstly, the concentration of ozone generated by the generator required careful control. In the literature synthesis, the concentration of O_3/O_2 was reported to be 2% approximately 0.5 mmol/min O_3.[284] As no such function was available on the ozone generator in the laboratory, external equipment will be required for this concentration assessment. Secondly, both coumarin substrates (**45** and **56**) obtained were low yields via this method, whereas literature citated reactions obtained 72 – 100% isolated yield for substrates (Table 61). Potentially, alternative oxidation methods of these coumarin substrates should be explored to limit side products formation.

Table 61. Ozonolysis reactions reported in literature (2% O_3/O_2 into a 0.15 M solution of alkene).[284] Starting materials, X = CH_2. Products, X = O (aldehyde or ketone).

Substrates	**Isolated yield/%**
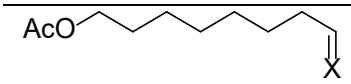	72
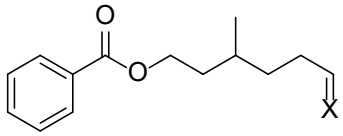	75
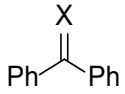	54
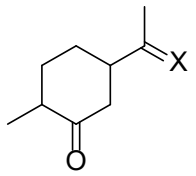	100
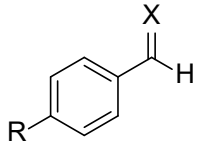 R = OAc, NO_2	81 (R = OAc), 100 (R = NO_2)

4.4 Conclusion and proposed future work

The 2-hydroxy-6-methoxyacetophenone (**21**) (Scheme 70) was successfully synthesized from ketone **60** as proposed at the beginning of this Chapter. The first procedure involved a two-step oxidation of **60** to form **61**. For batch reactions, chlorination of **60** required shielding from light to achieve the best selectivity of mono-chlorinated target compound **71**. When the reaction time was reduced to 3 hours by using microwave irradiation at higher temperatures, more starting material remained in the product mixture and reduced the ratio of **71**.

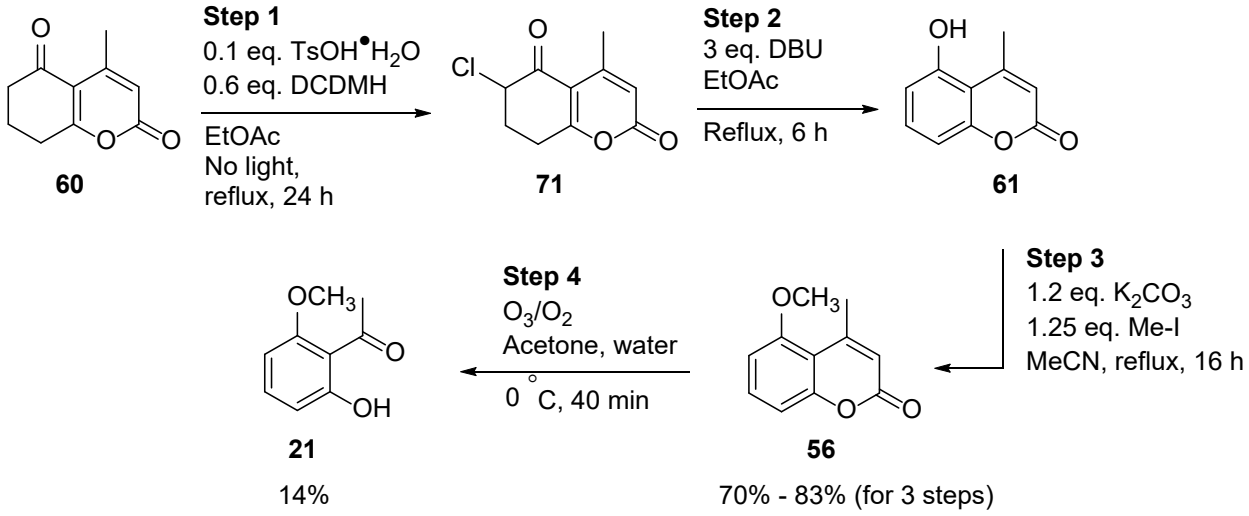

Scheme 70. The established synthetic scheme of synthesizing **21** from **60** in four steps. Yields were estimated by ^{1}H NMR spectroscopic methods.

At the same temperature and residence time, flow reactions were conducted successfully with higher selectivity than conventional and microwave assisted reactions without the need for light shielding and providing a more scalable solution as confirmed by steady state analysis (average, 1.46 g/ h or 6.2 - 6.5 mmol/ h for 90-95% estimated yield as stated in the Experimental procedure). Subsequent dehydrochlorination was a straightforward process using DBU in the same solvent as step 1. No extra evaporation or isolation of the product was required from step 1, minimizing the waste of solvent in multistep synthetic schemes. The *O*-methylation of **61** derived **56** by using the combination of potassium carbonate and iodomethane. The estimated yield by ^{1}H NMR spectroscopy with an internal standard was 70-83% over 3 steps (Scheme 70). Similarly, the crude mixture containing **61** was used directly to afford **56** and this compound could be easily purified

via column chromatography using hexane and ethyl acetate (from 34:2 to 33:2). Ozonolysis of **56** yielded **21** in 14%. Potentially, the concentration of O_3/O_2 can be re-assessed to control the rate of reaction and to improve the yield. In addition, exploring other oxidation methodologies of these coumarin substrates would be recommended as both tested coumarin substrates (**56** and **45**) did not provide yields as good as the simpler molecules reported in the literature.

In summary, the implementation of a flow reaction significantly reduced the reaction time for the chlorination step, enhancing process efficiency. The use of a sequential reaction strategy minimized the need for intermediate purification, thereby reducing solvent consumption and waste generation. Ethyl acetate (EtOAc) and acetonitrile (MeCN) were employed as solvents; among them, EtOAc is considered a relatively green solvent due to its low toxicity and good biodegradability. The green chemistry metrics for this synthetic route, including atom economy and reaction mass efficiency are summarized in Table 62.

Table 62. Summary of Green metrics of Scheme 69. AE = atom economy, RME = reaction mass efficiency. Yields are detailed in Experimental procedures, section 4.5.

Step	Yield	AE/%	RME/%
1	95	38	36.1
2	85 - 90	48	41 - 43
3	82 - 92	42	34 - 39
4	14	65	9

4.5 Experimental procedure

For General Information please refer to Section 2.5.

4.5.0 Synthesis of Section 4.1

4-hydroxy-2-methoxyacetophenone (41a)

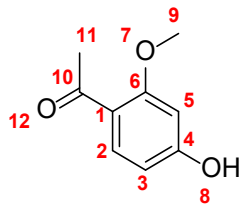

Chemical Formula: $C_9H_{10}O_3$
Exact Mass: 166.0630

The reagents of 3-methoxyphenol (X) (10 mmol, 1.24 g), acetic acid (15 mmol, 0.90 g) and Eaton's reagent (10 g) were mixed and stirred at 60 °C for 30 minutes. To the solution was added saturated $NaHCO_3$ solution (30 mL) and water (30 mL). The aqueous layer was extracted with ethyl acetate (60 mL × 3). The combined organic phase was dried by anhydrous Na_2SO_4 and concentrated in vacuo to afford a crude mixture. The title compound, 4-hydroxy-2-methxoyacetophenone (**41a**) and 2-hydroxy-4-methoxyacetophenone **(41b)** has a ratio of 1.27:1 measured by GC-MS total area% and were obtained by column chromatography purification (Hexane:EtOAc = 19:1 to 14:1).

Isolated yield: 0.55 g (33%).

^{1}H NMR (700 MHz, DMSO) δ/ppm 10.30 (s, 1H, H8), 7.59 (d, *J* = 8.6 Hz, 1H, H2), 6.48 (d, *J* = 2.2 Hz, 1H, H5), 6.42 (dd, *J* = 8.6, 2.2 Hz, 1H, H3), 3.84 (s, 3H, H9), 2.45 (s, 3H, H11).

^{1}H NMR (400 MHz, DMSO) δ/ppm 10.30 (s, 1H), 7.59 (d, *J* = 8.6 Hz, 1H), 6.48 (d, *J* = 2.2 Hz, 1H), 6.42 (dd, *J* = 8.6, 2.2 Hz, 1H), 3.84 (s, 3H), 2.45 (s, 3H).

^{13}C NMR (176 MHz, DMSO) δ/ppm 195.75 (C10), 163.14 (C6), 161.19 (C4), 131.95 (C2), 118.80 (C1), 107.72 (C3), 98.99 (C5), 55.45 (C9), 31.58 (C11).

^{13}C NMR (101 MHz, DMSO) δ/ppm 196.28, 163.67, 161.73, 132.48, 119.34, 108.26, 99.53, 55.98, 32.11.

2-hydroxy-4-methoxyacetophenone (41b)

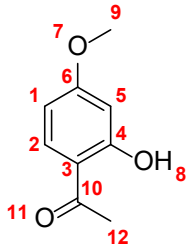

Chemical Formula: $C_9H_{10}O_3$
Exact Mass: 166.0630

Another product isolated from the synthesis for 4-hydroxy-2-methxoyacetophenone (**41a**) above.

Isolated yield: 0.49 g (30%).

^{1}H NMR (599 MHz, DMSO) δ/ppm 12.61 (s, 1H, H8), 7.81 (d, *J* = 8.9 Hz, 1H, H2), 6.49 (dd, *J* = 8.9, 2.5 Hz, 1H, H1), 6.44 (d, *J* = 2.5 Hz, 1H, H5), 3.79 (s, 3H, H9), 2.53 (s, 3H, H12).

^{13}C NMR (151 MHz, DMSO) δ/ppm 203.58 (C10), 166.15 (C6), 164.53 (C4), 133.72 (C2), 114.17 (C3), 107.69 (C1), 101.14 (C5), 56.14 (C9), 27.03 (C12).

^{1}H NMR (400 MHz, DMSO) δ/ppm 12.64 (s, 1H), 7.84 (d, *J* = 8.9 Hz, 1H), 6.53 (dd, *J* = 8.9, 2.5 Hz, 1H), 6.47 (d, *J* = 2.5 Hz, 1H), 3.82 (s, 3H), 2.57 (s, 3H).

^{13}C NMR (101 MHz, DMSO) δ/ppm 203.61, 166.19, 164.57, 133.75, 114.21, 107.72, 101.17, 56.17, 27.06.

4-methyl-2-oxo-2*H*-chromen-7-yl acetate (48)

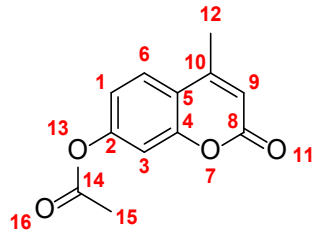

Chemical Formula: $C_{12}H_{10}O_4$
Exact Mass: 218.0579

A mixture of 7-hydroxy-4-methylcoumarin (10 mmol, 1.75 g), acetic acid (15 mmol, 0.90 g), and Eaton's reagent (10 g) was stirred at 60 °C overnight and then cooled to room temperature. To the solution was added saturated $NaHCO_3$ solution (30 mL) and water (30 mL). The aqueous layer was extracted with ethyl acetate (60 mL × 3). The combined organic phase was dried with anhydrous Na_2SO_4 and concentrated in vacuo. The 4-methyl-2-oxo-2*H*-chromen-7-yl acetate was obtained by column purification (Hexane:EtOAc = 5:1 to 4:1).

Isolated mass: 1.16 g.

^{1}H NMR (599 MHz, DMSO) δ/ppm 7.79 (d, *J* = 8.6 Hz, 1H, H6), 7.23 (d, *J* = 2.3 Hz, 1H, H3 7.15 (dd, *J* = 8.6, 2.3 Hz, 1H, H1) 6.36 (q, *J* = 1.3 Hz, 1H, H9), 2.41 (d, *J* = 1.3 Hz, 3H, H12), 2.28 (s, 3H, H15).

^{1}H NMR (400 MHz, DMSO) δ/ppm 7.82 (d, *J* = 8.7 Hz, 1H), 7.27 (d, *J* = 2.3 Hz, 1H), 7.19 (dd, *J* = 8.7, 2.3 Hz, 1H), 6.39 (q, *J* = 1.3 Hz, 1H), 3.63 (s, 5H), 2.44 (d, *J* = 1.3 Hz, 3H), 2.32 (s, 3H).

^{13}C NMR (151 MHz, DMSO) δ/ppm 169.24, 160.06, 153.95, 153.40, 153.33, 126.85 (C6), 118.87 (C1), 117.94, 114.16 (C9), 110.54 (C3), 21.31 (C15), 18.59 (C12).

^{13}C NMR (101 MHz, DMSO) δ/ppm 169.27, 160.09, 153.98, 153.43, 153.36, 126.88, 118.90, 117.97, 114.19, 110.58, 40.45, 21.34, 18.63.

^{1}H NMR (400 MHz, $CDCl_3$) δ 7.63 (d, *J* = 8.6 Hz, 1H), 7.14 (d, *J* = 2.7 Hz, 1H), 7.12 (dd, *J* = 8.6, 2.7 Hz, 1H), 6.29 (q, *J* = 1.3 Hz, 1H), 2.46 (d, *J* = 1.3 Hz, 3H), 2.36 (s, 3H).

^{13}C NMR (101 MHz, $CDCl_3$) δ 168.8 (C), 160.5 (C), 154.2 (C), 153.0 (C), 151.9 (C), 125.4 (CH), 118.1 (CH), 117.9 (C), 114.5 (CH), 110.5 (CH), 21.1 (CH_3), 18.7 (CH_3).

IR ν cm^{-1} 2332.6 (w), 1755.9 (s), 1725.2 (s), 1709.7 (m), 1616.3 (m), 1417.3 (w), 1393.8 (w), 1371.3 (m), 1264.9 (m), 1195.1 (s), 1156.3 (m), 1128.9 (s), 1070.8 (m), 1013.8 (m), 958.1 (m), 849.5 (s), 826.7 (m), 793.8 (w), 741.8 (w).

LC-MS (ESI - LC MeCN (TQD)): R_t 2.50 min, m/z 219.40 $[M+H]^+$ and 218.6 $[M]^+$; HR-MS Calculated for $C_{12}H_{11}O_4$ 219.0657, found: 219.0663 (Δ = 2.7 ppm).

Melting point 149.5-151.8 °C.

4.5.1 Synthesis of Section 4.3.1

Riboflavin tetraacetate (63)[324]

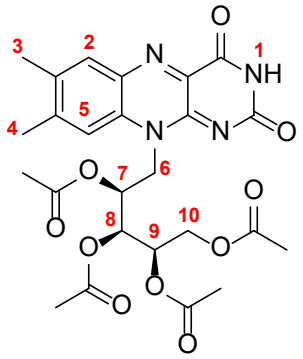

Chemical Formula: $C_{25}H_{28}N_4O_{10}$
Exact Mass: 544.1805

Triethylamine (2.79 mL, 20 mmol), riboflavin (**62**) (3.76 g, 10 mmol), and DMAP (0.0145 g, 1 mmol) were dissolved in acetic anhydride (10 mL). The mixture was heated until it began to boil. Upon initiation of a brief exothermic reaction, the heat source was removed. After the reaction subsided, gentle boiling was resumed and maintained until completion, as confirmed by TLC (DCM:MeOH = 15:1) analysis. The hot reaction mixture was poured into a vigorously stirred mixture of ice and water (~100 mL). Stirring was continued until the oily phase solidified. The resulting crude solid (5.04 g) was collected by filtration and used directly in the subsequent photoreaction.

^{1}H NMR (400 MHz, $CDCl_3$) δ/ppm 9.27 (s, 1H, H1), 8.04 (s, 1H, H2), 7.59 (s, 1H, H5), 5.43 (td, J = 6.0, 2.9 Hz, 2H, H6), 5.30 (s, 1H, H7 or H8 or H9), 4.93 (s, 1H, H7 or H8 or H9), 4.45 (dd, J = 12.4, 2.8 Hz, 2H, H10), 4.26 (m, 1H, H7 or H8 or H9), 2.59 (s, 3H), 2.46 (d, J = 0.9 Hz, 3H), 2.30 (s, 4H), 2.24 (d, J = 4.2 Hz, 5H), 2.12 (s, 3H, H3 or H4), 1.77 (s, 3H, H3 or H4).

Methyl (*E*)-3-(2-methoxyphenyl)but-2-enoate (58a)[290]

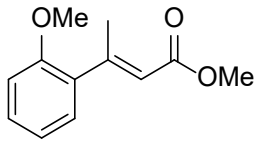

Chemical Formula: $C_{12}H_{14}O_3$
Exact Mass: 206.09

To a suspension of sodium hydride (0.46 g, 19 mmol) in THF (20 mL) at room temperature was added dropwise a solution of trimethyl phosphonoacetate (1.38 g, 7.6 mmol) in THF (6 mL). After 1 h, 2-methoxyacetophenone (**57**) (0.96 g, 6.4 mol) was added dropwise to the cooled solution maintained at 0 °C and the mixture stirred at room temperature. The reaction was monitored by TLC (DCM:MeOH = 9:1) (18 h) and water (30 mL) was added slowly to quench the reaction. The organic solvent was removed under reduced pressure and the residue extracted with ethyl acetate (40 mL × 3). The organic extract was dried over Na_2SO_4, and the solvent evaporated to give a crude oil (1.34 g) which was used without further purification.

^{1}H NMR (400 MHz, $CDCl_3$) δ/ppm 7.33-7.29 (m, 1H), 7.05 (m, *J* = 1.4 Hz, 1.8 Hz, 1H), 7.00 – 6.91 (m, 2H), 5.99 (q, *J* = 1.5 Hz, 1H), 3.83 (s, 3H), 3.56 (s, 3H), 2.18 (d, *J* = 1.5 Hz, 3H).

^{13}C NMR (100 MHz, $CDCl_3$) δ/ppm 166.01, 155.30, 153.96, 128.82, 128.00, 120.37, 118.30, 110.77, 55.54 (CH_3), 50.91 (CH_3), 26.91 (CH_3).

^{13}C NMR (101 MHz, $CDCl_3$) δ 166.01 (C), 155.30 (C), 153.96 (C), 128.82 (CH), 128.00 (CH), 120.37 (CH), 118.30 (CH), 110.77 (CH), 55.54 (CH_3), 50.91 (CH_3), 26.19 (CH_3).

NB: Although compound 5**8a** has been used as a synthetic intermediate in prior literature, its analytical data was not reported. The NMR spectrum above is provided for completeness.

(*E*)-3-(2-methoxyphenyl)but-2-enoic acid (59)[325-327]

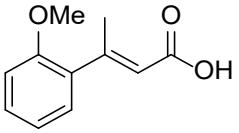

Chemical Formula: $C_{11}H_{12}O_3$
Exact Mass: 192.08

The crude methyl (*E*)-3-(2-methoxyphenyl)but-2-enoate (**59**) was subjected to hydrolysis. To the oil was added aqueous sodium hydroxide (2 M, 5 mL) and the solution heated to 90 °C for 3 h whilst monitoring the disappearance of the starting material by TLC (Hexane: EtOAc = 8:2). A small fraction is quenched with 4 M HCl and extracted with EtOAc. The reaction mixture was extracted with DCM (10 mL), then acidified with 4 M HCl to pH 3 and extracted with EtOAc (3 × 15 mL). The organic phase was dried over anhydrous Na_2SO_4 and concentrated under reduced pressure. The titled compound was purified by flush column chromatography (hexane:EtOAc = 25:1).

Isolated yield over two steps (57 – 58a – 59): 0.87 g (71%).

^{1}H NMR (400 MHz, DMSO) δ/ppm 12.20 (br. s, 1H), 7.33 (ddd, *J* = 8.4, 7.5, 1.8 Hz, 1H), 7.14 (dd, *J* = 7.5, 1.8 Hz, 1H), 7.05 (dd, *J* = 8.4, 1.0 Hz, 1H), 6.95 (td, *J* = 7.5, 1.0 Hz, 1H), 5.76 (q, *J* = 1.4 Hz, 1H), 3.79 (s, 3H), 2.37 (d, *J* = 1.4 Hz, 3H).

^{1}H NMR (400 MHz, $CDCl_3$) δ/ppm 7.37 – 7.30 (m, 1H), 7.19 (dd, *J* = 7.5, 1.8 Hz, 1H), 6.98 (td, *J* = 7.5, 1.1 Hz, 1H), 6.94 (dd, *J* = 8.3, 1.0 Hz, 1H), 5.97 (q, *J* = 1.3 Hz, 1H), 3.86 (s, 3H), 2.54 (d, *J* = 1.4 Hz, 3H).

^{13}C NMR (101 MHz, DMSO) δ/ppm 167.78 (C), 156.40 (C), 155.24 (C), 132.73 (C), 130.09 (CH), 128.89 (CH), 120.94 (CH), 120.19 (CH), 112.01 (CH), 55.92 (CH_3), 19.91 (CH_3).

^{13}C NMR (101 MHz, $CDCl_3$) δ/ppm 171.92, 159.62, 156.30, 132.92, 129.74, 128.76, 120.60, 118.60, 111.08, 55.48, 20.25.

IR (neat) ν_{max}/ cm^{-1} 2956 (OH), 1673 (C=O), 1621 (conjugated C=C).

LC-MS: R_t = 2.05 min, m/z 193.31 $[M+H]^+$; HR-MS calculated for $C_{11}H_{13}O_3$ 193.0865, found 193.0861 (Δ = -0.4 mDa; -2.1 ppm).

Melting point: 97.3-98.2 °C, literature 96-97 °C.[328]

(*Z*)-3-(2-methoxyphenyl)but-2-enoic acid (59a)[288]

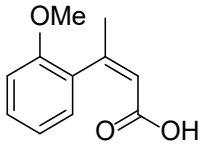

(*Z*)-3-(2-methoxyphenyl)but-2-enoic acid
Chemical Formula: $C_{11}H_{12}O_3$
Exact Mass: 192.08

The (*E*)-3-(2-methoxyphenyl)but-2-enoic acid (**59**) (2.11 g) and riboflavin tetraacetate (**63**) (0.3264 g) were dissolved in 90 mL MeCN and 90 mL MeOH. The flask was purged with O_2 before being stirred for the specified time under UV-light irradiation (~400 nm) and un oxygen atmosphere at 0.7 ml min^{-1} by flow reactor.[288] (Due to the limited isolated quantity of the title compound (< 20 mg), full characterization was precluded; only the NMR spectra and X-ray crystal structure are reported.)

^{1}H NMR (400 MHz, $CDCl_3$) δ/ppm 7.29 (m, 1H) 7.05 (m, 1H) 6.93 (m, 2H), 5.96 (q, *J* = 1.4 Hz 1H), 3.79 (s, 3H), 2.19 (d, *J* = 1.4 Hz, 3H).

^{13}C NMR (101 MHz, $CDCl_3$) δ/ppm 171.19, 155.43, 155.28, 129.70, 129.01, 127.98, 120.40, 118.44, 110.90, 55.46, 26.58.

^{13}C NMR - DEPT (101 MHz, $CDCl_3$) δ/ppm 129.01, 127.98, 120.40, 118.44, 110.90, 55.46, 26.58.

The structure and connectivity were confirmed by single crystal X-ray crystallography, performed by Dr Dmitry S. Yufit of the Durham University X-Ray Crystallography Service and has the unique identifier of '20srv225'.

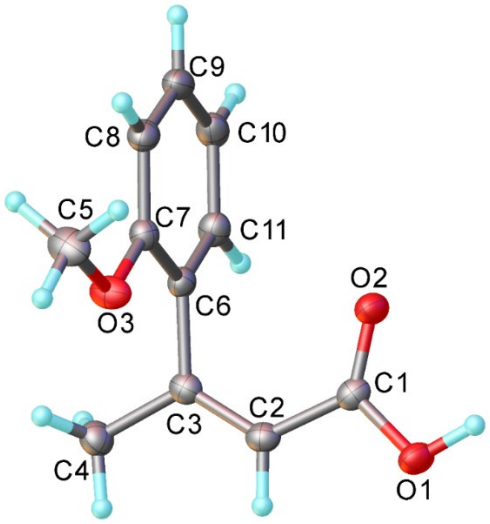

Space group	$P2_1/c$
a/Å	7.6921(3)
b/Å	6.5197(3)
c/Å	19.8946(7)
α/°	90
β/°	92.012(2)
γ/°	90

4-methyl-2*H*-chromen-2-ol (64)[288]

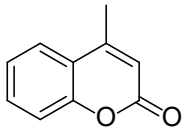

4-methyl-2*H*-chromen-2-one
Chemical Formula: $C_{10}H_8O_2$
Exact Mass: 160.0524

A proposed byproduct from the synthesis procedure for (*Z*)-3-(2-methoxyphenyl)but-2-enoic acid (**59a**).

^{1}H NMR (400 MHz, $CDCl_3$) δ/ppm 7.60 (m, 1H), 7.52 (m, 1H), 7.31 (m, 2H), 6.28 (d, *J* = 1.4 Hz 1H), 2.43 (d, *J* = 1.3 Hz 3H).

^{13}C NMR (101 MHz, $CDCl_3$) δ/ppm 160.81, 153.46, 152.47, 131.78, 124.61, 124.25, 119.94, 117.02, 115.05, 18.67.

^{13}C NMR-DEPT (101 MHz, $CDCl_3$) δ/ppm 131.78, 124.61, 124.25, 117.02, 115.05, 18.66.

LC-MS: R_t = 1.73 min, m/z 161.49 $[M+H]^+$.

NB: Due to the limited isolated quantity of the title compound (~ 15 mg), full characterization was precluded; only the NMR spectra and LC-MS is reported for isolated material and this data matches literature reference.[329]

4.5.2 Synthesis of Section 4.3.2

(2*E*,3*E*)-butane-2,3-dione dioxime (96)[330]

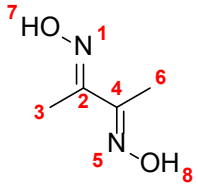

(2*E*,3*E*)-butane-2,3-dione dioxime
Chemical Formula: $C_4H_8N_2O_2$
Exact Mass: 116.0586

A solution of 2,3-biacetyl (8.6 g, 100 mmol), hydroxylamine hydrochloride (13.8 g, 200 mmol), and pyridine (19.0 g, 240 mmol) in methanol (100 mL) was heated at reflux for 1 hour. After cooling, ice water (500 mL) was added, and the resulting gray solid was filtered. Recrystallization from ethanol yielded (2*E*,3*E*)-butane-2,3-dione dioxime (96) as white crystal.

Isolated yield: 5.56 g (48%)

^{1}H NMR (400 MHz, DMSO-d_6) δ/ppm 11.38 (s, 2H, H7+H8), 1.93 (s, 6H, H1+H6).

^{13}C NMR (101 MHz, DMSO-d_6) δ/ppm 153.50 (C2+C4), 9.80 (C1+C6).

GC-MS R_t = 3.28 min, m/z 116.1 [M].

The structure and connectivity were confirmed by single crystal X-ray crystallography, performed by Dr Dmitry S. Yufit of the Durham University X-Ray Crystallography Service and has the unique identifier of ‘22srv214’.

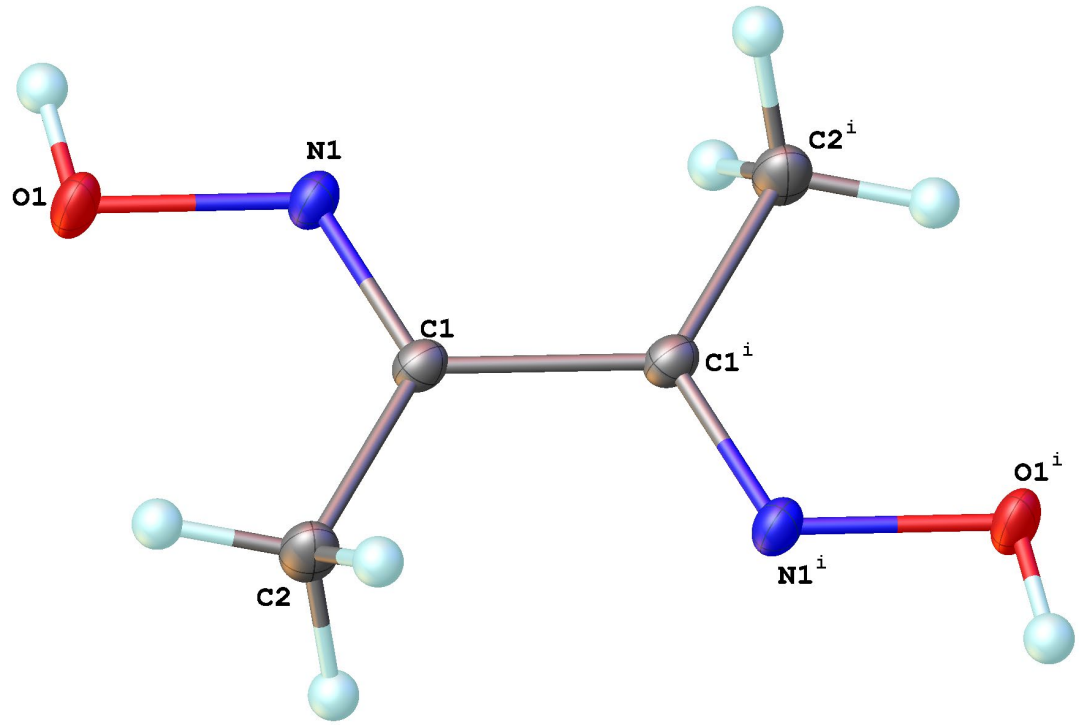

Space group	P -1
a/Å	4.4763(4)
b/Å	5.3582(4)
c/Å	5.8733(5)
α/°	101.018(3)
β/°	93.428(3)
γ/°	101.270(3)

Cobaloxime complex [Co(dmgH)(dmgH$_2$)Cl$_2$] (97)

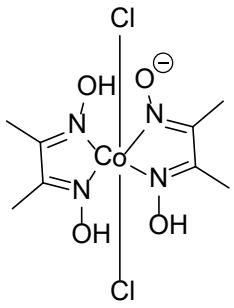

Chemical Formula: $C_8H_{15}Cl_2CoN_4O_4^-$
Exact Mass: 359.98

A solution of cobalt (II) chloride (520 mg, 4 mmol) and (2*E*,3*E*)-butane-2,3-dione dioxime (**96**) (928 mg, 8 mmol) in acetone (40 mL) was stirred at 40 °C for 12 hours. The resulting solid was filtered, washed with methanol to yield the target compound as a green powder which was used directly for next step.[330]

Cobaloxime complex Co(dmgH)$_2$ClPy] (69a)[331]

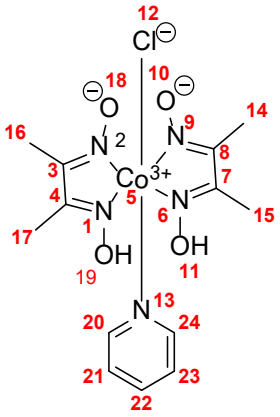

Chemical Formula: $C_{13}H_{19}ClCoN_5O_4$
Exact Mass: 403.05

A stirred suspension of [Co(dmgH)(dmgH$_2$)Cl$_2$] (**97**) (0.5 g, 1.4 mmol) and pyridine (0.13 mL, 1.4 mmol) in dichloromethane (10 mL) was treated with saturated NaHCO$_3$ solution (10 mL) and stirred at room temperature for 1 hour. The mixture was diluted with dichloromethane (10 mL) and washed with water (2 × 1 mL). The combined organic layers were dried over anhydrous Na$_2$SO$_4$,

filtered, and evaporated to yield [Co(dmgH)$_2$ClPy] as a brown crystalline solid.

Crude yield: 0.55 g (86.8%)

^{1}H NMR (400 MHz, $CDCl_3$) δ/ppm 8.30 – 8.22 (m, 2H, H20+H24), 7.73 (tt, *J* = 7.5, 1.5 Hz, 1H, H22), 7.28 – 7.23 (m, 2H, H21+H23), 2.41 (s, 12H, H12+H13+H14+H15).

^{13}C NMR (101 MHz, $CDCl_3$) δ/ppm 152.65 (C3+C4+C7+C8), 151.04 (C20+C24), 139.02 (C22), 125.72 (C21+C23), 13.14 (C12+C13+C14+C15).

NB: The NMR spectra above matched the literature data.[331]

3-Cyano-1-methylquinolinium perchlorate ($QuCN^+ClO_4^-$) (68)[332-334]

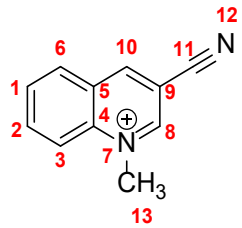

Chemical Formula: $C_{11}H_9N_2^+$
Exact Mass: 169.0760

To a stirred solution of 3-quinolinecarbonitrile (1 g, 6.5 mmol) in acetone (20 mL) was added iodomethane (2 mL, 32 mmol, 4 equiv.). The reaction mixture was heated to 65 °C and left to stir for 24 hours. On standing overnight at room temperature the crystalline ammonium iodide salt separated and was collected by filtration. The 3-cyano-1-methylquinolinium perchlorate was prepared by the addition of $NaClO_4$ (1.18 g, 9.6 mmol, 1.3 equiv.) to the iodide salt dissolved in H_2O (150 mL), with stirring at room temperature for 46 h. The precipitate was filtered off and purified by recrystallization from methanol (0.56 g).

^{1}H NMR (599 MHz, MeCN-d_3) δ/ppm 9.53 (d, J = 1.8 Hz, 1H), 9.49 (dd, J = 1.9, 0.9 Hz, 1H), 8.49 – 8.42 (m, 3H), 8.18 (ddd, J = 8.0, 5.6, 2.5 Hz, 1H), 4.62 (d, J = 0.7 Hz, 3H).
^{13}C NMR (151 MHz, MeCN-d_3) δ/ppm 152.27, 151.05, 139.24, 132.00, 131.53, 128.71, 119.29, 113.51, 106.85, 46.37.

LC-MS: R_t = 0.27 min, m/z 169.39 $[QuCN]^+$.

Melting point: 106.8 – 107.2 °C (No literature record).

4-methyl-7,8-dihydro-2*H*-chromene-2,5(6*H*)-dione (60)[335]

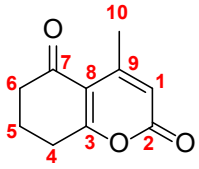

Chemical Formula: $C_{10}H_{10}O_3$
Exact Mass: 178.06

To a solution of cyclohexane-1,3-dione (**54**) (168.2 g, 1.5 mol) in absolute ethanol (500 mL) containing 1,8-diazabicyclo[5.4.0]undec-7-ene (DBU, 10.0 mL, 67 mmol) was added ethyl acetoacetate (292.8 g, 2.25 mol). The reaction mixture was heated at reflux for 24 hours, allowed to cool and the crystalline material which formed upon standing was isolated by filtration (69.0 g). The filtrate was left to further crystallise and a second crop was isolated (47.1 g). The title compound was afforded as a colourless crystalline solid.

Yield of crystalisation: 116.1 g (43%).

^{1}H NMR (599 MHz, $CDCl_3$) δ/ppm 5.95 (s, 1H, H1), 2.84 (t, *J* = 6.4 Hz, 2H, H4), 2.52 (t, *J* = 6.7 Hz, 2H, H6), 2.44 (d, *J* = 1.0 Hz, 3H, H10), 2.08 (q, *J* = 6.5 Hz, 2H, H5).

^{1}H NMR (400 MHz, $CDCl_3$) δ/ppm 5.98 (s, 1H, H1), 2.86 (t, *J* = 6.3 Hz, 2H, H4), 2.54 (t, *J* = 6.7 Hz, 2H, H6), 2.46 (d, *J* = 1.3 Hz, 3H, H10), 2.10 (q, *J* = 6.5 Hz, 2H, H5).

^{13}C NMR (151 MHz, $CDCl_3$) δ/ppm 195.42 (C7), 174.58 (C3), 159.46 (C2), 156.22 (C9), 114.73 (C8), 113.01 (C1), 38.49 (C6), 29.03 (C4), 22.66 (C10), 19.67 (C5).

IR (neat) ν_{max}/ cm^{-1} 3065 (w), 2970 (w, CH), 2890 (W, CH), 1717 (m/s, C=O), 1661 (s, C=O), 1610 (s), 1542 (s), 1396 (s), 1382 (s), 1298 (m), 1153 (m), 1031 (m), 931 (s), 827 (s), 754 (m), 560 (s), 510 (s), 467 (s).

LC-MS: R_t = 1.45 min, m/z 179.04 $[M+H]^+$; HR-MS calculated for $C_{10}H_{11}O_3$ 179.0708, found 179.0704 (Δ = -0.4 mDa; -2.2 ppm).

Melting point: 98.1 – 99.4 °C, literature 98 – 99.5 °C.[335]

The structure and connectivity were confirmed by single crystal X-ray crystallography, performed by Dr Toby Blundell of the Durham University X-Ray Crystallography Service and has the unique identifier of '24srv158'.

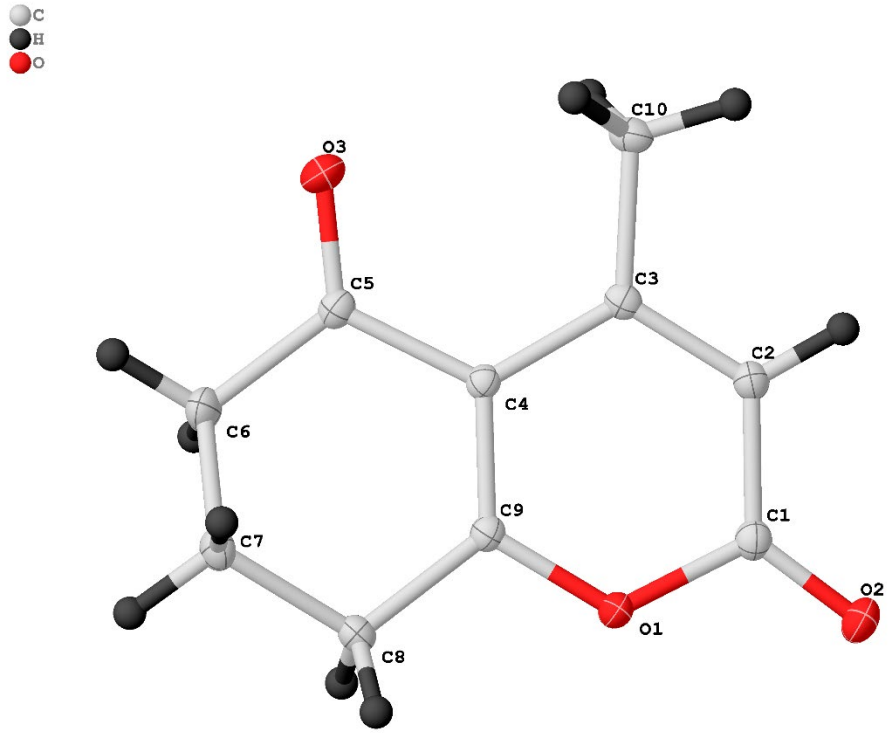

Space group	$P2_12_12_1$
a/Å	4.9882(2)
b/Å	7.4459(3)
c/Å	21.9013(8)
α/°	90
β/°	90
γ/°	90

6-chloro-4-methyl-7,8-dihydro-2*H*-chromene-2,5(6*H*)-dione (71)

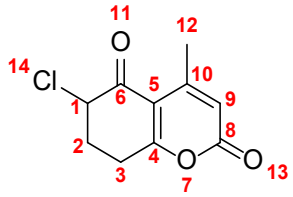

6-chloro-4-methyl-7,8-dihydro-2*H*-chromene-2,5(6*H*)-dione
Chemical Formula: $C_{10}H_9ClO_3$
Exact Mass: 212.0240

To a solution of 4-methyl-7,8-dihydro-2*H*-chromene-2,5(6*H*)-dione (**60**) (1.78 g, 10 mmol) in ethyl acetate (20 mL) was added 1,3-dichloro-5,5-dimethylhydantoin **72** (DCDMH) (1.18 g, 6 mmol) and *p*-toluenesulfonic acid monohydrate (0.19 g, 1 mmol). The reaction mixture was heated at reflux for 24 h, allowed to cool to room temperature and was washed with water (20 mL). The aqueous layer was extracted with ethyl acetate (3 ×15 mL). The combined organic layer was washed with saturated Na_2CO_3 (25 mL) and brine (30 mL), dried with anhydrous sodium sulfate, filtered, and concentrated to 2 mol dm^{-3}. The solution was directly used for 5-hydroxy-4-methylcoumarin (**61**) synthesis. A portion of the crude product was recrystallized from hexane:ethyl acetate (8:2) to afford the title compound as yellow crystals.

Mass of yielded product mixture without purification: 2.22 g.

Estimated yield by NMR: 95 %.

Yield by recrystallization: 80% (8.5 g, 50 mmol scale).

^{1}H NMR (400 MHz, DMSO) δ/ppm 6.20 (dq, J = 1.4, 0.7 Hz 1H, H9), 4.88 (dd, J = 8.9, 4.3 Hz,1H, H1), 3.01 (m, 2H, H3), 2.55 (m, 1H, H2), 2.39 (d, J = 13.8, 8.9, 6.8, 5.9 Hz, 3H, H12), 2.29 (m, 1H, H2).

^{13}C NMR (101 MHz, DMSO) δ/ppm 189.04 (C6), 174.85 (C4), 159.03 (C8), 156.26 (C10), 112.86 (C5+C9), 60.58 (C1), 28.85 (C2), 26.85 (C3), 22.28 (C12).

IR (neat) ν_{max}/ cm^{-1} 2919 (Aryl C-H), 1733(C=O), 1695(C=C), 1618(C=C).

LC-MS: R_t = 1.66 min, m/z 213.80 $[M+H]^+$; HR-MS calculated for $C_{10}H_{10}{}^{35}ClO_3$ 213.0318, found 213.0313 (Δ = -0.5 mDa; -2.3 ppm)

Melting point: 96.0 – 97.5 °C (No existing literature record).

The structure and connectivity were confirmed by single crystal X-ray crystallography, performed by Dr Toby Blundell of the Durham University X-Ray Crystallography Service and has the unique identifier of '23srv362'.

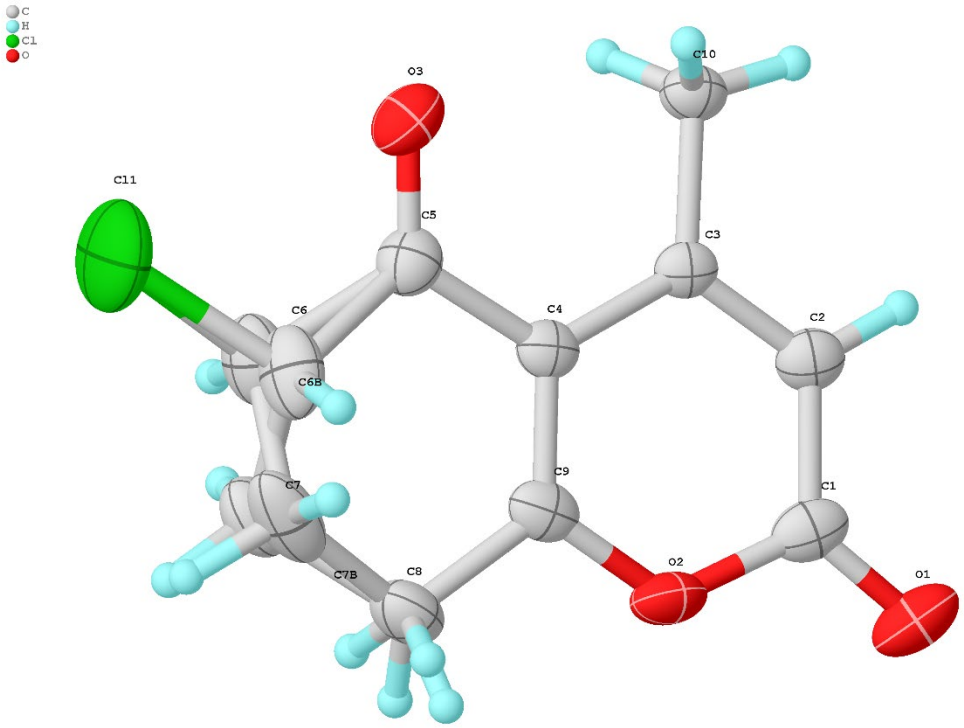

Space group	Pbca
a/Å	10.1493(4)
b/Å	9.8344(4)
c/Å	18.4999(6)
α/°	90
β/°	90
γ/°	90

5-hydroxy-4-methylcoumarin (61)[336]

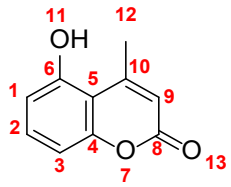

Chemical Formula: $C_{10}H_8O_3$
Exact Mass: 176.0473

To the solution of 6-chloro-4-methyl-7,8-dihydro-2*H*-chromene-2,5(6*H*)-dione **(71)** dissolved in ethyl acetate (2 M) was added 1,8-diazabicyclo[5.4.0]undec-7-ene (DBU, 45.7 g, 300 mmol). The reaction mixture was heated at reflux for 6 h, allowed to cool to room temperature and was washed with water (1 L), and 2% HCl (1 L). The aqueous layer was extracted with diethyl ether (2 × 2 L). The organic layers were combined, dried with Na_2SO_4, filtered, and evaporated in vacuo to afford the cream solid which was used directly for the synthesis of 2-hydroxy-6-methoxyacetophenone (**21**).

Mass of yielded product mixture without purification over two steps (**60** – **71** – **61**): 1.65 g.
Estimated yield by NMR: 85 - 90%.
^{1}H NMR (400 MHz, DMSO) δ/ppm 10.68 (s, 1H, H11), 7.36 (t, *J* = 8.2 Hz, 1H, H2), 6.78 (dd, *J* = 8.2, 1.5 Hz, 2H, H1+H3), 6.09 (m, 1H, H9), 2.57 (s, 3H, H12).
^{13}C NMR (101 MHz, DMSO) δ/ppm 160.14 (C8), 157.29 (C6 or C4), 155.31 (C6 or C4), 155.10 (C10), 132.56 (C2), 113.41 (C9), 111.69 (C1), 109.18 (C5), 107.68 (C3), 24.13 (C12).
(NMR sample was dissolved in $CDCl_3$ – DMSO co-solvent system in literature.[336])
IR (neat) ν = 3419 (br, OH) 1680 (s, CO) 1615 (s) 1468 (m, aromatic C-C).
LC-MS: R_t = 1.62 min, m/z 176.99 $[M+H]^+$; HR-MS calculated for $C_{10}H_9O_3$ 177.0552, found 177.0546 (Δ = -0.6 mDa; -3.4 ppm)
Melting point: 255.0 – 255.7 °C, literature 261-263 °C.[337]

5-methoxy-4-methylcoumarin (56)[315]

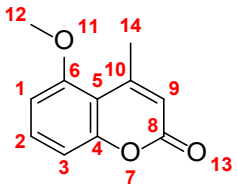

Chemical Formula: $C_{11}H_{10}O_3$
Exact Mass: 190.06

The crude compound prepared above, 5-hydroxy-4-methylcoumarin (**61**) (assume 1.9 g, 10 mmol) in acetonitrile (20 mL) was mixed with potassium carbonate (1.66 g, 12 mmol), dimethyl sulfate (1.58 g, 1.25 mmol) and heated at reflux for 16 h. The solvent was evaporated *in vacuo*. To the crude material was added water (20 mL) and extracted with ethyl acetate (3 × 25 mL). The combined organic layers were dried with Na_2SO_4, filtered, and concentrated in vacuo. White crystalline solid was obtained by recrystalisation from hexane and ethyl acetate (2:8). The title compound can also be purified by column chromatography (Hexane:EtOAc = 34:2 to 33:2).

Isolated yield over three steps (**60** – **71** – **61** - **56**): 23% (0.44 g).
Mass of yielded product mixture without purification over three steps (**60** – **71** – **61** - **56**): 1.78 g.
Estimated yield by NMR: 82 – 92%.
^{1}H NMR (400 MHz, DMSO) δ/ppm 7.54 (1H, t, *J* = 8.3 Hz, H2), 6.97 – 6.95 (1H, m, H3), 6.95 – 6.93 (1H, m, H1), 6.21 (1H, q, *J* = 1.3 Hz, H9), 3.89 (3H, s, H12), 2.54 (3H, d, *J* = 1.3 Hz, H14).
^{13}C NMR (101 MHz, DMSO) δ/ppm 159.85 (C8), 158.47 (C6), 155.10 (C4), 154.40 (C5), 132.83 (C2), 114.40 (C9), 110.20 (C10), 109.67 (C3), 107.54 (C1), 56.71 (C12), 24.31 (C14).
IR (neat) ν_{max}/ cm^{-1} 2935(m, aryl C-H), 1716(s, C=O), 1596 and 1564 and 1475 (s, benzene ring).
LC-MS: R_t = 2.00 min, m/z 191.09 $[M+H]^+$; HR-MS calculated for $C_{11}H_{11}O_3$ 191.0708, found 191.0709 (Δ = 0.5 ppm).
Melting point: 136.4 – 138.5 °C, literature 140 - 142 °C.[337]
The structure and connectivity were confirmed by single crystal X-ray crystallography, performed by Dr Toby Blundell of the Durham University X-Ray Crystallography Service and has the unique identifier of '23srv161'.

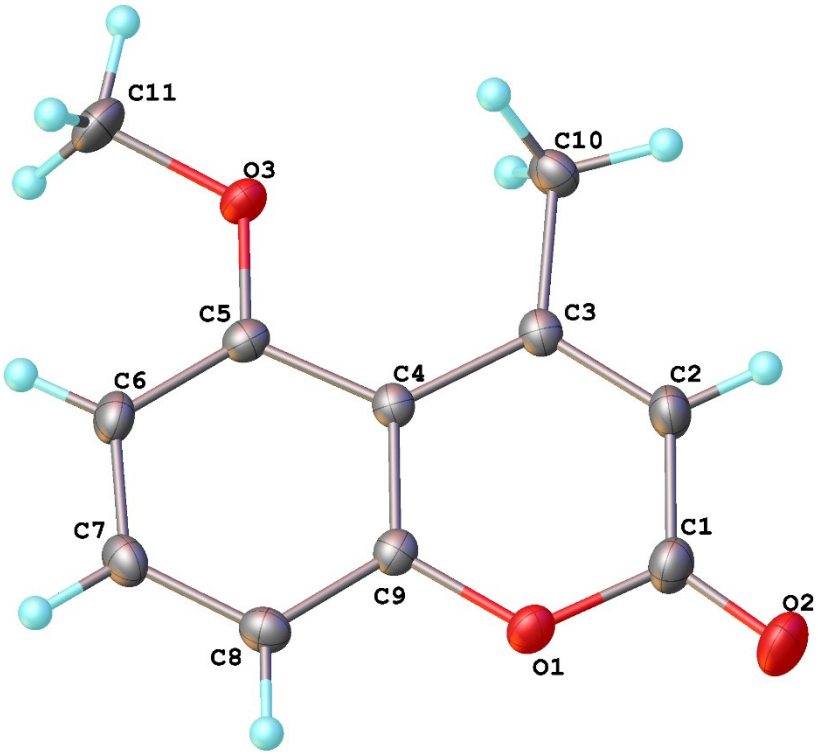

Space group	C2/c
a/Å	12.7199(4)
b/Å	9.5526(3)
c/Å	14.6729(5)
α/°	90
β/°	95.4391(14)
γ/°	90

1-(2-hydroxy-6-methoxyphenyl)ethan-1-one (21)[338]

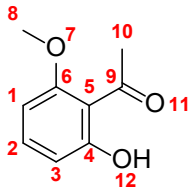

1-(2-hydroxy-6-methoxyphenyl)ethan-1-one
Chemical Formula: $C_9H_{10}O_3$
Exact Mass: 166.06

The solution of 5-methoxy-4-methylcoumarin **61** (0.57 g, 3 mmol) in acetone (19 mL) and water (1 mL) mixture was cooled to 0 °C. The stream of O_3/O_2 was generated (Electrolysis = 7) by triogen® LAB2B,[339] and supplied for 40 minutes. The reaction was sparged for 2 minutes with oxygen at the end. The solution was diluted with water (50 mL) and extracted with EtOAc (2 × 100 mL), dried over anhydrous Na_2SO_4, filtered and concentrated in vacuo to yield a yellow solid. A portion of the crude product was recrystallized from hexane:ethyl acetate (8:2) to afford the pale-yellow crystal.

Mass of yielded product mixture without purification: 0.42 g.

Estimated yield by NMR: 14%.

^{1}H NMR (599 MHz, DMSO) δ/ppm 11.79 (s, 1H, H12), 7.30 (t, *J* = 8.4 Hz, 1H, H2), 6.53 (dd, *J* = 8.4, 0.9 Hz, 1H, H1), 6.47 (dd, *J* = 8.4, 0.9 Hz, 1H, H3), 3.79 (s, 3H, H10), 2.49 (s, 3H, H8).

^{1}H NMR (400 MHz, DMSO) δ/ppm 11.85 (s, 1H), 7.33 (t, *J* = 8.3 Hz, 1H, H2), 6.51 (dd, *J* = 8.3, 0.9 Hz, 1H, H3), 3.83 (s, 3H, H10), 2.51 – 2.43 (s, 3H, H8).

^{13}C NMR (151 MHz, DMSO) δ/ppm 204.17 (C6), 160.43 (C5), 159.95 (C9), 134.67 (C2), 114.37 (C4), 109.84 (C3), 102.63 (C1), 56.34 (C10), 33.40 (C8).

^{13}C NMR (101 MHz, DMSO) δ/ppm 204.21 (C6), 160.53 (C5), 160.01 (C9), 134.74 (C2), 114.35 (C4), 109.88 (C3), 102.66 (C1), 56.37 (C10), 33.44 (C8).

IR (neat) ν = 2942 (br, OH) 1588 (s, C=O) 1454 (s) 1348 (s) 1290 (s) 1238 (s).

LC-MS: R_t = 2.33 min, m/z 167.11 $[M+H]^+$; HR-MS calculated for $C_9H_{11}O_3$ 167.0708, found 167.0712 (Δ = 0.4 mDa; 2.4 ppm).

Melting point: 55.9 – 57.5 °C, literature 53 - 57 °C.[280]

The structure and connectivity were confirmed by single crystal X-ray crystallography, performed by Dr Toby Blundell of the Durham University X-Ray Crystallography Service and has the unique identifier of '23srv402'.

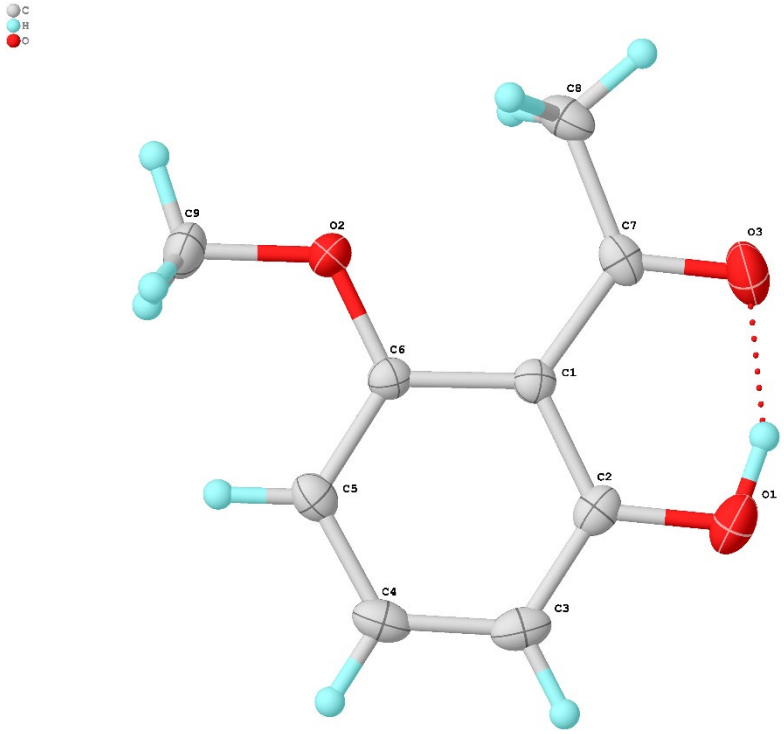

Space group	$P2_1/n$
a/Å	7.3563(7)
b/Å	8.8078(8)
c/Å	12.3331(11)
α/°	90
β/°	92.499(4)
γ/°	90

1-(2,4-dihydroxyphenyl)ethan-1-one (95)[340]

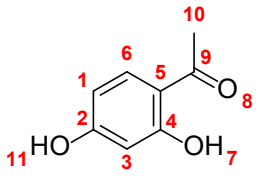

1-(2,4-dihydroxyphenyl)ethan-1-one
Chemical Formula: $C_8H_8O_3$
Exact Mass: 152.0473

The solution of 7-hydroxy-4-methylcoumarin (**56**) (0.53 g, 3 mmol) in a mixture of acetone (19 mL) and water (1 mL) was cooled to 0 °C. A stream of O_3/O_2 (Electrolysis = 8) was supplied for 23 minutes and the reaction was sparged for 2 minutes with oxygen. The solution was diluted with of water (50 mL) and extracted with EtOAc (2 × 100 mL), dried over sodium sulfate, filtered and concentrated in vacuo to yield the yellow solid. (The spectra below match literature.[341])

Estimated yield by NMR: 35%

^{1}H NMR (700 MHz, DMSO) δ/ppm 12.61 (s, 1H, OH), 10.65 (s, 1H, OH), 7.76 (d, *J* = 8.8 Hz, 1H, H6), 6.38 (dd, *J* = 8.8, 2.3 Hz, 1H, H3), 6.25 (d, *J* = 2.3 Hz, 1H, H1), 2.52 (s, 3H, H10).

^{1}H NMR (400 MHz, DMSO) δ/ppm 12.61 (s, 1H), 10.64 (s, 1H), 7.76 (d, *J* = 8.8 Hz, 1H), 6.38 (dd, *J* = 8.8, 2.4 Hz, 1H), 6.25 (d, *J* = 2.4 Hz, 1H), 2.52 (s, 3H).

^{13}C NMR (176 MHz, DMSO) δ/ppm 203.19 (C9), 165.35 (C4), 164.66 (C2), 134.19 (C6), 113.34 (C5), 108.59 (C3), 102.65 (C1), 26.83 (C10).

^{13}C NMR (101 MHz, DMSO) δ/ppm 203.19, 165.35, 164.67, 134.19, 113.34, 108.60, 102.76, 26.83.

References

1. K. C. Nicolaou, *Angewandte Chemie International Edition*, 2013, **52**, 131-146.
2. D. Kolb, *Experiential Learning: Experience As The Source Of Learning And Development*, 1984.
3. J. Fulford, F. Milton, D. Salas, A. Smith, A. Simler, C. Winlove and A. Zeman, *Cortex*, 2018, **105**, 26-40.
4. J. Pearson, *Nature Reviews Neuroscience*, 2019, **20**, 624-634.
5. F. Jin, S.-M. Hsu and Y. Li, *Vision*, 2024, **8**, 56.
6. A. Zeman, M. Dewar and S. Della Sala, *Cortex*, 2015, **73**, 378-380.
7. R. Keogh and J. Pearson, *Journal of Vision*, 2014, **14**, 7-7.
8. C. Aydin, *Memory*, 2018, **26**, 189-200.
9. Daniel L. Schacter, Donna R. Addis, D. Hassabis, Victoria C. Martin, R. N. Spreng and Karl K. Szpunar, *Neuron*, 2012, **76**, 677-694.
10. P. W. Atkins and J. De Paula, *Atkins' Physical chemistry*, Oxford University Press, Oxford, 10th ed. edn., 2014.
11. J. B. Foresman and A. Frisch, *Exploring chemistry with electronic structure methods*, Gaussian, Inc., Wallingford, CT, Third edition. edn., 2015.
12. B. Minto, *The Pyramid Principle: Logic in Writing and Thinking*, Pearson Education Limited, 2021.
13. Z. Wang, G. W. Walker, D. C. G. Muir and K. Nagatani-Yoshida, *Environmental Science & Technology*, 2020, **54**, 2575-2584.
14. A. J. M. Schoot Uiterkamp, *Journal of Integrative Environmental Sciences*, 2025, **22**, 2507611.
15. D. C. G. Muir, G. J. Getzinger, M. McBride and P. L. Ferguson, *Environmental Science & Technology*, 2023, **57**, 9119-9129.
16. R. Roundtable on Environmental Health Sciences, Medicine, H. Board on Population, P. Public Health and M. Institute of, in *Identifying and Reducing Environmental Health Risks of Chemicals in Our Society: Workshop Summary*, National Academies Press (US), Washington (DC), 2014.

17. M. Lancaster, in *Green Chemistry: An Introductory Text*, The Royal Society of Chemistry, 2016.
18. P. Anastas and N. Eghbali, *Chemical Society Reviews*, 2010, **39**, 301-312.
19. *Environmental Science & Technology*, 2003, **37**, 94A-101A.
20. C. A. Russell, *Ambix*, 1987, **34**, 169-180.
21. R. B. Silverman and M. W. Holladay, in *The Organic Chemistry of Drug Design and Drug Action (Third Edition)*, eds. R. B. Silverman and M. W. Holladay, Academic Press, Boston, 2014, DOI: https://doi.org/10.1016/B978-0-12-382030-3.00002-7, pp. 19-122.
22. E. M. Isin, C. S. Elmore, G. N. Nilsson, R. A. Thompson and L. Weidolf, *Chemical Research in Toxicology*, 2012, **25**, 532-542.
23. M. Raïssi, Y. Pellegrin, F.-X. Lefevre, M. Boujtita, D. Rousseau, T. Berthelot and F. Odobel, *Solar Energy*, 2020, **199**, 92-99.
24. Y. Koide, Y. Urano, S. Kenmoku, H. Kojima and T. Nagano, *Journal of the American Chemical Society*, 2007, **129**, 10324-10325.
25. S. A. Benner and A. M. Sismour, *Nat Rev Genet*, 2005, **6**, 533-543.
26. K. L. Garner, *Essays Biochem*, 2021, **65**, 791-811.
27. D.-K. Ro, E. M. Paradise, M. Ouellet, K. J. Fisher, K. L. Newman, J. M. Ndungu, K. A. Ho, R. A. Eachus, T. S. Ham, J. Kirby, M. C. Y. Chang, S. T. Withers, Y. Shiba, R. Sarpong and J. D. Keasling, *Nature*, 2006, **440**, 940-943.
28. J. H. Brooke, *The British Journal for the History of Science*, 1971, **5**, 363-392.
29. P. Ball, *Nature*, 2010, **468**, 1036-1036.
30. L. B. Slater, *Studies in History and Philosophy of Science Part A*, 2002, **33**, 1-33.
31. P. J. T. Morris and A. S. Travis, Routledge, 1 edn., 1997, DOI: 10.4324/9781315079097-42, pp. 715-739.
32. P. A. Wender, V. A. Verma, T. J. Paxton and T. H. Pillow, *Accounts of Chemical Research*, 2008, **41**, 40-49.
33. D. J. Newman and G. M. Cragg, *Journal of Natural Products*, 2020, **83**, 770-803.
34. M. Chhabra, in *Translational Biotechnology*, ed. Y. Hasija, Academic Press, 2021, DOI: https://doi.org/10.1016/B978-0-12-821972-0.00015-0, pp. 137-164.
35. D. J. Newman and G. M. Cragg, *Journal of Natural Products*, 2012, **75**, 311-335.

36. M. J. Yu, W. Zheng, B. M. Seletsky, B. A. Littlefield and Y. Kishi, in *Annual Reports in Medicinal Chemistry*, ed. J. E. Macor, Academic Press, 2011, vol. 46, pp. 227-241.
37. D. Uemura, K. Takahashi, T. Yamamoto, C. Katayama, J. Tanaka, Y. Okumura and Y. Hirata, *Journal of the American Chemical Society*, 1985, **107**, 4796-4798.
38. Y. Hirata and D. Uemura, *Pure and Applied Chemistry*, 1986, **58**, 701-710.
39. R. L. Bai, K. D. Paull, C. L. Herald, L. Malspeis, G. R. Pettit and E. Hamel, *Journal of Biological Chemistry*, 1991, **266**, 15882-15889.
40. T. D. Aicher, K. R. Buszek, F. G. Fang, C. J. Forsyth, S. H. Jung, Y. Kishi, M. C. Matelich, P. M. Scola, D. M. Spero and S. K. Yoon, *Journal of the American Chemical Society*, 1992, **114**, 3162-3164.
41. M. A. Jordan and L. Wilson, *Nature Reviews Cancer*, 2004, **4**, 253-265.
42. A. G. Atanasov, S. B. Zotchev, V. M. Dirsch, I. E. Orhan, M. Banach, J. M. Rollinger, D. Barreca, W. Weckwerth, R. Bauer, E. A. Bayer, M. Majeed, A. Bishayee, V. Bochkov, G. K. Bonn, N. Braidy, F. Bucar, A. Cifuentes, G. D'Onofrio, M. Bodkin, M. Diederich, A. T. Dinkova-Kostova, T. Efferth, K. El Bairi, N. Arkells, T.-P. Fan, B. L. Fiebich, M. Freissmuth, M. I. Georgiev, S. Gibbons, K. M. Godfrey, C. W. Gruber, J. Heer, L. A. Huber, E. Ibanez, A. Kijjoa, A. K. Kiss, A. Lu, F. A. Macias, M. J. S. Miller, A. Mocan, R. Müller, F. Nicoletti, G. Perry, V. Pittalà, L. Rastrelli, M. Ristow, G. L. Russo, A. S. Silva, D. Schuster, H. Sheridan, K. Skalicka-Woźniak, L. Skaltsounis, E. Sobarzo-Sánchez, D. S. Bredt, H. Stuppner, A. Sureda, N. T. Tzvetkov, R. A. Vacca, B. B. Aggarwal, M. Battino, F. Giampieri, M. Wink, J.-L. Wolfender, J. Xiao, A. W. K. Yeung, G. Lizard, M. A. Popp, M. Heinrich, I. Berindan-Neagoe, M. Stadler, M. Daglia, R. Verpoorte, C. T. Supuran and T. the International Natural Product Sciences, *Nature Reviews Drug Discovery*, 2021, **20**, 200-216.
43. Chemistry World, https://www.chemistryworld.com/industry/new-frontiers-in-synthesis-for-a-more-sustainable-future/4016243.article, (accessed September, 2024).
44. G. M. Cragg, D. J. Newman and K. M. Snader, *Journal of Natural Products*, 1997, **60**, 52-60.
45. D. J. Newman, G. M. Cragg and K. M. Snader, *Journal of Natural Products*, 2003, **66**, 1022-1037.
46. D. J. Newman and G. M. Cragg, *Journal of Natural Products*, 2007, **70**, 461-477.

47. D. J. Newman and G. M. Cragg, *Journal of Natural Products*, 2016, **79**, 629-661.
48. Halaven, https://www.halaven.com/-/media/Files/Halaven/HALAVEN-Full-Prescribing-Information.pdf, (accessed October, 2024).
49. M. A. Sierra and M. C. de la Torre, *Angewandte Chemie International Edition*, 2000, **39**, 1538-1559.
50. S. Kar, H. Sanderson, K. Roy, E. Benfenati and J. Leszczynski, *Chemical Reviews*, 2022, **122**, 3637-3710.
51. B. Török, in *Green Chemistry*, eds. B. Török and T. Dransfield, Elsevier, 2018, DOI: https://doi.org/10.1016/B978-0-12-809270-5.00003-0, pp. 49-89.
52. S. G. Warren and P. Wyatt, *Organic synthesis : the disconnection approach*, Wiley, Chichester, 2nd ed. edn., 2008.
53. J. Clayden, N. Greeves and S. G. Warren, *Organic chemistry*, Oxford University Press, Oxford, 2nd ed. / Jonathan Clayden, Nick Greeves, Stuart Warren. edn., 2012.
54. S. L. Schreiber, *Science*, 2000, **287**, 1964-1969.
55. M. D. Burke and S. L. Schreiber, *Angewandte Chemie International Edition*, 2004, **43**, 46-58.
56. W. R. Galloway and D. R. Spring, *Expert Opin Drug Discov*, 2009, **4**, 467-472.
57. W. R. J. D. Galloway, A. Isidro-Llobet and D. R. Spring, *Nature Communications*, 2010, **1**, 80.
58. I. N. Levine, *Quantum chemistry*, Prentice Hall, Englewood Cliffs, N.J, 5th ed. edn., 2000.
59. A. Streitwieser, *Molecular orbital theory for organic chemists*, Wiley, New York ;, 1961.
60. I. Fleming, *Frontier orbitals and organic chemical reactions*, Wiley, Chichester ;, 1978.
61. S. Haase, P. Tolvanen and V. Russo, *Processes*, 2022, **10**, 99.
62. D. Reay, C. Ramshaw and A. Harvey, in *Process Intensification (Second Edition)*, eds. D. Reay, C. Ramshaw and A. Harvey, Butterworth-Heinemann, Oxford, 2013, DOI: https://doi.org/10.1016/B978-0-08-098304-2.00001-8, pp. 1-25.
63. T. Van Gerven and A. Stankiewicz, *Industrial & Engineering Chemistry Research*, 2009, **48**, 2465-2474.
64. A. Stankiewicz and J. A. Moulijn, *Chemical Engineering Progress*, 2000, **96**, 22-33.

65. R. Porta, M. Benaglia and A. Puglisi, *Organic Process Research & Development*, 2016, **20**, 2-25.
66. I. R. Baxendale, L. Brocken and C. J. Mallia, *Green Processing and Synthesis*, 2013, **2**, 211-230.
67. P. A. Messina, K. C. Mange and W. J. Middleton, *Journal of Fluorine Chemistry*, 1989, **42**, 137-143.
68. C. O. Kappe, *Angewandte Chemie International Edition*, 2004, **43**, 6250-6284.
69. M. Ohring, in *Engineering Materials Science*, ed. M. Ohring, Academic Press, San Diego, 1995, DOI: https://doi.org/10.1016/B978-012524995-9/50035-0, pp. 559-610.
70. LibreTexts PHYSICS, https://phys.libretexts.org/Bookshelves/University_Physics/University_Physics_(OpenStax)/University_Physics_II_-_Thermodynamics_Electricity_and_Magnetism_(OpenStax)/08%3A_Capacitance/8.06%3A_Molecular_Model_of_a_Dielectric, (accessed November, 2024).
71. C. Gabriel, S. Gabriel, E. H. Grant, E. H. Grant, B. S. J. Halstead and D. Michael P. Mingos, *Chemical Society Reviews*, 1998, **27**, 213-224.
72. B. Ondruschka, W. Bonrath and D. Stuerga, in *Microwaves in Organic Synthesis*, 2012, DOI: https://doi.org/10.1002/9783527651313.ch2, pp. 57-103.
73. D. M. P. Mingos and D. R. Baghurst, *Chemical Society Reviews*, 1991, **20**, 1-47.
74. A. de la Hoz, A. Díaz-Ortiz and P. Prieto, in *Alternative Energy Sources for Green Chemistry*, eds. G. Stefanidis and A. Stankiewicz, The Royal Society of Chemistry, 2016, DOI: 10.1039/9781782623632-00001, p. 0.
75. A. M. Rodríguez, P. Prieto, A. de la Hoz, Á. Díaz-Ortiz, D. R. Martín and J. I. García, *ChemistryOpen*, 2015, **4**, 308-317.
76. A. d. l. Hoz and A. Loupy, *Microwaves in organic synthesis*, Wiley-VCH, Weinheim, 3rd, completely rev. and enl. ed. edn., 2012.
77. C. E. Wayne and R. P. Wayne, *Photochemistry*, Oxford University Press, Oxford, 1996.
78. *Principles and applications of photochemistry*, Wiley, Hoboken, N.J, 1st ed. edn., 2009.
79. N. Hoffmann, *Chemical Reviews*, 2008, **108**, 1052-1103.
80. J. Mattay and A. Griesbeck, *Photochemical Key Steps in Organic Synthesis: An Experimental Course Book*, Wiley, 2008.

81. P. Chuarienthong, N. Lourith and P. Leelapornpisid, *International Journal of Cosmetic Science*, 2010, **32**, 99-106.
82. M. Danihelová, J. Viskupičová and E. Šturdík, *Acta Chimica Slovaca*, 2012, **5**, 59-69.
83. *US Pat.,* 6423747, 2002.
84. K. B. Pandey and S. I. Rizvi, *Oxid Med Cell Longev*, 2009, **2**, 270-278.
85. M. P. Wilson and M. R. Schwarzman, *Environ Health Perspect*, 2009, **117**, 1202-1209.
86. A. P. Dicks, *Green Organic Chemistry in Lecture and Laboratory*, Taylor & Francis, 2011.
87. G. P. Taber, D. M. Pfisterer and J. C. Colberg, *Organic Process Research & Development*, 2004, **8**, 385-388.
88. Z. Amara, J. F. B. Bellamy, R. Horvath, S. J. Miller, A. Beeby, A. Burgard, K. Rossen, M. Poliakoff and M. W. George, *Nature Chemistry*, 2015, **7**, 489-495.
89. B. A. Anderson, M. M. Hansen, A. R. Harkness, C. L. Henry, J. T. Vicenzi and M. J. Zmijewski, *Journal of the American Chemical Society*, 1995, **117**, 12358-12359.
90. S. Arndt, B. Grill, H. Schwab, G. Steinkellner, U. Pogorevčnik, D. Weis, A. M. Nauth, K. Gruber, T. Opatz, K. Donsbach, S. R. Waldvogel and M. Winkler, *Green Chemistry*, 2021, **23**, 388-395.
91. D. M. Barnes, J. Ji, J. Zhang, S. A. King, S. J. Wittenberger and H. E. Morton, in *From Bench to Pilot Plant*, American Chemical Society, 2002, vol. 817, ch. 4, pp. 45-59.
92. K. M. J. Brands, J. F. Payack, J. D. Rosen, T. D. Nelson, A. Candelario, M. A. Huffman, M. M. Zhao, J. Li, B. Craig, Z. J. Song, D. M. Tschaen, K. Hansen, P. N. Devine, P. J. Pye, K. Rossen, P. G. Dormer, R. A. Reamer, C. J. Welch, D. J. Mathre, N. N. Tsou, J. M. McNamara and P. J. Reider, *Journal of the American Chemical Society*, 2003, **125**, 2129-2135.
93. A. Bruggink, E. C. Roos and E. de Vroom, *Organic Process Research & Development*, 1998, **2**, 128-133.
94. C. J. Cowden, R. D. Wilson*, B. C. Bishop, I. F. Cottrell, A. J. Davies and U.-H. Dolling, *Tetrahedron Letters*, 2000, **41**, 8661-8664.
95. D. J. Dale, P. J. Dunn, C. Golightly, M. L. Hughes, P. C. Levett, A. K. Pearce, P. M. Searle, G. Ward and A. S. Wood, *Organic Process Research & Development*, 2000, **4**, 17-22.

96. P. J. Dunn, S. Galvin and K. Hettenbach, *Green Chemistry*, 2004, **6**, 43-48.
97. S. Ghosh, A. S. Kumar and G. N. Mehta, *Beilstein J Org Chem*, 2010, **6**, 27.
98. V. Glaser, *GENETIC ENGINEERING & BIOTECHNOLOGY NEWS*, 2008, **28**, 30-+.
99. S. Koenig, *Scalable Green Chemistry: Case Studies from the Pharmaceutical Industry*, Jenny Stanford Publishing, 2013.
100. A. Kompella, B. R. K. Adibhatla, P. R. Muddasani, S. Rachakonda, V. K. Gampa and P. K. Dubey, *Organic Process Research & Development*, 2012, **16**, 1794-1804.
101. S. K. Ma, J. Gruber, C. Davis, L. Newman, D. Gray, A. Wang, J. Grate, G. W. Huisman and R. A. Sheldon, *Green Chemistry*, 2010, **12**, 81-86.
102. C. A. Martinez, S. Hu, Y. Dumond, J. Tao, P. Kelleher and L. Tully, *Organic Process Research & Development*, 2008, **12**, 392-398.
103. V. Pandarus, D. Desplantier-Giscard, G. Gingras, F. Béland, R. Ciriminna and M. Pagliaro, *Organic Process Research & Development*, 2013, **17**, 1492-1497.
104. C. K. Savile, J. M. Janey, E. C. Mundorff, J. C. Moore, S. Tam, W. R. Jarvis, J. C. Colbeck, A. Krebber, F. J. Fleitz, J. Brands, P. N. Devine, G. W. Huisman and G. J. Hughes, *Science*, 2010, **329**, 305-309.
105. A. K. Singh, R. E. Weaver, G. L. Powers, V. W. Rosso, C. Wei, D. A. Lust, A. S. Kotnis, F. T. Comezoglu, M. Liu, K. S. Bembenek, B. D. Phan, D. J. Vanyo, M. L. Davies, R. Mathew, V. A. Palaniswamy, W.-S. Li, K. Gadamsetti, C. J. Spagnuolo and W. J. Winter, *Organic Process Research & Development*, 2003, **7**, 25-27.
106. L. Wang, J. Shen, Y. Tang, Y. Chen, W. Wang, Z. Cai and Z. Du, *Organic Process Research & Development*, 2007, **11**, 487-489.
107. X. Xie and Y. Tang, *Appl Environ Microbiol*, 2007, **73**, 2054-2060.
108. The Presidential Green Chemistry Challenge Awards Program Summary of 2005 Award Entries and Recipients, https://www.epa.gov/sites/default/files/documents/award_entries_and_recipients2005.pdf , (accessed April, 2023).
109. Environmental Protection Agency, https://www.epa.gov/greenchemistry/presidential-green-chemistry-challenge-1997-greener-synthetic-pathways-award, (accessed April, 2023).
110. A. Demirbaş, *Energy Conversion and Management*, 2001, **42**, 1357-1378.

111. A. Corma, S. Iborra and A. Velty, *Chemical Reviews*, 2007, **107**, 2411-2502.
112. A. Arevalo-Gallegos, Z. Ahmad, M. Asgher, R. Parra-Saldivar and H. M. N. Iqbal, *International Journal of Biological Macromolecules*, 2017, **99**, 308-318.
113. BioRender, https://www.biorender.com/template/biorefinery-46106, (accessed August, 2025).
114. C.-H. Zhou, X. Xia, C.-X. Lin, D.-S. Tong and J. Beltramini, *Chemical Society Reviews*, 2011, **40**, 5588-5617.
115. M. E. Himmel, S.-Y. Ding, D. K. Johnson, W. S. Adney, M. R. Nimlos, J. W. Brady and T. D. Foust, *Science*, 2007, **315**, 804-807.
116. R. M. Gruska, A. Baryga, A. Kunicka-Styczyńska, S. Brzeziński, J. Rosicka-Kaczmarek, K. Miśkiewicz and T. Sumińska, *Molecules*, 2022, **27**, 5125.
117. A. Bayu, A. Abudula and G. Guan, *Fuel Processing Technology*, 2019, **196**, 106162.
118. A. F. Pires, N. G. Marnotes, O. D. Rubio, A. C. Garcia and C. D. Pereira, *Foods*, 2021, **10**, 1067.
119. Annual cheese production worldwide from 2015 to 2023, https://www.statista.com/statistics/1120911/cheese-production-worldwide/, (accessed June, 2023).
120. J. M. Rocha and A. Guerra, *European Food Research and Technology*, 2020, **246**, 2161-2174.
121. S. Cheng and S. I. Martínez-Monteagudo, *Asia-Pacific Journal of Chemical Engineering*, 2019, **14**, e2275.
122. A. Dutta, D. Dhara, P. K. Parida, A. Si, R. Yesuvadian, K. Jana and A. K. Misra, *RSC Advances*, 2017, **7**, 28853-28864.
123. M. Harju, H. Kallioinen and O. Tossavainen, *International Dairy Journal*, 2012, **22**, 104-109.
124. A. J. Mosquera-Martínez, J. U. Sepúlveda-Valencia, H. J. Ciro-Velásquez, S. Vargas-Díaz and L. Pérez-Escobar, *Applied Food Research*, 2023, **3**, 100272.
125. J.-J. Liu, G.-C. Zhang, E. J. Oh, P. Pathanibul, T. L. Turner and Y.-S. Jin, *Journal of Biotechnology*, 2016, **234**, 99-104.
126. T. Rheinberger, J. Wolfs, A. Paneth, H. Gojzewski, P. Paneth and F. R. Wurm, *Journal of the American Chemical Society*, 2021, **143**, 16673-16681.

127. Y. Chisti and K. Karimi, in *Encyclopedia of Sustainable Technologies (Second Edition)*, ed. M. A. Abraham, Elsevier, Oxford, 2024, DOI: https://doi.org/10.1016/B978-0-323-90386-8.00017-6, pp. 279-294.
128. B. Splechtna, I. Petzelbauer, U. Baminger, D. Haltrich, K. D. Kulbe and B. Nidetzky, *Enzyme and Microbial Technology*, 2001, **29**, 434-440.
129. I. Gavrila, P. Raffa and F. Picchioni, *Polymers*, 2018, **10**, 248.
130. R. Semproli, M. Simona Robescu, S. Sangiorgio, E. Pargoletti, T. Bavaro, M. Rabuffetti, G. Cappelletti, G. Speranza and D. Ubiali, *ChemPlusChem*, 2023, **88**, e202200331.
131. G. Bartoli, J. G. Fernández-Bolaños, G. Di Antonio, G. Foglia, S. Giuli, R. Gunnella, M. Mancinelli, E. Marcantoni and M. Paoletti, *The Journal of Organic Chemistry*, 2007, **72**, 6029-6036.
132. A. A. Rosatella, S. P. Simeonov, R. F. M. Frade and C. A. M. Afonso, *Green Chemistry*, 2011, **13**, 754-793.
133. F. G. Gonzalez, *Advances in Carbohydrate Chemistry*, 1956, **11**, 97-143.
134. J. K. N. Jones, *Journal of the Chemical Society (Resumed)*, 1945, DOI: 10.1039/JR9450000116, 116-119.
135. B. List and M. Turberg, *Synfacts*, 2019, **15**, 0428.
136. 2,4-Pentanedione, 99%, Thermo Scientific Chemicals, https://www.fishersci.co.uk/shop/products/2-4-pentanedione-99-thermo-scientific-1/11498076, (accessed April, 2023).
137. W. Zha, Z. Shao, J. W. Frost and H. Zhao, *Journal of the American Chemical Society*, 2004, **126**, 4534-4535.
138. M. Chia, T. J. Schwartz, B. H. Shanks and J. A. Dumesic, *Green Chemistry*, 2012, **14**, 1850-1853.
139. F. Rodrigues, Y. Canac and A. Lubineau, *Chemical Communications*, 2000, DOI: 10.1039/B006642G, 2049-2050.
140. A. P. Kozikowski, G. Q. Lin and J. P. Springer, *Tetrahedron Letters*, 1987, **28**, 2211-2214.
141. N. Ronaghi, D. M. Fialho, C. W. Jones and S. France, *The Journal of Organic Chemistry*, 2020, **85**, 15337-15346.
142. R. Zhang, A. Eronen, P. Vasko, X. Du, J. Install and T. Repo, *Green Chemistry*, 2022, **24**, 5052-5057.

143. S. Sato, Y. Naito and K. Aoki, *Carbohydrate Research*, 2007, **342**, 913-918.
144. A. K. Misra and G. Agnihotri, *Carbohydrate Research*, 2004, **339**, 1381-1387.
145. A. D. Sutton, J. K. Kim, R. Wu, C. B. Hoyt, D. B. Kimball, L. A. Silks, 3rd and J. C. Gordon, *ChemSusChem*, 2016, **9**, 2298-2300.
146. J. S. Yadav, B. V. S. Reddy, M. Sreenivas and G. Satheesh, *Synthesis-Stuttgart*, 2007, DOI: 10.1055/s-2007-966056, 1712-1716.
147. L. Nagarapu, M. V. Chary, A. Satyender, B. Supriya and R. Bantu, *Synthesis-Stuttgart*, 2009, DOI: 10.1055/s-0029-1216865, 2278-2282.
148. L. Yan, G. F. Dai, J. L. Yang, F. W. Liu and H. M. Liu, *Bioorg Med Chem Lett*, 2007, **17**, 3454-3457.
149. B. C, Durham University, 2020.
150. F. P. Byrne, S. Jin, G. Paggiola, T. H. M. Petchey, J. H. Clark, T. J. Farmer, A. J. Hunt, C. Robert McElroy and J. Sherwood, *Sustainable Chemical Processes*, 2016, **4**, 7.
151. US FDA Guidance, Compliance, & Regulatory Information, https://www.fda.gov/drugs/guidance-compliance-regulatory-information/guidances-drugs,
152. R. K. Montgomery, S. D. Krasinski, J. N. Hirschhorn and R. J. Grand, *Journal of Pediatric Gastroenterology and Nutrition*, 2007, **45**, S131-S137.
153. G. Chen, T. Leong, S. Kentish, M. Ashokkumar and G. Martin, 2019, DOI: 10.1016/B978-0-12-815056-6.00008-5, pp. 267-304.
154. M. I. G. Siso, *Bioresource Technology*, 1996, **57**, 1-11.
155. L. H. Pignolet, A. S. Waldman, L. Schechinger, G. Govindarajoo, J. S. Nowick and L. Ted, *Journal of Chemical Education*, 1998, **75**, 1430.
156. C. T. d. Carvalho, W. B. d. B. Lima, F. G. M. de Medeiros, J. M. d. M. Dantas, C. E. de Araújo Padilha, E. S. dos Santos, G. R. de Macêdo and F. C. de Sousa Júnior, *Preparative Biochemistry & Biotechnology*, 2021, **51**, 714-722.
157. *US Pat.,* 6660313 B2, 2003.
158. *WO Pat.,* 2013/084244 Al, 2013.
159. Creative Enzymes, https://www.creative-enzymes.com/product/native-kluyveromyces-lactis-galactosidase_928.html, (accessed June, 2025).
160. J. L. Baret, in *Methods in Enzymology*, Academic Press, 1987, vol. 136, pp. 411-423.

161. L. H. Jin, Y. Li, X. H. Ren and J. H. Lee, *Journal of Microbiology and Biotechnology*, 2015, **25**, 1291-1298.
162. Immobilization of Lactase Enzyme on Alginate Beads - A Quick Test, https://www.chemedx.org/article/immobilization-lactase-enzyme-alginate-beads-quick-test, (accessed April, 2023).
163. Making milk lactose free, https://www.youtube.com/watch?v=wYyqZWWU9GU, (accessed April, 2023).
164. C.-Y. Ko, J.-M. Liu, K.-I. Chen, C.-W. Hsieh, Y.-L. Chu and K.-C. Cheng, *Food Biophysics*, 2018, **13**, 353-361.
165. K. Y. Lee and D. J. Mooney, *Progress in Polymer Science*, 2012, **37**, 106-126.
166. N. K. Sachan, S. Pushkar, A. Jha and A. Bhattcharya, *J. Pharm. Res*, 2009, **2**, 1191-1199.
167. C. H. Goh, P. W. S. Heng and L. W. Chan, *Carbohydrate Polymers*, 2012, **88**, 1-12.
168. S. Sellimi, I. Younes, H. B. Ayed, H. Maalej, V. Montero, M. Rinaudo, M. Dahia, T. Mechichi, M. Hajji and M. Nasri, *International Journal of Biological Macromolecules*, 2015, **72**, 1358-1367.
169. T. Buranachai, N. Praphairaksit and N. Muangsin, *AAPS PharmSciTech*, 2010, **11**, 1128-1137.
170. K. N. Ghimire, K. Inoue, K. Ohto and T. Hayashida, *Bioresource Technology*, 2008, **99**, 32-37.
171. H. Paudyal, B. Pangeni, K. Inoue, H. Kawakita, K. Ohto, K. N. Ghimire and S. Alam, *Bioresource Technology*, 2013, **148**, 221-227.
172. S. Nazeri, S. Azarian, M. Fattahi, R. Sedaghat, F. Tofighi Zavareh, Z. Aghazadeh, M. Abdollahi and A. Mirshafiey, *Immunopharmacology and immunotoxicology*, 2017, **39**, 1-7.
173. O. D. Frent, L. G. Vicas, N. Duteanu, C. M. Morgovan, T. Jurca, A. Pallag, M. E. Muresan, S. M. Filip, R.-L. Lucaciu and E. Marian, *International Journal of Molecular Sciences*, 2022, **23**, 12108.
174. K. Majore and I. Ciprovica, *Foods*, 2022, **11**.
175. K. Majore and I. Ciproviča, *Proceedings of the Latvian Academy of Sciences. Section B. Natural, Exact, and Applied Sciences.*, 2020, **74**, 263-269.
176. Y. S. Song, H. U. Lee, C. Park and S. W. Kim, *Food Chemistry*, 2013, **136**, 689-694.

177. A. E. Al-Muftah and I. M. Abu-Reesh, *Biochemical Engineering Journal*, 2005, **23**, 139-153.
178. V. Gekas and M. Lopezleiva, *Process Biochemistry*, 1985, **20**, 2-12.
179. Physics LibreTexts, https://phys.libretexts.org/Bookshelves/College_Physics/College_Physics_1e_(OpenStax)/12%3A_Fluid_Dynamics_and_Its_Biological_and_Medical_Applications/12.01%3A_Flow_Rate_and_Its_Relation_to_Velocity,
180. 2,4-Pentanedione, https://www.chembk.com/en/chem/2,4-Pentanedione, (accessed April, 2023).
181. Vapourtec, chrome-extension://efaidnbmnnnibpcajpcglclefindmkaj/https://www.vapourtec.com/wp-content/uploads/2015/10/Vapourtec_Dispersion.pdf, (accessed April, 2025).
182. AM Technology, https://www.amt.uk/flow-reactors, (accessed April, 2025).
183. IUPAC Gold Book, https://goldbook.iupac.org/terms/view/S05962, (accessed August, 2025).
184. Organic Chemistry Portal, https://www.organic-chemistry.org/topics/flowchemistry.shtm, (accessed August, 2025).
185. fReactor, https://freactor.com/learningIntroReactors.html, (accessed August, 2025).
186. A. A. Belyaev, A. V. Arutyunov and V. S. Arutyunov, *Theoretical Foundations of Chemical Engineering*, 2023, **57**, 861-868.
187. T. M. de Winter, Y. Balland, A. E. Neski, L. Petitjean, H. C. Erythropel, M. Moreau, J. Hitce, P. Coish, J. B. Zimmerman and P. T. Anastas, *ACS Sustainable Chemistry & Engineering*, 2018, **6**, 11196-11199.
188. LAMDA, https://www.powderdosing.info/features, (accessed August, 2025).
189. ACS Publications, https://researcher-resources.acs.org/publish/author_guidelines?coden=joceah, (accessed June, 2025).
190. Royal Society of Chemistry, https://www.rsc.org/journals-books-databases/author-and-reviewer-hub/authors-information/prepare-and-format/experimental-reporting-requirements/#presentation-of-experimental-data, (accessed June, 2025).
191. O. V. Dolomanov, L. J. Bourhis, R. J. Gildea, J. A. K. Howard and H. Puschmann, *Journal of Applied Crystallography*, 2009, **42**, 339-341.

192. G. Sheldrick, *Acta Crystallographica Section A*, 2015, **71**, 3-8.
193. G. Sheldrick, *Acta Crystallographica Section C*, 2015, **71**, 3-8.
194. D.-L. Li, X.-M. Li, T.-G. Li, H.-Y. Dang, P. Proksch and B.-G. Wang, *Chemical and Pharmaceutical Bulletin*, 2008, **56**, 1282-1285.
195. F. Epifano, S. Genovese, L. Menghini and M. Curini, *Phytochemistry*, 2007, **68**, 939-953.
196. A. del Olmo, J. Calzada and M. Nuñez, *Critical Reviews in Food Science and Nutrition*, 2017, **57**, 3084-3103.
197. J.-F. Sun, X. Lin, X.-F. Zhou, J. Wan, T. Zhang, B. Yang, X.-W. Yang, Z. Tu and Y. Liu, *The Journal of Antibiotics*, 2014, **67**, 451-457.
198. J. Shi, J. Liu, D. Kang, Y. Huang, W. Kong, Y. Xiang, X. Zhu, Y. Duan and Y. Huang, *ACS Omega*, 2019, **4**, 6630-6636.
199. K.-S. Kim, X. Cui, D.-S. Lee, W. Ko, J. H. Sohn, J. H. Yim, R.-B. An, Y.-C. Kim and H. Oh, *International Journal of Molecular Sciences*, 2014, **15**, 23749-23765.
200. Y. Ruan, C. Han, D. Wang, Y. Inoue, Y. Amen, A. Othman, Y. Mittraphab, M. Nagata and K. Shimizu, *Natural Product Research*, 2023, **37**, 4089-4098.
201. S. K. Haraguchi, A. A. Silva, G. J. Vidotti, P. V. Dos Santos, F. P. Garcia, R. B. Pedroso, C. V. Nakamura, C. M. A. De Oliveira and C. C. Da Silva, *Molecules*, 2011, **16**, 1166-1180.
202. B. Adalat, F. Rahim, W. Rehman, Z. Ali, L. Rasheed, Y. Khan, T. A. Farghaly, S. Shams, M. Taha, A. Wadood, S. A. A. Shah and M. H. Abdellatif, *Pharmaceuticals*, 2023, **16**, 208.
203. M. Larsen, H. Kromann, A. Kharazmi and S. F. Nielsen, *Bioorganic & Medicinal Chemistry Letters*, 2005, **15**, 4858-4861.
204. W. Ma, X. Zhang, Y. Ma, D. Chen, L. Wang, C. Zhao and W. Yang, *Polymer Chemistry*, 2017, **8**, 3574-3585.
205. A. Alamri, M. H. El-Newehy and S. S. Al-Deyab, *Chemistry Central Journal*, 2012, **6**, 111.
206. F. I. Zubkov and V. V. Kouznetsov, *Molecules*, 2023, **28**, 370.
207. H. Ahmadpourmir, H. Attar, J. Asili, V. Soheili, S. F. Taghizadeh and A. Shakeri, *Natural Products and Bioprospecting*, 2024, **14**, 28.

208. G. Mohammadi Ziarani, Z. Kheilkordi and F. Mohajer, *Journal of the Iranian Chemical Society*, 2020, **17**, 247-282.
209. K. M. Adki and Y. A. Kulkarni, *Life Sciences*, 2020, **250**, 117544.
210. J. Stefanska and R. Pawliczak, *Mediators Inflamm*, 2008, **2008**, 106507.
211. H. Surburg and J. Panten, *Common Fragrance and Flavor Materials : Preparation, Properties and Uses*, John Wiley & Sons, Incorporated, Newark, GERMANY, 2016.
212. G. Wejnerowska and I. Narloch, *Molecules*, 2021, **26**, 6896.
213. W. Denis and P. B. Dunbar, *Journal of Industrial & Engineering Chemistry*, 1909, **1**, 256-257.
214. J.-J. Chen, J.-Y. Cho, T.-L. Hwang and I.-S. Chen, *Journal of Natural Products*, 2008, **71**, 71-75.
215. Q.-W. Niu, N.-H. Chen, Z.-N. Wu, D. Luo, Y.-Y. Li, Y.-B. Zhang, Q.-G. Li, Y.-L. Li and G.-C. Wang, *Natural Product Research*, 2019, **33**, 2230-2235.
216. *CN Pat.,* 103044390 A, 2012.
217. N. Morales-Camilo, C. O. Salas, C. Sanhueza, C. Espinosa-Bustos, S. Sepúlveda-Boza, M. Reyes-Parada, F. Gonzalez-Nilo, M. Caroli-Rezende and A. Fierro, *Chemical Biology & Drug Design*, 2015, **85**, 685-695.
218. C. Battilocchio, B. J. Deadman, N. Nikbin, M. O. Kitching, I. R. Baxendale and S. V. Ley, *Chemistry – A European Journal*, 2013, **19**, 7917-7930.
219. J. Park, P. Khloya, Y. Seo, S. Kumar, H. K. Lee, D. K. Jeon, S. Jo, P. K. Sharma and W. Namkung, *PLoS One*, 2016, **11**, e0149131.
220. *WO Pat.,* 051478, 2011.
221. D. R. R. Moreno, G. Giorgi, C. O. Salas and R. A. Tapia, *Molecules*, 2013, **18**, 14797-14806.
222. I. Yavari, R. Mohsenzadeh and P. Ravaghi, *The Journal of Organic Chemistry*, 2022, **87**, 2616-2623.
223. E. D. D. Calder, S. A. I. Sharif, F. I. McGonagle and A. Sutherland, *The Journal of Organic Chemistry*, 2015, **80**, 4683-4696.
224. S. Kumar, N. Vashisht, Aruna and S. P. Sharma, *Russian Journal of Organic Chemistry*, 2021, **57**, 1508-1512.

225. H. Chen, J. Xie, D. Xing, J. Wang, J. Tang, Z. Yi, F. Xia, W.-W. Qiu and F. Yang, *Organic & Biomolecular Chemistry*, 2019, **17**, 1062-1066.
226. N. A. A. Elkanzi, H. Hrichi, R. A. Alolayan, W. Derafa, F. M. Zahou and R. B. Bakr, *ACS Omega*, 2022, **7**, 27769-27786.
227. Z. Gao, F. Wang, J. Qian, H. Yang, C. Xia, J. Zhang and G. Jiang, *Organic Letters*, 2021, **23**, 1181-1187.
228. *US Pat.,* 20090054400A1, 2009.
229. *CN Pat.,* 103570661 A 2014.
230. G. Gudipudi, S. R. Sagurthi, S. Perugu, G. Achaiah and G. L. David Krupadanam, *RSC Advances*, 2014, **4**, 56489-56501.
231. P. Saling, 1993.
232. Z. Zheng, Q. Liu, X. Peng, Z. Jin and J. Wu, *Organic Letters*, 2024, **26**, 917-921.
233. Z. Mincheva, J. Velkov, G. Boireau, J. Barry and C. Fugier, *Synthetic Communications*, 1995, **25**, 149-155.
234. *CN Pat.,* 101768065 B 2014.
235. E. Yoshioka, H. Tamenaga and H. Miyabe, *Tetrahedron Letters*, 2014, **55**, 1402-1405.
236. H.-J. Lo, C.-Y. Lin, M.-C. Tseng and R.-J. Chein, *Angewandte Chemie International Edition*, 2014, **53**, 9026-9029.
237. SciFinder, https://scifinder-n.cas.org/search/catalogItem/6745a3c835b8cf4021cb9a69/1, (accessed November, 2024).
238. N. M. F. S. A. Cerqueira, A. M. F. Oliveira-Campos, P. J. Coelho, L. H. M. de Carvalho, A. Samat and R. Guglielmetti, *Helvetica Chimica Acta*, 2002, **85**, 442-450.
239. R. Ravichandran, *Journal of Molecular Catalysis A: Chemical*, 1998, **130**, L205-L207.
240. F. Albericio, N. Kneib-Cordonier, S. Biancalana, L. Gera, R. I. Masada, D. Hudson and G. Barany, *The Journal of Organic Chemistry*, 1990, **55**, 3730-3743.
241. Y. Suzuki and H. Takahashi, *CHEMICAL & PHARMACEUTICAL BULLETIN*, 1983, **31**, 1751-1753.
242. H. F. Anwar, University of Oslo, 2009.
243. T. V. Hansen and L. Skattebol, *Organic Syntheses*, 2012, **89**, 220-229.
244. N. U. Hofslokken and L. Skattebol, *Acta Chemica Scandinavica*, 1999, **53**, 258-262.
245. T. V. Hansen and L. Skattebol, *Organic Syntheses*, 2005, **82**, 64-68.

246. Ø. W. Akselsen, L. Skattebøl and T. V. Hansen, *Tetrahedron Letters*, 2009, **50**, 6339-6341.
247. F. Alonso, I. P. Beletskaya and M. Yus, *Chemical Reviews*, 2002, **102**, 4009-4092.
248. X. Ma, S. Liu, Y. Liu, G. Gu and C. Xia, *Scientific Reports*, 2016, **6**, 25068.
249. I. Markish and O. Arrad, *Industrial & Engineering Chemistry Research*, 1995, **34**, 2125-2127.
250. Y. Satkar, V. Ramadoss, P. D. Nahide, E. García-Medina, K. A. Juárez-Ornelas, A. J. Alonso-Castro, R. Chávez-Rivera, J. O. C. Jiménez-Halla and C. R. Solorio-Alvarado, *RSC Advances*, 2018, **8**, 17806-17812.
251. L. Wang, C. Feng, Y. Zhang and J. Hu, *Molecules*, 2020, **25**.
252. D. Georgiev, B. W. Saes, H. J. Johnston, S. K. Boys, A. Healy and A. N. Hulme, *Molecules*, 2016, **21**, 88.
253. D. E. Pearson, R. D. Wysong and C. V. Breder, *The Journal of Organic Chemistry*, 1967, **32**, 2358-2360.
254. H. Xu, L. Hu, G. Zhu, Y. Zhu, Y. Wang, Z.-G. Wu, Y. Zi and W. Huang, *RSC Advances*, 2022, **12**, 7115-7119.
255. S. Fujisaki, H. Eguchi, A. Omura, A. Okamoto and A. Nishida, *Bulletin of the Chemical Society of Japan*, 1993, **66**, 1576-1579.
256. R. Hemelaere, F. Carreaux and B. Carboni, *European Journal of Organic Chemistry*, 2015, **2015**, 2470-2481.
257. Y. Zhao, Z. Li, C. Yang, R. Lin and W. Xia, *Beilstein Journal of Organic Chemistry*, 2014, **10**, 622-627.
258. X. Xiong and Y.-Y. Yeung, *ACS Catalysis*, 2018, **8**, 4033-4043.
259. R. Nouch, M. Cini, M. Magre, M. Abid, M. Diéguez, O. Pàmies, S. Woodward and W. Lewis, *Chemistry – A European Journal*, 2017, **23**, 17195-17198.
260. C. A. Marques, M. Selva and P. Tundo, *The Journal of Organic Chemistry*, 1994, **59**, 3830-3837.
261. M. La Torre, W. Maton, E. Cleator and M. Jouffroy, *Synthesis*, 2023, **55**, 1394-1400.
262. P. P. Cellier, J.-F. Spindler, M. Taillefer and H.-J. Cristau, *Tetrahedron Letters*, 2003, **44**, 7191-7195.

263. C. J. Crawford, Y. Qiao, Y. Liu, D. Huang, W. Yan, P. H. Seeberger, S. Oscarson and S. Chen, *Organic Process Research & Development*, 2021, **25**, 1573-1578.
264. D. Li, J. Huang and R. B. Kaner, *Accounts of Chemical Research*, 2009, **42**, 135-145.
265. S. Giri, M. Bhaumik, R. Das, V. K. Gupta and A. Maity, *Applied Catalysis B: Environmental*, 2017, **202**, 207-216.
266. C. Egan-Morriss, R. L. Kimber, N. A. Powell and J. R. Lloyd, *Nanoscale Advances*, 2022, **4**, 654-679.
267. Y. Era, J. A. Dennis, S. Wallace and L. E. Horsfall, *Green Chemistry*, 2021, **23**, 8886-8890.
268. Y. Era, J. A. Dennis, L. E. Horsfall and S. Wallace, *JACS Au*, 2022, **2**, 2446-2452.
269. M. Asikainen, O. Jauhiainen, O. Aaltonen and A. Harlin, *Green Chemistry*, 2013, **15**, 3230-3235.
270. R. C. Brewster, J. T. Suitor, A. W. Bennett and S. Wallace, *Angewandte Chemie International Edition*, 2019, **58**, 12409-12414.
271. P. Ciesielski and P. Metz, *Bioorganic & Medicinal Chemistry*, 2017, **25**, 6175-6177.
272. D. Sang, H. Yue, Z. Zhao, P. Yang and J. Tian, *The Journal of Organic Chemistry*, 2020, **85**, 6429-6440.
273. B. Åkermark, *Acta Chemica Scandinavica*, 1970, **24**, 1459-1460.
274. E. Yoshioka, H. Tanaka, S. Kohtani and H. Miyabe, *Organic Letters*, 2013, **15**, 3938-3941.
275. G. A. Olah, *Friedel-Crafts and related reactions*, Interscience Publishers, New York, 1963.
276. R. Murashige, Y. Hayashi, S. Ohmori, A. Torii, Y. Aizu, Y. Muto, Y. Murai, Y. Oda and M. Hashimoto, *Tetrahedron*, 2011, **67**.
277. in *Comprehensive Organic Name Reactions and Reagents*, DOI: https://doi.org/10.1002/9780470638859.conrr334, pp. 1496-1500.
278. L. A. González, S. Robledo, Y. Upegui, G. Escobar and W. Quiñones, *Molecules*, 2021, **26**, 7067.
279. J. Wang, R.-G. Zhou, T. Wu, T. Yang, Q.-X. Qin, I. Li, B. Yang and J. Yang, *Journal of Chemical Research*, 2012, **36**, 121-122.

280. J. Greb, T. Drennhaus, M. K. T. Klischan, Z. W. Schroeder, W. Frey and J. Pietruszka, *Chemistry – A European Journal*, 2023, **29**, e202300941.
281. J. Tang, K. Qian, B.-N. Zhang, Y. Chen, P. Xia, D. Yu, Y. Xia, Z.-Y. Yang, C.-H. Chen, S. L. Morris-Natschke and K.-H. Lee, *Bioorganic & Medicinal Chemistry*, 2010, **18**, 4363-4373.
282. A. Russell, *Organic syntheses : an annual publication of satisfactory methods for the preparation of organic chemicals.*, 1941, **21**, 22-27.
283. Merk, https://www.sigmaaldrich.com/GB/en/product/aldrich/39410?srsltid=AfmBOor4AyAbsZv8YpxShpXgIdkaehNgkEuoHvMnni9GjypY_vr8P4X1, (accessed July, 2025).
284. C. E. Schiaffo and P. H. Dussault, *The Journal of Organic Chemistry*, 2008, **73**, 4688-4690.
285. M. Lončarić, D. Gašo-Sokač, S. Jokić and M. Molnar, *Biomolecules*, 2020, **10**, 151.
286. S. Prateeptongkum, N. Duangdee and P. Thongyoo, *ARKIVOC*, 2014, **2015**.
287. S. Tyndall, K. F. Wong and M. A. VanAlstine-Parris, *The Journal of Organic Chemistry*, 2015, **80**, 8951-8953.
288. J. B. Metternich and R. Gilmour, *Journal of the American Chemical Society*, 2016, **138**, 1040-1045.
289. U. Matern, P. Lüer and D. Kreusch, in *Comprehensive Natural Products Chemistry*, eds. S. D. Barton, K. Nakanishi and O. Meth-Cohn, Pergamon, Oxford, 1999, DOI: https://doi.org/10.1016/B978-0-08-091283-7.00026-6, pp. 623-637.
290. J. Jin, Q. Xu and W. Deng, *Chinese Journal of Chemistry*, 2017, **35**, 397-400.
291. Q. Yang, Z. Jia, L. Li, L. Zhang and S. Luo, *Organic Chemistry Frontiers*, 2018, **5**, 237-241.
292. W. T. Brady and C. H. Shieh, *Journal of Heterocyclic Chemistry*, 1984, **21**, 1337-1339.
293. D. Walker and J. D. Hiebert, *Chemical Reviews*, 1967, **67**, 153-195.
294. Y. Wang, W. Liu, W. Ren and Y. Shi, *Organic Letters*, 2015, **17**, 4976-4979.
295. Z. Rappoport, *The chemistry of enols*, Wiley, Chichester, 1990.
296. X. He, Y.-W. Zheng, T. Lei, W.-Q. Liu, B. Chen, K. Feng, C.-H. Tung and L.-Z. Wu, *Catalysis Science & Technology*, 2019, **9**, 3337-3341.

297. P. Winget, E. J. Weber, C. J. Cramer and D. G. Truhlar, *Physical Chemistry Chemical Physics*, 2000, **2**, 1231-1239.
298. N. A. Romero and D. A. Nicewicz, *Chemical Reviews*, 2016, **116**, 10075-10166.
299. D. C. Grills, D. E. Polyansky and E. Fujita, *ChemSusChem*, 2017, **10**, 4359-4373.
300. J. L. Hodgson, M. Namazian, S. E. Bottle and M. L. Coote, *The Journal of Physical Chemistry A*, 2007, **111**, 13595-13605.
301. P. Winget, C. J. Cramer and D. G. Truhlar, *Theoretical Chemistry Accounts*, 2004, **112**, 217-227.
302. J. Conradie, *Journal of Physics: Conference Series*, 2015, **633**, 012045.
303. ALS Electrochemistry & Spectroelectrochemistry, https://www.als-japan.com/1810.html, (accessed March, 2025).
304. P. Natarajan and B. König, *European Journal of Organic Chemistry*, 2021, **2021**, 2145-2161.
305. K. Ohkubo, T. Kobayashi and S. Fukuzumi, *Angewandte Chemie International Edition*, 2011, **50**, 8652-8655.
306. Y. Zhang, University of Durham, 2023.
307. S. Moulay, *Current Organic Chemistry*, 2018, **22**, 1986-2016.
308. N. Sarki, V. Goyal, K. Natte and R. V. Jagadeesh, *Advanced Synthesis & Catalysis*, 2021, **363**, 5028-5046.
309. S. Ouk, S. Thiébaud, E. Borredon and P. Le Gars, *Applied Catalysis A: General*, 2003, **241**, 227-233.
310. S. Ouk, S. Thiebaud, E. Borredon, P. Legars and L. c. Lecomte, *Tetrahedron Letters*, 2002, **43**, 2661-2663.
311. U. Tilstam, *Organic Process Research & Development*, 2012, **16**, 1150-1153.
312. M. R. Saidi and F. Rajabi, *Phosphorus, Sulfur, and Silicon and the Related Elements*, 2003, **178**, 2343-2348.
313. Y. Chen, *Chemistry – A European Journal*, 2019, **25**, 3405-3439.
314. S. Bleus, J. Semerel and W. Dehaen, *Green Chemistry*, 2024, **26**, 3903-3908.
315. N. Myung, S. Connelly, B. Kim, S. J. Park, I. A. Wilson, J. W. Kelly and S. Choi, *Chemical Communications*, 2013, **49**, 9188-9190.
316. F. Rajabi and M. R. Saidi, *Synthetic Communications*, 2004, **34**, 4179-4188.

317. Y. Hu, L. Shan, T. Qiu, L. Liu and J. Chen, *European Journal of Medicinal Chemistry*, 2021, **223**, 113739.
318. S. Ma, D.-C. Fang, B. Ning, M. Li, L. He and B. Gong, *Chemical Communications*, 2014, **50**, 6475-6478.
319. S. Xu, *Yaoxue Xuebao*, 2001, **36**, 269-273.
320. J. S. Bandar, A. Tanaset and T. H. Lambert, *Chemistry*, 2015, **21**, 7365-7368.
321. S. V. Ley, I. R. Baxendale, R. N. Bream, P. S. Jackson, A. G. Leach, D. A. Longbottom, M. Nesi, J. S. Scott, R. I. Storer and S. J. Taylor, *Journal of the Chemical Society, Perkin Transactions 1*, 2000, DOI: 10.1039/B006588I, 3815-4195.
322. S. V. Ley, I. R. Baxendale, G. Brusotti, M. Caldarelli, A. Massi and M. Nesi, *Il Farmaco*, 2002, **57**, 321-330.
323. Y. Yamaguchi, I. Akimoto, K. Motegi, T. Yoshimura, K. Wada, N. Nishizono and K. Oda, *Chemical and Pharmaceutical Bulletin*, 2013, **61**, 997-1001.
324. A. Barthel, L. Trieschmann, D. Ströhl, R. Kluge, G. Böhm and R. Csuk, *Archiv der Pharmazie*, 2009, **342**, 445-452.
325. X. Zhang, Q. Chen, R. Song, J. Xu, W. Tian, S. Li, Z. Jin and Y. R. Chi, *ACS Catalysis*, 2020, **10**, 5475-5482.
326. M. Croisy-Delcey, E. Bisagni, C. Huel, D. Zilberfarb and A. Croisy, *Journal of Heterocyclic Chemistry*, 1991, **28**, 65-71.
327. J. Wu, C. Mou and Y. R. Chi, *Chinese Journal of Chemistry*, 2018, **36**, 333-337.
328. R. E. Dean, A. Midgley, E. N. White and D. McNeil, *Journal of the Chemical Society (Resumed)*, 1961, DOI: 10.1039/JR9610002773, 2773-2779.
329. Z. Shi and C. He, *The Journal of Organic Chemistry*, 2004, **69**, 3669-3671.
330. X.-Y. Huang, R. Ding, Z.-Y. Mo, Y.-L. Xu, H.-T. Tang, H.-S. Wang, Y.-Y. Chen and Y.-M. Pan, *Organic Letters*, 2018, **20**, 4819-4823.
331. S. Hou, H. Yang, B. Cheng, H. Zhai and Y. Li, *Chemical Communications*, 2017, **53**, 6926-6929.
332. P. Bolduc, A. Jacques and S. K. Collins, *Journal of the American Chemical Society*, 2010, **132**, 12790-12791.
333. R. M. G. Roberts, D. Ostović and M. M. Kreevoy, *Faraday Discussions of the Chemical Society*, 1982, **74**, 257-265.

334. S. Fukuzumi, M. Nishimine, K. Ohkubo, N. V. Tkachenko and H. Lemmetyinen, *The Journal of Physical Chemistry B*, 2003, **107**, 12511-12518.
335. J. Oehldrich and J. M. Cook, *The Journal of Organic Chemistry*, 1977, **42**, 889-894.
336. N. Takeuti, T. Kasama, Y. Aida, J. Oki, I. Maruyama, K. Watanabe and S. Tobinaga, *CHEMICAL & PHARMACEUTICAL BULLETIN*, 1991, **39**, 1415-1421.
337. R. N. Gourley, J. Grimshaw and P. G. Millar, *Journal of the Chemical Society C: Organic*, 1970, DOI: 10.1039/J39700002318, 2318-2323.
338. F. Munafò, M. Nigro, N. Brindani, J. Manigrasso, I. Geronimo, G. Ottonello, A. Armirotti and M. De Vivo, *European Journal of Medicinal Chemistry*, 2023, **248**, 115044.
339. Asynt, https://www.asynt.com/product/ozone-generator/, (accessed June, 2025).
340. K. Hu, Z.-h. Yang, S.-S. Pan, H.-j. Xu and J. Ren, *European Journal of Medicinal Chemistry*, 2010, **45**, 3453-3458.
341. Z. Yang, Y. Wang, M. Ablise, A. Maimaiti, Z. Mutalipu, T. Yan, Z.-Y. Liu and A. Aihaiti, *Bioorganic Chemistry*, 2024, **149**, 107498.